Harvesting entanglement from quantum fields:

from theory to proposed superconducting implementations

by

Adam Teixido-Bonfill

A thesis
presented to the University of Waterloo
in fulfillment of the
thesis requirement for the degree of
Doctor of Philosophy
in
Applied Mathematics (Quantum Information)

Waterloo, Ontario, Canada, 2025

© Adam Teixido-Bonfill 2025

Examining Committee Membership

The following served on the Examining Committee for this thesis. The decision of the Examining Committee is by majority vote.

External Examiner:	Natalie Klco Assistant Professor, Dept. of Physics, Duke University
Supervisor(s):	Eduardo Martín-Martínez Professor, Dept. of Applied Mathemathics, University of Waterloo
Internal Member:	Florian Girelli Associate Professor, Dept. of Applied Mathematics, University of Waterloo
Internal-External Member:	Adrian Lupascu Associate Professor, Dept. of Physics & Astronomy, University of Waterloo Associate Professor, Institute for Quantum Computing, University of Waterloo
Other Member(s):	Graeme Smith Associate Professor, Dept. of Applied Mathematics, University of Waterloo Associate Professor, Institute for Quantum Computing, University of Waterloo

Author's Declaration

This thesis consists of material all of which I authored or co-authored: see Statement of Contributions included in the thesis. This is a true copy of the thesis, including any required final revisions, as accepted by my examiners.

I understand that my thesis may be made electronically available to the public.

Statement of contributions

This thesis contains results from the following works:

1. **A. Teixidó-Bonfill**, and E. Martín-Martínez, "Derivative coupling enables genuine entanglement harvesting in causal communication" Phys. Rev. D **110**, 105016 (2024).

2. M. H. Zambianco, **A. Teixidó-Bonfill**, and E. Martín-Martínez, "Interference of communication and field correlations in entanglement harvesting" Phys. Rev. D **110**, 025016 (2024).

3. **A. Teixidó-Bonfill**, X. Dai, A. Lupascu, E. Martín-Martínez, "Towards an experimental implementation of entanglement harvesting in superconducting circuits: effect of detector gap variation on entanglement harvesting", arXiv:2505.01516, (2025).

Results from papers 1 and 2 appear in Chapter 2 of this thesis. I was responsible for doing the calculations and writing the first draft for article 1, and the text then was edited collaboratively with my supervisor. For paper 2, I obtained the results and proofs provided in Section 2.5 and all the calculations included in Appendix A. The rest of the text for this work was first drafted by Matheus H. Zambianco, and then edited collaboratively by all co-authors.

The results in Chapter 3 do not appear in a published work as of the time of writing of this thesis, but are part of a work in progress which we plan to submit for publication [1].

Results from paper 3 appear in Chapter 4. I produced the calculations and plots for this work. X. Dai was involved in initial discussions, and worked on a code to predict the gap variation in experimental setups, with results appearing in Section 4.2.1 on the part titled "Approximated linear dependence of the gap on the instantaneous transversal coupling strength". I wrote the first draft of the article, and then edited it collabovatively with the other co-authors.

Additional contributions published during my PhD but not included explicitly in this thesis are:

4. **A. Teixidó-Bonfill**, J. Schindler, D. Šafránek, "Entropic partial orderings of quantum measurements", Phys. Scr. **100** 015298, (2025).

5. **A. Teixidó-Bonfill**, "Data processing makes POVMs coarser and observational entropies larger", arXiv:2209.04549, (2022).

Abstract

Entanglement harvesting is a relativistic quantum information protocol through which initially uncorrelated particle detectors become entangled by locally interacting with a quantum field. This process allows one to extract and repurpose the entanglement naturally present in quantum fields, even from spacelike-separated regions. Entanglement harvesting has not been realized in the lab, but multiple experimental platforms to realize it have been proposed, among which superconducting circuits stand out due to their controllability and ability to implement strong interactions of detectors with 1+1 dimensional quantum fields.

In this thesis, we start by investigating entanglement harvesting using particle detectors coupled to a massless scalar field through its derivative, a coupling that captures important features of light-matter interaction and is naturally realized in superconducting circuits. We show that detectors in causal contact can still harvest genuine entanglement from the field, with harvested entanglement peaking when the detectors are fully light-connected. Additionally, we find that communication and harvesting contributions to the detectors' entanglement can interfere both constructively and destructively. Surprisingly, this implies that the presence of entanglement in the field can sometimes inhibit, rather than enhance, the entangling of the detectors.

We then broaden the analysis to more general entanglement harvesting protocols involving detectors with arbitrary number of energy levels and a general class of couplings to the field. Furthermore, we study the longitudinal (diagonal) and transversal (off-diagonal) components of the detector-field interaction. We show that at leading order, entanglement harvesting is dominated by the component transversal to the detectors' initial state. Through an explicit qubit model, we further illustrate how increasing the strength of longitudinal coupling can suppress harvested entanglement via higher-order effects.

Finally, motivated by the prospect of experimental realizations, we introduce a variable-gap detector model that bridges the gap between idealized Unruh-DeWitt particle detectors and existing implementations in superconducting circuits. Using parameters tailored to potential experimental setups, we investigate entanglement harvesting in both spacelike-separated and causally connected scenarios. We find that, while variations in the energy gap reduce the ability to harvest entanglement in spacelike scenarios, detectors in causal contact detectors can still become entangled through their interaction with the field. Notably, our analysis shows that (due to the derivative coupling nature of the model) even for causally connected detectors, there are setups where entanglement primarily originates from the field's correlations. This demonstrates the potential for genuine entanglement harvesting in the lab and opens the door to near-future entanglement harvesting experiments in superconducting circuits.

Acknowledgements

I could never thank enough my partner, Hanne Silverans. You have been a bright light in my life for these last two years, with your smile and your jokes, and not to mention your neverending love, support and thoughtfulness. The PhD journey became a lighter weight, a more enjoyable walk, with you at my side. I look forward to many more adventures with you.

I profusely thank my supervisor, Eduardo Martín-Martínez. You introduced me to this interesting research area where we can tinker with quantum mechanics, information theory, thermodynamics and general relativity at the same time. Your genuine excitement for research is contagious, and I appreciate all that I learned from you: from how to present and write, to how to collaborate and supervise. Your words of praise, which helped me see the work I have accomplished, boosted my motivation. I also appreciate the freedom you gave me, which flourished into a project and a collaboration with other authors. Thank you for fostering a safe and comfortable environment in our research group, which facilitates interactions among us, your students, sparking research, and also, friendships. In the end, thank you for always having our best interest at heart.

The PhD would not have been the same have not been for all the people that I have met at Waterloo. Thank you to Damià Canyameres, Ireneo James Membere, Caroline Lima, Héctor Maeso-García, José Polo-Gómez, Evan Peters, Daniel Quiles-Pastor, Boris Ragula, Tales Rick Perche, Bruno de Souza Leão Torres, Eirini Telali, Erickson Tjoa, Kelly Wurtz, Yale Yauk, and Matheus Zambianco, which made this last years much more enjoyable; to Adrian Lupascu, who allowed me to connect more directly with experiments and for inviting me to attend the superconducting devices group meetings, which has been a formative experience as a theorist; to Achim Kempf, who gave us access to the Physics of Information Lab, a perfect place for all the theoretical physics students in the University of Waterloo to collaborate, and to Joseph Schindler and Dominik Šafránek, for the very interesting conversations on quantum thermodynamics and observational entropy, and for the great experience of working together.

I thank the financial support from the "La Caixa" foundation, through the Postgraduate Fellowships Abroad program, which gave me two years of PhD to fully dedicate my time to research, the part of the PhD which I love the most.

Last but not least, thank you to my parents and my sibling for their support and encouragement all the way to here, and for reminding me to take care of myself, even when living at the other side of the ocean.

Dedication

To my grandparents, and the family they raised.

Table of Contents

Examining Committee Membership ii

Author's Declaration iii

Statement of contributions iv

Abstract v

Acknowledgements vi

Dedication vii

List of Figures xiii

List of Tables xviii

1 Introduction 1

2 Harvesting entanglement in the presence of communication 6

2.1 Entanglement harvesting from the field derivative 7

2.1.1 Motivation for coupling to the field derivative 7

2.1.2 Reviewing the free real scalar quantum field 7

2.1.3 Harvesting protocol with derivative coupling 9

2.2 Communication vs genuine harvesting . . . 12
2.3 Canceling out the communication contribution to entanglement . . . 15
2.4 Entanglement harvesting in curved spacetimes . . . 17
2.5 General results for guaranteeing constructive interference . . . 24
2.6 Entanglement through communication and harvesting can interfere destructively . . . 31
2.6.1 Examples in Minkowski spacetime . . . 32
2.6.2 Example in a cosmological spacetime . . . 40

3 Harvesting entanglement with general couplings: longitudinal and transversal components 44

3.1 Entanglement harvesting separating the contributions of longitudinal and transversal interactions . . . 45
3.1.1 Analytic expression for the longitudinal evolution . . . 47
3.1.2 Perturbatively including the transversal evolution . . . 50
3.1.3 Evolution of the detectors . . . 52
3.2 Splitting longitudinal and transversal interactions with respect to the initial state . . . 52
3.2.1 Evolution of the detectors . . . 54
3.2.2 Negativity for the detectors . . . 56
3.3 Effect of a nonperturbative longitudinal interaction . . . 58
3.3.1 Initializing the field in the vacuum state . . . 62
3.3.2 Choice of smearing and switching functions . . . 63
3.3.3 Effect of the longitudinal coupling strength on the evolution of the negativity . . . 65

4 Harvesting entanglement in a proposed superconducting implementation 67

4.1 Review of superconducting tunable couplers . . . 67
4.1.1 Quantized transmission line . . . 67
4.1.2 Tunable coupler and flux qubit . . . 70

4.1.3 Coupling the superconducting circuit to the transmission line 72
4.2 A variable gap particle detector as a model of flux qubit and tunable coupler 75
4.2.1 Simplifying the TC+FQ circuit model 75
4.2.2 Result of the simplifications of the TC+FQ circuit model 78
4.2.3 Comparison of the variable gap detector to UDW detectors 80
4.3 Entanglement Harvesting with detectors of variable gap 81
4.3.1 Harvesting from the vacuum 84
4.4 Genuine entanglement harvesting 86
4.5 Exploring the effects of the implementation features on entanglement harvesting 87
4.5.1 Fixed vs tunable parameters 88
4.5.2 Explored switching functions 90
4.5.3 Effect of duration and delay 91
4.5.4 Spacelike harvesting for finite duration switchings 99
4.5.5 Effect of the distance between detectors 104

5 Conclusions and Outlook **112**

References **119**

APPENDICES **129**

A Appendices for Chapter 2 **130**
A.1 Communication at leading order through a mediating system 130
A.2 Inequality between negativity and its communication and harvesting contributions 132
A.3 Examples of symmetries that satisfy Corollary 1 133
A.4 Further simplifications of the hypotheses of Corollary 1 137
A.5 Simplifying the symmetries for the most common entanglement harvesting scenarios 141

A.5.1 Sufficient symmetries for harvesting and communication collaboration in Minkowski spacetime . . . 141
A.5.2 Sufficient symmetries for constructive interference between harvesting and communication in FRW spacetimes . . . 145
A.6 Alternative symmetry conditions for detectors prescribed in Fermi normal coordinates . . . 147
A.6.1 Conditions for the time reversibility and spatial reflection symmetry of Fermi normal coordinates . . . 147
A.6.2 Simplified conditions to satisfy Corollary 1 when detectors are prescribed in the Fermi normal coordinates . . . 155
A.7 Additional symmetries when swapping the times at which the detectors are switched . . . 158

B Appendices for Chapter 3 **160**
B.1 Computing the transversal picture Hamiltonian . . . 160
B.2 Perturbative expansion of the longitudinal evolution . . . 162
B.3 Interaction picture state in the longitudinal basis . . . 165
B.4 Evolution of the state of the detectors . . . 171
B.4.1 Summary of components of the detectors' state . . . 178
B.4.2 Evolution of the state components for detectors initialized in pure product states . . . 184
B.5 Eigenvalues of perturbed rank one Hermitian operators . . . 185
B.6 Computing expectation values for displacement and field operators . . . 188
B.6.1 Zero-mean Gaussian states . . . 189
B.6.2 Vacuum state . . . 190

C Appendices for Chapter 4 **192**
C.1 Relating the variable gap detector and the spin-boson model . . . 192
C.2 Computing the outcome of the harvesting protocol . . . 194
C.3 Simplifying the integrals needed to compute negativity . . . 197

C.3.1 Symmetric switching functions equal up to a time shift and equal detectors . . . 197
C.3.2 Changing variables to partially decouple time integrals . . . 200
C.4 Spacelike harvesting in the large cutoff limit . . . 201

List of Figures

2.1 Spacetime diagram depicting with grey ellipses the regions where detectors A and B interact (strongly) with the field. The diagram shows the delay t_Δ and separation $\boldsymbol{x}_\Delta$, and the yellow shaded regions indicate null separation from the detector A. 10

2.2 Contributions to the negativity $\mathcal{N}$, see Eq. (2.21), for a series of derivative coupling and amplitude coupling scenarios. The correlations $|\mathcal{M}|$ which contribute to $\mathcal{N}$ are split between the $|\mathcal{M}^+|$ term (genuine harvesting) the $|\mathcal{M}^-|$ term (acquired by communication). The setup uses the Gaussian switching and smearing functions given in Eq. (2.34), $\Omega T = 4$, $|x_\Delta|/T = 5$, $\sigma/T = 0.05$. The amplitude coupling in 1+1D has an IR cutoff of $\Lambda T = 0.02$, see, e.g. [2]. The $\overline{\lambda}$ is an adimensional coupling constant, whose definition depends on the scenario: for *derivative coupling*, $\overline{\lambda} = \lambda$ in $1+1$D and $\overline{\lambda} = \lambda/T$ in 3+1D. For *amplitude coupling*, $\overline{\lambda} = \lambda T$ in $1+1$D and $\overline{\lambda} = \lambda$ in 3+1D. The brown vertical lines denote maximum light contact, and the light yellow coloured regions show the size of the strong support of the switching function of a detector, taken to be $[-3.5T, 3.5T]$. 18

2.3 Non-symmetric switching function for different values of the asymmetry parameter α. 35

2.4 Results for an entanglement harvesting setup in Minkowski spacetime with non-symmetric switchings. The physical parameters used are: $\Omega T = 5$, $d/T = 2.1$, and $\sigma/T = 0.3$. In the horizontal axis, we have $\Delta t = t_{\text{B}} - t_{\text{A}}$. The solid vertical lines (yellow) represent the lightcones. Figures (a), (c), and (e) correspond to the case $\alpha = 2.35$, whereas Figures (b), (d), and (f) display the case $\alpha = 0$, where we have the standard Gaussian switching. The appearance of an even symmetry with respect to Δt in the plots is explained by Appendix A.7. 36

2.5 Numerical results for the negativity (top) and the communication-assisted negativity (bottom) as a function of the proper time d between the centers of the detectors and the time delay Δt between the centers of the switchings. The entanglement harvesting setup is in Minkowski spacetime with Gaussian switchings of different length scales, and the physical parameters used are: $\Omega T_{\text{A}} = 4$, $\sigma/T_{\text{A}} = 0.2$, and $T_{\text{B}}/T_{\text{A}} = 1.3$. 38

2.6 Correlations ($\mathcal{M}$) and negativity ($\mathcal{N}$), divided into harvested ($\mathcal{M}^+, \mathcal{N}^+$) and communication ($\mathcal{M}^-, \mathcal{N}^-$) components as a function of the time delay Δt between the switchings. The harvesting setup is in Minkowski spacetime, with Gaussian switchings with different time scales, and the physical parameters used are: $\Omega T_{\text{A}} = 4$, $d/T = 3$, $\sigma/T_{\text{A}} = 0.2$, and $T_{\text{B}}/T_{\text{A}} = 1.3$. The reason for the symmetries with respect to the sign of Δt are explained in Appendix A.7. 39

2.7 Numerical results for De Sitter spacetime. The parameters used are: $\Omega T = 4$, $d/T = 2$, $\sigma/T = 0.1$, and $H = 0.1$. Here, $\Delta t = t_{\text{B}} - t_{\text{A}}$ 43

3.1 Choice of switching function for the transversal interaction. 64

3.2 Numerical results for the scenario of the current section 3.3, with detector gap $\Omega = 9$, distance between detectors $d = 1$, and detector size $\sigma = 0.1$. The transversal interaction is turned on at time $t = 0$ and turned off at $t = 1$, smoothly, according to Eq. (3.107). The longitudinal interaction is constantly turned on, and we test different longitudinal coupling strengths, indicated by the value of $\lambda_{\parallel}$. 66

4.1 Lumped circuit model of a resistance-less transmission line. 68

4.2 Circuit model of a flux qubit. The γ_i indicate the phase variable of the i-th Josephson junction. 70

4.3 Circuit model of the tunable coupler connected to the flux qubit. The tunable coupler connects to the transmission line through the points a and b. 71

4.4 Lumped circuit model of a transmission line coupled to the TC+FQ circuit of Figure 4.3, depicted as a dashed box. 72

4.5 The blue dots show the superconducting qubit transition frequency $\Omega/2\pi$ for each transversal coupling strength γ_x. This frequency is computed from the numerical diagonalization of the Hamiltonian (4.15), with parameters chosen to match [3]. The red line is the linear best fit. 79

4.6 (a) Gaussian switching shape, with 5 standard deviations shown. (b) Cosine ramps switching shape with $S_f = 0.4$. (c) Isosceles trapezoid switching shape with $S_f = 0.4$. 90

4.7 Plots for the scenario 1 of Table 4.1: $\lambda \to 0$, $\Delta\Omega \to 0$. **The following applies to Figures 4.7, 4.8, 4.9, 4.10, 4.11 and 4.12:** The first row shows $\mathcal{N}/\lambda^2$, with white indicating $\mathcal{N} = 0$, while darker colors indicate progressively smaller but non-zero $\mathcal{N}$. The second row shows the harvesting estimator $|\mathcal{M}^+|/(|\mathcal{M}^-| + |\mathcal{M}^+|)$, which goes from 0 (all entanglement acquired by communication) to 1 (all entanglement from genuine harvesting). The horizontal axes indicate the switching timescale or duration T and the vertical axes indicate the delay t_Δ between switchings. Each column explores a different switching function, which are, from left to right: Gaussian, cosine ramps with $S_f = 0$, isosceles trapezoid with $S_f = 0.2$. The horizontal solid line indicates full lightlike contact. For the compact switchings, the detectors' interactions are spacelike below the lower dashed lines and timelike above the upper dashed lines. Outside the region enclosed by the dashed yellow lines, only the 5σ tails of the Gaussian switchings overlap. 92

4.8 Analogous to Figure 4.7, but for scenario 2 of Table 4.1, with $\lambda = -0.1$ and gap variation $\Delta\Omega = -0.5$. 93

4.9 Analogous to Figure 4.7, but for scenario 3 of Table 4.1, with $\lambda = -0.3$ and gap variation $\Delta\Omega/(2\pi) = -1.6\,\mathrm{GHz}$. 94

4.10 Analogous to Figure 4.7, but for scenario 4 of Table 4.1, with $\lambda = -0.65$ and gap variation $\Delta\Omega/(2\pi) = -3.4\,\mathrm{GHz}$. 95

4.11 Analogous to Figure 4.7, but for scenario 5 of Table 4.1, with $\lambda = -1$ and gap variation $\Delta\Omega/(2\pi) = -5.2\,\mathrm{GHz}$. 96

4.12 Analogous to Figure 4.7, but for scenario 6 of Table 4.1, with $\lambda = 0.1$ and gap variation $\Delta\Omega = 0.5$. 97

4.13 Spacetime diagrams with gray rectangles representing the detectors' interactions. (a) Case $t_\Delta = t_d - T$, with t_d fixed. The entanglement harvested in this case is shown in Figure 4.14 ($t_d = 1\,\mathrm{ns}$) and Figure 4.15 ($t_d = 0.5\,\mathrm{ns}$). (b) Case $t_d = T$, $t_\Delta = 0$. The entanglement harvested in this case is shown in in Figure 4.16. 100

4.14 Negativity acquired by spacelike detectors. To ensure the negativity is the largest, we explore the boundary where interactions become spacelike, by choosing $t_\Delta = t_d - T$, with $t_d = 1\,\text{ns}$. This arrangement is depicted in the spacetime diagram of Figure 4.13(a). **The following applies to Figures 4.14, 4.15, and 4.16:** The plots' horizontal axes are the switching durations T and the vertical axes are the portion of the switching function that is flat S_f and at full coupling. The switching function for the left column is the cosine ramps and for the right column the isosceles trapezoid. The rows respectively correspond to the scenarios 1, 2, 3 and 6 of Table 4.1. 101

4.15 Negativity acquired by spacelike detectors. The plots are analogous to Figure 4.14, with the only difference being that the distance between detectors is reduced so that $t_d = 0.5\,\text{ns}$. 102

4.16 Negativity acquired by spacelike detectors. The plots are analogous to Figure 4.14, with the exceptions of fixing $t_\Delta = 0$ and allowing the distance between detectors to vary as $t_d = T$, as depicted in the spacetime diagram of Figure 4.13(b). Moreover, the rows show the scenarios 1, 2, 3, 4 and 6 of Table 4.1. 103

4.17 Scenario 1 of Table 4.1, with $\lambda \to 0$, $\Delta\Omega \to 0$. **The following applies to Figures 4.17, 4.18, 4.19, 4.20, 4.21 and 4.22:** The first row shows $\mathcal{N}/\lambda^2$, with $\mathcal{N} = 0$ in white. The second row shows $|\mathcal{M}^+|/(|\mathcal{M}^-| + |\mathcal{M}^+|)$, which goes from 0 (all entanglement from communication) to 1 (all entanglement from harvesting). t_d is the signaling time and t_Δ the delay between switchings. The columns use, from left to right, the switching functions: 1) Gaussian, $T = 0.07\,\text{ns}$, 2) cosine ramps, $T = 0.21\,\text{ns}$, $S_f = 0$, 3) isosceles trapezoid, $T = 0.16\,\text{ns}$, $S_f = 0.2$. The diagonal solid lines indicate full lightlike contact. Outside the dashed lines, either there is no light contact (compact switchings) or only the 5σ tails of the Gaussian can interact. To aid visualization, the values of negativity larger than the thresholds indicated in the legend are plotted yellow. 105

4.18 Analogous to Figure 4.17, but for scenario 2 of Table 4.1, with $\lambda = -0.1$, $\Delta\Omega/(2\pi) = -0.5\,\text{GHz}$. Moreover, each column of plots uses, from left to right, Gaussian switching with $T = 0.075\,\text{ns}$, cosine ramps switching with $T = 0.22\,\text{ns}$, $S_f = 0$, and isosceles trapezoid switching with $T = 0.17\,\text{ns}$, $S_f = 0.2$. 106

4.19 Analogous to Figure 4.17, but for scenario 3 of Table 4.1, with $\lambda = -0.3$, $\Delta\Omega/(2\pi) = -1.6\,\text{GHz}$. Moreover, each column of plots uses, from left to right, Gaussian switching with $T = 0.09\,\text{ns}$, cosine ramps switching with $T = 0.27\,\text{ns}$, $S_f = 0$, and isosceles trapezoid switching with $T = 0.21\,\text{ns}$, $S_f = 0.2$. 107

4.20 Analogous to Figure 4.17, but for scenario 4 of Table 4.1, with $\lambda = -0.65$, $\Delta\Omega/(2\pi) = -3.4\,\text{GHz}$. Moreover, each column of plots uses, from left to right, Gaussian switching with $T = 0.13\,\text{ns}$, cosine ramps switching with $T = 0.38\,\text{ns}$, $S_f = 0$, and isosceles trapezoid switching with $T = 0.29\,\text{ns}$, $S_f = 0.2$. 108

4.21 Analogous to Figure 4.17, but for scenario 5 of Table 4.1, with $\lambda = -1$, $\Delta\Omega/(2\pi) = -5.2\,\text{GHz}$. Moreover, each column of plots uses, from left to right, Gaussian switching with $T = 0.23\,\text{ns}$, cosine ramps switching with $T = 0.71\,\text{ns}$, $S_f = 0$, and isosceles trapezoid switching with $T = 0.54\,\text{ns}$, $S_f = 0.2$. 109

4.22 Analogous to Figure 4.17, but for scenario 6 of Table 4.1, with $\lambda = 0.1$, $\Delta\Omega/(2\pi) = 0.5\,\text{GHz}$. Moreover, each column of plotss uses, from left to right, Gaussian switching with $T = 0.065\,\text{ns}$, cosine ramps switching with $T = 0.2\,\text{ns}$, $S_f = 0$, and isosceles trapezoid switching with $T = 0.15\,\text{ns}$, $S_f = 0.2$. 110

C.1 $\mathcal{N}/\lambda^2$ plotted against the cutoff frequency $\Omega_{\text{cut}}/(2\pi)$, for $\Omega^0/(2\pi) = 7.3\,\text{GHz}$, $\Delta\Omega = 0$, $|t_\Delta| = t_d - T$ (spacelike detector interactions). The cutoff frequency $\Omega_{\text{cut}}/(2\pi) = 50\text{GHz}$, used throughout this work, is highlighted with a vertical dashed line. The subfigures are for: (a) Cosine ramps switching, $T = 0.2\,\text{ns}$, $S_f = 0$, $t_d = 1\,\text{ns}$. (b) Isosceles trapezoid switching, $T = 0.16\,\text{ns}$, $S_f = 0.2$, $t_d = 1\,\text{ns}$. (c) Isosceles trapezoid switching, $T = 0.16\,\text{ns}$, $S_f = 0.2$, $t_d = 0.16\,\text{ns}$. We emphasize that for all the scenarios analyzed the detectors are in strict spacelike separation. 200

List of Tables

4.1 This table depicts the scenarios that will be explored in the present section. The $\to 0$ corresponds to the weak coupling limit. The qubit transition frequency variation follows $\Delta\Omega/(2\pi) \approx 5.2 \cdot \lambda\,\mathrm{GHz}$. 89

Chapter 1

Introduction

It is well established that the vacuum state of a quantum field contains entanglement between degrees of freedom located in different spacetime regions, including those that are spacelike separated [4, 5, 6, 7, 8]. In fact, Bell inequalities can be violated by performing measurements of local observables of space-like separated regions [9]. In later years, a family of relativistic quantum information protocols known as *entanglement harvesting* was developed to operationally access this entanglement. In these protocols, a pair of initially uncorrelated particle detectors interact locally with a quantum field and may become entangled by extracting correlations present in the field state. Entanglement harvesting was first explored by Valentini and Reznik [9, 10, 11] and further developed later on for different kinds of fields and backgrounds (see, e.g., [2, 12, 13, 14, 15, 16, 17, 18, 19, 20, 21, 22, 23, 24, 25]).

Particle detector models are internally simple quantum systems that couple locally to the quantum field. These detectors offer a physically implementable way to probe entanglement in quantum field theory, avoiding the divergences that often affect field-theoretic calculations. A widely used example of detector model is the Unruh-DeWitt (UDW) detector [26, 27, 28, 29, 30], which captures essential features of light–matter interaction [31, 14]. Entanglement harvesting with detectors has been explored across various field types and spacetime backgrounds [12, 13, 14, 19, 21, 18], and holds promise both for understanding the entanglement structure of QFT [32, 33, 34, 35, 36, 37, 38] and as a way to harness non-locality resources in quantum information [39]. Despite its significance, entanglement harvesting has not been experimentally realized as of the time of the writing of this thesis. Implementations have been proposed in linear ion traps [40], superconducting circuits [41, 42, 43], in graphene [44], in Bose-Einstein condensates [45,

46] and in nonlinear crystals [47, 48, 49, 50], but so far no direct experimental test of entanglement harvesting has been performed.

When two detectors interact with spacelike separated regions of a quantum field, any entanglement they acquire must originate from preexisting correlations in the field, since no communication between them is possible in such case (see, e.g., [51, 52, 53, 54]). However, as noted in [55], this is no longer the case when the detectors are causally connected. In such scenarios, entanglement can arise not only from genuine harvesting but also through communication mediated by the field. The total entanglement acquired by the detectors can thus be understood as a combination of two contributions: *communication-mediated* entanglement and *genuinely harvested* entanglement.

This distinction has been explored primarily within the UDW detector model, where detectors couple linearly to the field amplitude. Previous work showed that, for massless fields in 1+1 and 3+1 dimensional Minkowski spacetime, the entanglement acquired by light-connected detectors is dominated by communication effects rather than genuine harvesting [55]. Genuine harvesting was found to contribute meaningfully only in higher dimensions ($n \geq 5$) or when the field has sufficient mass. More recent work has extended this analysis to curved spacetimes, showing that caustics and secondary null geodesics can enable genuinely harvested entanglement even in causally connected setups [56]. In this thesis, we show that it is possible to construct configurations where genuine harvesting dominates for 1+1D and 3+1D Minkowski spacetime with massless fields, even when the causal contact between detectors is maximum. This allows us to maximize the genuinely harvested entanglement even in scenarios where communication is possible. To observe this behavior, we depart from the standard amplitude coupling and instead consider detectors coupled to the derivative of the field amplitude.

Derivative coupled detector models have primarily been used to address infrared divergences that arise for massless fields in low dimensional spacetimes [57, 58, 59, 60, 61, 62, 19, 63, 64]. While amplitude coupling IR divergences can be regularized via cutoffs, the resulting detector dynamics retain some dependence on the chosen cutoff [2, 59, 60]. Derivative coupling, by contrast, avoids such IR issues naturally. Additionally, in 1+1D, the short-distance behavior of the derivative coupling resembles that of amplitude coupling in 3+1D [60, 62]. Furthermore, dualities between the amplitude and derivative couplings were identified in [65]. These features make the derivative model a useful tool for exploring 3+1D-like behavior in simpler 1+1D settings.

Beyond its theoretical usefulness, the derivative coupling has direct connections to experimentally accessible systems. It more accurately captures certain features of light-matter interactions [66, 14], and it can be implemented in superconducting circuits [67, 3].

This implementation consists of a superconducting qubit coupled to a transmission line, modeled as a 1+1D massless scalar field, as will be presented in the latter parts of this thesis. Typically, the interaction between the qubit and the transmission line is modeled using the spin-boson model [68] with an Ohmic bosonic bath, see, e.g., [69, 70, 3]. This description turns out to be none other than derivative coupling in the language of particle detectors [67].

Another topic studied in the present thesis relates to previous literature which seemed to support that communication and harvesting contributions to detector entanglement always add constructively. Then, one would expect to find more entanglement when communication occurs through the field, rather than when it does not occur, such as when detectors are in spacelike separation. However, perhaps surprisingly, we show that communication does not always contribute positively to entanglement.

Namely, we find that, in general, the contribution of the communication component and the contribution from the harvesting of preexisting entanglement in the field can actually *interfere*. This interference can be constructive, amplifying even more the amount of entanglement acquired by the detectors, but also destructive so that the harvesting contribution and the communication contribution cancel and the detectors fail to get entangled. This phenomenon is not apparent in the setups considered in recent studies in which this splitting is analyzed (such as [55, 56, 50]). We show that this phenomenon was not visible because for all the commonly chosen highly symmetric setups (see, e.g., [71, 72, 22, 73, 74, 75, 76, 77, 78, 79, 80]) both sources of entanglement contribute constructively to entangle the detectors. In this thesis, we provide sufficient conditions, fulfilled by commonly explored scenarios, such that the interference between the two sources is guaranteed to be constructive.

Then, guided by these conditions, we provide examples of causally connected detectors which do not get entangled due to destructive interference, even though communication alone or genuine harvesting alone would have entangled the detectors. These examples are provided both in Minkowski and De Sitter spacetimes. Conversely, we also find scenarios where the constructive interference is stronger than in the setups commonly explored in the literature, further enhancing the entanglement acquired by the detectors.

The last major topic explored in this thesis is the modeling of a proposed experimental realization of entanglement harvesting in a superconducting circuit platform. The implementation of entanglement harvesting in superconducting circuits leverages the ability of these circuits to create "artificial atoms" that can strongly couple to the electromagnetic field [81, 82]. Specifically, the interaction can reach the ultra-strong coupling regime. At such strong couplings, the rotating wave approximation, commonly used to describe light-

matter interaction [83], breaks down [69]. Notably, this approximation is not present in UDW detector models used in RQI. A key advantage of using superconducting circuits for RQI experiments is their high tunability, allowing for circuits with switchable coupling that can reach the ultra-strong regime [84, 85, 3]. This enables superconducting circuit platforms to access regimes where the amounts of harvested entanglement become significant. In these setups, the interaction of superconducting qubits with the field inside a microwave waveguide can be switched on and off within fractions of nanosecond, allowing these detectors to probe fields in spacelike separated regions.

Our first goal is to strengthen the connection between experimentally implemented particle detectors in superconducting circuits and the idealized UDW detector models commonly employed in RQI. We begin with a complete circuit model of the superconducting implementation. Then, we review the series of approximations upon it that result in a model that resembles an UDW detector coupled to a 1+1D scalar massless field, but that retains crucial implementation specific features of the superconducting circuit platform. These features, which allow to better model realistic experiments, include: a variable energy gap, coupling to the derivative of the field amplitude, and a soft UV cutoff. Among these features, derivative coupling stands out for, as previously discussed in this introduction, naturally removing IR divergences [57, 58, 59, 60, 61, 62, 19, 63, 64], better modeling light-matter interactions in some regimes [14, 66, 67], and its duality with amplitude coupling [65]. The impact of the cutoff and its relation to the detector spatial localization has been previously analyzed in [67]. However, the variable energy gap has only been explored in very idealized scenarios outside of superconducting circuits and in timelike connection [79, 80]. In this study, the variation of the energy gap is dictated by the experimental constraints in the superconducting circuit implementation. Using the implementation of [3], the variation of the gap is linked to the strength of the coupling, which is time dependent. This is a constraint whose effect has not yet been fully explored in the context of RQI protocols.

Once the model is established, we study how these implementation specific features affect entanglement harvesting. We examine entanglement harvesting both for spacelike separated and causally connected detectors. To do so, we use the tools described at the start of the thesis, developed in [55], to split the entanglement into sources: communication through the field or harvesting of preexisting field entanglement. This split allows us to identify situations where entanglement is genuinely harvested even in causal contact.

The thesis is organized as follows, in chapter 2, we explore entanglement harvesting for detectors in causal contact. In section 2.1, we set up a simple entanglement harvesting setup with derivative coupling. Then, section 2.2 describes why and how to split the harvesting and communication contributions to entanglement acquired by detectors. Sec-

tion 2.3 compares the communication contributions for amplitude and derivative coupling, and provides examples where derivative coupling allows to genuinely harvest entanglement while in full causal communication. Then, section 2.4 reviews a more general protocol of entanglement harvesting that applies to curved spacetimes, to establish notation and build the necessary tools that will be used later on. Section 2.5 presents the conditions that the spacetime, the detectors, and the field Feynmann propagator should meet to guarantee constructive interference of communication and harvesting. In section 2.6, we show numerical examples in Minkowski and De Sitter spacetimes where these conditions are violated. There, we find that interference can go through the full range from completely destructive to fully constructive.

The chapter 3 studies the effect of longitudinal and transversal interactions for an even more general class of entanglement harvesting protocols than the ones presented in Chapter 2. Firstly, section 3.1 presents entanglement harvesting for detectors with an arbitrary number of energy levels, which couple to the field through a general class of couplings. The coupling is split into longitudinal (diagonal) and transversal (off-diagonal) parts, with evolution solved exactly for the longitudinal part and perturbatively for the transversal part. Then, section 3.2 shows that the contributions to negativity at leading order are always dominated by the interaction that is transversal to the initial state of the detectors. Finally, section 3.3 explores an example for qubit detectors with transversal and longitudinal coupling, for increasingly large amounts of longitudinal coupling, until higher order effects make the longitudinal coupling contribute, detrimentally, to negativity.

In chapter 4, we connect the superconducting implementation of detectors to the theoretical models usually used in relativistic quantum information, and study the particular effects of the implementation on entanglement harvesting. The chapter starts with a section 4.1 that provides the circuit model for implementing particle detectors as a superconducting device. Then, section 4.2 describes the simplifications that turn the detector implementation model into a UDW-like detector with implementation-specific features such as a variable gap and derivative coupling. Section 4.3 illustrates the entanglement harvesting protocol for a pair of variable gap, derivatively coupled detectors. Section 4.4 delineates how to separate the communication and genuine harvesting contributions to the entanglement acquired by causally connected detectors. Section 4.5 shows how the implementation-specific features such as gap variation affect entanglement harvesting.

Lastly, chapter 5 summarizes the main results and conclusions of each chapter.

Chapter 2

Harvesting entanglement in the presence of communication

Entanglement harvesting is often studied for particle detectors that interact with space-like separated regions of the quantum field. In such scenarios, detectors cannot communicate, guaranteeing that any entanglement gathered by the detectors is extracted from the field. However, this restriction to keep the detectors space-like separated is forgone in this chapter. Then, as [55] pointed out, for causally connected detectors, entanglement can arise not only from harvesting preexisting correlations in the field but also from communicating via the field. In this chapter, we start by presenting the counterintuitive case of communication contribution vanishing at the same time as entanglement becomes the largest, suggesting that a large amount of entanglement is genuinely harvested. This phenomenon can occur for—but is not limited to—detectors that couple to the field derivative. Then, we move onto the topic of interference between the communication and harvesting contributions to entanglement. In previous studies, these two contributions seem to always add up, increasing the total entanglement [55, 56, 50]. We show that instead the two sources of entanglement—communication and harvesting—can interfere with each other, sometimes canceling out entirely. This interference was previously missed because entanglement harvesting setups are usually highly symmetric, see for example [71, 72, 22, 73, 74, 75, 76, 77, 78, 79, 80]. Such symmetries guarantee the interference to be constructive, which is a result also presented in this chapter.

In this chapter, we use natural units $\hbar = c = 1$, indicate spacetime points as x, denote their coordinates as x^ρ, and use the Einstein summation convention over spacetime indices such as ρ. We will also denote coordinates as $(t, \boldsymbol{x})$ when t can be interpreted as a time coordinate. Then, $\boldsymbol{x}$ denotes an n-dimensional vector of spatial coordinates.

2.1 Entanglement harvesting from the field derivative

To establish the context and notation, we summarize the entanglement harvesting protocol along the lines of, for example, [2]. However, the protocol presented below differs in the following: using particle detectors that linearly couple to the time derivative of the field, instead of the more common choice of coupling to the value of the field itself.

2.1.1 Motivation for coupling to the field derivative

In the usual Unruh-DeWitt particle detector model [26, 27, 28], the coupling between the detector and the field is linear in the field amplitude. Even if less popular, derivative coupling, where the detector couples linearly to the (proper) time derivative of the field, has been widely used in the literature to avoid infrared divergences that affect amplitude coupling in low dimensional massless field theories [57, 58, 59, 60, 61, 62, 19, 63, 64]. Although such divergences can be regularized with cutoffs, the states of the detectors after interacting with the field depend, even if weakly, on the chosen cutoff [2, 59, 60]. Derivative coupling eliminates this dependence and, in 1+1 dimensions, has a similar short-distance behavior to amplitude coupling in 3+1 dimensions [60, 62]. Dualities between amplitude and derivative coupling have also been identified [65]. Moreover, derivative coupling better captures aspects of the interaction between atoms and the electromagnetic field [14, 66]. Additionally, this coupling is realizable in superconducting circuits: superconducting qubits coupled to transmission lines effectively implement derivative coupling. This implementation is also often modeled in the literature as the spin-boson model with an Ohmic bath [68, 69, 70, 67, 3].

Notably, derivative coupling has not been used to explore the distinction between the two sources of entanglement: communication through the field and harvesting preexisting field entanglement. This distinction was originally explored using amplitude coupling in [55]. We analyze this split for the derivative coupling case later in this chapter, using the summary of entanglement harvesting that follows.

2.1.2 Reviewing the free real scalar quantum field

First, we give an overview of the theory of free real scalar quantum fields on $(n+1)$-dimensional Minkowski (flat) spacetime. If we fix some inertial frame with coordinates

$(t, \boldsymbol{x})$, the action of a free real scalar field of mass m is given by

$$S[\phi] = \int \mathrm{d}t\, \mathrm{d}^n\boldsymbol{x} \left(\frac{1}{2}(\partial_t \phi)^2 - \frac{1}{2}(\nabla\phi)^2 - \frac{1}{2}m^2\phi^2 \right). \tag{2.1}$$

Here, we indicate the gradient by $\nabla = (\partial_{x^1}, \ldots, \partial_{x^n})^\top$. Applying the Euler-Lagrange equations to $S[\phi]$ shows that $\phi(t, \boldsymbol{x})$ satisfies the Klein-Gordon equation,

$$(\Box + m^2)\phi(t, \boldsymbol{x}) = 0, \tag{2.2}$$

with the d'Alembert operator $\Box = \partial_t^2 - \nabla^2$ and the Laplace operator $\nabla^2 = \partial_{x^1}^2 + \ldots + \partial_{x^n}^2$. The following plane waves are a complete, orthonormal set of solutions to Eq. (2.2),

$$u_{\boldsymbol{k}}(t, \boldsymbol{x}) = \frac{e^{\mathrm{i}(\boldsymbol{k}\cdot\boldsymbol{x} - \omega_k t)}}{\sqrt{2(2\pi)^n \omega_{\boldsymbol{k}}}}, \quad \boldsymbol{k} \in \mathbb{R}^n, \tag{2.3}$$

with $\omega_{\boldsymbol{k}} = \sqrt{\boldsymbol{k}^2 + m^2}$. Specifically, these solutions are orthonormal with respect to the Klein-Gordon inner product, which means that they satisfy

$$(u_{\boldsymbol{k}}, u_{\boldsymbol{k}'})_{\mathrm{KG}} = \delta(\boldsymbol{k} - \boldsymbol{k}'), \quad (u^*_{\boldsymbol{k}}, u^*_{\boldsymbol{k}'})_{\mathrm{KG}} = -\delta(\boldsymbol{k} - \boldsymbol{k}'), \quad (u_{\boldsymbol{k}}, u^*_{\boldsymbol{k}'})_{\mathrm{KG}} = 0. \tag{2.4}$$

Here, $(\,.\,,.\,)_{\mathrm{KG}}$ is defined to be, for any two solutions ϕ_1, ϕ_2 of the Klein-Gordon equation,

$$(\phi_1, \phi_2)_{\mathrm{KG}} = \mathrm{i} \int \mathrm{d}^n\boldsymbol{x} \phi_1^*(t, \boldsymbol{x}) \partial_t \phi_2(t, \boldsymbol{x}) - \partial_t \phi_1^*(t, \boldsymbol{x}) \phi_2(t, \boldsymbol{x}). \tag{2.5}$$

Importantly, any classical solution $\phi(t, \boldsymbol{x})$ to Eq. (2.2) can be expressed as a linear combination of the mode functions $u_{\boldsymbol{k}}(t, \boldsymbol{x})$ and their complex conjugates:

$$\phi(t, \boldsymbol{x}) = \int \mathrm{d}^n\boldsymbol{k} \big(a^*_{\boldsymbol{k}} u^*_{\boldsymbol{k}}(t, \boldsymbol{x}) + a_{\boldsymbol{k}} u_{\boldsymbol{k}}(t, \boldsymbol{x}) \big), \tag{2.6}$$

where $a_{\boldsymbol{k}}$ are constant complex coefficients. Upon canonical quantization, the field ϕ becomes a field operator $\hat{\phi}$, expanded in plane-wave modes,

$$\hat{\phi}(t, \boldsymbol{x}) = \int \frac{\mathrm{d}^n\boldsymbol{k}}{\sqrt{2(2\pi)^n \omega_{\boldsymbol{k}}}} (e^{\mathrm{i}(\omega_k t - \boldsymbol{k}\cdot\boldsymbol{x})} \hat{a}^\dagger_{\boldsymbol{k}} + e^{\mathrm{i}(\boldsymbol{k}\cdot\boldsymbol{x} - \omega_k t)} \hat{a}_{\boldsymbol{k}}), \tag{2.7}$$

where we substituted the value of $u_{\boldsymbol{k}}(t, \boldsymbol{x})$ using the expression (2.3), and $\omega_{\boldsymbol{k}} = \sqrt{\boldsymbol{k}^2 + m^2}$. Moreover, the coefficients $a_{\boldsymbol{k}}$ and $a^*_{\boldsymbol{k}}$ were respectively promoted to the annihilation and

creation operators, $\hat{a}_{\boldsymbol{k}}$ and $\hat{a}^\dagger_{\boldsymbol{k}}$. These ladder operators obey the canonical commutation relations $[\hat{a}_{\boldsymbol{k}}, \hat{a}^\dagger_{\boldsymbol{k}'}] = \delta^n(\boldsymbol{k} - \boldsymbol{k}')\hat{\mathbb{1}}$.

Additionally, one can identify a Lagrangian for the free field associated to the choice of frame $(t, \boldsymbol{x})$. This Lagrangian can be found starting from the expression for the action in equation (2.1) and removing the integral over time. Then, by Legendre transforming the Lagrangian, the resulting Hamiltonian after quantization is

$$\hat{H}_{\text{FREE},\,\phi} = \int \mathrm{d}^n\boldsymbol{x} \left(\frac{1}{2}\hat{\pi}^2 + \frac{1}{2}(\nabla\hat{\phi})^2 + \frac{1}{2}m^2\hat{\phi}^2 \right), \tag{2.8}$$

with $\hat{\pi} = \partial_t\hat{\phi}$ the field's canonical momentum. Notably, this Hamiltonian can be rewritten in terms of the ladder operators,

$$\hat{H}_{\text{FREE},\,\phi} = \frac{1}{2}\int \mathrm{d}^n\boldsymbol{k}\, \omega_{\boldsymbol{k}} \big(\hat{a}^\dagger_{\boldsymbol{k}}\hat{a}_{\boldsymbol{k}} + \hat{a}_{\boldsymbol{k}}\hat{a}^\dagger_{\boldsymbol{k}}\big). \tag{2.9}$$

This Hamiltonian mirrors that of a collection of independent quantum harmonic oscillators, with each field mode labeled by $\boldsymbol{k} \in \mathbb{R}^n$ and associated with a frequency $\omega_{\boldsymbol{k}}$.

2.1.3 Harvesting protocol with derivative coupling

In order to perform the entanglement harvesting protocol, we consider a pair of detectors to couple to the field, labeled as A and B. We take these detectors to be inertial and comoving with the frame $(t, \boldsymbol{x})$. Moreover, the detectors are two-level quantum systems that interact locally with the quantum field. Each detector has a free Hamiltonian whose eigenstates are labeled as the ground state $|g_\nu\rangle$ and the excited state $|e_\nu\rangle$, with $\nu \in \{\mathrm{A}, \mathrm{B}\}$. The free Hamiltonian of each detector sets an energy gap Ω_ν between the two states,

$$\hat{H}_{\text{FREE},\,\nu} = \Omega_\nu \, |e_\nu\rangle\langle e_\nu| \,, \quad \nu \in \mathrm{A}, \mathrm{B}. \tag{2.10}$$

The detectors couple to the derivative of the field amplitude in accordance to the following Unruh-DeWitt interaction Hamiltonian (in the interaction picture) [26, 27, 28]:

$$\begin{aligned} \hat{H}_{\mathrm{I}}(t) &= \hat{H}_{\mathrm{A}}(t) + \hat{H}_{\mathrm{B}}(t), \\ \hat{H}_\nu(t) &= \lambda_\nu \chi_\nu(t) \hat{\mu}_\nu(t) \int \mathrm{d}^n\boldsymbol{x}\, F_\nu(\boldsymbol{x}) \partial_t\hat{\phi}(t, \boldsymbol{x}). \end{aligned} \tag{2.11}$$

Notice that the field operator that appears in the interaction is $\partial_t\hat{\phi}(t, \boldsymbol{x})$ instead of the usual $\hat{\phi}(t, \boldsymbol{x})$. The interaction strength is controlled by λ_ν, $\chi_\nu(t)$ and $F_\nu(\boldsymbol{x})$ respectively

are the switching function and the smearing function, which localize the interaction in time and space. The monopole moment of each detector is given by

$$\hat{\mu}_\nu(t) = e^{\mathrm{i}\Omega_\nu t}\hat{\sigma}_\nu^+ + e^{-\mathrm{i}\Omega_\nu t}\hat{\sigma}_\nu^-, \tag{2.12}$$

where $\hat{\sigma}_\nu^+ = |e_\nu\rangle\langle g_\nu| = (\hat{\sigma}_\nu^-)^\dagger$.

For simplicity, we take the detectors to be equal, with $\lambda = \lambda_\nu$ and $\Omega = \Omega_\nu$. Moreover, we use the same switching and smearing functions for both detectors, up to a spacetime translation,

$$\chi_\nu(t) = \chi(t - t_\nu), \;\; F_\nu(\boldsymbol{x}) = F(\boldsymbol{x} - \boldsymbol{x}_\nu). \tag{2.13}$$

The delay between switchings $t_\Delta = t_\mathrm{B} - t_\mathrm{A}$ and the separation $\boldsymbol{x}_\Delta = \boldsymbol{x}_\mathrm{B} - \boldsymbol{x}_\mathrm{A}$ control the causal relations between the localized interactions, as depicted in Figure 2.1.

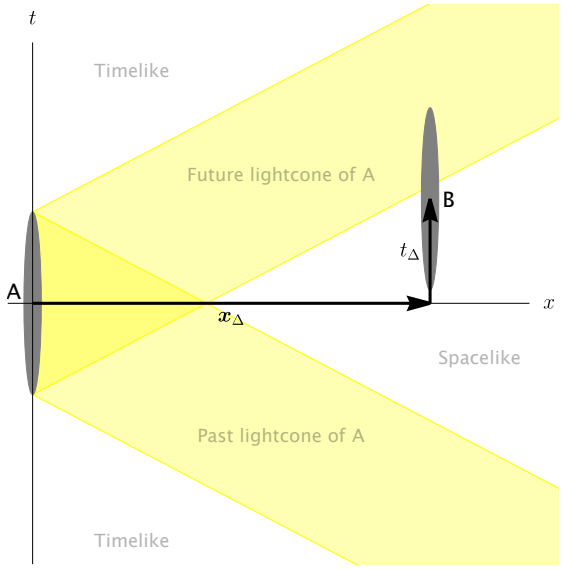


Figure 2.1: Spacetime diagram depicting with grey ellipses the regions where detectors A and B interact (strongly) with the field. The diagram shows the delay t_Δ and separation $\boldsymbol{x}_\Delta$, and the yellow shaded regions indicate null separation from the detector A.

The evolution of the initial state of the full system initially in a state $\hat{\rho}_0$ yields the evolved state $\hat{\rho} = \hat{U}\hat{\rho}_0\hat{U}^\dagger$. We can evaluate the time evolution operator $\hat{U}$ through its

Dyson series:

$$\hat{U} = \underbrace{\hat{\mathbb{1}}}_{\hat{U}^{(0)}} \underbrace{-\mathrm{i}\int \mathrm{d}t\, \hat{H}_{\mathrm{I}}(t)}_{\hat{U}^{(1)}} \underbrace{-\int \mathrm{d}t \int^{t} \mathrm{d}t'\, \hat{H}_{\mathrm{I}}(t)\hat{H}_{\mathrm{I}}(t')}_{\hat{U}^{(2)}} + \mathcal{O}(\lambda^3). \tag{2.14}$$

Denoting $\hat{\rho}^{(i,j)} = \hat{U}^{(i)}\hat{\rho}_0\hat{U}^{(j)\dagger}$, the final state becomes

$$\hat{\rho} = \hat{\rho}_0 + \hat{\rho}^{(1,0)} + \hat{\rho}^{(0,1)} + \hat{\rho}^{(2,0)} + \hat{\rho}^{(1,1)} + \hat{\rho}^{(0,2)} + \mathcal{O}(\lambda^3). \tag{2.15}$$

To study the entanglement the detectors acquire through the interaction, we need to start in an initially uncorrelated detector state, and after the interaction trace out the field, yielding $\hat{\rho}_{\mathrm{AB}} = \mathrm{Tr}_{\phi}(\hat{\rho})$, and then look at the correlations in the evolved state $\hat{\rho}_{\mathrm{AB}}$. Again to take a simple case, let us take the common starting assumption that the detectors and the field start uncorrelated and in their ground states,

$$\hat{\rho}_0 = |g_{\mathrm{A}}\rangle\langle g_{\mathrm{A}}| \otimes |g_{\mathrm{B}}\rangle\langle g_{\mathrm{B}}| \otimes |0\rangle\langle 0|\,. \tag{2.16}$$

where $|0\rangle$ is the Minkowski vacuum. Due to the choice of initial state, all the contributions to $\hat{\rho}_{\mathrm{AB}}$ which are of odd order in λ vanish.

Under the given assumptions, the final state of the detectors to leading order in the coupling strength, represented in matrix form in the basis $\{|g_{\mathrm{A}}g_{\mathrm{B}}\rangle, |e_{\mathrm{A}}g_{\mathrm{B}}\rangle, |g_{\mathrm{A}}e_{\mathrm{B}}\rangle, |e_{\mathrm{A}}e_{\mathrm{B}}\rangle\}$ is

$$\hat{\rho}_{\mathrm{AB}} = \begin{pmatrix} 1-2\mathcal{L} & 0 & 0 & \mathcal{M}^* \\ 0 & \mathcal{L} & \mathcal{L}_{\mathrm{AB}} & 0 \\ 0 & \mathcal{L}^*_{\mathrm{AB}} & \mathcal{L} & 0 \\ \mathcal{M} & 0 & 0 & 0 \end{pmatrix} + \mathcal{O}(\lambda^4), \tag{2.17}$$

where the local noise is

$$\begin{aligned} \mathcal{L} = \lambda^2 \int \mathrm{d}t\, \mathrm{d}t'\, \mathrm{d}^n\boldsymbol{x}\, \mathrm{d}^n\boldsymbol{x}'\, \chi(t)\chi(t')F(\boldsymbol{x})F(\boldsymbol{x}') \\ \times e^{\mathrm{i}\Omega\Delta t} W^*_{tt'}(\Delta t, \Delta\boldsymbol{x}), \end{aligned} \tag{2.18}$$

and

$$\begin{aligned} \mathcal{L}_{\mathrm{AB}} = \lambda^2 e^{-\mathrm{i}\Omega t_\Delta} \int \mathrm{d}t\, \mathrm{d}t'\, \mathrm{d}^n\boldsymbol{x}\, \mathrm{d}^n\boldsymbol{x}'\, \chi(t)\chi(t')F(\boldsymbol{x})F(\boldsymbol{x}') \\ \times e^{\mathrm{i}\Omega\Delta t} W^*_{tt'}(\Delta t - t_\Delta, \Delta\boldsymbol{x} - \boldsymbol{x}_\Delta), \\ \mathcal{M} = -\lambda^2 e^{\mathrm{i}\Omega(t_{\mathrm{A}}+t_{\mathrm{B}})} \int \mathrm{d}t\, \mathrm{d}t'\, \mathrm{d}^n\boldsymbol{x}\, \mathrm{d}^n\boldsymbol{x}'\, \chi(t)\chi(t')F(\boldsymbol{x})F(\boldsymbol{x}') \\ \times e^{\mathrm{i}\Omega(t+t')} W_{tt'}(|\Delta t - t_\Delta|, \Delta\boldsymbol{x} - \boldsymbol{x}_\Delta), \end{aligned} \tag{2.19}$$

where $\Delta t = t - t'$ and $\Delta \boldsymbol{x} = \boldsymbol{x} - \boldsymbol{x}'$, $t_\Delta = t_{\text{B}} - t_{\text{A}}$, $\boldsymbol{x}_\Delta = \boldsymbol{x}_{\text{B}} - \boldsymbol{x}_{\text{A}}$, and $W_{tt'} = \partial_t \partial_{t'} W$, where W is the Wightman function of the vacuum of $(n+1)$-dimensional Minkowski spacetime,[1]

$$\begin{aligned} W(\Delta t, \Delta \boldsymbol{x}) &= \langle 0 | \hat{\phi}(t, \boldsymbol{x}) \hat{\phi}(t', \boldsymbol{x}') | 0 \rangle \\ &= \int \frac{\mathrm{d}^n \boldsymbol{k}}{2(2\pi)^n \omega_{\boldsymbol{k}}} e^{-\mathrm{i}\omega_{\boldsymbol{k}} \Delta t + \mathrm{i}\boldsymbol{k}\cdot\Delta \boldsymbol{x}}. \end{aligned} \tag{2.20}$$

To quantify the amount of entanglement between the detectors, we use the *negativity* [86, 87, 88]. This entanglement quantifier is a common choice in the entanglement harvesting literature (see, e.g. [2, 14, 56, 22]), since it is an entanglement measure even for mixed states and it is easy to compute. Furthermore, for a system of two qubits, negativity is a faithful entanglement measure. Negativity is equal to the absolute sum of the *negative eigenvalues* of the partially transposed density matrix of the two qubits $\hat{\rho}^{\top_{\text{A}}}$. For the final state $\hat{\rho}_{\text{AB}}$ given in Eq. (2.17) the negativity is [11, 2]:

$$\mathcal{N} = \max(|\mathcal{M}| - \mathcal{L}, 0) + \mathcal{O}(\lambda^4). \tag{2.21}$$

This expression reveals that entanglement arises from a competition between the nonlocal correlation term $\mathcal{M}$ and the local noise term $\mathcal{L}$. For detectors in causal contact, the entanglement created between the detectors can be traced to two different sources [55]. On the one hand, the detectors can get entangled via communication through the field (*signaling*) and, on the other hand, the detectors can get entangled by extracting the entanglement already present [4, 5] in the field state (*harvesting*). In the next section, we are going to review how one can distinguish between these two different contributions.

2.2 Communication vs genuine harvesting

When two space-like separated detectors entangle, the entanglement must be extracted from preexisting field correlations. However, when detectors are in causal contact, they can gain entanglement in two ways: 1) by genuinely harvesting entanglement from the state of the field, and 2) by exchanging information through the field. In this section, we review how to decompose the detectors' correlations into two components, respectively sourced by genuine harvesting and by communication. This will give us an estimator for how much of the correlations, and therefore of the entanglement, comes from each source.

[1] Notice that in the more common case where the detectors couple to the amplitude instead of the derivative, the expressions in Eq. (2.19) remain the same except for replacing $W_{tt'} \to W$.

This decomposition into harvesting and communication, originally introduced in [55], is based on the symmetric and antisymmetric parts of the two-point field correlator.

For an arbitrary field state $\hat{\rho}_\phi$, the two-point correlator is defined as

$$W(\mathsf{x},\mathsf{x}') = \langle \hat{\phi}(\mathsf{x})\hat{\phi}(\mathsf{x}')\rangle_{\hat{\rho}_\phi}\,, \tag{2.22}$$

which can be divided into symmetric and antisymmetric parts,

$$W^{\pm}(\mathsf{x},\mathsf{x}') = \frac{W(\mathsf{x},\mathsf{x}') \pm W(\mathsf{x}',\mathsf{x})}{2}. \tag{2.23}$$

Since $W(\mathsf{x}',\mathsf{x}) = W^*(\mathsf{x},\mathsf{x}')$, we have that W^+ and W^- respectively are the real and imaginary parts of W, and

$$\begin{aligned} W^+(\mathsf{x},\mathsf{x}') &= \frac{1}{2}\,\langle\{\hat{\phi}(\mathsf{x}),\hat{\phi}(\mathsf{x}')\}\rangle_{\hat{\rho}_\phi}\,, \\ W^-(\mathsf{x},\mathsf{x}') &= \frac{1}{2}\,\langle[\hat{\phi}(\mathsf{x}),\hat{\phi}(\mathsf{x}')]\rangle_{\hat{\rho}_\phi}\,. \end{aligned} \tag{2.24}$$

In [55], it was argued that W^+ reflects the preexisting correlations in the field state, while W^- mediates communication through the field. Thus, only W^+ can be associated to genuinely harvested entanglement. We summarize the evidence to support this in the following:

1. The expectation value of the field commutator $[\hat{\phi}(\mathsf{x}),\hat{\phi}(\mathsf{x}')]$ is independent of the state (see, among many others, [53, 55]). Therefore, W^- is unaffected by any preexisting field correlations, which are dictated by the initial field state. In turn, any detector correlations mediated solely by W^- remain the same regardless of the amount of correlations and entanglement initially present in the field. Therefore, the contributions of W^- to the detectors' entanglement cannot reflect entanglement being harvested from the field.

   Conversely, the expectation value of the field anticommutator $\{\hat{\phi}(\mathsf{x}),\hat{\phi}(\mathsf{x}')\}$ does depend on the sate. Therefore, any change in the preexisting field correlations is only captured by W^+, which is consistent with associating W^+ to harvested entanglement

2. The communication between two detectors at leading order is exclusively mediated by W^-, with no contribution whatsoever from W^+, as shown in [51, 52, 53, 54]. Therefore, this points towards detectors' correlations caused by W^- being communication-mediated and detectors' correlations caused by W^+ being genuinely harvested from

the field. This argument holds at leading order, which is enough for the calculations in the present thesis that distinguish between communication and harvesting contributions.

This result is not exclusive to detectors, but rather holds in general for any two systems A, B that couple to the interaction picture observables $\hat{C}_{\rm A}(t)$ and $\hat{C}_{\rm B}(t')$ of a third system C. Specifically, at leading order, communication between A and B is exclusively mediated by $[\hat{C}_{\rm A}(t), \hat{C}_{\rm B}(t')]$. Furthermore, even non-perturbatively, A and B can only communicate if $[\hat{C}_{\rm A}(t), \hat{C}_{\rm B}(t')]$ is non-zero. In other words, communication between A and B is impossible if they only couple to commuting interaction picture observables of the mediating system C (see, e.g., Appendix A.1).

3. The field commutator fulfills $[\hat{\phi}(\mathsf{x}), \hat{\phi}(\mathsf{x}')] = \mathrm{i}E(\mathsf{x},\mathsf{x}')\hat{\mathbb{1}}$, where $E(\mathsf{x},\mathsf{x}')$ is the causal propagator. $E(\mathsf{x},\mathsf{x}')$ is equal to the retarded minus the advanced Green's functions (see, e.g. [89]). If the quantum field theory were to be replaced by a classical field theory (where there is no entanglement) the role of the commutator would be played by the Poisson bracket and the communication through the classical field would be mediated by this very same propagator. In other words, in classical field theory, these Green's functions are what mediates communication between interacting field sources. Moreover, the Green's functions, and thus W^-, vanish outside the light cone for Klein-Gordon fields such as the ones we consider. This is required to prevent signaling between space-like regions and directly relates to the axiom of microcausality in quantum field theory.

   Conversely, the field anticommutator $\{\hat{\phi}(\mathsf{x}), \hat{\phi}(\mathsf{x}')\}$ has support even for spacelike separated events, and thus W^+ exclusively sources spacelike entanglement harvesting.

In the expression (2.21) for negativity, the term $\mathcal{M}$ accounts for the correlations between the detectors that contribute positively to entanglement. We split this term $\mathcal{M}$ by source,

$$\mathcal{M} = \mathcal{M}^+ + \mathcal{M}^-, \tag{2.25}$$

with $\mathcal{M}^+$ being sourced by preexisting field correlations and $\mathcal{M}^-$ being sourced from communication. This is done by defining $\mathcal{M}^\pm$ analogously to $\mathcal{M}$ in (2.19) but keeping only contributions from $W^\pm$.

Finally, based on the equation (2.21) for negativity, we define the *harvested negativity* $\mathcal{N}^+$ and the *communication-assisted negativity* $\mathcal{N}^-$ as[2]

$$\mathcal{N}^\pm = \max\{|\mathcal{M}^\pm| - \mathcal{L}, 0\} + \mathcal{O}(\lambda^4). \tag{2.26}$$

[2]A remark to avoid confusion: notice that $\mathcal{M}^-$ can be non-zero while $\mathcal{N}^- = 0$ if the local noise terms conspire appropriately, or even $\mathcal{N} \neq 0$ while $\mathcal{N}^\pm = 0$, a case that will appear in the plots of the examples of

2.3 Canceling out the communication contribution to entanglement

Now we move onto showing how the behavior of the imaginary part of the two-point function W^- (and therefore of $\mathcal{M}^-$) is affected by coupling to $\partial_t\hat{\phi}$ instead of $\hat{\phi}$. Moreover, we limit our exploration to massless fields, with $m = 0$ and thus $\omega_{\boldsymbol{k}} = |k|$. Remarkably, we can find regimes in flat spacetime where the communication-mediated correlations $\mathcal{M}^-$ become zero in when the light-like contact and the entanglement gathered by the detectors are maximum.

Denoting as W_n^- the antisymmetric part of the two-point function of the vacuum of $(n+1)$-dimensional Minkowski spacetime (for a derivation of the expressions below see, e.g., [55]),

$$W_1^-(\mathsf{x},\mathsf{x}') = -\frac{\mathrm{i}}{4}\big(\Theta(|\Delta x|+\Delta t) - \Theta(|\Delta x|-\Delta t)\big), \tag{2.27}$$

$$W_2^-(\mathsf{x},\mathsf{x}') = -\frac{\mathrm{i}\,\mathrm{sgn}(\Delta t)}{4\pi}\frac{\Theta\left(\Delta t^2 - \Delta\boldsymbol{x}^2\right)}{\sqrt{\Delta t^2 - \Delta\boldsymbol{x}^2}}, \tag{2.28}$$

and, for odd $n \geq 3$,

$$\begin{aligned} W_n^-(\mathsf{x},\mathsf{x}') = \sum_{j=0}^{\frac{n-3}{2}} \frac{\mathrm{i}a_j}{|\Delta\boldsymbol{x}|^{n-2-j}}\big(&\delta^{(j)}(\Delta t + |\Delta\boldsymbol{x}|) \\ &- (-1)^j\delta^{(j)}(\Delta t - |\Delta\boldsymbol{x}|)\big), \end{aligned} \tag{2.29}$$

where a_j are real numbers and $\delta^{(j)}$ are the Dirac delta distribution's j-th derivative.

The two time derivatives of W_n^- that appear in $\mathcal{M}^-$ in Eq. (2.19) are the only change introduced by coupling to $\partial_t\hat{\phi}$ instead of $\hat{\phi}$. Therefore, for amplitude coupling, as discussed in the section above and in [55], communication is mediated by W_n^-, while, for derivative coupling, the communication is mediated by $\partial_t\partial_{t'}W_n^-$.

For $n = 1$,

$$\partial_t\partial_{t'}W_1^-(\mathsf{x},\mathsf{x}') = \frac{\mathrm{i}}{4}\big(\delta^{(1)}(\Delta t + |\Delta x|) + \delta^{(1)}(\Delta t - |\Delta x|)\big). \tag{2.30}$$

the section 2.6. This means that communication-assisted harvesting can occur even if $\mathcal{N}^- = 0$. However, even in such a case the preexisting field correlations are responsible for entanglement occurring between the detectors. If field correlations were not there, there would be no entanglement between the detectors at all.

For $n = 2$, the following closed expression is valid for any x, x' that are not light-connected:

$$\begin{aligned}&\partial_t\partial_{t'}W_2^-(\mathsf{x},\mathsf{x}')\\&= \frac{\mathrm{i}\,\mathrm{sgn}(\Delta t)}{4\pi}\frac{(2\Delta t^2+\Delta\boldsymbol{x}^2)\,\Theta(\Delta t^2-\Delta\boldsymbol{x}^2)}{(\Delta t^2-\Delta\boldsymbol{x}^2)^{5/2}},\end{aligned} \tag{2.31}$$

and, in any case, for any x, x' the distribution can be evaluated from the following integral form:

$$\partial_t\partial_{t'}W_2^-(\mathsf{x},\mathsf{x}') = -\frac{\mathrm{i}}{4\pi}\int_0^\infty \mathrm{d}\omega\,\omega^2\sin(\omega\Delta t)J_0(\omega|\Delta\boldsymbol{x}|), \tag{2.32}$$

where J_0 is the Bessel function of the first kind of order zero.

Furthermore, for odd $n \geq 3$,

$$\begin{aligned}\partial_t\partial_{t'}W_n^-(\mathsf{x},\mathsf{x}') = \sum_{j=0}^{\frac{n-3}{2}}\frac{-\mathrm{i}a_j}{|\Delta\boldsymbol{x}|^{n-2-j}}\big(&\delta^{(j+2)}(\Delta t+|\Delta\boldsymbol{x}|)\\&-(-1)^j\delta^{(j+2)}(\Delta t-|\Delta\boldsymbol{x}|)\big).\end{aligned} \tag{2.33}$$

Here, notice that for large enough distances $|\Delta\boldsymbol{x}|$, the term with $j = \frac{n-3}{2}$ dominates, decaying as $|\Delta\boldsymbol{x}|^{-\frac{n-1}{2}}$. Interestingly, in this long-distance regime, at least for n odd, $\partial_t\partial_t W_n^-$ has a behaviour akin to W_{n+4}^-, except that it keeps the $|\Delta\boldsymbol{x}|$ decay of W_n^-.

These expressions show that both W_n^- and $\partial_t\partial_{t'}W_n^-$ are only supported in the light-cone (and inside the light-cone for W_1^-, W_2^- and $\partial_t\partial_{t'}W_2^-$), so one might expect that $\mathcal{M}^-$ peaks at the light-cone. This is the case when coupling to the amplitude in $1+1$ and $3+1$ dimensions, with, for example, Gaussian switching functions [55]. However, this changes when we couple to the derivative. Then, $\mathcal{M}^-$ can reach zero even in full light contact (in $1+1$ D) or in partial light contact (in $3+1$ D), as we show next.

For simplicity, consider Gaussian profiles for both centered switching and smearing functions (see Eq. (2.13)),

$$\chi(t) = e^{-\frac{t^2}{T^2}},\ F(\boldsymbol{x}) = \frac{1}{(\sqrt{\pi}\sigma)^n}e^{-\frac{\boldsymbol{x}^2}{\sigma^2}}, \tag{2.34}$$

where T is the interaction time-scale, and σ is the size of the detector. Then, from

Eq. (2.19),

$$\mathcal{M} = CT \int \mathrm{d}t_- \, \mathrm{d}^n \boldsymbol{x}_- \frac{e^{-\frac{t_-^2}{2T^2} - \frac{\boldsymbol{x}_-^2}{2\sigma^2}}}{(\sqrt{2\pi}\sigma)^n} W_{tt'}(|t_- - t_\Delta|, \boldsymbol{x}_- - \boldsymbol{x}_\Delta),$$
$$C = -\sqrt{\frac{\pi}{2}} \lambda^2 e^{\mathrm{i}\Omega(t_\mathrm{A}+t_\mathrm{B}) - \frac{1}{2}(\Omega T)^2}, \tag{2.35}$$

where we took the change of variables $t_\pm = t \pm t'$, $\boldsymbol{x}_\pm = \boldsymbol{x} \pm \boldsymbol{x}'$ and then integrated over t_+ and $\boldsymbol{x}_+$. To better understand how $\mathcal{M}^-$ for $n = 1$ becomes zero in full causal contact, we integrate over t_- analytically. Using that $W_{tt'} = \partial_t \partial_{t'} W$ together with Eq. (2.30),

$$\mathcal{M}_1^- = \frac{\mathrm{i}C}{4} \int \mathrm{d}x_- \left(\frac{|x_- - x_\Delta| + t_\Delta}{T} e^{-\frac{1}{2}\left(\frac{|x_- - x_\Delta| + t_\Delta}{T}\right)^2} \right.$$
$$\left. + \frac{|x_- - x_\Delta| - t_\Delta}{T} e^{-\frac{1}{2}\left(\frac{|x_- - x_\Delta| - t_\Delta}{T}\right)^2} \right) \frac{e^{-\frac{x_-^2}{2\sigma^2}}}{\sqrt{2\pi}\sigma}, \tag{2.36}$$

which becomes easier to interpret in the point-like detector limit, where $\sigma \to 0$, and for $(|x_\Delta| + |t_\Delta|) \gg T$, so that the causal relationships are well-defined. In these regimes,

$$\mathcal{M}_1^- \approx \frac{\mathrm{i}C}{4} \frac{|x_\Delta| - |t_\Delta|}{T} e^{-\frac{1}{2}\left(\frac{|x_\Delta| - |t_\Delta|}{T}\right)^2}. \tag{2.37}$$

Therefore, for derivative coupling in $1+1$ dimensions, $|\mathcal{M}^-|$ is gaussianly suppressed as we move away from the light-cone, but actually cancels on the light-cone itself (where $|x_\Delta| = |t_\Delta|$), as seen in Figure 2.2(a). Simultaneously, $|\mathcal{M}^+|$ and $|\mathcal{M}|$ reach a maximum at maximum light-like communication, causing the detectors to gather the most entanglement, and this entanglement being genuinely harvested from the field.

For derivative coupling in $3+1$ dimensions, $\mathcal{M}^-$ results from integrating a Gaussian against $\delta^{(2)}$ (in the pointlike limit $\sigma \to 0$), which causes $|\mathcal{M}^-|$ to have three peaks, as seen in Figure 2.2(b), with communication reaching zero in between these peaks, even though the detectors are in causal contact. This phenomenon allows to genuinely harvest entanglement from a massless field also in 3+1 dimensions even in partial light-like contact, contrarily to the amplitude coupling case [55].

2.4 Entanglement harvesting in curved spacetimes

For the sake of completeness and to establish notation, we generalize the entanglement harvesting protocol presented in section 2.1 to the context of general spacetimes, following

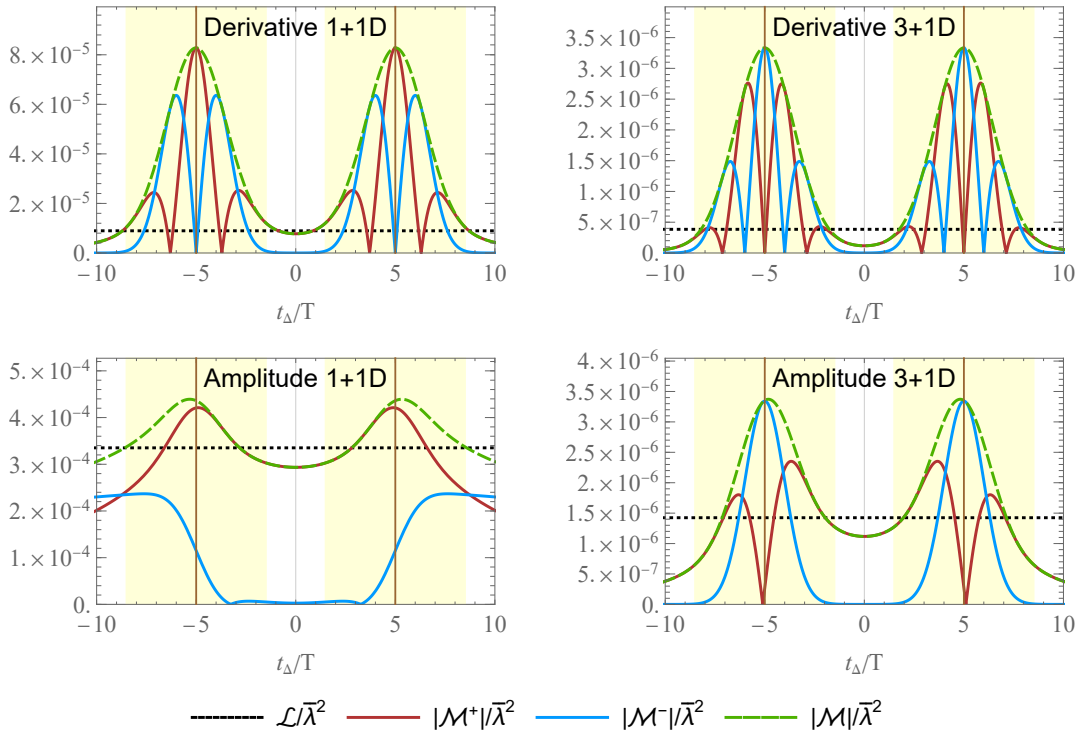


Figure 2.2: Contributions to the negativity $\mathcal{N}$, see Eq. (2.21), for a series of derivative coupling and amplitude coupling scenarios. The correlations $|\mathcal{M}|$ which contribute to $\mathcal{N}$ are split between the $|\mathcal{M}^+|$ term (genuine harvesting) the $|\mathcal{M}^-|$ term (acquired by communication). The setup uses the Gaussian switching and smearing functions given in Eq. (2.34), $\Omega T = 4$, $|x_\Delta|/T = 5$, $\sigma/T = 0.05$. The amplitude coupling in 1+1D has an IR cutoff of $\Lambda T = 0.02$, see, e.g. [2]. The $\overline{\lambda}$ is an adimensional coupling constant, whose definition depends on the scenario: for *derivative coupling*, $\overline{\lambda} = \lambda$ in $1+1$D and $\overline{\lambda} = \lambda/T$ in 3+1D. For *amplitude coupling*, $\overline{\lambda} = \lambda T$ in $1+1$D and $\overline{\lambda} = \lambda$ in 3+1D. The brown vertical lines denote maximum light contact, and the light yellow coloured regions show the size of the strong support of the switching function of a detector, taken to be $[-3.5T, 3.5T]$.

for example [90, 91]. Consider two Unurh-DeWitt detectors [26, 27, 28, 29, 30], A and B, following timelike trajectories $\mathsf{z}_{\mathrm{A}}(\tau_{\mathrm{A}})$ and $\mathsf{z}_{\mathrm{B}}(\tau_{\mathrm{B}})$ in an arbitrary $n+1$ dimensional curved spacetime M. The quantities τ_{A} and τ_{B} are the respective proper times of the detectors.

The detectors are two-level quantum systems with the following internal Hamiltonians,

$$\hat{H}_{\mathrm{FREE},\,\nu} = \Omega_\nu \hat{\sigma}^+_\nu \hat{\sigma}^-_\nu\,, \quad \nu \in \mathrm{A}, \mathrm{B}. \tag{2.38}$$

Here, Ω_ν represents the (proper) internal energy gap, while $\hat{\sigma}_\nu^+ = |e_\nu\rangle\langle g_\nu|$ and $\hat{\sigma}_\nu^- = |g_\nu\rangle\langle e_\nu|$ are ladder operators between the respective ground ($|g_\nu\rangle$) and excited ($|e_\nu\rangle$) states. Next, we describe a common way to couple these detectors to a massless real scalar quantum field $\hat{\phi}(\mathsf{x})$ defined on the spacetime M.

The first step is to quantize the field. Consider a free massless real scalar field $\phi(\mathsf{x})$ in M, which is assumed to satisfy the Klein-Gordon equation,

$$(\nabla^\rho \nabla_\rho - \xi R)\phi(\mathsf{x}) = 0. \tag{2.39}$$

Here, ξ is a constant that determines the coupling strength to curvature, R is the scalar curvature, and ∇_ρ denotes the covariant derivative. Next, assume $\{u_{\boldsymbol{k}}(\mathsf{x}), u^*_{\boldsymbol{k}}(\mathsf{x}')\}$ to be a complete, orthonormal set of solutions to Eq. (2.39) [92, 93]. Then, any classical solution $\phi(\mathsf{x})$ is a linear combination of $u_{\boldsymbol{k}}(\mathsf{x})$ and $u^*_{\boldsymbol{k}}(\mathsf{x}')$,

$$\phi(\mathsf{x}) = \int \mathrm{d}^n \boldsymbol{k}\ (a^*_{\boldsymbol{k}} u^*_{\boldsymbol{k}}(\mathsf{x}) + a_{\boldsymbol{k}} u_{\boldsymbol{k}}(\mathsf{x})), \tag{2.40}$$

where $a_{\boldsymbol{k}}$ are constant complex coefficients. After canonically quantizing the field, the field amplitude $\phi(\mathsf{x})$ becomes an operator,

$$\hat{\phi}(\mathsf{x}) = \int \mathrm{d}^n \boldsymbol{k}\ (u^*_{\boldsymbol{k}}(\mathsf{x})\hat{a}^\dagger_{\boldsymbol{k}} + u_{\boldsymbol{k}}(\mathsf{x})\hat{a}_{\boldsymbol{k}}), \tag{2.41}$$

with the coefficients $a_{\boldsymbol{k}}$ promoted to operators. Specifically, $\hat{a}_{\boldsymbol{k}}$ and $\hat{a}^\dagger_{\boldsymbol{k}}$ are the usual ladder operators, which satisfy the bosonic canonical commutation relations, namely

$$[\hat{a}_{\boldsymbol{k}}, \hat{a}^\dagger_{\boldsymbol{k}'}] = \delta^n(\boldsymbol{k} - \boldsymbol{k}'). \tag{2.42}$$

Let us move onto specifying the interaction between the detector and the quantum field using the covariant Unruh-DeWitt model [90]. For this model, the interaction occurs within a region of spacetime, according to the following interaction Hamiltonian density [3]:

$$\hat{H}_{\mathrm{I}}(\mathsf{x}) = \lambda\big[\Lambda_{\mathrm{A}}(\mathsf{x})\hat{\mu}_{\mathrm{A}}(\tau_{\mathrm{A}}) + \Lambda_{\mathrm{B}}(\mathsf{x})\hat{\mu}_{\mathrm{B}}(\tau_{\mathrm{B}})\big]\hat{\phi}(\mathsf{x}). \tag{2.43}$$

[3] Usually, this construction assumes that there exists a foliation in which $\Lambda_\nu(\tau_\nu, \boldsymbol{x}) = \chi_\nu(\tau_\nu)F_\nu(\boldsymbol{x})$. This is justified by the assumption that internal forces keep the detector cohesive. The center of mass follows the trajectory $\mathsf{z}_\nu(\tau_\nu)$ that defines the detector's proper time τ_ν, serving as its internal clock. For further details and justification, see [90, 91], where this model is shown to be suitable for systems like atomic probes.

Here, λ is the interaction strength, $\Lambda_\nu(\mathsf{x})$ are the spacetime smearing functions, which localize the interaction in space and time, and the detectors' operators $\hat{\mu}_\nu$ are the monopole moments, given by

$$\hat{\mu}_\nu(\tau_\nu) = e^{\mathrm{i}\Omega_\nu\tau_\nu}\hat{\sigma}_\nu^+ + e^{-\mathrm{i}\Omega_\nu\tau_\nu}\hat{\sigma}_\nu^-. \tag{2.44}$$

The evolution of the joint state of the detectors and the field, in the interaction picture, is given by the unitary

$$\hat{U} = \mathcal{T}\exp\left(-\mathrm{i}\int \mathrm{d}V \hat{h}_\mathrm{I}(\mathsf{x})\right), \tag{2.45}$$

where the $\mathcal{T}$ indicates that we are using the time ordered exponential[4]. Moreover, $\mathrm{d}V$ is the invariant spacetime volume element. For a given choice of coordinates $(t, \boldsymbol{x})$, the volume element takes the form $\mathrm{d}V = \mathrm{d}t\mathrm{d}^n\boldsymbol{x}\sqrt{-g}$, where g is the determinant of the metric tensor.

Take the full system to be initialized in the interaction picture state

$$\hat{\rho}_0 = |\psi_\mathrm{A}\rangle\langle\psi_\mathrm{A}| \otimes |\psi_\mathrm{B}\rangle\langle\psi_\mathrm{B}| \otimes \hat{\rho}_{\phi,0}, \tag{2.46}$$

where $|\psi_\mathrm{A}\rangle$ and $|\psi_\mathrm{B}\rangle$ are arbitrary pure states of the detectors. With this choice, notice that there are no correlations between detectors in their initial state. Nonetheless, the detectors can evolve to a mutually entangled state, after time evolution turns the state $\hat{\rho}_0$ into $\hat{\rho} = \hat{U}\hat{\rho}_0\hat{U}^\dagger$, using Eq. (2.45). This can occur even if the detectors are spacelike separated, for instance, when $\hat{\rho}_{\phi,0}$ is the vacuum. This is so because the detectors harvest preexisting entanglement in the field's initial state. The process of extracting entanglement from the field to two localized detectors has become known as *entanglement harvesting* [40, 2]. For example, when the field's initial state is the Minkowski vacuum, it is well known that there is entanglement in the field between degrees of freedom in regions that are spacelike [4, 5, 11] and timelike [94, 95, 43] separated.

As an additional assumption to simplify the final result, consider the initial state of the field $\hat{\rho}_{\phi,0}$ to have a vanishing one-point function and three-point function,

$$\mathrm{Tr}\left(\hat{\rho}_{\phi,0}\hat{\phi}(\mathsf{x})\right) = 0, \mathrm{Tr}\left(\hat{\rho}_{\phi,0}\hat{\phi}(\mathsf{x})\hat{\phi}(\mathsf{x}')\hat{\phi}(\mathsf{x}'')\right) = 0. \tag{2.47}$$

[4]Notice that for detectors that are not point-like, but rather are smeared in space, there is ambiguity in the time ordering. Nonetheless, reference [91] shows that the evolution will not depend on the ordering chosen, as long as predictions are kept at leading order in the interaction strength, λ, and suitable initial states are chosen. For the purposes of the present chapter, we assume that a physically motivated choice of time ordering has been taken.

Similar assumptions are commonly taken in entanglement harvesting protocols. Moreover, the assumption holds for a large variety of states, including the Minkowski vacuum in flat spacetime and the conformal vacuum in DeSitter. Additionally, it is also true for any Fock states as well as any zero mean Gaussian states such as thermal states and the squeezed vacuum.[5]

Finding a closed form expression for the time evolved state $\hat{\rho} = \hat{U}\hat{\rho}_0\hat{U}^\dagger$ is not possible in general. So, instead, we take a perturbative approach in λ. Thus, we expand the time evolution operator $\hat{U}$ via a Dyson series:

$$\hat{U} = \underbrace{\hat{\mathbb{1}}}_{\hat{U}^{(0)}} \underbrace{-\mathrm{i}\int \mathrm{d}V_1 \hat{h}_{\mathrm{I}}(\mathsf{x}_1)}_{\hat{U}^{(1)}} \underbrace{-\int \mathrm{d}V_1 \int \mathrm{d}V_2 \hat{h}_{\mathrm{I}}(\mathsf{x}_1)\hat{h}_{\mathrm{I}}(\mathsf{x}_2)\,\Theta\left(t(\mathsf{x}_1) - t(\mathsf{x}_2)\right)}_{\hat{U}^{(2)}} + \mathcal{O}(\lambda^3), \tag{2.48}$$

where $\Theta(t)$ is the Heaviside step function, and t is the time parameter with respect to which we defined the time ordering. Next, denoting $\hat{\rho}^{(i,j)} = \hat{U}^{(i)}\hat{\rho}_0\hat{U}^{(j)\dagger}$, the evolved state becomes

$$\hat{\rho} = \hat{\rho}_0 + \hat{\rho}^{(1,0)} + \hat{\rho}^{(0,1)} + \hat{\rho}^{(2,0)} + \hat{\rho}^{(1,1)} + \hat{\rho}^{(0,2)} + \mathcal{O}(\lambda^3). \tag{2.49}$$

To study the entanglement that the detectors acquire through the interaction, we need to trace out the field, yielding $\hat{\rho}_{\mathrm{AB}} = \mathrm{Tr}_\phi(\hat{\rho})$, the detectors' evolved state. The terms in $\hat{\rho}_{\mathrm{AB}}$ of order λ and λ^3 cancel out, due to the assumption on the initial state of the field stated in equation (2.47), leaving

$$\hat{\rho}_{\mathrm{AB}} = \mathrm{Tr}_\phi\,\hat{\rho} = \hat{\rho}_{\mathrm{AB},0} + \hat{\rho}^{(2,0)}_{\mathrm{AB}} + \hat{\rho}^{(1,1)}_{\mathrm{AB}} + \hat{\rho}^{(0,2)}_{\mathrm{AB}} + \mathcal{O}(\lambda^4)\,. \tag{2.50}$$

In order to express this state in matrix form, we consider states $|\zeta_{\mathrm{A}}\rangle$ and $|\zeta_{\mathrm{B}}\rangle$ so that $\{|\psi_{\mathrm{A}}\psi_{\mathrm{B}}\rangle\,, |\psi_{\mathrm{A}}\zeta_{\mathrm{B}}\rangle\,, |\zeta_{\mathrm{A}}\psi_{\mathrm{B}}\rangle\,, |\zeta_{\mathrm{A}}\zeta_{\mathrm{B}}\rangle\}$ is an orthonormal basis. Without losing generality, we assume that these states relate to the previously defined ground and excited states of the detectors as follows,

$$\begin{aligned} |g_\nu\rangle &= \cos\alpha_\nu\,|\psi_\nu\rangle - e^{\mathrm{i}\beta_\nu}\sin\alpha_\nu\,|\zeta_\nu\rangle\,, \\ |e_\nu\rangle &= e^{-\mathrm{i}\beta_\nu}\sin\alpha_\nu\,|\psi_\nu\rangle + \cos\alpha_\nu\,|\zeta_\nu\rangle\,, \end{aligned} \tag{2.51}$$

for some $\alpha_\nu, \beta_\nu \in [0, 2\pi]$. Then, using the results from [96], in the basis $\{|\psi_{\mathrm{A}}\psi_{\mathrm{B}}\rangle\,,\ |\psi_{\mathrm{A}}\zeta_{\mathrm{B}}\rangle\,,\ |\zeta_{\mathrm{A}}\psi_{\mathrm{B}}\rangle\,,\ |\zeta_{\mathrm{A}}\zeta_{\mathrm{B}}\rangle\}$, we get

$$\hat{\rho}_{\mathrm{AB}} = \begin{bmatrix} 1-\mathcal{L}_{\mathrm{AA}}-\mathcal{L}_{\mathrm{BB}} & \mathcal{X}^* & \mathcal{Y}^* & \mathcal{M}^* \\ \mathcal{X} & \mathcal{L}_{\mathrm{BB}} & \mathcal{L}^*_{\mathrm{AB}} & 0 \\ \mathcal{Y} & \mathcal{L}_{\mathrm{AB}} & \mathcal{L}_{\mathrm{AA}} & 0 \\ \mathcal{M} & 0 & 0 & 0 \end{bmatrix} + O(\lambda^4)\,, \tag{2.52}$$

[5] What is more, for all the mentioned examples of field states, all the odd-point functions vanish.

with

$$\begin{aligned}\mathcal{L}_{\mu\nu} =& \cos^2\alpha_\mu \cos^2\alpha_\nu\, L_{\mu\nu}(\Omega_\mu,\Omega_\nu)\\ &- \cos^2\alpha_\mu \sin^2\alpha_\nu\, e^{-2\mathrm{i}\beta_\nu}\, L_{\mu\nu}(\Omega_\mu,-\Omega_\nu)\\ &- \sin^2\alpha_\mu \cos^2\alpha_\nu\, e^{2\mathrm{i}\beta_\mu}\, L_{\mu\nu}(-\Omega_\mu,\Omega_\nu)\\ &+ \sin^2\alpha_\mu \sin^2\alpha_\nu\, e^{2\mathrm{i}(\beta_\mu-\beta_\nu)}\, L_{\mu\nu}(-\Omega_\mu,-\Omega_\nu),\end{aligned} \tag{2.53}$$

$$\begin{aligned}\mathcal{M} =& \cos^2\alpha_{\mathrm{A}} \cos^2\alpha_{\mathrm{B}}\, M(\Omega_{\mathrm{A}},\Omega_{\mathrm{B}})\\ &- \cos^2\alpha_{\mathrm{A}} \sin^2\alpha_{\mathrm{B}}\, e^{2\mathrm{i}\beta_{\mathrm{B}}}\, M(\Omega_{\mathrm{A}},-\Omega_{\mathrm{B}})\\ &- \sin^2\alpha_{\mathrm{A}} \cos^2\alpha_{\mathrm{B}}\, e^{2\mathrm{i}\beta_{\mathrm{A}}}\, M(-\Omega_{\mathrm{A}},\Omega_{\mathrm{B}})\\ &+ \sin^2\alpha_{\mathrm{A}} \sin^2\alpha_{\mathrm{B}}\, e^{2\mathrm{i}(\beta_{\mathrm{A}}+\beta_{\mathrm{B}})}\, M(-\Omega_{\mathrm{A}},-\Omega_{\mathrm{B}}),\end{aligned} \tag{2.54}$$

where

$$L_{\mu\nu}(\Omega_\mu,\Omega_\nu) = \lambda^2 \int \mathrm{d}V\mathrm{d}V' e^{\mathrm{i}(\Omega_\mu\tau_\mu(\mathsf{x})-\Omega_\nu\tau_\nu(\mathsf{x}'))}\Lambda_\mu(\mathsf{x})\Lambda_\nu(\mathsf{x}')W(\mathsf{x}',\mathsf{x}), \tag{2.55}$$

$$M(\Omega_{\mathrm{A}},\Omega_{\mathrm{B}}) = -\lambda^2 \int \mathrm{d}V\mathrm{d}V' e^{\mathrm{i}(\Omega_{\mathrm{A}}\tau_{\mathrm{A}}(\mathsf{x})+\Omega_{\mathrm{B}}\tau_{\mathrm{B}}(\mathsf{x}'))}\Lambda_{\mathrm{A}}(\mathsf{x})\Lambda_{\mathrm{B}}(\mathsf{x}')G_{\mathrm{F}}(\mathsf{x},\mathsf{x}'). \tag{2.56}$$

The terms $\mathcal{L}_{\mu\nu}$ and $\mathcal{M}$ are usually called *local noise* and *non-local correlations*, respectively. The expressions for $\mathcal{X}$ and $\mathcal{Y}$ are cumbersome and, since we will not use them here, we refer the interested reader to reference [96]. In equations (2.55) and (2.56), $W(\mathsf{x},\mathsf{x}')$ is the *Wightman function*,

$$W(\mathsf{x},\mathsf{x}') = \mathrm{Tr}\Big[\hat{\phi}(\mathsf{x})\hat{\phi}(\mathsf{x}')\hat{\rho}_{\phi,0}\Big], \tag{2.57}$$

whereas $G_{\mathrm{F}}(\mathsf{x},\mathsf{x}')$ represents the *Feynman propagator*, which can be written as

$$\begin{aligned}G_{\mathrm{F}}(\mathsf{x},\mathsf{x}') &= \mathrm{Tr}\Big[\mathcal{T}\hat{\phi}(\mathsf{x})\hat{\phi}(\mathsf{x}')\hat{\rho}_{\phi,0}\Big]\\ &= \Theta\big(t(\mathsf{x})-t(\mathsf{x}')\big)W(\mathsf{x},\mathsf{x}') + \Theta\big(t(\mathsf{x}')-t(\mathsf{x})\big)W(\mathsf{x}',\mathsf{x}).\end{aligned} \tag{2.58}$$

Remember that $\Theta(t)$ is the Heaviside step function, and t is the time coordinate with respect to which we defined the time ordering.

Again, to quantify the amount of entanglement between the detectors, we use the *negativity* [86, 87], which is an entanglement measure even for mixed states, and is faithful for systems of two qubits. Negativity can be computed as the absolute sum of the *negative*

eigenvalues of the partially transposed density matrix $\hat{\rho}^{\top_A}$. In particular, for the state $\hat{\rho}_{AB}$ described by Eq. (2.52) we have [2]

$$\mathcal{N} = \max\{0, \mathcal{V}\} + \mathcal{O}(\lambda^4), \tag{2.59}$$

with

$$\mathcal{V} = \sqrt{|\mathcal{M}|^2 + \left(\frac{\mathcal{L}_{AA} - \mathcal{L}_{BB}}{2}\right)^2} - \frac{\mathcal{L}_{AA} + \mathcal{L}_{BB}}{2}. \tag{2.60}$$

According this expression, entanglement emerges as a competition between the non-local term $\mathcal{M}$ and the local noise terms ($\mathcal{L}_{AA}$ and $\mathcal{L}_{BB}$). For the particular case $\mathcal{L}_{AA} = \mathcal{L}_{BB} = \mathcal{L}$ (such as for identical inertial detectors in flat spacetime), the negativity reads

$$\mathcal{N} = \max\{0, |\mathcal{M}| - \mathcal{L}\} + \mathcal{O}(\lambda^4). \tag{2.61}$$

In section 2.2 we described how to separate, for detectors in causal contact, the two sources from which entanglement between detectors can arise [55]: communication mediated by the field (*signaling*) and preexisting entanglement in the field state (*harvesting*). As a short reminder, this required splitting $\mathcal{M}$ into

$$\mathcal{M} = \mathcal{M}^+ + \mathcal{M}^-, \tag{2.62}$$

with $\mathcal{M}^-$ accounting for correlations gained via *signaling* and $\mathcal{M}^+$ accounting for correlations gained via *harvesting*. This is achieved by defining $\mathcal{M}^\pm$ in the same way as $\mathcal{M}$ from (2.54), but only retaining the contributions from $W^\pm$. In other words, by substituting the $G_F(\mathsf{x}, \mathsf{x}')$ in Eq. (2.56) by the corresponding $G_F^\pm(\mathsf{x}, \mathsf{x}')$, defined as

$$G_F^\pm(\mathsf{x}, \mathsf{x}') = \Theta\big(t(\mathsf{x}) - t(\mathsf{x}')\big)W^\pm(\mathsf{x}, \mathsf{x}') + \Theta\big(t(\mathsf{x}') - t(\mathsf{x})\big)W^\pm(\mathsf{x}', \mathsf{x}). \tag{2.63}$$

Furthermore, the *harvested negativity* $\mathcal{N}^+$ and the *communication-assisted negativity* $\mathcal{N}^-$ are now defined in terms of

$$\mathcal{V}^\pm = \sqrt{|\mathcal{M}^\pm|^2 + \left(\frac{\mathcal{L}_{AA} - \mathcal{L}_{BB}}{2}\right)^2} - \frac{\mathcal{L}_{AA} + \mathcal{L}_{BB}}{2}, \tag{2.64}$$

so that

$$\mathcal{N}^\pm = \max\{\mathcal{V}^\pm, 0\} + \mathcal{O}(\lambda^4). \tag{2.65}$$

2.5 General results for guaranteeing constructive interference

It is commonly observed in previous literature that the acquired entanglement $\mathcal{N}$ is larger than both $\mathcal{N}^{\pm}$, which indicates that communication and preexisting field correlations work together to entangle the detectors. However, this is not the case in general. There are situations where communication and field correlations can "destructively interfere", resulting in small $\mathcal{N}$ even if both $\mathcal{N}^{\pm}$ are relatively large. In this section, we will explore this phenomenon by describing all the ways in which the contributions from communication and preexisting field correlations can add up to build entanglement. Then, we explore a set of transformations of the harvesting setup that turn scenarios where communication and genuine harvesting contributions to $|\mathcal{M}|$ cancel each other into scenarios where they collaborate. After this, we provide a set of (easy to check) sufficient conditions under which communication and harvesting are always collaborating constructively.

For this exploration, we will focus on the study of the correlation term $|\mathcal{M}|$ which always contributes positively to $\mathcal{N}$. The current section specifically presents how communication (through $\mathcal{M}^{-}$) and field correlations (through $\mathcal{M}^{+}$) determine $|\mathcal{M}|$ and therefore $\mathcal{N}$. The local noise terms, $\mathcal{L}_{\text{AA}}$ and $\mathcal{L}_{\text{BB}}$, of course, also affect entanglement, however, they are local to each detector and hence independent of communication and correlations acquired of the detectors, and thus are ignored in the present section.

Starting from the most general scenario, $|\mathcal{M}|$ can be small even if $|\mathcal{M}^{+}|$ and $|\mathcal{M}^{-}|$ are relatively large, because

$$\begin{aligned} |\mathcal{M}|^2 &= |\mathcal{M}^{+} + \mathcal{M}^{-}|^2 \\ &= |\mathcal{M}^{+}|^2 + |\mathcal{M}^{-}|^2 + 2|\mathcal{M}^{+}||\mathcal{M}^{-}|\cos\Delta\gamma. \end{aligned} \tag{2.66}$$

Here, $\Delta\gamma$ is the relative phase between the complex numbers $\mathcal{M}^{+}$ and $\mathcal{M}^{-}$. This phase $\Delta\gamma$ controls how communication ($\mathcal{M}^{-}$) interferes with field correlations ($\mathcal{M}^{+}$). The interference can be *fully destructive*, making $|\mathcal{M}|$ the smallest,

$$|\Delta\gamma| = \pi \iff |\mathcal{M}| = ||\mathcal{M}^{+}| - |\mathcal{M}^{-}||, \tag{2.67}$$

fully constructive, making $|\mathcal{M}|$ the largest,

$$|\Delta\gamma| = 0 \iff |\mathcal{M}| = |\mathcal{M}^{+}| + |\mathcal{M}^{-}|, \tag{2.68}$$

or exactly *in between*, with $\mathcal{M}^{+}$ and $\mathcal{M}^{-}$ so that

$$|\Delta\gamma| = \pi/2 \iff |\mathcal{M}| = \sqrt{|\mathcal{M}^{+}|^2 + |\mathcal{M}^{-}|^2}. \tag{2.69}$$

In the two latter cases, communication and field correlations collaborate to increase $|\mathcal{M}|$ and thus $\mathcal{N}$. As we will see, the last relation, Eq. (2.69), turns out to be commonly fulfilled for the simplest choices of UDW detector model, as will be explored in Proposition 3

Next, we explore how to transform a setup from a destructive interference to a constructive interference scenario. Concretely, we will show how to transform the parameters of the harvesting setup to change the sign $\cos\Delta\gamma$ in Eq (2.66). In order to find such transformation, it is convenient to denote as $\mathcal{M}_{G_{\rm F}^*}$ the term $\mathcal{M}$ after complex conjugating the propagator $G_{\rm F}$. Then,

$$\mathcal{M} = \mathcal{M}^+ + \mathcal{M}^-,\ \mathcal{M}_{G_{\rm F}^*} = \mathcal{M}^+ - \mathcal{M}^-. \tag{2.70}$$

Consequently,

$$\mathcal{M}^{\pm}_{G_{\rm F}^*} = \pm\mathcal{M}^{\pm}, \tag{2.71}$$

which implies

$$|\mathcal{M}_{G_{\rm F}^*}|^2 = |\mathcal{M}^+|^2 + |\mathcal{M}^-|^2 - 2|\mathcal{M}^+||\mathcal{M}^-|\cos\Delta\gamma, \tag{2.72}$$

where $\Delta\gamma$ is the relative phase between the original terms $\mathcal{M}^+$ and $\mathcal{M}^-$. Observe that, as we were searching for, the term with $\cos\Delta\gamma$, which controls the interference, has the opposite sign in $|\mathcal{M}_{G_{\rm F}^*}|$ compared to in $|\mathcal{M}|$. Meanwhile, the communication and field correlations contributions retain the same size, $|\mathcal{M}^{\pm}_{G_{\rm F}^*}| = |\mathcal{M}^{\pm}|$.

Therefore, if we find an operation that conjugates $G_{\rm F}$, we could use it to turn destructive interference into constructive, as previously described. The next proposition shows how one can achieve that by changing the initial state of the particle detectors or, equivalently, transforming the parameters of the particle detector model.

Proposition 1. *Consider an operation that transforms arbitrary states of the detectors $\nu = A,\ B$ as follows*

$$\begin{aligned}&\cos\alpha_\nu\,|g_\nu\rangle + e^{\mathrm{i}\beta_\nu}\sin\alpha_\nu\,|e_\nu\rangle\\ &\to \sin\alpha_\nu\,|g_\nu\rangle + e^{\mathrm{i}\beta_\nu}\cos\alpha_\nu\,|e_\nu\rangle\,.\end{aligned} \tag{2.73}$$

Let $\widetilde{\mathcal{M}}$ be $\mathcal{M}$ after performing this transformation on the initial state of the detectors. Then,

$$\begin{aligned}&|\widetilde{\mathcal{M}}|^2 = |\mathcal{M}^+|^2 + |\mathcal{M}^-|^2 - 2|\mathcal{M}^+||\mathcal{M}^-|\cos\Delta\gamma,\\ &|\widetilde{\mathcal{M}}^{\pm}| = |\mathcal{M}^{\pm}|.\end{aligned} \tag{2.74}$$

Therefore, swapping the populations in the ground and excited state (while keeping the relative phase between them) changes the sign of $\cos\Delta\gamma$. Thus, this swap turns any destructive

interference into constructive, while keeping the communication and genuine harvesting contributions unchanged.

Equivalently, the transformation in Eq. (2.73) can be implemented by reversing the energy gaps $\Omega_\nu \to -\Omega_\nu$ and the relative phases $\beta_\nu \to -\beta_\nu$.

Proof. To prove the proposition, use Eq. (2.54) to see that

$$\begin{aligned}(\mathcal{M}_{G_{\mathrm{F}}^*})^* =& \big[\cos^2\alpha_{\mathrm{A}}\cos^2\alpha_{\mathrm{B}}\, M(-\Omega_{\mathrm{A}},-\Omega_{\mathrm{B}}) \\ &- \cos^2\alpha_{\mathrm{A}}\sin^2\alpha_{\mathrm{B}}\, e^{-2\mathrm{i}\beta_{\mathrm{B}}}\, M(-\Omega_{\mathrm{A}},\Omega_{\mathrm{B}}) \\ &- \sin^2\alpha_{\mathrm{A}}\cos^2\alpha_{\mathrm{B}}\, e^{-2\mathrm{i}\beta_{\mathrm{A}}}\, M(\Omega_{\mathrm{A}},-\Omega_{\mathrm{B}}) \\ &+ \sin^2\alpha_{\mathrm{A}}\sin^2\alpha_{\mathrm{B}}\, e^{-2\mathrm{i}(\beta_{\mathrm{A}}+\beta_{\mathrm{B}})}\, M(\Omega_{\mathrm{A}},\Omega_{\mathrm{B}})\big] \\ =&\widetilde{\mathcal{M}}. \end{aligned} \tag{2.75}$$

Here we used that

$$\big(M_{G_{\mathrm{F}}^*}(\Omega_{\mathrm{A}},\Omega_{\mathrm{B}})\big)^* = M(-\Omega_{\mathrm{A}},-\Omega_{\mathrm{B}}), \tag{2.76}$$

which in turn follows from Eq. (2.56) and $\Lambda_\nu = \Lambda_\nu^*$.

Finally, substituting $\widetilde{\mathcal{M}} = \mathcal{M}_{G_{\mathrm{F}}^*}^*$ into Eqs. (2.71) and (2.72) provides the identities stated in the proposition. □

Notice that according to this result, the stronger the destructive interference is in $\mathcal{M}$, the stronger the corresponding constructive interference is in $\widetilde{\mathcal{M}}$.

Now, we are ready to explore the conditions that enforce $\cos\Delta\gamma = 0$.

Proposition 2. *Let $\mathcal{M}_{G_F^*}$ be $\mathcal{M}$ after complex conjugating G_F, as in Eq. (2.70). Then,*

$$\begin{aligned}|\mathcal{M}| = |\mathcal{M}_{G_F^*}| &\iff |\mathcal{M}| = \sqrt{|\mathcal{M}^+|^2 + |\mathcal{M}^-|^2} \\ &\iff \cos\Delta\gamma = 0. \end{aligned} \tag{2.77}$$

Proof. The proof follows directly from comparing equations (2.66) and (2.72). □

Therefore, $|\mathcal{M}| = |\mathcal{M}_{G_{\mathrm{F}}^*}|$ is a **sufficient condition** for both the communication $\mathcal{M}^-$ and field correlations $\mathcal{M}^+$ to positively contribute to negativity. Notice that, because of Eq. (2.75), the result of Proposition 2 also holds if we use $\widetilde{\mathcal{M}}$ instead of $\mathcal{M}_{G_{\mathrm{F}}^*}$. Therefore, if $|\mathcal{M}|$ does not change under transforming the initial states as in Eq. (2.73), then there cannot be destructive interference. Furthermore, whenever $|\mathcal{M}| = |\mathcal{M}_{G_{\mathrm{F}}^*}|$, interference is

locked in the middle ground with $\cos\Delta\gamma = 0$, and the contributions $\mathcal{N}^-$ and $\mathcal{N}^+$ to the entanglement between the detectors satisfy

$$\mathcal{N} \geq \sqrt{(\mathcal{N}^+)^2 + (\mathcal{N}^-)^2} \Rightarrow \mathcal{N} \geq \mathcal{N}^-,\ \mathcal{N} \geq \mathcal{N}^+, \tag{2.78}$$

as proven in Appendix A.2.

Next, we will provide a framework to find symmetries of the harvesting setup that enforce the condition $|\mathcal{M}| = |\mathcal{M}_{G_{\text{F}}^*}|$. This framework is based on performing coordinate transformations in the integral for $\mathcal{M}$. To keep this method as general as possible and simultaneously simplify the derivation, we use the order λ^2 contribution to $\hat{\rho}_{\text{AB}}$, denoted by $\hat{\rho}^{(2)}_{\text{AB}}$ (the expression is provided in reference [96]). Working with the basis generated by the tensor product of the general states $|\psi_\nu\rangle$ and $|\zeta_\nu\rangle$, as defined before in Eq. (2.51), we can write

$$\begin{aligned}\mathcal{M} &= \langle\zeta_{\text{A}}\chi_{\text{B}}|\hat{\rho}^{(2)}_{\text{AB}}|\psi_{\text{A}}\psi_{\text{B}}\rangle\,, \\ &= -\lambda^2 \int \mathrm{d}V\mathrm{d}V' P_{\text{A}}(\mathsf{x})P_{\text{B}}(\mathsf{x}')G_{\text{F}}(\mathsf{x},\mathsf{x}').\end{aligned} \tag{2.79}$$

where we have defined[6]

$$P_\nu(\mathsf{x}) = \Lambda_\nu(\mathsf{x})\,\langle\zeta_\nu|\hat{\mu}_\nu(\tau_\nu(\mathsf{x}))|\psi_\nu\rangle\,. \tag{2.80}$$

Notice that the terms $P_\nu(\mathsf{x})$ conveniently group the contributions to $\mathcal{M}$ due to each detector. The condition $|\mathcal{M}| = |\mathcal{M}_{G_{\text{F}}^*}|$ thus becomes equivalent to

$$\begin{aligned}&\left|\int \mathrm{d}V\mathrm{d}V' P_{\text{A}}(\mathsf{x})P_{\text{B}}(\mathsf{x}')G_{\text{F}}(\mathsf{x},\mathsf{x}')\right| \\ &= \left|\int \mathrm{d}V\mathrm{d}V' P^*_{\text{A}}(\mathsf{x})P^*_{\text{B}}(\mathsf{x}')G_{\text{F}}(\mathsf{x},\mathsf{x}')\right|.\end{aligned} \tag{2.81}$$

Now, consider a map $\boldsymbol{T}$ taking a pair of points $\mathsf{x},\mathsf{x}' \in \mathsf{M}$ to another pair as follows,

$$\boldsymbol{T}(\mathsf{x},\mathsf{x}') = (T_1(\mathsf{x},\mathsf{x}'), T_2(\mathsf{x},\mathsf{x}')). \tag{2.82}$$

To see the effect of this map on pairs of coordinates, consider a pair of charts (φ,φ') mapping pairs of spacetime points (x,x') to the coordinates $(x^\rho, x'^\rho) \in \mathbb{R}^{n+1}$. We can

[6]Here we write $\tau_\nu(\mathsf{x})$ to represent the value of τ_ν when the center of mass of detector ν is in the same leaf (of the Fermi-Walker foliation where the spacetime smearing factorizes as mentioned in footnote 1) as the spacetime point x.

see that $\boldsymbol{T}$ induces a map between the coordinates of pairs of events $(y^\rho, y'^\rho) \to (x^\rho, x'^\rho)$ through

$$(\varphi, \varphi') \circ \boldsymbol{T}^{-1} \circ (\varphi^{-1}, \varphi'^{-1}), \tag{2.83}$$

i.e., through the composition of $\boldsymbol{T}^{-1}$ with the chart pair (φ, φ'). Specifically, the coordinates (y^ρ, y'^ρ) of the pair of points $(\mathsf{y}, \mathsf{y}')$ are sent to the the coordinates (x^ρ, x'^ρ) of the pair of points $(T_1^{-1}(\mathsf{y}, \mathsf{y}'), T_2^{-1}(\mathsf{y}, \mathsf{y}'))$. Then, for integrals like the ones in Eq. (2.81), we can use the map (2.83) as a "change of variables", as follows[7]

$$\begin{aligned}
\mathcal{A} &= \int \mathrm{d}V \mathrm{d}V' A(\mathsf{y}, \mathsf{y}') \\
&= \int \mathrm{d}^{n+1} y^\rho \, \mathrm{d}^{n+1} y'^\rho \sqrt{g(y^\rho) g'(y'^\rho)} A(y^\rho, y'^\rho) \\
&= \int \mathrm{d}^{n+1} x^\rho \, \mathrm{d}^{n+1} x'^\rho \sqrt{g\big(T_1(x^\rho, x'^\rho)\big)\, g'\big(T_2(x^\rho, x'^\rho)\big)} \\
&\qquad \times |J(x^\rho, x'^\rho)| A\big(\boldsymbol{T}(x^\rho, x'^\rho)\big),
\end{aligned} \tag{2.84}$$

where g and g' are the determinant of the metric in the coordinates defined by φ and φ' respectively. Moreover,

$$J(x^\rho, x'^\rho) = \det\left[\frac{\partial(y^\rho, y'^\rho)}{\partial(x^\sigma, x'^\sigma)}\right] \tag{2.85}$$

is the determinant of the Jacobian matrix of the change of variables. For convenience, let us define

$$\mathfrak{j}(x^\rho, x'^\rho) = \frac{\sqrt{g\big(T_1(x^\rho, x'^\rho)\big)\, g'\big(T_2(x^\rho, x'^\rho)\big)}}{\sqrt{g(x^\rho) g'(x'^\rho)}} |J(x^\rho, x'^\rho)|, \tag{2.86}$$

Notice that $\mathfrak{j}(x^\rho, x'^\rho)$ is invariant under changes of coordinates. Therefore, we can write Eq. (2.84) in an explicitly coordinate independent way,

$$\mathcal{A} = \int \mathrm{d}V \mathrm{d}V' \, \mathfrak{j}(\mathsf{x}, \mathsf{x}') A\big(\boldsymbol{T}(\mathsf{x}, \mathsf{x}')\big). \tag{2.87}$$

Now, consider a different integral,

$$\mathcal{B} = \int \mathrm{d}V \mathrm{d}V' B(\mathsf{x}, \mathsf{x}'). \tag{2.88}$$

[7]Notice that when we replace a function of points in spacetime $A(\mathsf{x}, \mathsf{x}')$ by $A(x^\rho, x'^\rho)$ we are abusing notation and what we actually mean is $A(\mathsf{x}, \mathsf{x}') = A(\varphi^{-1}(x^\rho), \varphi'^{-1}(x'^\rho)) \equiv A(x^\rho, x'^\rho)$.

Then, observe that in order to impose the condition $|\mathcal{A}| = |\mathcal{B}|$ it is sufficient to find a constant angle θ such that

$$\mathfrak{j}(\mathsf{x},\mathsf{x}')A\big(\boldsymbol{T}(\mathsf{x},\mathsf{x}')\big) = e^{\mathrm{i}\theta}B(\mathsf{x},\mathsf{x}'). \tag{2.89}$$

Applying this result to our condition in Eq. (2.81), we obtain the following theorem.

Theorem 1. *Consider any transformation $\boldsymbol{T} = (T_1, T_2)$ that acts on two copies of the spacetime M, as in equation (2.82). Let P_{A} and P_{B} be given by equation (2.80).*

Assume there is a constant angle θ such that

$$\frac{P^*_{\mathrm{A}}\big(T_1(\mathsf{x},\mathsf{x}')\big)P^*_{\mathrm{B}}\big(T_2(\mathsf{x},\mathsf{x}')\big)G_{\mathrm{F}}\big(\boldsymbol{T}(\mathsf{x},\mathsf{x}')\big)\mathfrak{j}(\mathsf{x},\mathsf{x}')}{P_{\mathrm{A}}(\mathsf{x})P_{\mathrm{B}}(\mathsf{x}')G_{\mathrm{F}}(\mathsf{x},\mathsf{x}')} = e^{\mathrm{i}\theta}. \tag{2.90}$$

Then, $|\mathcal{M}| = |\mathcal{M}_{G^*_F}|$, and therefore by Proposition 2,

$$|\mathcal{M}| = \sqrt{|\mathcal{M}^+|^2 + |\mathcal{M}^-|^2}. \tag{2.91}$$

Which means that $\cos\Delta\gamma = 0$ in Eq. (2.66) and that, in particular, the contributions of communication and preexisting field correlations cannot interfere destructively.

It turns out that we can simplify the condition expressed by Eq. (2.90) if, for a given spacetime and field configuration, $\mathfrak{j}(\mathsf{x},\mathsf{x}') = 1$ and the map $\boldsymbol{T}$ preserves the Feynman propagator. This simplification is detailed in the following Corollary.

Corollary 1. *Assume that the map $\boldsymbol{T} = (T_1, T_2)$ satisfies*

$$\begin{aligned} &g\big(T_1(x^\rho, x'^\rho)\big)\, g'\big(T_2(x^\rho, x'^\rho)\big)|J(x^\rho, x'^\rho)|^2 = g(x^\rho)g'(x'^\rho),\\ &G_{\mathrm{F}}\big(\boldsymbol{T}(\mathsf{x},\mathsf{x}')\big) = G_{\mathrm{F}}(\mathsf{x},\mathsf{x}'), \end{aligned} \tag{2.92}$$

Then, the condition

$$P^*_{\mathrm{A}}\big(T_1(\mathsf{x},\mathsf{x}')\big)P^*_{\mathrm{B}}\big(T_2(\mathsf{x},\mathsf{x}')\big) = e^{\mathrm{i}\theta}P_{\mathrm{A}}(\mathsf{x})P_{\mathrm{B}}(\mathsf{x}'), \tag{2.93}$$

with θ some constant, becomes sufficient to have

$$|\mathcal{M}| = \sqrt{|\mathcal{M}^+|^2 + |\mathcal{M}^-|^2}. \tag{2.94}$$

In order to apply this result to physical situations, it will be helpful to further simplify this corollary when certain symmetries are present in the detector dynamics. Several of these possible symmetries are explored in Appendix A.3. From there, we derive that in many cases, which happen to frequently appear in the literature, communication and field correlations must "collaborate" to generate entanglement between detectors. Moreover, this collaboration happens in the very specific way described by Eq. (2.94). Concretely, in Appendix A.3 we provide conditions on the particle detectors, field, and spacetime of entanglement harvesting setups so that Eq. (2.94) holds. It is important to have in mind that these conditions are only *sufficient* to force $\cos\Delta\gamma = 0$ and, in turn, to rule out destructive interference. Nonetheless, as we shall see in the next section, it is easy to find setups even with fully constructive interference ($\Delta\gamma = 0$) or fully destructive interference ($\Delta\gamma = \pi$) just by violating these conditions. Therefore, even if these conditions are not necessary, they seem to be present in all cases that we know of where Eq. (2.94) holds. For conciseness, the following proposition presents a simplified version of these conditions, which will guide the exploration of harvesting setups in the next section.

Proposition 3. *Consider entanglement harvesting setups where*

1. *Spacetime is flat.*
2. *The field is initially prepared in the Minkowski vacuum, and the detectors start both in their ground state or both in their excited state.*
3. *The detectors are inertial and comoving.*
4. *Spacetime smearings are separable in the detectors' comoving frame, i.e.,* $\Lambda_\nu(t,\boldsymbol{x}) = \chi_\nu(t)F_\nu(\boldsymbol{x})$.
5. *The proper energy gaps are equal,* $\Omega_{\text{A}} = \Omega_{\text{B}}$.
6. *In the comoving frame, for some time* t_{R}*, it is satisfied that either*

$$\chi_\nu(t+t_{\text{R}}) = \chi_\nu(t_{\text{R}}-t),\ \ \nu = A, B, \tag{2.95}$$
$$\text{or}\ \ \chi_{\text{A}}(t+t_{\text{R}}) = \chi_{\text{B}}(t-t_{\text{R}}). \tag{2.96}$$

Then, the following relationship holds,

$$|\mathcal{M}| = \sqrt{|\mathcal{M}^+|^2 + |\mathcal{M}^-|^2}. \tag{2.97}$$

The reader familiar with entanglement harvesting will likely recognize these conditions as being satisfied for many cases analyzed in previous literature. Therefore, very often we see this kind of "collaboration" between the communication-assisted term and the genuine harvesting term when it comes to detectors getting entangled while they are in causal contact.

For the harvesting setups specified by this proposition, fulfilling either Eq. (2.95) or Eq. (2.96) makes the setup symmetric under a certain map $\boldsymbol{T}$ in the way described by Corollary 1. When Eq. (2.95) holds, the setup becomes symmetric under the following time reversal around t_{R},

$$\boldsymbol{T}(t_{\mathrm{R}}+t,\boldsymbol{x},t_{\mathrm{R}}+t',\boldsymbol{x}')=(t_{\mathrm{R}}-t,\boldsymbol{x},t_{\mathrm{R}}-t',\boldsymbol{x}'), \tag{2.98}$$

where the coordinates are chosen to be the standard Minkowski coordinates. Similarly, when Eq. (2.96) holds, the setup becomes symmetric under a different time reversal around t_{R} which also includes a time coordinate swap,

$$\boldsymbol{T}(t_{\mathrm{R}}+t,\boldsymbol{x},t_{\mathrm{R}}+t',\boldsymbol{x}')=(t_{\mathrm{R}}-t',\boldsymbol{x},t_{\mathrm{R}}-t,\boldsymbol{x}'). \tag{2.99}$$

The reasons for why the whole setup is symmetric are that, first, Minkowski spacetime and the corresponding vacuum are symmetric under time reversal at all times, allowing t_{R} to have an arbitrary value. Second, the conditions over the initial states of the detectors, their trajectories, gaps, and switching functions are sufficient to ensure that the field-detector interactions are time reversal symmetric around some t_{R}. The details of how Proposition 3 guarantees Corollary 1 are provided in Appendices A.3, A.4 and A.5. Appendix A.6 shows three more general versions of Proposition 3 for arbitrary harvesting setups that follow the covariant prescription of [90].

In summary, the symmetries in Proposition 3 forbid destructive interference. However, it is not difficult to think of physical scenarios where these symmetries are violated. We will illustrate this in the next section, where we will show scenarios with both destructive interference and stronger constructive interference than those described by Proposition 3.

2.6 Entanglement through communication and harvesting can interfere destructively

In this section, we will present concrete examples both for detectors in Minkowski spacetime and in cosmological scenarios where the assumptions of Proposition 3 (and their

generalizations to cosmological spacetimes) are not satisfied. Concretely, we will analyze scenarios where both the communication-assisted and genuine harvesting contributions to negativity will be greater than the actual negativity acquired by the detectors, showing a destructive interference between the communication contribution to entanglement and the entanglement acquired through harvesting. Moreover, most cases previously studied in the literature satisfy the conditions of Proposition 3 and therefore the two contributions to entanglement while in causal contact were constructively interfering in a particular way, satisfying

$$|\mathcal{M}| = \sqrt{|\mathcal{M}^{+}|^2 + |\mathcal{M}^{-}|^2}. \tag{2.100}$$

However, we will see that it is possible to find scenarios where $|\mathcal{M}|$ is actually larger than (2.100) (strong constructive interference) and cases where it is less than (2.100) (destructive interference). This showcases that most of the setups previously studied in the literature are in a very particular middle ground between constructive and destructive interference of communication and harvesting.

2.6.1 Examples in Minkowski spacetime

First, let us consider two detectors in 3 + 1 Minkowski spacetime. We adopt coordinates $x^{\rho} = (t, \boldsymbol{x})$ where the metric reads

$$\mathrm{d}s^2 = -\mathrm{d}t^2 + \mathrm{d}\boldsymbol{x}^2. \tag{2.101}$$

As usual for two inertial comoving detectors, we will assume that the localization of both detectors A and B is given by spacetime smearing functions which can be split into a switching and spatial smearing in the coordinates $(t, \boldsymbol{x})$, i.e, $\Lambda_{\nu}(\mathsf{x}) = \chi_{\nu}(t)F_{\nu}(\boldsymbol{x})$. More concretely, we assume that the detectors' centers of mass follow inertial trajectories described by $\boldsymbol{z}_{\mathrm{A}}(t) = \boldsymbol{x}_{\mathrm{A}}$ and $\boldsymbol{z}_{\mathrm{B}}(t) = \boldsymbol{x}_{\mathrm{B}}$, where $\boldsymbol{x}_{\mathrm{A}}$ and $\boldsymbol{x}_{\mathrm{B}}$ are constant 3-vectors. We will assume that both detectors start in their respective ground states and that the state of the field is initially prepared in the Minkowski vacuum, the expressions for $\mathcal{L}_{\mu\nu}$ and $\mathcal{M}$ (see Eqs. (2.53) and (2.54)) can be written in the following form (with $\Omega_{\mathrm{A}} = \Omega_{\mathrm{B}} = \Omega$):

$$\begin{aligned}
\mathcal{L}_{\mu\nu} &= \frac{\lambda^2}{2(2\pi)^3} \int \mathrm{d}t\mathrm{d}t' e^{-\mathrm{i}\Omega(t-t')} \chi_{\mu}(t)\chi_{\nu}(t') K_{\mu\nu}(t,t'), \\
\mathcal{M} &= -\frac{\lambda^2}{2(2\pi)^3} \int_{-\infty}^{\infty} \mathrm{d}t \int_{-\infty}^{t} \mathrm{d}t'\; Q_{\mathrm{AB}}(t,t').
\end{aligned} \tag{2.102}$$

Where we have defined the auxiliary functions

$$Q_{\mathrm{AB}}(t,t') = e^{\mathrm{i}\Omega(t+t')} K_{\mathrm{AB}}(t,t') \left(\chi_{\mathrm{A}}(t)\chi_{\mathrm{B}}(t') + \chi_{\mathrm{A}}(t')\chi_{\mathrm{B}}(t)\right), \tag{2.103}$$

$$K_{\mu\nu}(t,t') = 2(2\pi)^3 \int \mathrm{d}^3\boldsymbol{x}\mathrm{d}^3\boldsymbol{x}' F_\mu(\boldsymbol{x})F_\nu(\boldsymbol{x}')W(t,\boldsymbol{x};t',\boldsymbol{x}'). \tag{2.104}$$

To follow a common choice in the literature, for the spatial smearing function, we take a Gaussian profile, namely

$$F_\nu(\boldsymbol{x}) = \frac{1}{(\sqrt{\pi}\sigma)^3} e^{-\frac{1}{2}\left(\frac{|\boldsymbol{x}-\boldsymbol{x}_\nu|}{\sigma}\right)^2}. \tag{2.105}$$

For this particular choice of smearing (2.104) simplifies to

$$K_{\mu\nu}(t,t') = \int \frac{\mathrm{d}\boldsymbol{k}^3}{|\boldsymbol{k}|} e^{\mathrm{i}\boldsymbol{k}\cdot(\boldsymbol{x}_\mu-\boldsymbol{x}_\nu)} e^{-|\boldsymbol{k}|^2\sigma^2} e^{-\mathrm{i}|\boldsymbol{k}|\Delta t}. \tag{2.106}$$

Notice that in the equation for $\mathcal{M}$, the Heaviside theta function that appears in the definition of the Feynman propagator, Eq. (2.58), is implemented as a nested integral in the time variable t. To evaluate Eq. (2.106), we will consider separately the cases $\mu = \nu$ (same detectors) and $\mu \neq \nu$ (different detectors). First, for $\mu \neq \nu$, we have $K_{\mathrm{AB}}(t,t') = K_{\mathrm{BA}}(t,t')$, which evaluates to

$$K_{\mathrm{AB}}(t,t') = \frac{2\pi\mathrm{i}}{d}\left[\mathcal{I}(\Delta t + d) - \mathcal{I}(\Delta t - d)\right]. \tag{2.107}$$

Here, $\Delta t = t - t'$, $d = |\boldsymbol{x}_{\mathrm{A}} - \boldsymbol{x}_{\mathrm{B}}|$, and

$$\mathcal{I}(z) = \frac{\sqrt{\pi}}{2\sigma} e^{-\frac{z^2}{4\sigma^2}} - \frac{\mathrm{i}}{\sigma}\mathcal{D}\left(\frac{z}{2\sigma}\right), \tag{2.108}$$

where $\mathcal{D}(x) = \frac{\sqrt{\pi}}{2}e^{-x^2}\operatorname{erfi} x$ is the Dawson function[8]. For $\mu = \nu$, we have

$$K_{\nu\nu}(t,t') = \frac{2\pi}{\sigma^2}\left[1 - \frac{\Delta t}{\sqrt{2}\sigma}\left(\mathrm{i}\sqrt{\frac{\pi}{2}}e^{-\frac{\Delta t^2}{4\sigma^2}} + \sqrt{2}\mathcal{D}\left(\frac{\Delta t}{2\sigma}\right)\right)\right]. \tag{2.110}$$

Finally, the term $\mathcal{M}^-$ associated with signalling can be written as

$$\mathcal{M}^- = -\frac{\lambda^2}{2(2\pi)^3}\int_{-\infty}^{\infty}\mathrm{d}t\int_{-\infty}^{t}\mathrm{d}t'\; Q^-_{\mathrm{AB}}(t,t'). \tag{2.111}$$

[8]The Dawson function is defined as

$$\mathcal{D}(x) \coloneqq e^{-x^2}\int_0^x \mathrm{d}y\, e^{-y^2}. \tag{2.109}$$

Here, the only difference between $Q^{-}_{\mathrm{AB}}(t,t')$ and $Q_{\mathrm{AB}}(t,t')$ is the replacement $K_{\mathrm{AB}}(t,t') \to K^{-}_{\mathrm{AB}}(t,t')$, where

$$K^{-}_{\mathrm{AB}}(t,t') = \frac{\pi^{3/2}\mathrm{i}}{\sigma d}\left[e^{-\frac{(\Delta t+d)^2}{4\sigma^2}} - e^{-\frac{(\Delta t-d)^2}{4\sigma^2}}\right]. \tag{2.112}$$

To proceed with the numerical evaluation of all the relevant terms, we need to define an expression for the switching function of the detectors. Notice that, in the current setup, conditions 1 through 5 of Proposition 3 are satisfied. Therefore, to create a numerical scenario where the conditions of the proposition are not satisfied we need to pick a switching function that violates condition 6. For this, we can employ switchings that contradict both equation (2.95) and equation (2.96). One way to achieve this is by making the switching functions asymmetric. In particular, we are going to choose skew-normal distributions [97], namely

$$S(t;\alpha) = N(\alpha)e^{-\frac{t^2}{T^2}}\left(1+\mathrm{erf}\left(\frac{\alpha t}{T}\right)\right). \tag{2.113}$$

Here, $N(\alpha)$ stands for a dimensionless normalization factor that ensures that the maximum value of $S(t;\alpha)$ is 1. Denoting by $t_{\max}(\alpha)$ the point such that $S(t_{\max}(\alpha);\alpha) = 1$, we can define the switchings for $j = \mathrm{A},\mathrm{B}$ as follows:

$$\chi_\nu(t;\alpha) = S(t - t_{\max}(\alpha) - t_\nu). \tag{2.114}$$

In this way, we ensure that the maximum of the switching happens at $t = t_\nu$ (see figure 2.3).

Using the switching of Eq. (2.114), we numerically evaluated the expressions for $\mathcal{M}$, $\mathcal{M}^{\pm}$ and $\mathcal{L}_{\nu\nu}$, thus obtaining results for the negativity $\mathcal{N}$ and the two contributions $\mathcal{N}^{\pm}$.

We display in Figure 2.4 different regimes where the conditions in Eqs. (2.95) and (2.96) are not fulfilled and the interference between $\mathcal{M}^{+}$ and $\mathcal{M}^{-}$ affects the detectors' ability to become entangled in different ways. In Fig. 2.4 we present side-to-side results for the case of asymmetric switching functions ($\alpha = 2.35$, left column) and symmetric Gaussian switching ($\alpha = 0$, right column). Figures 2.4a and 2.4b show $|\mathcal{M}|$ and $|\mathcal{M}^{\pm}|$, Figures 2.4c and 2.4d show the relative phases between $\mathcal{M}^{+}$ and $\mathcal{M}^{-}$, and Figures 2.4e and 2.4f show $\mathcal{N}$ and $\mathcal{N}^{\pm}$.

Specifically, in the case $\alpha = 2.35$ (see Figures 2.4a, 2.4c, 2.4e), there exists a range of values of $\Delta t = t_{\mathrm{B}} - t_{\mathrm{A}}$ that causes the communication-assisted negativity $\mathcal{N}^{-}$ to exceed the negativity itself. Moreover, we have identified values of Δt where $\mathcal{N}^{-}$ is non-zero even though $\mathcal{N} = 0$.

For $\alpha = 0$, condition 6 of Proposition 3 is met, so Eq. (2.97) holds. This means the relative phase between $\mathcal{M}^{+}$ and $\mathcal{M}^{-}$ is $\pm\pi/2$, leading to constructive interference. In

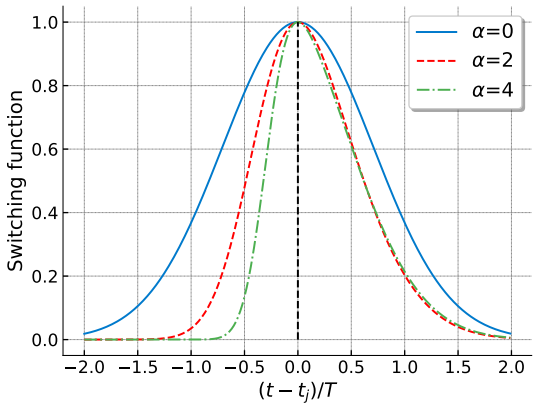


Figure 2.3: Non-symmetric switching function for different values of the asymmetry parameter α.

contrast, for $\alpha = 2.35$, there are regions with destructive and constructive interference. Moreover, notice that the constructive interference gets stronger than in the $\pm\pi/2$ relative phase scenario.

Another way of violating condition 6 of Proposition (3) is to use different shapes for the switching functions of each detector. Indeed, by choosing Gaussian switchings of different widths we can violate the condition in Eq. (2.97). Namely, we can choose

$$\chi_\nu(t) = e^{-\left(\frac{t-t_\nu}{T_\nu}\right)^2}, \tag{2.115}$$

with $T_{\mathrm{A}} \neq T_{\mathrm{B}}$.

We illustrate the case of switching with two different widths in Figures 2.5 and 2.6. We see that there is an asymmetry in how the detectors are entangled depending on which detector switches on first, with an advantage when $\Delta t > 0$ (the detector with shorter switching time (A) couples to the field before the detector with a longer switching time (B)). However, we note that the contributions to negativity, $\mathcal{N}^+$, and $\mathcal{N}^-$, do not depend on the order of coupling. This means that the asymmetry of the negativity with respect to Δt is due to interference alone because of how the relative phases change depending on which detector couples first.

Concretely, when detector B couples first ($\Delta t < 0$) the interference is destructive, reducing the extracted entanglement. Conversely, when A couples first ($\Delta t > 0$) we have constructive interference between the two contributions, with an effect even stronger than

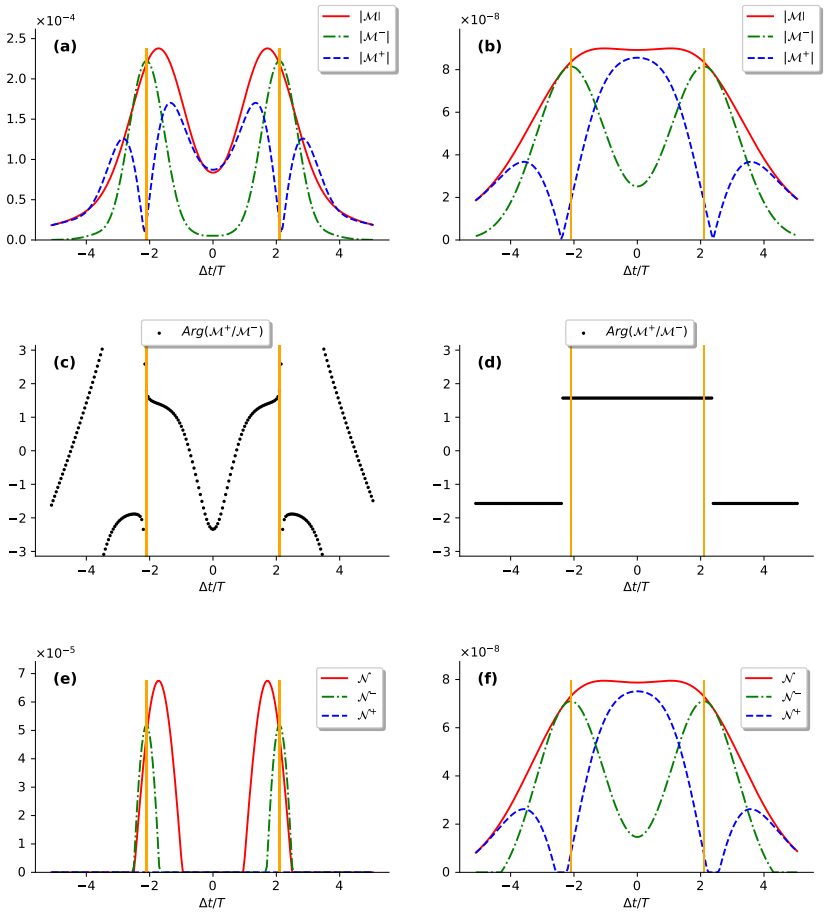


Figure 2.4: Results for an entanglement harvesting setup in Minkowski spacetime with non-symmetric switchings. The physical parameters used are: $\Omega T = 5$, $d/T = 2.1$, and $\sigma/T = 0.3$. In the horizontal axis, we have $\Delta t = t_{\mathrm{B}} - t_{\mathrm{A}}$. The solid vertical lines (yellow) represent the lightcones. Figures (a), (c), and (e) correspond to the case $\alpha = 2.35$, whereas Figures (b), (d), and (f) display the case $\alpha = 0$, where we have the standard Gaussian switching. The appearance of an even symmetry with respect to Δt in the plots is explained by Appendix A.7.

that in Eq. (2.100). Hence, in a configuration with a different switching duration in each detector, maximizing entanglement requires carefully timing the detectors' interactions to avoid the adverse effects of destructive interference.

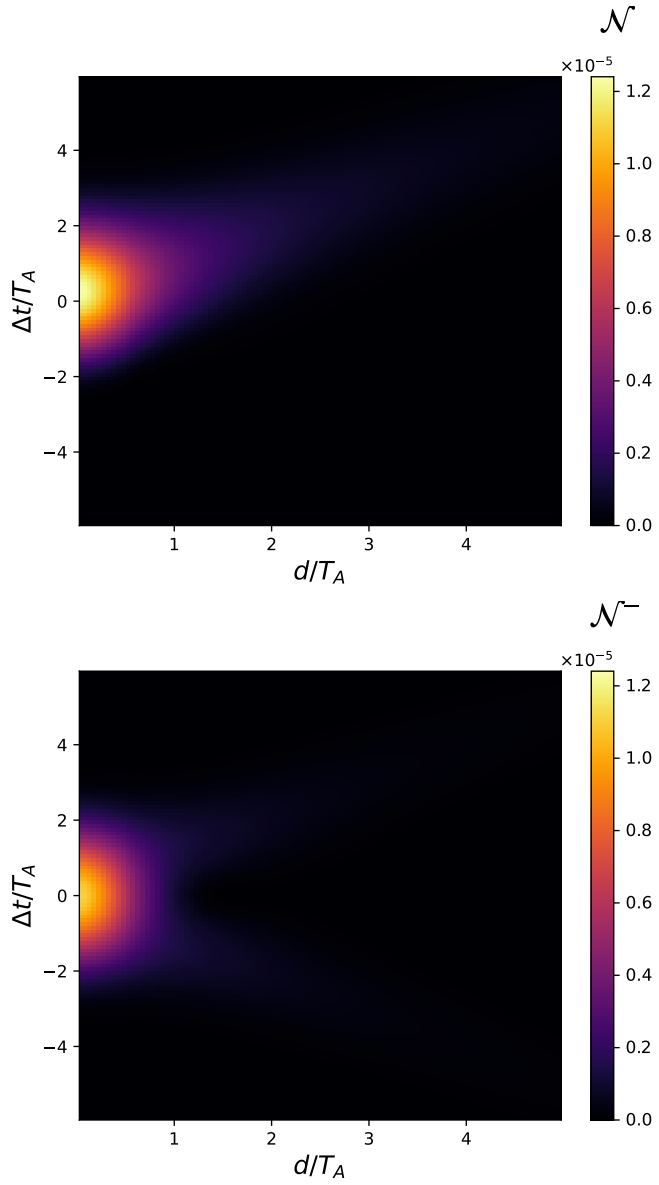


Figure 2.5: Numerical results for the negativity (top) and the communication-assisted negativity (bottom) as a function of the proper time d between the centers of the detectors and the time delay Δt between the centers of the switchings. The entanglement harvesting setup is in Minkowski spacetime with Gaussian switchings of different length scales, and the physical parameters used are: $\Omega T_{\mathrm{A}} = 4$, $\sigma/T_{\mathrm{A}} = 0.2$, and $T_{\mathrm{B}}/T_{\mathrm{A}} = 1.3$.

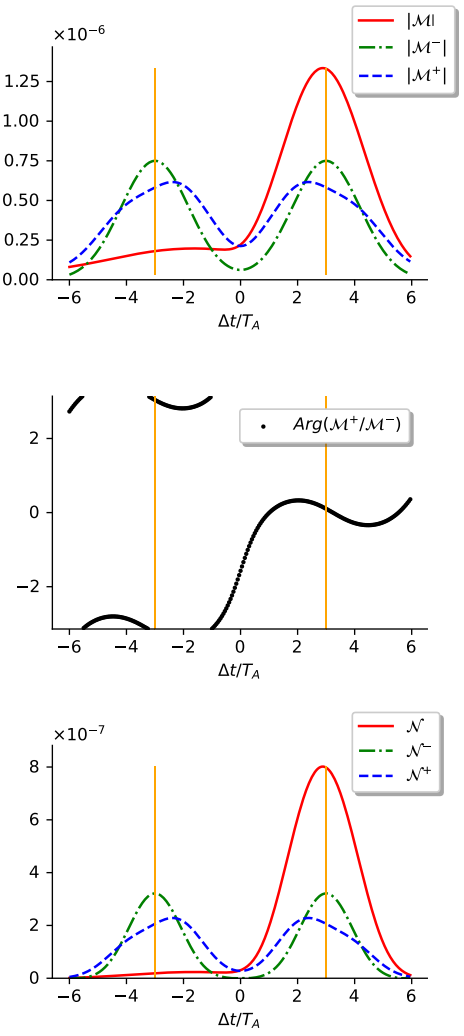


Figure 2.6: Correlations ($\mathcal{M}$) and negativity ($\mathcal{N}$), divided into harvested ($\mathcal{M}^+, \mathcal{N}^+$) and communication ($\mathcal{M}^-, \mathcal{N}^-$) components as a function of the time delay Δt between the switchings. The harvesting setup is in Minkowski spacetime, with Gaussian switchings with different time scales, and the physical parameters used are: $\Omega T_{\mathrm{A}} = 4$, $d/T = 3$, $\sigma/T_{\mathrm{A}} = 0.2$, and $T_{\mathrm{B}}/T_{\mathrm{A}} = 1.3$. The reason for the symmetries with respect to the sign of Δt are explained in Appendix A.7.

2.6.2 Example in a cosmological spacetime

By working in a spacetime that has no time-reversal symmetry, we can also construct an entanglement harvesting setup where the interference between the contributions from field correlations and communication violate condition (2.97). As a particular example, we shall consider a spatially flat FRW spacetime, a setting where entanglement harvesting has been studied in the past (see, e.g., [98]). In comoving coordinates $(t, \boldsymbol{x}) = (t, x, y, z)$ the line element reads

$$\mathrm{d}s^2 = -\mathrm{d}t^2 + a(t)^2(\mathrm{d}x^2 + \mathrm{d}y^2 + \mathrm{d}z^2). \tag{2.116}$$

Or, introducing a new time coordinate η

$$\eta(t) = \int_0^t \mathrm{d}t' \frac{1}{a(t')}, \tag{2.117}$$

we explicitly reveal the conformally flat nature of the metric:

$$\mathrm{d}s^2 = -a(\eta)^2(\mathrm{d}t^2 + \mathrm{d}x^2 + \mathrm{d}y^2 + \mathrm{d}z^2). \tag{2.118}$$

We now consider a scalar quantum field $\hat{\phi}$ conformally coupled to curvature so that the field satisfies Eq. (2.39) with $\xi = \frac{1}{6}$. In this case, it can be shown (see, e.g., [99]) that the field $\hat{\psi}(\mathsf{x}) = a(\eta)\hat{\phi}(\mathsf{x})$ satisfies the Minkowski Klein-Gordon equation. Therefore, the field modes of $\hat{\phi}(\mathsf{x})$ and the Wightman function $W(\mathsf{x}, \mathsf{x}')$ for this case can be obtained from the ones from the Minkowski case by simply introducing additional multiplicative scale factors $a(\eta)$.

Now, in order to concretely find setups where the interference between $\mathcal{M}^+$ and $\mathcal{M}^-$ leads to a novel behavior of the negativity, the guiding principle will be the violation of a more general version of Proposition 3 that applies to FRW spacetimes. As demonstrated in Appendix A.5.2, we can derive the following proposition:

Proposition 4. *Consider entanglement harvesting setups where*

1. *Spacetime is FRW as in Eq. (2.116).*
2. *The scale factor satisfies* $a(t+t_{\mathrm{R}}) = a(t_{\mathrm{R}}-t)$.
3. *Both detectors are comoving with the Hubble flow and are initially both in the ground state or both in the excited state.*
4. *The field is massless, conformally coupled to curvature, and initially in the conformal vacuum.*
5. *Spacetime smearings factorize in the comoving frame as the product of a function of only time and a function of only space, i.e.,* $\Lambda_j(t,\boldsymbol{x}) = \mathfrak{T}_j(t)\mathfrak{X}_j(\boldsymbol{x})$.
6. *The proper energy gaps are equal,* $\Omega_{\mathrm{A}} = \Omega_{\mathrm{B}}$.
7. *In the comoving frame, for some time* t_{R}*, it is satisfied that either*

$$\mathfrak{T}_j(t+t_{\mathrm{R}}) = \mathfrak{T}_j(t_{\mathrm{R}}-t),\ \ j=A,B, \tag{2.119}$$
$$\text{or}\ \ \mathfrak{T}_{\mathrm{A}}(t+t_{\mathrm{R}}) = \mathfrak{T}_{\mathrm{B}}(t-t_{\mathrm{R}}). \tag{2.120}$$

Then, the following relationship holds,

$$|\mathcal{M}| = \sqrt{|\mathcal{M}^{+}|^2 + |\mathcal{M}^{-}|^2}. \tag{2.121}$$

Assuming that the initial state of the field is the conformal vacuum and that the detectors both start in their respective ground states, the terms $\mathcal{L}_{\mu\nu}$, $\mathcal{M}$ and $\mathcal{M}^{-}$ will be given by the same equations (2.102) and (2.111) under the replacement

$$\mathrm{d}t\mathrm{d}t' \to \frac{\mathrm{d}t\mathrm{d}t'}{a(t)a(t')}. \tag{2.122}$$

In the auxiliary functions $K_{\mathrm{AB}}(t,t')$ and $K_{\nu\nu}(t,t')$ of equations 2.107 and (2.110), we also need to perform the replacement $\Delta t = t-t' \to \Delta\eta = \eta(t)-\eta(t')$. Therefore, the numerical methods applied to compute $\mathcal{N}$ in the subsection 2.6.1 and all associated terms transition smoothly to this case. All that remains is to specify a particular example of FRW spacetime and choose the shape and switching functions to model our detectors. As a concrete

example let us choose the scale factor to be that of De Sitter spacetime:

$$a(t) = e^{Ht}. \tag{2.123}$$

As for the detectors, let us choose both the switchings and the spatial smearing functions to be Gaussians. That is, the functions $\chi_\nu(t)$ will be given by

$$\chi_\nu(t) = e^{-\left(\frac{t-t_\nu}{T}\right)^2}. \tag{2.124}$$

The smearing functions $F_\nu(t, \boldsymbol{x})$ are given by

$$F_\nu(t, \boldsymbol{x}) = \frac{1}{(\sqrt{2\pi}\sigma a(t))^3} e^{-\frac{1}{2}\left(\frac{|\boldsymbol{x}-\boldsymbol{x}_\nu|}{\sigma}\right)^2}. \tag{2.125}$$

where the detector expands with the expansion of the universe and the scale factor in the denominator comes from the L^1 normalization of the smearing function:

$$\int \mathrm{d}\boldsymbol{x}^3 a(t)^3 F_\nu(\boldsymbol{x}, t_0) = 1. \tag{2.126}$$

Notice that even if we choose

$$\mathfrak{T}_\nu(t) = a(t)^{-3}\chi_\nu(t), \tag{2.127}$$
$$\mathfrak{X}_\nu(\boldsymbol{x}) = a(t)^3 F_\nu(t, \boldsymbol{x}). \tag{2.128}$$

to ensure consistency with assumption 5 of Proposition 4, it is clear that the form of the expansion factor, Eq. (2.123) automatically leads to the violation of the conditions expressed by Eqs. (2.119) and (2.120). Therefore, in the present setup, we have no guarantee that the relation (2.121) holds.

A particular case of this kind of setup is displayed in Figure 2.7. Analogously to the instances examined in the Minkowski case, it is observed that the components $\mathcal{M}^\pm$ exhibit interference, leading to scenarios where the communication-mediated negativity surpasses the total negativity. Additionally, around the region $\Delta t/T = 0$, we observe that the harvested negativity ($\mathcal{N}^+$) can also exceed the value of the negativity ($\mathcal{N}$). This means that despite the detectors' capability to extract preexisting correlations from the field, the entanglement acquired through communication destructively interferes with the harvested entanglement, resulting in the overall entanglement being less than each component individually.

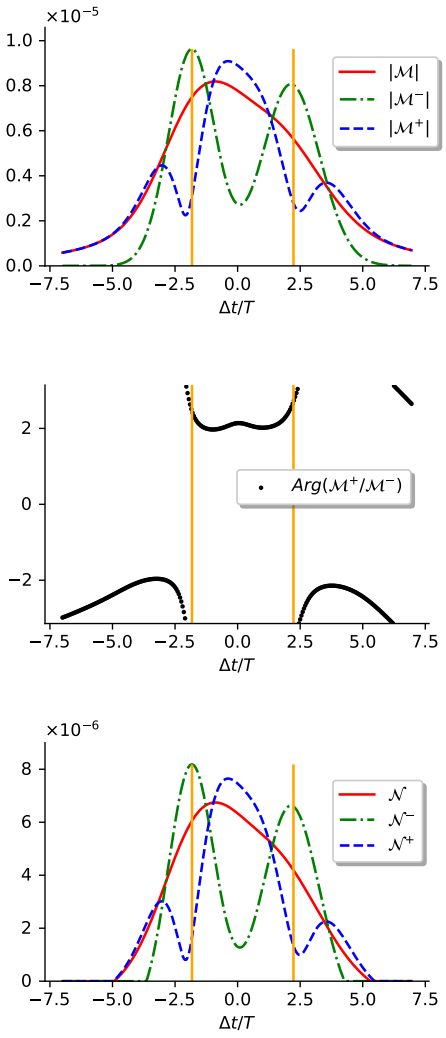


Figure 2.7: Numerical results for De Sitter spacetime. The parameters used are: $\Omega T = 4$, $d/T = 2$, $\sigma/T = 0.1$, and $H = 0.1$. Here, $\Delta t = t_{\rm B} - t_{\rm A}$

Chapter 3

Harvesting entanglement with general couplings: longitudinal and transversal components

In this chapter, we reach the peak of the progression of this thesis towards increasingly general entanglement harvesting protocols of two detectors. This progression started with an entanglement harvesting protocol for derivative coupling in flat spacetime in section 2.1 and then continued with a more general protocol for harvesting in curved spacetimes in section 2.4. In this chapter, we forgo the assumption of the detectors being qubits, and allow instead an arbitrary number of detector energy levels. Moreover, particle detectors usually have simple couplings, such as the product of the monopole operator and field operator depicted in the Unruh-DeWitt model of Eq. (2.43). These couplings are useful to obtain clear and concise results. However, these simplifying choices lack the flexibility to accommodate the range of couplings that appear in implementations of entanglement harvesting in superconducting circuits. To surpass this limitation, we allow to couple general operators of the detectors to field operators. Furthermore, we split the coupling into longitudinal and transversal parts with respect to a preferred detector basis, and analyze the contributions of these two parts to entanglement harvesting. Throughout this chapter, $\hbar = c = 1$ is assumed.

Note of clarification. A version of this chapter will appear in an upcoming paper [1], which is currently a work in progress.

3.1 Entanglement harvesting separating the contributions of longitudinal and transversal interactions

In this section, we provide a general entanglement harvesting protocol, where a pair of arbitrary detectors couple to a real scalar quantum field. We consider a general form of coupling, which we then split into longitudinal and transversal parts, which contribute differently to the entanglement detectors can harvest. This split allows us to provide analytical expressions for the time evolution for detectors without transversal coupling. Then, we perturbatively add back the transversal interaction, to obtain the time evolution for general interactions. Therefore, in the obtained expressions, the longitudinal coupling is included non-perturbatively and the transversal coupling is included up to second order.

Consider the following interaction Hamiltonian in the interaction picture,

$$\hat{H}_{\mathrm{I}}(t) = \sum_{\nu} \hat{\lambda}^{\nu}(t)\hat{\phi}^{\alpha^{\nu}}(t). \tag{3.1}$$

Here, $\hat{\lambda}^{\nu}$ are arbitrary Hermitian operators of the detector $\nu \in \{A, B\}$. Moreover, $\hat{\phi}^{\alpha^{\mathrm{A}}}$ and $\hat{\phi}^{\alpha^{\mathrm{B}}}$ are Hermitian operators of the field, defined through the following notation,

$$\hat{\phi}^{\alpha}(t) = \mathrm{i}\int_{\mathbb{R}^n} \mathrm{d}^n\boldsymbol{k}\, \alpha(t,\boldsymbol{k})\hat{a}^{\dagger}_{\boldsymbol{k}} - \alpha^{*}(t,\boldsymbol{k})\hat{a}_{\boldsymbol{k}}. \tag{3.2}$$

The creation and annihilation operators $\hat{a}^{\dagger}_{\boldsymbol{k}}$ and $\hat{a}_{\boldsymbol{k}}$ satisfy the canonical commutation relations $[\hat{a}_{\boldsymbol{k}}, \hat{a}^{\dagger}_{\boldsymbol{k}'}] = \delta(\boldsymbol{k}-\boldsymbol{k}')\hat{\mathbb{1}}$.

For example, in flat spacetime, the field amplitude operator can be expanded in plane waves as follows,

$$\hat{\phi}(t,\boldsymbol{x}) = \int_{\mathbb{R}^n} \frac{\mathrm{d}^n\boldsymbol{k}}{\sqrt{2(2\pi)^n\omega_{\boldsymbol{k}}}}\Big(e^{\mathrm{i}(\omega_{\boldsymbol{k}}t-\boldsymbol{k}\cdot\boldsymbol{x})}\hat{a}^{\dagger}_{\boldsymbol{k}} + e^{\mathrm{i}(\boldsymbol{k}\cdot\boldsymbol{x}-\omega_{\boldsymbol{k}}t)}\hat{a}_{\boldsymbol{k}}\Big), \tag{3.3}$$

where $\omega_{\boldsymbol{k}} = \sqrt{m^2+|\boldsymbol{k}|^2}$, with m the mass of the field. Notice that $\hat{\phi}(t,\boldsymbol{x})$ can be rewritten in terms of the notation prescribed in Eq. (3.2),

$$\hat{\phi}(t,\boldsymbol{x}) = \hat{\phi}^{u_{\boldsymbol{x}}}(t), \quad u_{\boldsymbol{x}}(t,\boldsymbol{k}) = \frac{e^{\mathrm{i}(\omega_{\boldsymbol{k}}t-\boldsymbol{k}\cdot\boldsymbol{x})}}{\sqrt{2(2\pi)^n\omega_{\boldsymbol{k}}}}. \tag{3.4}$$

Additionally, smeared field amplitudes, which commonly appear in Unruh-DeWitt (UDW) detector models [26, 27, 28, 29, 30], can be expressed similarly, as shown next. Given a

spatial smearing $F(\boldsymbol{x})$, the corresponding smeared $\hat{\phi}(t,\boldsymbol{x})$ is equal to

$$\int_{\mathbb{R}^n} \mathrm{d}^n\boldsymbol{x}\, F(\boldsymbol{x})\hat{\phi}(t,\boldsymbol{x}) = \hat{\phi}^f(t),$$
$$f(t,\boldsymbol{k}) = \frac{e^{\mathrm{i}\omega_{\boldsymbol{k}}t}\widetilde{F}(-\boldsymbol{k})}{\sqrt{2(2\pi)^n\omega_{\boldsymbol{k}}}}. \tag{3.5}$$

Here, we used the following Fourier transform convention,

$$\widetilde{F}(\boldsymbol{k}) = \int_{\mathbb{R}^n} \mathrm{d}^n\boldsymbol{x}\, e^{\mathrm{i}\boldsymbol{k}\cdot\boldsymbol{x}}F(\boldsymbol{x}). \tag{3.6}$$

Next, we define *longitudinal* and *transversal* with respect to a choice of orthonormal basis for the detectors. A usual choice would be to pick the energy eigenbases of the detectors' free Hamiltonians, but we do not limit ourselves to this choice. Instead, let $\{|i_{\mathrm{A}}\rangle\}$ and $\{|j_{\mathrm{B}}\rangle\}$ be arbitrary orthonormal bases for the detectors A and B, respectively. Then, all operators can be split into longitudinal and transversal parts with respect to these bases. For example,

$$\hat{\lambda}^\nu = \hat{\lambda}^\nu_\parallel + \hat{\lambda}^\nu_\perp, \tag{3.7}$$

by taking the longitudinal part $\hat{\lambda}^\nu_\parallel$ to be the diagonal components of $\hat{\lambda}^\nu$ in the $\{|i_\nu\rangle\}$ basis, and $\hat{\lambda}^\nu_\perp$ being the off-diagonal components. Then, we split the interaction Hamiltonian accordingly,

$$\begin{aligned}
\hat{H}_{\mathrm{I}}(t) &= \hat{H}_\parallel(t) + \hat{H}_\perp(t),\\
\hat{H}_\parallel(t) &= \sum_\nu \hat{\lambda}^\nu_\parallel(t)\hat{\phi}^{\alpha^\nu}(t),\\
\hat{H}_\perp(t) &= \sum_\nu \hat{\lambda}^\nu_\perp(t)\hat{\phi}^{\alpha^\nu}(t).
\end{aligned} \tag{3.8}$$

The advantage of this split is that the longitudinal evolution can be solved analytically using a Magnus expansion, as presented next. Specifically, by longitudinal evolution we mean the evolution without transversal interaction, which is

$$\hat{U}^\parallel(t) = \mathcal{T}\exp\left(-\mathrm{i}\int_{t_\parallel}^t \mathrm{d}t_1\, \hat{H}_\parallel(t_1)\right). \tag{3.9}$$

Here, $\mathcal{T}\exp$ denotes the time-ordered exponential, and the evolution occurs from a time $t_\parallel$ to a time t.

Moreover, we consider

$$\begin{aligned}\hat{\lambda}^{\nu}_{\parallel}(t) &= \lambda^{\nu}_{\parallel}\hat{\chi}^{\nu}_{\parallel}(t),\\ \hat{\lambda}^{\nu}_{\perp}(t) &= \lambda^{\nu}_{\perp}\hat{\chi}^{\nu}_{\perp}(t),\end{aligned} \tag{3.10}$$

where $\lambda^{\nu}_{\parallel}$ and $\lambda^{\nu}_{\perp}$ are parameters that tune the strength of the longitudinal and the transversal interactions, and can be used to perform perturbative expansions. The $\hat{\chi}^{\nu}_{\parallel}(t)$ and $\hat{\chi}^{\nu}_{\perp}(t)$ act as operator versions of switching functions, and include the possibility to turn on and off the interaction independently for different detector energy levels. For simplicity, we consider $\lambda_{\parallel}$ and $\lambda_{\perp}$ to be parameters that govern the longitudinal and transversal coupling strength for both detectors,

$$\begin{aligned}\lambda^{\mathrm{A}}_{\parallel} &= a^{\mathrm{A}}_{\parallel}\lambda_{\parallel}, \quad \lambda^{\mathrm{B}}_{\parallel} = a^{\mathrm{B}}_{\parallel}\lambda_{\parallel},\\ \lambda^{\mathrm{A}}_{\perp} &= a^{\mathrm{A}}_{\perp}\lambda_{\perp}, \quad \lambda^{\mathrm{B}}_{\perp} = a^{\mathrm{B}}_{\perp}\lambda_{\perp},\end{aligned} \tag{3.11}$$

where $a^{\mathrm{A}}_{\parallel}$, $a^{\mathrm{B}}_{\parallel}$, $a^{\mathrm{A}}_{\perp}$, $a^{\mathrm{B}}_{\perp}$ are coefficients of order zero in $\lambda_{\parallel}$, $\lambda_{\perp}$.

3.1.1 Analytic expression for the longitudinal evolution

According to the Magnus expansion,

$$\hat{U}^{\parallel}(t) = e^{\hat{\Omega}(t)}, \quad \hat{\Omega}(t) = \sum_{k=1}^{\infty}\hat{\Omega}_k(t), \tag{3.12}$$

$$\begin{aligned}\hat{\Omega}_1(t) &= -\mathrm{i}\int_{t_{\parallel}}^{t}\mathrm{d}t_1\,\hat{H}_{\parallel}(t_1),\\ \hat{\Omega}_2(t) &= -\frac{1}{2}\int_{t_{\parallel}}^{t}\mathrm{d}t_1\int_{t_{\parallel}}^{t_1}\mathrm{d}t_2\,[\hat{H}_{\parallel}(t_1),\hat{H}_{\parallel}(t_2)],\end{aligned} \tag{3.13}$$

and the $\hat{\Omega}_3$, $\hat{\Omega}_4$, ... are integrals of nested commutators of $\hat{H}_{\parallel}$, which are are zero. These nested commutators are zero because

$$\begin{aligned}[\hat{H}_{\parallel}(t_1),\hat{H}_{\parallel}(t_2)] &= 2\sum_{\mu\nu}\hat{\lambda}^{\mu}_{\parallel}(t_1)\hat{\lambda}^{\nu}_{\parallel}(t_2)W^{\mu\nu-}(t_1,t_2),\\ W^{\mu\nu-}(t_1,t_2) &= \mathrm{i}\int_{\mathbb{R}^n}\mathrm{d}^n\boldsymbol{k}\;\mathrm{Im}\big(\alpha^{\mu *}(t_1,\boldsymbol{k})\alpha^{\nu}(t_2,\boldsymbol{k})\big),\end{aligned} \tag{3.14}$$

and $[\hat{H}_\parallel(t), \hat{\lambda}^\nu_\parallel(t')] = 0$. In order to find Eq. (3.14), we used $[\hat{\lambda}^\mu_\parallel(t_1), \hat{\lambda}^\nu_\parallel(t_2)] = 0$, which holds due to $\hat{\lambda}^\mu_\parallel(t_1)$ and $\hat{\lambda}^\nu_\parallel(t_2)$ being diagonal on the same basis. Moreover, we used Eq. (3.2) to find

$$[\hat{\phi}^{\alpha^\mu}(t_1), \hat{\phi}^{\alpha^\nu}(t_2)] = 2W^{\mu\nu-}(t_1, t_2)\hat{\mathbb{1}}. \tag{3.15}$$

Substituting Eqs. (3.8) and (3.14) into Eq. (3.13),

$$\begin{aligned}
\hat{\Omega}_1(t) &= -\mathrm{i}\sum_\nu \hat{\phi}^{\hat{\beta}^\nu}(t), \\
\hat{\beta}^\nu(t, \boldsymbol{k}) &= \int_{t_\parallel}^t \mathrm{d}t_1\, \hat{\lambda}^\nu_\parallel(t_1)\alpha^\nu(t_1, \boldsymbol{k}), \\
\hat{\Omega}_2(t) &= \sum_{\mu\nu} \hat{\Omega}^{\mu\nu}(t), \\
\hat{\Omega}^{\mu\nu}(t) &= -\int_{t_\parallel}^t \mathrm{d}t_1 \int_{t_\parallel}^{t_1} \mathrm{d}t_2\, \hat{\lambda}^\mu_\parallel(t_1)\hat{\lambda}^\nu_\parallel(t_2)W^{\mu\nu-}(t_1, t_2).
\end{aligned} \tag{3.16}$$

Here, we defined detector controlled field operators,

$$\hat{\phi}^{\hat{\beta}} = \mathrm{i}\int_{\mathbb{R}^n} \mathrm{d}^n\boldsymbol{k}\, \hat{\beta}(\boldsymbol{k})\hat{a}^\dagger_{\boldsymbol{k}} - \hat{\beta}^\dagger(\boldsymbol{k})\hat{a}_{\boldsymbol{k}}, \tag{3.17}$$

where $\hat{\beta}(\boldsymbol{k})$ are detector operators that share a common eigenbasis among all $\boldsymbol{k}$, i.e. $[\hat{\beta}(\boldsymbol{k}), \hat{\beta}(\boldsymbol{k}')] = 0$. Using this definition,

$$\hat{\phi}^{\hat{\beta}^\nu}(t) = \int_{t_\parallel}^t \mathrm{d}t_1\, \hat{\lambda}^\nu_\parallel(t_1)\hat{\phi}^{\alpha^\nu}(t_1). \tag{3.18}$$

Finally, the non-perturbative expression for $\hat{U}^\parallel$ is

$$\hat{U}^\parallel(t) = e^{\hat{\Omega}_2(t)}\hat{D}_{\hat{\beta}^{\mathrm{A}}(t)+\hat{\beta}^{\mathrm{B}}(t)}, \tag{3.19}$$

where the operator $e^{\hat{\Omega}_2(t)}$ acts only on the detectors. Moreover, we defined controlled displacement operators as

$$\hat{D}_{\hat{\beta}} = e^{-\mathrm{i}\hat{\phi}^{\hat{\beta}}}. \tag{3.20}$$

This definition is analogous to displacement operators,

$$\hat{D}_\alpha = e^{-\mathrm{i}\hat{\phi}^\alpha} = \exp\left\{\int_{\mathbb{R}^n} \mathrm{d}^n\boldsymbol{k}\, \alpha(\boldsymbol{k})\hat{a}^\dagger_{\boldsymbol{k}} - \alpha^*(\boldsymbol{k})\hat{a}_{\boldsymbol{k}}\right\}. \tag{3.21}$$

Since below Eq. (3.17) we required that $\hat{\beta}(\boldsymbol{k})\,|b\rangle = \beta^b(\boldsymbol{k})\,|b\rangle$ for some detector basis $\{|b\rangle\}$, then

$$\hat{D}_{\hat{\beta}} = \sum_b |b\rangle\langle b|\,\hat{D}_{\beta^b}, \tag{3.22}$$

manifesting the controlled displacement nature of $\hat{D}_{\hat{\beta}}$.

In particular, for the basis $\{|i_{\mathrm{A}} j_{\mathrm{B}}\rangle\}$ where longitudinal operators diagonalize, we get

$$\hat{D}_{\hat{\beta}^{\mathrm{A}}(t)+\hat{\beta}^{\mathrm{B}}(t)} = \sum_{ij} |i_{\mathrm{A}} j_{\mathrm{B}}\rangle\langle i_{\mathrm{A}} j_{\mathrm{B}}|\,\hat{D}_{\beta_i^{\mathrm{A}}(t)+\beta_j^{\mathrm{B}}(t)}. \tag{3.23}$$

where

$$\begin{aligned}
&\hat{\beta}^\nu(t,\boldsymbol{k})\,|i_\nu\rangle = \beta_i^\nu(t,\boldsymbol{k})\,|i_\nu\rangle\,,\\
&\beta_i^\nu(t,\boldsymbol{k}) = \int_{t_\parallel}^{t} \mathrm{d}t_1\,\lambda_{\parallel,i}^\nu(t_1)\alpha^\nu(t_1,\boldsymbol{k}),\\
&\hat{\lambda}_\parallel^\nu(t)\,|i_\nu\rangle = \lambda_{\parallel,i}^\nu(t)\,|i_\nu\rangle\,.
\end{aligned} \tag{3.24}$$

In summary, $\hat{D}_{\hat{\beta}^{\mathrm{A}}(t)+\hat{\beta}^{\mathrm{B}}(t)}$ applies $\hat{D}_{\beta_i^{\mathrm{A}}(t)+\beta_j^{\mathrm{B}}(t)}$ on the field when the state of the detectors is $|i_{\mathrm{A}} j_{\mathrm{B}}\rangle$. Moreover, in the basis $\{|i_{\mathrm{A}} j_{\mathrm{B}}\rangle\}$, the unitary $e^{\hat{\Omega}_2(t)}$ can be understood as adding relative phases between the detector basis states

$$\begin{aligned}
&e^{\hat{\Omega}_2(t)} = \sum_{ij} e^{\Omega_{2,ij}(t)}\,|i_{\mathrm{A}} j_{\mathrm{B}}\rangle\langle i_{\mathrm{A}} j_{\mathrm{B}}|\,,\\
&\Omega_{2,ij} = -\vartheta_{ii}^{\mathrm{AA}} - \vartheta_{jj}^{\mathrm{BB}} - \vartheta_{ij}^{\mathrm{AB}} - \vartheta_{ji}^{\mathrm{BA}}\,,
\end{aligned} \tag{3.25}$$

$$\vartheta_{ij}^{\mu\nu}(t) = \int_{t_\parallel}^{t} \mathrm{d}t_1 \int_{t_\parallel}^{t_1} \mathrm{d}t_2\,\lambda_{\parallel,i}^\mu(t_1)\lambda_{\parallel,j}^\nu(t_2)W^{\mu\nu-}(t_1,t_2). \tag{3.26}$$

Combining the results above,

$$\hat{U}^\parallel(t) = \sum_{ij} e^{\Omega_{2,ij}(t)}\,|i_{\mathrm{A}} j_{\mathrm{B}}\rangle\langle i_{\mathrm{A}} j_{\mathrm{B}}|\,\hat{D}_{\beta_i^{\mathrm{A}}(t)+\beta_j^{\mathrm{B}}(t)}, \tag{3.27}$$

where we used definitions from Eqs. (3.21), (3.24) and (3.25).

3.1.2 Perturbatively including the transversal evolution

This subsection derives the time evolution of the interaction picture state $\hat{\rho}(t)$ under couplings with both longitudinal and transversal components. In Sec. 3.1.1, we obtained the exact longitudinal evolution, $\hat{U}^{\parallel}(t)$. However, the same non-perturbative procedure cannot be applied to compute the transversal part of the evolution. Instead, we are going to include the transversal interaction perturbatively.

Firstly, we define the *transversal picture*. The transversal picture state $\hat{\rho}_{\mathrm{T}}(t)$ is

$$\hat{\rho}_{\mathrm{T}}(t) = \hat{U}^{\parallel\dagger}(t)\hat{\rho}(t)\hat{U}^{\parallel}(t), \tag{3.28}$$

where $\hat{\rho}(t)$ is the usual interaction picture state. Then, $\hat{\rho}_{\mathrm{T}}(t)$ evolves according to

$$\begin{aligned}
&\hat{\rho}_{\mathrm{T}}(t) = \hat{\mathcal{U}}(t)\hat{\rho}_{\mathrm{T},0}\hat{\mathcal{U}}^{\dagger}(t),\\
&\hat{\mathcal{U}}(t) = \mathcal{T}\exp\left(-\mathrm{i}\int_{t_0}^{t}\mathrm{d}t_1\,\hat{H}_{\mathrm{T}}(t_1)\right).
\end{aligned} \tag{3.29}$$

Here, $\mathcal{T}$ is used to denote the time-ordered exponential, t_0 is the initial time, $\hat{\rho}_{\mathrm{T},0} = \hat{\rho}_{\mathrm{T}}(t_0)$ is the initial state, and

$$\hat{H}_{\mathrm{T}}(t) = \hat{U}^{\parallel\dagger}(t)\hat{H}_{\perp}(t)\hat{U}^{\parallel}(t). \tag{3.30}$$

In other words, $\hat{H}_{\mathrm{T}}$ is the transversal picture version of the $\hat{H}_{\perp}$ defined in equation (3.8). This transversal Hamiltonian can be rewritten as

$$\begin{aligned}
&\hat{H}_{\mathrm{T}} = \sum_{\nu}\hat{\lambda}^{\nu}_{\mathrm{T}}\big(\hat{\phi}^{\alpha^\nu} + \hat{m}_{\parallel}^{\mathrm{A}^\nu} + \hat{m}_{\parallel}^{\mathrm{B}^\nu}\big),\\
&\hat{\lambda}^{\nu}_{\mathrm{T}} = \hat{U}^{\parallel\dagger}\hat{\lambda}^{\nu}_{\perp}\hat{U}^{\parallel},\\
&\hat{m}_{\parallel}^{\mu^\nu}(t) = 2\mathrm{i}\int_{t_{\parallel}}^{t}\mathrm{d}t_1\,\hat{\lambda}^{\mu}_{\parallel}(t_1)W^{\mu\nu-}(t_1,t),
\end{aligned} \tag{3.31}$$

as shown in Appendix B.1. Notice that the terms $\hat{\lambda}^{\mathrm{A}}_{\mathrm{T}}\hat{m}_{\parallel}^{\mathrm{B}^{\mathrm{A}}}$ and $\hat{\lambda}^{\mathrm{B}}_{\mathrm{T}}\hat{m}_{\parallel}^{\mathrm{A}^{\mathrm{B}}}$ in $\hat{H}_{\mathrm{T}}$ reveal the presence of a field-mediated interaction between the detectors.

Next, we perturbatively compute $\hat{\rho}_{\mathrm{T}}(t)$ by performing a Dyson expansion of $\hat{\mathcal{U}}(t)$,

$$\hat{\mathcal{U}}(t) = \hat{\mathcal{U}}^{(0)}(t) + \hat{\mathcal{U}}^{(1)}(t) + \hat{\mathcal{U}}^{(2)}(t) + \mathcal{O}\big(\lambda_{\perp}^{3}\big), \tag{3.32}$$

$$\begin{aligned}
&\hat{\mathcal{U}}^{(0)}(t) = \hat{\mathbb{1}},\\
&\hat{\mathcal{U}}^{(1)}(t) = -\mathrm{i}\int_{t_0}^{t}\mathrm{d}t_1\,\hat{H}_{\mathrm{T}}(t_1),\\
&\hat{\mathcal{U}}^{(2)}(t) = -\int_{t_0}^{t}\mathrm{d}t_1\int_{t_0}^{t_1}\mathrm{d}t_2\,\hat{H}_{\mathrm{T}}(t_1)\hat{H}_{\mathrm{T}}(t_2).
\end{aligned} \tag{3.33}$$

Then, the time-evolved density operator for the state of the detectors and the field is,

$$\hat{\rho}_{\mathrm{T}} = \hat{\rho}_{\mathrm{T},0} + \hat{\rho}_{\mathrm{T}}^{(1,0)} + \hat{\rho}_{\mathrm{T}}^{(0,1)} + \hat{\rho}_{\mathrm{T}}^{(2,0)} + \hat{\rho}_{\mathrm{T}}^{(1,1)} + \hat{\rho}_{\mathrm{T}}^{(0,2)} + \mathcal{O}\big(\lambda_{\perp}^{3}\big)\,, \tag{3.34}$$

where we dropped the t dependencies for simplicity of notation.

The corrections are

$$\hat{\rho}_{\mathrm{T}}^{(i,j)} = \hat{\mathcal{U}}^{(i)}\hat{\rho}_{\mathrm{T},0}\hat{\mathcal{U}}^{(j)\dagger}\,. \tag{3.35}$$

Since we are interested in finding $\hat{\rho}(t)$, we turn $\hat{\rho}_{\mathrm{T}}(t)$ back to the interaction picture, using

$$\hat{\rho}(t) = \hat{U}^{\parallel}(t)\hat{\rho}_{\mathrm{T}}(t)\hat{U}^{\parallel\dagger}(t). \tag{3.36}$$

Then,

$$\hat{\rho} = \hat{\rho}^{(0,0)} + \hat{\rho}^{(1,0)} + \hat{\rho}^{(0,1)} + \hat{\rho}^{(2,0)} + \hat{\rho}^{(1,1)} + \hat{\rho}^{(0,2)} + \mathcal{O}\big(\lambda_{\perp}^{3}\big)\,, \tag{3.37}$$

$$\hat{\rho}^{(i,j)} = \hat{U}^{\parallel}\hat{\mathcal{U}}^{(i)}\hat{U}_{0}^{\parallel\dagger}\hat{\rho}_{0}\hat{U}_{0}^{\parallel}\hat{\mathcal{U}}^{(j)\dagger}\hat{U}^{\parallel\dagger}\,, \tag{3.38}$$

with $\hat{\rho}_0 = \hat{U}_0^{\parallel}\hat{\rho}_{\mathrm{T},0}\hat{U}_0^{\parallel\dagger}$ the initial state, and $\hat{U}_0^{\parallel} = \hat{U}^{\parallel}(t_0)$.

This result can be restated in terms of the unitary $\hat{U}(t)$ that dictates time evolution, $\hat{\rho}(t) = \hat{U}(t)\hat{\rho}_0\hat{U}^{\dagger}(t)$. Specifically, we find

$$\hat{U} = \hat{U}^{\parallel}\Big(\hat{\mathcal{U}}^{(0)} + \hat{\mathcal{U}}^{(1)} + \hat{\mathcal{U}}^{(2)} + \mathcal{O}\big(\lambda_{\perp}^{3}\big)\Big)\hat{U}_{0}^{\parallel\dagger}. \tag{3.39}$$

Here, one can check that perturbatively expanding $\hat{U}$ with respect to $\hat{H}_{\parallel}$ recovers the usual Dyson expansion for $\hat{U}$ in terms of $\hat{H}_{\mathrm{I}}$. This consistency check is provided in Appendix B.2.

From now on, let us now choose $t_{\parallel} = t_0$, which implies $\hat{\rho}_0 = \hat{\rho}_{\mathrm{T},0}$ and $\hat{U}_0^{\parallel} = \hat{\mathbb{1}}$. Then, Eq. (3.38) simplifies to

$$\hat{\rho}^{(i,j)} = \hat{U}^{\parallel}\hat{\mathcal{U}}^{(i)}\hat{\rho}_{0}\hat{\mathcal{U}}^{(j)\dagger}\hat{U}^{\parallel\dagger}\,. \tag{3.40}$$

Furthermore, we provide expressions for $\hat{\rho}(t)$ in the chosen detector bases $\{|i_{\mathrm{A}}\rangle\}$ and $\{|j_{\mathrm{B}}\rangle\}$ in Appendix B.3.

3.1.3 Evolution of the detectors

In order to study the evolution of the detectors, we trace over the field,

$$\hat{\rho}_{\mathrm{AB}}(t) = \mathrm{Tr}_{\phi}\, \hat{\rho}(t). \tag{3.41}$$

We now apply this to the expression of Eq. (3.37), which includes the transversal coupling perturbatively,

$$\begin{aligned}\hat{\rho}_{\mathrm{AB}} = \hat{\rho}_{\mathrm{AB}}^{(0,0)} + \hat{\rho}_{\mathrm{AB}}^{(1,0)} + \hat{\rho}_{\mathrm{AB}}^{(0,1)} \\ + \hat{\rho}_{\mathrm{AB}}^{(2,0)} + \hat{\rho}_{\mathrm{AB}}^{(1,1)} + \hat{\rho}_{\mathrm{AB}}^{(0,2)} + \mathcal{O}\big(\lambda_{\perp}^{3}\big),\end{aligned} \tag{3.42}$$

where we defined $\hat{\rho}_{\mathrm{AB}}^{(k,l)} = \mathrm{Tr}_{\phi}\, \hat{\rho}^{(k,l)}$, for any indices k, l. The expressions for the components of $\hat{\rho}_{\mathrm{AB}}^{(k,l)}$ in the preferred detector basis $\{|i_{\mathrm{A}} j_{\mathrm{B}}\rangle\}$ are provided in Appendix B.4.1.

In order to study the amount of entanglement in $\hat{\rho}_{\mathrm{AB}}$ we need an entanglement measure that applies to mixed states. In this work, we use negativity, which is an entanglement monotone and is faithful for systems of two qubits [86, 87, 88]. The negativity of a general bipartite state, such as $\hat{\rho}_{\mathrm{AB}}$, is

$$\mathcal{N}(\hat{\rho}_{\mathrm{AB}}) = \frac{\big|\big|\hat{\rho}_{\mathrm{AB}}^{\top_{\mathrm{A}}}\big|\big|_1 - 1}{2}. \tag{3.43}$$

Here, $\hat{\rho}_{\mathrm{AB}}^{\top_{\mathrm{A}}}$ denotes the partial transpose of $\hat{\rho}_{\mathrm{AB}}$ with respect to the subsystem A, and $||\hat{\sigma}||_1 = \mathrm{Tr}\sqrt{\hat{\sigma}^{\dagger}\hat{\sigma}}$ is the trace norm, which is equal to the sum of the singular values of $\hat{\sigma}$. Equivalently, $\mathcal{N}(\hat{\rho}_{\mathrm{AB}})$ equals the absolute sum of the negative eigenvalues of $\hat{\rho}_{\mathrm{AB}}^{\top_{\mathrm{A}}}$. The latter is the characterization that we will use to compute negativity in the next sections.

3.2 Splitting longitudinal and transversal interactions with respect to the initial state

Let us explore the entanglement obtained by detectors that start in an arbitrary pure product state. We will use the expressions for $\hat{\rho}$ and $\hat{\rho}_{\mathrm{AB}}$ obtained in the previous section to separate longitudinal and transversal contributions to the evolution. Specifically, we choose the initial state at time t_0 to be

$$\hat{\rho}_0 = |\psi_{\mathrm{A}}\rangle\langle\psi_{\mathrm{A}}| \otimes |\psi_{\mathrm{B}}\rangle\langle\psi_{\mathrm{B}}| \otimes \hat{\rho}_{\phi,0}, \tag{3.44}$$

where $\hat{\rho}_{\phi,0}$ is the initial state of the field, and $|\psi_{\text{A}}\rangle$ and $|\psi_{\text{B}}\rangle$ are arbitrary initial pure states for the detectors.

In general, we have freedom to choose the bases $\{|i_{\text{A}}\rangle\}$ and $\{|j_{\text{B}}\rangle\}$ used to define longitudinal and transversal operators. For our current choice of initial state in Eq. (3.44), it is convenient to pick

$$|0_{\text{A}}\rangle \coloneqq |\psi_{\text{A}}\rangle\,, \quad |0_{\text{B}}\rangle \coloneqq |\psi_{\text{B}}\rangle\,, \tag{3.45}$$

and then complete the orthonormal bases as preferred to obtain $\{|i_{\text{A}}\rangle\}$ and $\{|j_{\text{B}}\rangle\}$. Notice that $|0_{\text{A}}\rangle$ and $|0_{\text{B}}\rangle$ are not necessarily the ground state for the detectors. Here, the index 0 solely indicates that these states are the first element of the basis. In other words, for each detector, we have split the operators into longitudinal and transversal parts with respect to an orthogonal basis that contains the initial state as first element. Under this choice, we can rewrite the initial state as

$$\hat{\rho}_0 = |0_{\text{A}}0_{\text{B}}\rangle\langle 0_{\text{A}}0_{\text{B}}| \otimes \hat{\rho}_{\phi,0}. \tag{3.46}$$

Then, given $t_{\parallel} = t_0$,

$$\hat{\rho} = \hat{\rho}^{(0,0)} + \mathcal{O}\big(\lambda_{\perp}\big)\,, \tag{3.47}$$

$$\begin{aligned}\hat{\rho}^{(0,0)}(t) &= \hat{U}^{\parallel}(t)\hat{\rho}_0\hat{U}^{\parallel\dagger}(t) \\ &= |0_{\text{A}}0_{\text{B}}\rangle\langle 0_{\text{A}}0_{\text{B}}| \otimes \hat{D}_{\beta_0^{\text{A}}(t)+\beta_0^{\text{B}}(t)}\hat{\rho}_{\phi,0}\hat{D}^{\dagger}_{\beta_0^{\text{A}}(t)+\beta_0^{\text{B}}(t)},\end{aligned} \tag{3.48}$$

from using Eqs. (3.27) and (3.40). Therefore, if there is no transversal interaction with respect to the initial state, i.e. $\lambda_{\perp} = 0$, then the detectors remain in the initial state. The same is not true for the field, upon which the longitudinal interaction causes a time dependent displacement of its state.

For general interactions, we include the transversal interaction perturbatively, as described in subsection 3.1.2, expanding the state as

$$\hat{\rho} = \hat{\rho}^{(0,0)} + \hat{\rho}^{(1,0)} + \hat{\rho}^{(0,1)} + \hat{\rho}^{(2,0)} + \hat{\rho}^{(1,1)} + \hat{\rho}^{(0,2)} + \mathcal{O}\big(\lambda_{\perp}^3\big)\,. \tag{3.49}$$

The expressions for these in the preferred basis can be obtained from particularizing the results of Appendix B.3 to the choice of initial state of Eq. (3.46).

3.2.1 Evolution of the detectors

Now, we study $\hat{\rho}_{\text{AB}}$ given the initial state of Eq. (3.46). Specifically, we provide the form of the terms in the expansion

$$\hat{\rho}_{\text{AB}} = \hat{\rho}_{\text{AB}}^{(0,0)} + \hat{\rho}_{\text{AB}}^{(1,0)} + \hat{\rho}_{\text{AB}}^{(0,1)} + \hat{\rho}_{\text{AB}}^{(2,0)} + \hat{\rho}_{\text{AB}}^{(1,1)} + \hat{\rho}_{\text{AB}}^{(0,2)} + \mathcal{O}\big(\lambda_{\perp}^{3}\big). \tag{3.50}$$

In order to do so, it is convenient to split the following operators,

$$\hat{H}_{\text{T}} = \sum_{\nu} \hat{H}_{\text{T}}^{\nu}, \;\; \hat{\mathcal{U}}^{(1)} = \sum_{\nu} \hat{\mathcal{U}}^{\nu}, \;\; \hat{\mathcal{U}}^{(2)} = \sum_{\mu\nu} \hat{\mathcal{U}}^{\mu\nu}, \tag{3.51}$$

so that

$$\begin{aligned}
\hat{H}_{\text{T}}^{\nu} &= \hat{\lambda}_{\text{T}}^{\nu} \hat{\phi}_{\text{T}}^{\alpha^{\nu}}, \\
\hat{\mathcal{U}}^{\nu}(t) &= -\mathrm{i} \int_{t_0}^{t} \mathrm{d}t_1 \, \hat{H}_{\text{T}}^{\nu}(t_1), \\
\hat{\mathcal{U}}^{\mu\nu}(t) &= -\int_{t_0}^{t} \mathrm{d}t_1 \int_{t_0}^{t_1} \mathrm{d}t_2 \, \hat{H}_{\text{T}}^{\mu}(t_1) \hat{H}_{\text{T}}^{\nu}(t_2),
\end{aligned} \tag{3.52}$$

and define the field operators

$$\begin{aligned}
\hat{U}_{ij}^{\parallel} &= \langle i_{\text{A}} j_{\text{B}} | \hat{U}^{\parallel} | i_{\text{A}} j_{\text{B}} \rangle \,, \\
\hat{\mathcal{U}}_{iji'j'}^{\nu} &= \langle i_{\text{A}} j_{\text{B}} | \, \hat{\mathcal{U}}^{\nu} \, | i'_{\text{A}} j'_{\text{B}} \rangle \,, \\
\hat{\mathcal{U}}_{iji'j'}^{\mu\nu} &= \langle i_{\text{A}} j_{\text{B}} | \, \hat{\mathcal{U}}^{\mu\nu} \, | i'_{\text{A}} j'_{\text{B}} \rangle \,.
\end{aligned} \tag{3.53}$$

Going back to the expression for $\hat{\rho}_{\text{AB}}$, the zeroth order in $\lambda_{\perp}$ can be obtained from Eq. (3.48),

$$\hat{\rho}_{\text{AB}}^{(0,0)} = |0_{\text{A}} 0_{\text{B}}\rangle\langle 0_{\text{A}} 0_{\text{B}}| \,. \tag{3.54}$$

The first order contributions in $\lambda_{\perp}$, given $t_{\parallel} = t_0$ and Eq. (3.40), are

$$\begin{aligned}
\hat{\rho}_{\text{AB}}^{(1,0)} &= |\xi_{\text{A}} 0_{\text{B}}\rangle\langle 0_{\text{A}} 0_{\text{B}}| + |0_{\text{A}} \xi_{\text{B}}\rangle\langle 0_{\text{A}} 0_{\text{B}}| \,, \\
\hat{\rho}_{\text{AB}}^{(0,1)} &= \hat{\rho}_{\text{AB}}^{(1,0)\dagger}.
\end{aligned} \tag{3.55}$$

Here, $|\xi_{\nu}\rangle$ are orthogonal to the initial states,

$$\langle \xi_{\text{A}} | 0_{\text{A}} \rangle = \langle \xi_{\text{B}} | 0_{\text{B}} \rangle = 0, \tag{3.56}$$

and fulfill

$$
\begin{aligned}
|\xi_\nu\rangle &= \sum_{i\neq 0} \xi_i^\nu \, |i_\nu\rangle \,, \\
\xi_i^{\mathrm{A}} &= \big\langle \hat{U}_{00}^{\parallel\dagger} \hat{U}_{i0}^{\parallel} \hat{\mathcal{U}}_{i000}^{\mathrm{A}} \big\rangle_{\hat{\rho}_{\phi,0}}, \\
\xi_j^{\mathrm{B}} &= \big\langle \hat{U}_{00}^{\parallel\dagger} \hat{U}_{0j}^{\parallel} \hat{\mathcal{U}}_{0j00}^{\mathrm{B}} \big\rangle_{\hat{\rho}_{\phi,0}}.
\end{aligned} \tag{3.57}
$$

Here, we denote expectation values as

$$
\big\langle \hat{A} \big\rangle_{\hat{\rho}_\phi} = \mathrm{Tr}_\phi\big(\hat{A}\hat{\rho}_\phi\big). \tag{3.58}
$$

The contributions of order $\lambda_\perp^2$ are

$$
\begin{aligned}
\hat{\rho}_{\mathrm{AB}}^{(2,0)} &= \big(|\upsilon_{\mathrm{AA}} 0_{\mathrm{B}}\rangle + |0_{\mathrm{A}} \upsilon_{\mathrm{BB}}\rangle + |\mathrm{M}\rangle \big) \langle 0_{\mathrm{A}} 0_{\mathrm{B}}| \,, \\
\hat{\rho}_{\mathrm{AB}}^{(1,1)} &= \hat{L}_{\mathrm{AA}} \otimes |0_{\mathrm{B}}\rangle\langle 0_{\mathrm{B}}| + |0_{\mathrm{A}}\rangle\langle 0_{\mathrm{A}}| \otimes \hat{L}_{\mathrm{BB}} + \hat{L}_{\mathrm{AB}} + \hat{L}_{\mathrm{AB}}^\dagger, \\
\hat{\rho}_{\mathrm{AB}}^{(0,2)} &= \hat{\rho}_{\mathrm{AB}}^{(2,0)\dagger},
\end{aligned} \tag{3.59}
$$

where

$$
\begin{aligned}
|\upsilon_{\nu\nu}\rangle &= \sum_i \upsilon_i^{\nu\nu} \, |i_\nu\rangle \,, \\
\upsilon_i^{\mathrm{AA}} &= \big\langle \hat{U}_{00}^{\parallel\dagger} \hat{U}_{i0}^{\parallel} \hat{\mathcal{U}}_{i000}^{\mathrm{AA}} \big\rangle_{\hat{\rho}_{\phi,0}}, \\
\upsilon_j^{\mathrm{BB}} &= \big\langle \hat{U}_{00}^{\parallel\dagger} \hat{U}_{0j}^{\parallel} \hat{\mathcal{U}}_{0j00}^{\mathrm{BB}} \big\rangle_{\hat{\rho}_{\phi,0}},
\end{aligned} \tag{3.60}
$$

$$
\begin{aligned}
|\mathrm{M}\rangle &= \sum_{i\neq 0} \sum_{j\neq 0} M_{ij} \, |i_{\mathrm{A}} j_{\mathrm{B}}\rangle \,, \\
M_{ij} &= \big\langle \hat{U}_{00}^{\parallel\dagger} \hat{U}_{ij}^{\parallel} (\hat{\mathcal{U}}_{ij00}^{\mathrm{AB}} + \hat{\mathcal{U}}_{ij00}^{\mathrm{BA}}) \big\rangle_{\hat{\rho}_{\phi,0}},
\end{aligned} \tag{3.61}
$$

$$
\begin{aligned}
\hat{L}_{\nu\nu} &= \sum_{i\neq 0} \sum_{i'\neq 0} L_{ii'}^{\nu\nu} \, |i_\nu\rangle\langle i'_\nu| \,, \\
\hat{L}_{\mathrm{AB}} &= \sum_{i\neq 0} \sum_{j\neq 0} L_{ij}^{\mathrm{AB}} \, |i_{\mathrm{A}} 0_{\mathrm{B}}\rangle\langle 0_{\mathrm{A}} j_{\mathrm{B}}| \,, \\
L_{ii'}^{\mathrm{AA}} &= \big\langle \big(\hat{\mathcal{U}}_{i'000}^{\mathrm{A}}\big)^\dagger \hat{U}_{i'0}^{\parallel\dagger} \hat{U}_{i0}^{\parallel} \hat{\mathcal{U}}_{i000}^{\mathrm{A}} \big\rangle_{\hat{\rho}_{\phi,0}}, \\
L_{jj'}^{\mathrm{BB}} &= \big\langle \big(\hat{\mathcal{U}}_{0j'00}^{\mathrm{B}}\big)^\dagger \hat{U}_{0j'}^{\parallel\dagger} \hat{U}_{0j}^{\parallel} \hat{\mathcal{U}}_{0j00}^{\mathrm{B}} \big\rangle_{\hat{\rho}_{\phi,0}}, \\
L_{ij}^{\mathrm{AB}} &= \big\langle \big(\hat{\mathcal{U}}_{0j00}^{\mathrm{B}}\big)^\dagger \hat{U}_{0j}^{\parallel\dagger} \hat{U}_{i0}^{\parallel} \hat{\mathcal{U}}_{i000}^{\mathrm{A}} \big\rangle_{\hat{\rho}_{\phi,0}}.
\end{aligned} \tag{3.62}
$$

Further expressions for the expectation values ξ_i^{ν}, $\upsilon_i^{\nu\nu}$, M_{ij} and $L_{ij}^{\mu\nu}$ are provided in Appendix B.4.2.

Compiling the results above into a single expression,

$$\begin{aligned}\hat{\rho}_{\mathrm{AB}} = {} & |0_{\mathrm{A}}0_{\mathrm{B}}\rangle\langle 0_{\mathrm{A}}0_{\mathrm{B}}| + \big(\,|\xi_{\mathrm{A}}0_{\mathrm{B}}\rangle + |0_{\mathrm{A}}\xi_{\mathrm{B}}\rangle\big)\langle 0_{\mathrm{A}}0_{\mathrm{B}}| \\ & + |0_{\mathrm{A}}0_{\mathrm{B}}\rangle\big(\langle\xi_{\mathrm{A}}0_{\mathrm{B}}| + \langle 0_{\mathrm{A}}\xi_{\mathrm{B}}|\,\big) \\ & + \big(\,|\upsilon_{\mathrm{AA}}0_{\mathrm{B}}\rangle + |0_{\mathrm{A}}\upsilon_{\mathrm{BB}}\rangle + |\mathrm{M}\rangle\big)\langle 0_{\mathrm{A}}0_{\mathrm{B}}| \\ & + |0_{\mathrm{A}}0_{\mathrm{B}}\rangle\big(\langle\upsilon_{\mathrm{AA}}0_{\mathrm{B}}| + \langle 0_{\mathrm{A}}\upsilon_{\mathrm{BB}}| + \langle\mathrm{M}|\,\big) \\ & + \hat{L}_{\mathrm{AA}}\otimes|0_{\mathrm{B}}\rangle\langle 0_{\mathrm{B}}| + |0_{\mathrm{A}}\rangle\langle 0_{\mathrm{A}}|\otimes\hat{L}_{\mathrm{BB}} + \hat{L}_{\mathrm{AB}} + \hat{L}_{\mathrm{AB}}^{\dagger} \\ & + \mathcal{O}\big(\lambda_{\perp}^{3}\big).\end{aligned} \tag{3.63}$$

3.2.2 Negativity for the detectors

Next, we study the amount of entanglement in $\hat{\rho}_{\mathrm{AB}}$ by obtaining an expression for the negativity $\mathcal{N}(\hat{\rho}_{\mathrm{AB}})$. We show that, at leading order in $\lambda_{\perp}$, $\mathcal{N}(\hat{\rho}_{\mathrm{AB}})$ is a function of solely the quantities ξ_i^{A}, ξ_j^{B}, M_{ij} and $L_{ii'}^{\mathrm{AA}}$, $L_{jj'}^{\mathrm{BB}}$.

Specifically, the negativity of the detectors is, at leading order in $\lambda_{\perp}$,

$$\mathcal{N}(\hat{\rho}_{\mathrm{AB}}) = \mathcal{N}\big((\hat{\sigma}_2 - |\psi_1\rangle\langle\psi_1|)^{\top_{\mathrm{A}}}\big) + \mathcal{O}\big(\lambda_{\perp}^{3}\big), \tag{3.64}$$

where

$$\begin{aligned}|\psi_1\rangle &= \big(\,|\xi_{\mathrm{A}}0_{\mathrm{B}}\rangle\,\big)^{*} + |0_{\mathrm{A}}\xi_{\mathrm{B}}\rangle\,, \\ \hat{\sigma}_2 &= \big(\hat{L}_{\mathrm{AA}}\big)^{*}\otimes|0_{\mathrm{B}}\rangle\langle 0_{\mathrm{B}}| + |0_{\mathrm{A}}\rangle\langle 0_{\mathrm{A}}|\otimes\hat{L}_{\mathrm{BB}} + \hat{M} + \hat{M}^{\dagger}, \\ \hat{M} &= \sum_{i\neq 0}\sum_{j\neq 0} M_{ij}\,|0_{\mathrm{A}}j_{\mathrm{B}}\rangle\langle i_{\mathrm{A}}0_{\mathrm{B}}|\,.\end{aligned} \tag{3.65}$$

These expressions use the definitions of the previous subsection 3.2.1 and $(\,.\,)^{*}$ denotes complex conjugating the coefficients in the $\{|i_{\mathrm{A}}j_{\mathrm{B}}\rangle\}$ basis. Moreover, $\mathcal{N}\big((\hat{\sigma}_2 - |\psi_1\rangle\langle\psi_1|)^{\top_{\mathrm{A}}}\big)$ equals the absolute sum of the negative eigenvalues of $\hat{\sigma}_2 - |\psi_1\rangle\langle\psi_1|$, which is of order $\lambda_{\perp}^{2}$.

In order to show this result, we need to compute the partial transpose of $\hat{\rho}_{\mathrm{AB}}$,

$$\begin{aligned}\hat{\rho}_{\mathrm{AB}}^{\top_{\mathrm{A}}} = {} & |0_{\mathrm{A}}0_{\mathrm{B}}\rangle\langle 0_{\mathrm{A}}0_{\mathrm{B}}| + |\psi_1\rangle\langle 0_{\mathrm{A}}0_{\mathrm{B}}| + |0_{\mathrm{A}}0_{\mathrm{B}}\rangle\langle\psi_1| \\ & + |\psi_2\rangle\langle 0_{\mathrm{A}}0_{\mathrm{B}}| + |0_{\mathrm{A}}0_{\mathrm{B}}\rangle\langle\psi_2| + \hat{\sigma}_2 + \mathcal{O}\big(\lambda_{\perp}^{3}\big),\end{aligned} \tag{3.66}$$

where we used the definitions in Eq. (3.65) together with

$$
\begin{aligned}
|\psi_2\rangle &= \big(\,|\upsilon_{\mathrm{AA}}0_{\mathrm{B}}\rangle\,\big)^* + |0_{\mathrm{A}}\upsilon_{\mathrm{BB}}\rangle + |\mathrm{L}_{\mathrm{AB}}\rangle\,,\\
|\mathrm{L}_{\mathrm{AB}}\rangle &= \sum_{i\neq 0}\sum_{j\neq 0} L_{ij}^{\mathrm{BA}}\,|i_{\mathrm{A}}j_{\mathrm{B}}\rangle\,.
\end{aligned}
\tag{3.67}
$$

Remember that $(\,.\,)^*$ denotes complex conjugating the coefficients in the $\{|i_{\mathrm{A}}j_{\mathrm{B}}\rangle\}$ basis. In order to compute $\mathcal{N}(\hat{\rho}_{\mathrm{AB}})$, we need to know the eigenvalues of $\hat{\rho}_{\mathrm{AB}}^{\mathsf{T}_{\mathrm{A}}}$. The Appendix B.5 describes how to perturbatively find the eigenvalues of $\hat{\rho}_{\mathrm{AB}}^{\mathsf{T}_{\mathrm{A}}}$. The main result of this appendix is that the negative eigenvalues of $\hat{\rho}_{\mathrm{AB}}^{\mathsf{T}_{\mathrm{A}}}$ are the same as the negative eigenvalues of $\hat{\sigma}_2 - |\psi_1\rangle\langle\psi_1|$.

Remarkably, for the case studied in this section, i.e. detectors initialized in longitudinal states, not only the leading order contribution to $\mathcal{N}(\hat{\rho}_{\mathrm{AB}})$ is of order $\lambda_\perp^2$, but it is also of order zero in $\lambda_\parallel$. This can be seen from the expressions for ξ_i^ν, $\upsilon_i^{\nu\nu}$, M_{ij} and $L_{ij}^{\mu\nu}$ provided in Appendix B.4.2. Such expressions are non-perturbative in $\lambda_\parallel$, but if we expand them with respect to $\lambda_\parallel$, then we obtain, at leading order

$$
\begin{aligned}
\xi_i^\nu &= -\mathrm{i}\int_{t_0}^{t}\mathrm{d}t_1\,\lambda_{\perp,i0}^{\nu}(t_1)\big\langle\hat{\phi}^{\alpha^\nu}(t_1)\big\rangle_{\hat{\rho}_{\phi,0}} + \mathcal{O}(\lambda_\parallel),\\
\upsilon_i^{\nu\nu} &= -\sum_{s\neq i,0}\int_{t_0}^{t}\mathrm{d}t_1\int_{t_0}^{t_1}\mathrm{d}t_2\,\lambda_{\perp,is}^{\nu}(t_1)\lambda_{\perp,s0}^{\nu}(t_2)W^{\nu\nu}(t_1,t_2) + \mathcal{O}(\lambda_\parallel),\\
M_{ij} &= -\int_{t_0}^{t}\mathrm{d}t_1\int_{t_0}^{t}\mathrm{d}t_2\,\lambda_{\perp,i0}^{\mathrm{A}}(t_1)\lambda_{\perp,j0}^{\mathrm{B}}(t_2)G^{\mathrm{AB}}(t_1,t_2) + \mathcal{O}(\lambda_\parallel),\\
L_{ij}^{\mu\nu} &= \int_{t_0}^{t}\mathrm{d}t_1\int_{t_0}^{t}\mathrm{d}t_2\,\lambda_{\perp,i0}^{\mu}(t_1)\lambda_{\perp,0j}^{\nu}(t_2)W^{\nu\mu}(t_2,t_1) + \mathcal{O}(\lambda_\parallel),
\end{aligned}
\tag{3.68}
$$

where we defined

$$
\begin{aligned}
W^{\mu\nu}(t_1,t_2) &= \langle\hat{\phi}^{\alpha^\mu}(t_1)\hat{\phi}^{\alpha^\nu}(t_2)\rangle_{\hat{\rho}_{\phi,0}},\\
G^{\mu\nu}(t_1,t_2) &= \Theta(t_1-t_2)W^{\mu\nu}(t_1,t_2) + \Theta(t_2-t_1)W^{\nu\mu}(t_2,t_1).
\end{aligned}
\tag{3.69}
$$

Notice that $G^{\mu\nu}(t_1,t_2)$ is the time ordered version of $W^{\mu\nu}(t_1,t_2)$. Additionally, this definition is compatible with the $W^{\mu\nu-}$ previously introduced in equation (3.14). Specifically,

$$
W^{\mu\nu-}(t_1,t_2) = \frac{W^{\mu\nu}(t_1,t_2) - W^{\nu\mu}(t_2,t_1)}{2}.
\tag{3.70}
$$

The expressions above justify that $\mathcal{N}(\hat{\rho}_{\text{AB}})$ is dominated by the coupling that is transversal to the detectors' initial state. This holds for any initial state of the field $\hat{\rho}_{\phi,0}$, but is only true in the perturbative regime, where $\lambda_\perp$ and $\lambda_\parallel$ are small. In other words,

$$\mathcal{N}(\hat{\rho}_{\text{AB}}) \propto \lambda_\perp^2 \big(1 + \mathcal{O}(\lambda_\perp) + \mathcal{O}(\lambda_\parallel)\big). \tag{3.71}$$

Conversely, there are at least two regimes where the effect of the longitudinal interaction can become relevant: 1) if $\lambda_\parallel$ is large, and 2) if the longitudinal interaction is kept on for a long time. We will explore the first case in the next section with an example qubit detector.

3.3 Effect of a nonperturbative longitudinal interaction

Now, we look into the the effects of the longitudinal coupling in entanglement harvesting for a particular example. In light of the previous section, where the longitudinal interaction did not affect leading order negativity, we will use the non-perturbative results in $\lambda_\parallel$ to explore higher order effects for this parameter.

For this example, we will consider a massless scalar quantum field in (1+1)-dimensional Minkowski space. In this case, the amplitude of the field can be written as a particular case of Eq. (3.3),

$$\hat{\phi}(t,x) = \int_{\mathbb{R}} \frac{\mathrm{d}k}{\sqrt{4\pi|k|}} \Big(e^{\mathrm{i}(|k|t-kx)} \hat{a}_k^\dagger + e^{-\mathrm{i}(|k|t-kx)} \hat{a}_k \Big). \tag{3.72}$$

As a simple model of detector, we will take a pair of qubit UDW detectors. However, we will couple the detectors to the derivative of the field amplitude $\partial_t \hat{\phi}(t, \boldsymbol{x})$, since this is the implementation that can be experimentally realized in superconducting circuits, as seen for example in [67, 3].

Consider UDW detectors with energy gaps Ω_ν and respectively denote their ground and excited states as $|g_\nu\rangle$ and $|e_\nu\rangle$. This energy eigenbasis is now our preferred longitudinal basis. Then, the following interaction Hamiltonian introduces both longitudinal and transversal interactions,

$$\hat{H}_{\text{I}}(t) = \sum_\nu \hat{\lambda}^\nu(t) \int \mathrm{d}^n\boldsymbol{x}\, F_\nu(\boldsymbol{x}) \partial_t \hat{\phi}(t, \boldsymbol{x}), \tag{3.73}$$

where the smearing function $F_\nu(x)$ controls where the detector ν couples to the field, and

$$\hat{\lambda}^\nu(t) = \lambda^\nu_\perp \chi^\nu_\perp(t)\hat{\mu}_\nu(t) + \lambda^\nu_\parallel \chi^\nu_\parallel(t)\,|e_\nu\rangle\langle e_\nu|\,. \tag{3.74}$$

Here $\chi^\nu_\perp$ and $\chi^\nu_\parallel$ are switching functions for the transversal and longitudinal interactions. These switching functions localize the interaction in time and take on real values. The operator $\hat{\mu}_\nu(t)$ is called monopole moment operator and is defined as

$$\hat{\mu}_\nu(t) = e^{\mathrm{i}\Omega_\nu t}\hat{\sigma}^+_\nu + e^{-\mathrm{i}\Omega_\nu t}\hat{\sigma}^-_\nu, \tag{3.75}$$

where $\hat{\sigma}^+_\nu = |e_\nu\rangle\langle g_\nu| = (\hat{\sigma}^-_\nu)^\dagger$. Now, we can recast this Hamiltonian in the form of Eq. (3.1), with the objective to then use the results described in previous sections. First, we recognize that for the chosen longitudinal basis,

$$\hat{\lambda}^\nu_\perp(t) = \lambda^\nu_\perp \chi^\nu_\perp(t)\hat{\mu}_\nu(t), \quad \hat{\lambda}^\nu_\parallel(t) = \lambda^\nu_\parallel \chi^\nu_\parallel(t)\,|e_\nu\rangle\langle e_\nu|\,. \tag{3.76}$$

Additionally, analogously to Eq. (3.5), we find that

$$\begin{aligned}\int_{\mathbb{R}^n} \mathrm{d}^n\boldsymbol{x}\, F_\nu(\boldsymbol{x})\partial_t\hat{\phi}(t,\boldsymbol{x}) &= \hat{\phi}^{\alpha^\nu}(t),\\ \alpha^\nu(t,k) &= e^{\mathrm{i}|k|t}\sqrt{\frac{|k|}{4\pi}}\widetilde{F}^*_\nu(k),\end{aligned} \tag{3.77}$$

where we used that $F_\nu(x)$ is real, so that $\widetilde{F}_\nu(-k) = \widetilde{F}^*_\nu(k)$.

Next, consider the detectors to be initialized in their ground states,

$$\hat{\rho}_0 = |g_{\mathrm{A}}g_{\mathrm{B}}\rangle\langle g_{\mathrm{A}}g_{\mathrm{B}}| \otimes \hat{\rho}_{\phi,0}. \tag{3.78}$$

This is a longitudinal state of the energy eigenbasis of the detectors, and thus we can use the results from section 3.2. In particular, the effects of the longitudinal interaction will only appear beyond leading order on the longitudinal interaction strength.

Under the choices above, the state of the detectors $\hat{\rho}_{\mathrm{AB}}$ in the basis $\{|g_{\mathrm{A}}g_{\mathrm{B}}\rangle,\ |e_{\mathrm{A}}g_{\mathrm{B}}\rangle,\ |g_{\mathrm{A}}e_{\mathrm{B}}\rangle,\ |e_{\mathrm{A}}e_{\mathrm{B}}\rangle\}$ at any given point in time becomes

$$\begin{aligned}\hat{\rho}_{\mathrm{AB}} = &\begin{pmatrix} 1 - L^{\mathrm{AA}} - L^{\mathrm{BB}} & \xi^{\mathrm{A}*} & \xi^{\mathrm{B}*} & M^* \\ \xi^{\mathrm{A}} & L^{\mathrm{AA}} & L^{\mathrm{AB}} & 0 \\ \xi^{\mathrm{B}} & L^{\mathrm{AB}*} & L^{\mathrm{BB}} & 0 \\ M & 0 & 0 & 0 \end{pmatrix}\\ &+ \mathcal{O}(\lambda^3_\perp).\end{aligned} \tag{3.79}$$

This expression follows from the equations in subsection 3.2.1, after dropping the subindices indices for succinctness. Moreover, we used the following property of the Dyson expansion: the trace for the approximation of $\hat{\rho}_{\mathrm{AB}}$ is 1, even when the Dyson expansion is truncated to a finite number of terms.

Following subsection 3.2.2, the negativity of $\hat{\rho}_{\mathrm{AB}}$ at leading order is the absolute sum of negative eigenvalues of

$$\hat{\sigma}_2 - |\psi_1\rangle\langle\psi_1| = \begin{pmatrix} 0 & 0 & 0 & 0 \\ 0 & L^{\mathrm{AA}} - |\xi^{\mathrm{A}}|^2 & M^* - \xi^{\mathrm{A}*}\xi^{\mathrm{B}*} & 0 \\ 0 & M - \xi^{\mathrm{A}}\xi^{\mathrm{B}} & L^{\mathrm{BB}} - |\xi^{\mathrm{B}}|^2 & 0 \\ 0 & 0 & 0 & 0 \end{pmatrix}. \tag{3.80}$$

The eigenvalues of this matrix can be found analytically, from which one finds that

$$\mathcal{N}(\hat{\rho}_{\mathrm{AB}}) = \max\{0, \mathcal{V}\} + \mathcal{O}(\lambda_\perp^3), \tag{3.81}$$

with

$$\mathcal{V} = \sqrt{|M - \xi^{\mathrm{A}}\xi^{\mathrm{B}}|^2 + \left(\frac{L_{\mathrm{AA}} - |\xi^{\mathrm{A}}|^2 - L_{\mathrm{BB}} + |\xi^{\mathrm{B}}|^2}{2}\right)^2} + \frac{|\xi^{\mathrm{A}}|^2 + |\xi^{\mathrm{B}}|^2}{2} - \frac{\mathcal{L}_{\mathrm{AA}} + \mathcal{L}_{\mathrm{BB}}}{2}. \tag{3.82}$$

This expression simplifies for the case $L = L_{\mathrm{AA}} = L_{\mathrm{BB}}$, $\xi = \xi_{\mathrm{A}} = \xi_{\mathrm{B}}$, turning into

$$\mathcal{N}(\hat{\rho}_{\mathrm{AB}}) = \max\left\{0, |M - \xi^2| + |\xi|^2 - L\right\} + \mathcal{O}(\lambda_\perp^3). \tag{3.83}$$

We obtain the quantities ξ^ν, $L^{\mu\nu}$, M by particularizing the expressions of Appendix B.4.2 to the current scenario,

$$\xi^\nu = -\mathrm{i}\lambda_\perp^\nu \int_{t_0}^{t} \mathrm{d}t_1\, e^{\zeta^{(\nu,0)}(t,t_1)} \chi_\perp^\nu(t_1) e^{\mathrm{i}\Omega_\nu t_1} \left\langle \hat{D}_{\beta^\nu(t)-\beta^\nu(t_1)} \hat{\phi}^{\alpha^\nu}(t_1) \right\rangle_{\hat{\rho}_{\phi,0}}, \tag{3.84}$$

$$\begin{aligned} L^{\mu\nu} = \lambda_\perp^\mu \lambda_\perp^\nu \int_{t_0}^{t} \mathrm{d}t_1 \int_{t_0}^{t} \mathrm{d}t_2\, e^{\zeta^{(\mu,\nu)}(t,t_1,t_2)} \chi_\perp^\mu(t_1) \chi_\perp^\nu(t_2) \\ \times \left\langle \hat{\phi}^{\alpha^\nu}(t_2) \hat{D}_{\beta^\mu(t)-\beta^\nu(t)+\beta^\nu(t_2)-\beta^\mu(t_1)} \hat{\phi}^{\alpha^\mu}(t_1) \right\rangle_{\hat{\rho}_{\phi,0}} e^{\mathrm{i}(\Omega_\mu t_1 - \Omega_\nu t_2)}, \end{aligned} \tag{3.85}$$

$$\begin{aligned} M = -\lambda_\perp^{\mathrm{A}} \lambda_\perp^{\mathrm{B}} \int_{t_0}^{t} \mathrm{d}t_1 \int_{t_0}^{t_1} \mathrm{d}t_2\, e^{\zeta^{(\mathrm{AB},0)}(t,t_1,t_2) + \mathrm{i}(\Omega_{\mathrm{A}} t_1 + \Omega_{\mathrm{B}} t_2)} \chi_\perp^{\mathrm{A}}(t_1) \chi_\perp^{\mathrm{B}}(t_2) \\ \times \left\langle \hat{D}_{\beta^{\mathrm{A}}(t)+\beta^{\mathrm{B}}(t)-\beta^{\mathrm{A}}(t_1)-\beta^{\mathrm{B}}(t_2)} \hat{\phi}^{\alpha^{\mathrm{A}}}(t_1) \hat{\phi}^{\alpha^{\mathrm{B}}}(t_2) \right\rangle_{\hat{\rho}_{\phi,0}} + \mathrm{A} \leftrightarrow \mathrm{B}. \end{aligned} \tag{3.86}$$

where by $\mathrm{A} \leftrightarrow \mathrm{B}$ we mean swapping the labels A and B. Moreover, we denoted

$$\begin{aligned}\beta^{\nu}(t,k) &= \lambda_{\parallel}^{\nu}\int_{t_0}^{t}\mathrm{d}t_1\,\chi_{\parallel}^{\nu}(t_1)\alpha^{\nu}(t_1,k)\\ &= \lambda_{\parallel}^{\nu}(4\pi)^{-\frac{1}{2}}|k|^{\frac{1}{2}}\widetilde{F}_{\nu}^{*}(k)\int_{t_0}^{t}\mathrm{d}t_1\,\chi_{\parallel}^{\nu}(t_1)e^{\mathrm{i}|k|t},\end{aligned} \tag{3.87}$$

$$\begin{aligned}\zeta^{(\nu,0)}(t,t_1) &= \vartheta^{\nu\nu}(t_1)-\vartheta^{\nu\nu}(t)+C^{\nu\nu}(t,t_1),\\ &= -(\lambda_{\parallel}^{\nu})^2\int_{t_1}^{t}\mathrm{d}t_1'\int_{t_1}^{t_1'}\mathrm{d}t_2'\,\chi_{\parallel}^{\nu}(t_1')\chi_{\parallel}^{\nu}(t_2')W^{\nu\nu-}(t_1',t_2'),\end{aligned} \tag{3.88}$$

$$\begin{aligned}\zeta^{(\mu,\nu)}(t,t_1,t_2) &= \vartheta^{\mu\mu}(t_1)-\vartheta^{\nu\nu}(t_2)-\vartheta^{\mu\mu}(t)+\vartheta^{\nu\nu}(t)\\ &\quad-\vartheta^{\mu\nu}(t)+\vartheta^{\nu\mu}(t)+C^{\mu\mu}(t,t_1)-C^{\nu\mu}(t,t_1)\\ &\quad+C^{\mu\nu}(t,t_2)-C^{\nu\nu}(t,t_2)-C^{\mu\nu}(t_1,t_2),\end{aligned} \tag{3.89}$$

$$\zeta^{(\nu,\nu)}(t,t_1,t_2) = \zeta^{(\nu,0)}(t_2,t_1), \tag{3.90}$$

$$\begin{aligned}\zeta^{(\mathrm{AB},0)}(t,t_1,t_2) &= -\sum_{\mu\nu}\vartheta^{\mu\nu}(t)+\sum_{\nu}C^{\nu\mathrm{A}}(t,t_1)+C^{\nu\mathrm{B}}(t,t_2)\\ &\quad+\vartheta^{\mathrm{AA}}(t_1)+2\vartheta^{\mathrm{AB}}(t_1)+\vartheta^{\mathrm{BB}}(t_2)-C^{\mathrm{AB}}(t_1,t_2),\end{aligned} \tag{3.91}$$

with $\zeta^{(\mathrm{BA},0)}$ equal to $\zeta^{(\mathrm{AB},0)}$ with all A and B labels swapped. Finally,

$$\begin{aligned}\vartheta^{\mu\nu}(t) &= \lambda_{\parallel}^{\mu}\lambda_{\parallel}^{\nu}\int_{t_0}^{t}\mathrm{d}t_1\int_{t_0}^{t_1}\mathrm{d}t_2\,\chi_{\parallel}^{\mu}(t_1)\chi_{\parallel}^{\nu}(t_2)W^{\mu\nu-}(t_1,t_2),\\ C^{\mu\nu}(t,t') &= \lambda_{\parallel}^{\mu}\lambda_{\parallel}^{\nu}\int_{t_0}^{t}\mathrm{d}t_1\int_{t_0}^{t'}\mathrm{d}t_2\,\chi_{\parallel}^{\mu}(t_1)\chi_{\parallel}^{\nu}(t_2)W^{\mu\nu-}(t_1,t_2),\\ W^{\mu\nu-}(t_1,t_2) &= \frac{\mathrm{i}}{4\pi}\int_{-\infty}^{\infty}\mathrm{d}k\,|k|\,\mathrm{Im}\big(e^{\mathrm{i}|k|(t_2-t_1)}\widetilde{F}_{\mu}(k)\widetilde{F}_{\nu}^{*}(k)\big),\end{aligned} \tag{3.92}$$

where the last equality comes from substituting Eq. (3.77) into the definition of $W^{\mu\nu-}$ given in Eq. (3.14).

3.3.1 Initializing the field in the vacuum state

Next, we choose the field to be initialized in its vacuum state,

$$\hat{\rho}_{\phi,0} = |0_\phi\rangle\langle 0_\phi| \,. \tag{3.93}$$

This assumption allows us to evaluate field expectation values by using the tools from Appendix B.6, resulting in

$$\begin{aligned}
\xi^\nu &= -\mathrm{i}\lambda_\perp^\nu \lambda_\parallel^\nu \int_{t_0}^{t} \mathrm{d}t_1 \int_{t_1}^{t} \mathrm{d}t_2\, e^{\mathrm{i}\Omega_\nu t_1 - \varrho^\nu(t,t_1)} \chi_\perp^\nu(t_1)\chi_\parallel^\nu(t_2) W^{\nu\nu\nu}(t_2,t_1), \\
\varrho^\nu(t,t_1) &= (\lambda_\parallel^\nu)^2 \int_{t_1}^{t} \mathrm{d}t_1' \int_{t_1}^{t_1'} \mathrm{d}t_2'\, \chi_\parallel^\nu(t_1')\chi_\parallel^\nu(t_2') W^{\nu\nu\nu}(t_1',t_2'),
\end{aligned} \tag{3.94}$$

which fulfills $\varrho^\nu(t',t) = \varrho^{\nu *}(t,t')$, and $\mathrm{Re}\left(\varrho^\nu(t,t_1)\right) \geq 0$. As an intermediate step to obtain the equation above, we showed that

$$\left\langle \hat{D}_{\beta^\nu(t)-\beta^\nu(t_1)} \right\rangle_{|0_\phi\rangle\langle 0_\phi|} e^{\zeta^{(\nu,0)}(t,t_1)} = e^{-\varrho^\nu(t,t_1)}. \tag{3.95}$$

For succinctness, we only provide the integrals for $L^{\nu\nu}$, since L^{AB} is not needed to compute negativity.

$$\begin{aligned}
L^{\nu\nu} = (\lambda_\perp^\nu)^2 \int_{t_0}^{t} \mathrm{d}t_1 \int_{t_0}^{t} \mathrm{d}t_2\, e^{\mathrm{i}\Omega_\nu(t_1-t_2) - \varrho^\nu(t_2,t_1)} \chi_\perp^\nu(t_1) \\
\times \chi_\perp^\nu(t_2)\Big(W^{\nu\nu\nu}(t_2,t_1) - (\lambda_\parallel^\nu)^2 \int_{t_1}^{t_2} \mathrm{d}t_1'\, \chi_\parallel^\nu(t_1') \\
\times W^{\nu\nu\nu}(t_1',t_1) \int_{t_1}^{t_2} \mathrm{d}t_2'\, \chi_\parallel^\nu(t_2') W^{\nu\nu\nu}(t_2,t_2') \Big),
\end{aligned} \tag{3.96}$$

Lastly, for M,

$$\begin{aligned}
M = -\lambda_\perp^{\mathrm{A}} \lambda_\perp^{\mathrm{B}} \int_{t_0}^{t} \mathrm{d}t_1 \int_{t_0}^{t} \mathrm{d}t_2\, e^{-\varrho^{\mathrm{A}}(t,t_1) - \varrho^{\mathrm{B}}(t,t_2) - G_\parallel^{\mathrm{AB}}(t,t_1,t_2)} \\
\times e^{\mathrm{i}(\Omega_{\mathrm{A}} t_1 + \Omega_{\mathrm{B}} t_2)} \chi_\perp^{\mathrm{A}}(t_1)\chi_\perp^{\mathrm{B}}(t_2)\big(G^{\mathrm{AB}}(t_1,t_2) - B^{\mathrm{AB}}(t,t_1,t_2) \big),
\end{aligned} \tag{3.97}$$

where we defined

$$\begin{aligned}
G_\parallel^{\mathrm{AB}}(t,t_1,t_2) &= \lambda_\parallel^{\mathrm{A}} \lambda_\parallel^{\mathrm{B}} \int_{t_1}^{t} \mathrm{d}t_1' \int_{t_2}^{t} \mathrm{d}t_2'\, \chi_\parallel^{\mathrm{A}}(t_1')\chi_\parallel^{\mathrm{B}}(t_2') G^{\mathrm{AB}}(t_1',t_2'), \\
B^{\mu\nu}(t,t_1,t_2) &= \big(\mathcal{B}^{\mu\mu}(t,t_1,t_1) + \mathcal{B}^{\nu\mu}(t,t_2,t_1) \big)\big(\mathcal{B}^{\mu\nu}(t,t_1,t_2) + \mathcal{B}^{\nu\nu}(t,t_2,t_2) \big), \\
\mathcal{B}^{\mu\nu}(t,t_1,t_2) &= \lambda_\parallel^\mu \int_{t_1}^{t} \mathrm{d}t_1'\, \chi_\parallel^\mu(t_1') W^{\mu\nu}(t_1',t_2).
\end{aligned} \tag{3.98}$$

The equations (3.94) until (3.98) also hold more generally, for fields initialized in Gaussian states for which the expectation value of $\hat{\phi}$ is zero. Examples of such states, besides the vacuum, are thermal states.

3.3.2 Choice of smearing and switching functions

We will consider the smearing functions to be Gaussian, and use detectors of equal shape and size,

$$F_\nu(x) = F(x - x_\nu), \quad F(x) = \frac{1}{\sqrt{\pi}\sigma} e^{-\frac{x^2}{\sigma^2}}, \tag{3.99}$$

with $d = |x_{\text{A}} - x_{\text{B}}|$ being the distance between the detectors. Then,

$$\widetilde{F}_\nu(k) = e^{\mathrm{i}kx_\nu}\widetilde{F}(k), \quad \widetilde{F}(k) = e^{-\frac{1}{4}k^2\sigma^2} \tag{3.100}$$

and substituting into Eq. (3.77),

$$\alpha^\nu(t,k) = e^{\mathrm{i}(|k|t - kx_\nu)}\sqrt{\frac{|k|}{4\pi}} e^{-\frac{1}{4}k^2\sigma^2}, \tag{3.101}$$

and into Eq. (B.153),

$$\begin{aligned} W^{\mu\nu}(t_1,t_2) &= \int_{-\infty}^{\infty} \mathrm{d}k\, \alpha^{\mu *}(t_1,k)\alpha^\nu(t_2,k) \\ &= \frac{1}{4\pi}\int_{-\infty}^{\infty} \mathrm{d}k\, |k| e^{-\frac{1}{2}k^2\sigma^2} e^{\mathrm{i}|k|(t_2-t_1)+\mathrm{i}k(x_\mu - x_\nu)} \\ &= \frac{1}{2\pi}\int_0^{\infty} \mathrm{d}k\, k e^{-\frac{1}{2}k^2\sigma^2} \cos\big(k(x_\mu - x_\nu)\big) e^{\mathrm{i}k(t_2-t_1)}, \end{aligned} \tag{3.102}$$

and taking into account that $W^{\mu\nu -} = \mathrm{i}\,\mathrm{Im}(W^{\mu\nu})$,

$$W^{\mu\nu -}(t_1,t_2) = \frac{\mathrm{i}}{2\pi}\int_0^{\infty} \mathrm{d}k\, k e^{-\frac{1}{2}k^2\sigma^2} \cos\big(k(x_\mu - x_\nu)\big) \sin\big(k(t_2 - t_1)\big). \tag{3.103}$$

Remarkably, this integral has an analytical solution,

$$\begin{aligned} W^{\mu\nu -}(t_1,t_2) &= \frac{\mathrm{i}}{4\pi}\big(J^-(t_1 - t_2 + |x_\mu - x_\nu|) + J^-(t_1 - t_2 - |x_\mu - x_\nu|)\big), \\ J^-(t) &= -\int_0^{\infty} \mathrm{d}k\, |k| e^{-\frac{1}{2}k^2\sigma^2} \sin(kt) \\ &= -\frac{\sqrt{\pi}}{\sqrt{2}\sigma^3} t e^{-\frac{t^2}{2\sigma^2}}. \end{aligned} \tag{3.104}$$

Analogously, we can define $W^{\mu\nu+} = \mathrm{Re}(W^{\mu\nu})$ and obtain that

$$\begin{aligned} W^{\mu\nu+}(t_1, t_2) &= \frac{\mathrm{i}}{4\pi}\big(J^+(t_1 - t_2 + |x_\mu - x_\nu|) + J^+(t_1 - t_2 - |x_\mu - x_\nu|)\big), \\ J^+(t) &= \int_0^\infty \mathrm{d}k\, |k| e^{-\frac{1}{2}k^2\sigma^2} \cos(kt) \\ &= \frac{1}{\sigma^2} - \frac{\sqrt{2}}{\sigma^3} t\mathcal{D}\left(\frac{t}{\sqrt{2}\sigma}\right). \end{aligned} \tag{3.105}$$

where $\mathcal{D}(x) = \frac{\sqrt{\pi}}{2} e^{-x^2} \operatorname{erfi} x$ is the Dawson function[1], with $\operatorname{erfi} z = -\mathrm{i} \operatorname{erf} z$ the imaginary error function.

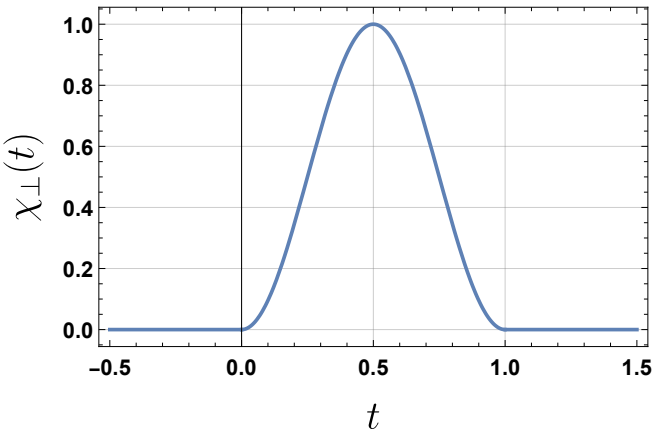


Figure 3.1: Choice of switching function for the transversal interaction.

Moving onto the choice of the longitudinal and transversal switching functions $\chi_\parallel^\nu(t)$ and $\chi_\perp^\nu(t)$, we take

$$\chi_\parallel^\nu(t) = 1, \qquad \chi_\perp^\nu(t) = \begin{cases} \sin(\pi t)^2 & 0 < t < 1, \\ 0 & \text{otherwise}, \end{cases} \tag{3.107}$$

where $\chi_\perp^{\mathrm{A}}(t) = \chi_\perp^{\mathrm{B}}(t)\chi_\perp(t)$ is illustrated in Figure 3.1. Note that $\chi_\perp(t)$ is a function with a continuous derivative, supported on the interval $[0, 1]$, meaning that the transversal interaction lasts for exactly one unit of time. The choice $\chi_\parallel^\nu(t) = 1$ means that the longitudinal

[1]The Dawson function is defined as

$$\mathcal{D}(x) \coloneqq e^{-x^2} \int_0^x \mathrm{d}y\, e^{-y^2}. \tag{3.106}$$

coupling is constantly active for both detectors. This setup represents the simplest case without any control over the longitudinal coupling. Our goal is to examine how much a constant, unintended longitudinal interaction can affect the amount of harvested entanglement.

Notice that even though the longitudinal interaction is always turned on, $\hat{\rho}_{\text{AB}}$ only starts to change at the time $t = 0$.[2] Accordingly, we choose the initial time to be $t_0 = 0$.

3.3.3 Effect of the longitudinal coupling strength on the evolution of the negativity

For simplicity, let us now consider equal coupling strengths for both detectors $\lambda_\perp = \lambda_\perp^{\text{A}} = \lambda_\perp^{\text{B}}$, $\lambda_\parallel = \lambda_\parallel^{\text{A}} = \lambda_\parallel^{\text{B}}$, and equal energy gaps, $\Omega = \Omega^{\text{B}} = \Omega^{\text{B}}$. Combining these with the choices of smearing and switching functions provided above and with the equations from subsection 3.3.1, we obtain $\xi = \xi^{\text{A}} = \xi^{\text{B}}$, $L = L^{\text{AA}} = L^{\text{BB}}$. Therefore, we can use the formula (3.83) for the negativity,

$$\mathcal{N}(\hat{\rho}_{\text{AB}}) = \max\left\{0, |M - \xi^2| + |\xi|^2 - L\right\} + \mathcal{O}(\lambda_\perp^3). \tag{3.108}$$

Note that $|M - \xi^2| + |\xi|^2 - L$ is proportional to $\lambda_\perp^2$. Therefore, instead of plotting $\mathcal{N}(\hat{\rho}_{\text{AB}})$, we will plot $\mathcal{N}(\hat{\rho}_{\text{AB}})/\lambda_\perp^2$ at leading order, which is independent of the value of $\lambda_\perp$.

After numerically integrating (3.94), (3.96) and (3.97), under the choices of smearing and switching of subsection 3.3.2, we obtain Figure 3.2. These figure shows the effects of progressively higher values of $\lambda_\parallel$. These plots reach regimes where higher order effects on $\lambda_\parallel$ are significant, and thus the non-perturbative expressions on $\lambda_\parallel$ that we are using become relevant to obtain the correct result.

[2] This is only true because the initial state of the detectors, chosen in equation (3.78), is longitudinal, like the interaction for $t < 0$.

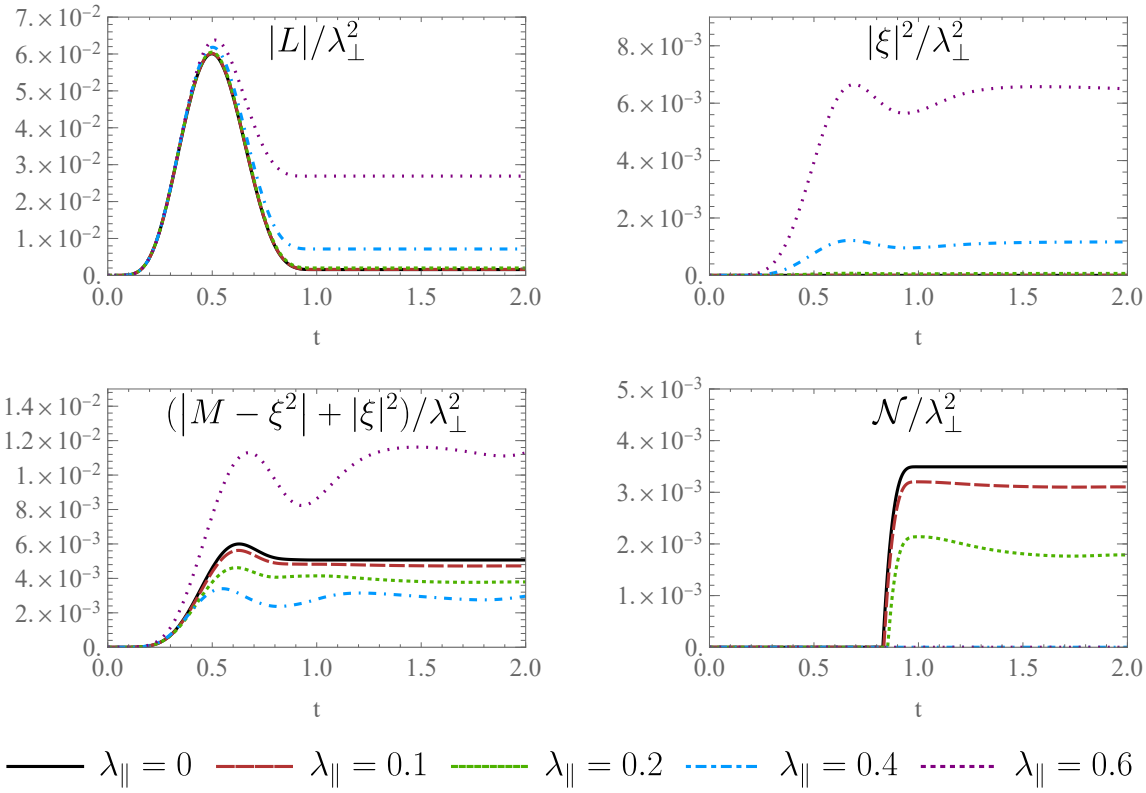


Figure 3.2: Numerical results for the scenario of the current section 3.3, with detector gap $\Omega = 9$, distance between detectors $d = 1$, and detector size $\sigma = 0.1$. The transversal interaction is turned on at time $t = 0$ and turned off at $t = 1$, smoothly, according to Eq. (3.107). The longitudinal interaction is constantly turned on, and we test different longitudinal coupling strengths, indicated by the value of $\lambda_\parallel$.

Chapter 4

Harvesting entanglement in a proposed superconducting implementation

4.1 Review of superconducting tunable couplers

In this section we will analyze the superconducting circuit model behind implementing tunable coupling of a superconducting qubit to a transmission line [3]. Namely, in this implementation, we can tune the coupling between superconducting qubits and a transmission line from zero coupling to the ultra-strong coupling regime in a matter of fractions of nanosecond. We will review the derivation of the Hamiltonian of this device, which will be useful for Section 4.2 where we relate it to the typical particle detector models employed in the literature of entanglement harvesting. To model the system we will follow a circuit model approach, similarly to the Supplementary material of [69] and to [100, 101].

4.1.1 Quantized transmission line

Superconducting transmission lines provide an experimental system where dynamical degrees of freedom of the electromagnetic field can be simplified into a one-dimensional real scalar quantum field theory. Although it is well-known in the literature of superconducting quantum devices, for convenience and notation setting purposes, we include here a brief derivation of the Hamiltonian of the transmission line from its lumped circuit model depicted in Figure 4.1.

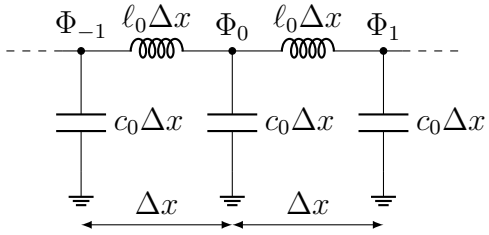


Figure 4.1: Lumped circuit model of a resistance-less transmission line.

The Hamiltonian of this lumped circuit model is

$$H_{\text{TL},\Delta x} = \frac{1}{2}\sum_i \frac{(\Phi_{i+1}-\Phi_i)^2}{\ell_0 \Delta x} + \frac{q_i^2}{c_0 \Delta x}, \tag{4.1}$$

where ℓ_0 and c_0 respectively are the inductance and capacitance per unit length. The variables Φ_i and q_i respectively are the flux and charge for the node i, and are defined as

$$\Phi_i(t) = \int_{-\infty}^{t} \mathrm{d}t'\, V_i(t'),\ q_i(t) = \int_{-\infty}^{t} \mathrm{d}t'\, I_i(t'), \tag{4.2}$$

where V_i and I_i respectively are the voltage and intensity from the node i to ground.

To get the Hamiltonian of the transmission line, we take the continuum limit, $\Delta x \to 0$, obtaining

$$H_{\text{TL}} = \frac{1}{2}\int \mathrm{d}x\, \frac{\partial_x \Phi(x)^2}{\ell_0} + \frac{q(x)^2}{c_0}, \tag{4.3}$$

where

$$\partial_t \Phi(x) = \frac{\delta H_{\text{TL}}}{\delta q(x)} = \frac{q(x)}{c_0}. \tag{4.4}$$

After quantization, $\hat{H}_{\text{TL}}$ can be recognized as the Hamiltonian of a 1D real massless scalar quantum field. Its Heisenberg picture amplitude operator $\hat{\Phi}$ is given by

$$\hat{\Phi}(t,x) = \sqrt{\hbar Z_0}\int \frac{\mathrm{d}k}{\sqrt{4\pi|k|}}(e^{\mathrm{i}(\omega_k t - kx)}\hat{a}_k^\dagger + \text{H.c.})\,. \tag{4.5}$$

Here, $Z_0 = \sqrt{\frac{\ell_0}{c_0}}$ is the characteristic impedance of the transmission line, $\omega_k = v|k|$ is the frequency of the the mode of wavenumber k and $v = 1/\sqrt{c_0\ell_0}$ is the speed of light in the

transmission line. The $\hat{a}_k$ and $\hat{a}_k^\dagger$ are the annihilation and creation operators of the mode k, which fulfill $[\hat{a}_k, \hat{a}_{k'}^\dagger] = \delta(k - k')$. Using these definitions, one finds that

$$\hat{H}_{\text{TL}} = \frac{1}{2} \int \mathrm{d}k \, \hbar\omega_k \Big(\hat{a}_k^\dagger \hat{a}_k + \hat{a}_k \hat{a}_k^\dagger \Big). \tag{4.6}$$

To give an idea about the physical scales of the system, typical parameters for the transmission line are (see e.g., [102, 70])

$$v \approx 1.2 \cdot 10^8 \, \mathrm{m\,s^{-1}}, \;\; Z_0 \approx 50 \, \Omega. \tag{4.7}$$

We will use these values throughout this work.

There is a frequency scale beyond which electromagnetic signals in the transmission line get attenuated. This attenuation increases drastically beyond the superconducting gap. For aluminum, commonly used for superconducting transmission lines, the superconducting gap is 75 GHz [103]. Therefore, the experimental implementation introduces an effective UV cutoff scale. The effects of the cutoff and finite size of the superconducting qubits were explored in [67], and become more relevant for shorter interactions.

In this work, we consider an exponential cutoff at a frequency scale of $\Omega_{\text{cut}}/(2\pi) = 50\,\text{GHz}$. This cutoff value was found in [70] by matching experimental measurements with the renormalized frequency of the coupled qubit (which is cutoff dependent), under the renormalization model of [104, 68]. To implement the cutoff, we modify the field operator that interacts with the qubit as follows,

$$\hat{\Phi}_{\text{C}}(t, x) = \sqrt{\hbar Z_0} \int \mathrm{d}k \, \frac{\text{C}(\omega_k)}{\sqrt{4\pi|k|}} (e^{\mathrm{i}(\omega_k t - kx)} \hat{a}_k^\dagger + \text{H.c.}) \, . \tag{4.8}$$

Here, we added the exponentially decreasing weight

$$\text{C}(\omega) = e^{-\frac{|\omega|}{2\Omega_{\text{cut}}}} . \tag{4.9}$$

As discussed in [67], this implementation of the cutoff is equivalent to the qubit interacting with a spatially smeared version of the field. Specifically,

$$\hat{\Phi}_{\text{C}}(t, x) = \int \mathrm{d}x' \, F_{\text{eff}}(x' - x) \hat{\Phi}(t, x'), \tag{4.10}$$

where the effective smearing function $F_{\text{eff}}(x)$ is

$$F_{\text{eff}}(x) = \frac{1}{2\pi} \int \mathrm{d}k \; \text{C}(\omega_k) e^{\mathrm{i}kx} = \frac{1}{2\pi v} \widetilde{\text{C}}\left(\frac{x}{v}\right), \tag{4.11}$$

with the following Fourier transform convention

$$\widetilde{f}(k) = \int \mathrm{d}x\, f(x) e^{\mathrm{i}kx}. \tag{4.12}$$

The expression for $F_{\text{eff}}(x)$ follows from comparing Eqs. (4.5) and (4.8) to see that $\widetilde{F}_{\text{eff}}(k) = \mathrm{C}(\omega_k)$, and then using the inverse Fourier transform together with $\omega_k = v|k|$. Notice that $F_{\text{eff}}(x) \in \mathbb{R}$ and $F_{\text{eff}}(x) = F_{\text{eff}}(-x)$, due to $\widetilde{F}_{\text{eff}}(k) \in \mathbb{R}$ and $\widetilde{F}_{\text{eff}}(k) = \widetilde{F}_{\text{eff}}(-k)$.

In particular, for the exponential cutoff chosen in Eq. (4.9),

$$F_{\text{eff}}(x) = \frac{2\Omega_{\text{cut}}}{\pi v} \frac{1}{1 + \left(\frac{2\Omega_{\text{cut}}}{v} x\right)^2}. \tag{4.13}$$

4.1.2 Tunable coupler and flux qubit

Here we describe the superconducting circuit which performs the role of the detector in the entanglement harvesting implementation. Following the proposal of [3], this circuit consists of a flux qubit tunably coupled to the transmission line. This circuit is made out of Josephson junctions, which can be implemented as a small insulating gap between superconducting materials. In circuit diagrams, Josephson junctions are indicated as crosses. In practice, Josephson junctions always have a capacitance in parallel, indicated by drawing the crosses in a box.

Consider the flux qubit depicted in Figure 4.2. The qubit subspace consists of the two lowest energy levels of the circuit. The flux qubit consists of a superconducting loop with Josephson junctions. The loop is threaded by an external magnetic flux f_ε, which can be tuned arbitrarily and is chosen so that the qubit is in the symmetry point, i.e. in a minimum of the qubit frequency.

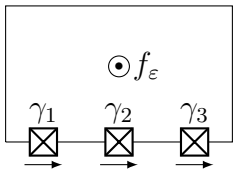


Figure 4.2: Circuit model of a flux qubit. The γ_i indicate the phase variable of the i-th Josephson junction.

The tunable coupler is an additional loop with Josphson junctions, threaded by an external flux f_β, shown in Figure 4.3. From now on, we will refer to the two lowest energy levels of the combined circuit presented in Figure 4.3 as the *qubit subspace*, which differs from the qubit subspace of the flux qubit.

The transmission line is connected at a and b, which makes the phase operator $\hat{\gamma}_5$ couple to the transmission line. Then, the parameter f_β allows to tune the coupling strength between the qubit and the transmission line, by changing the size of $\hat{\gamma}_5$ in the qubit subspace.

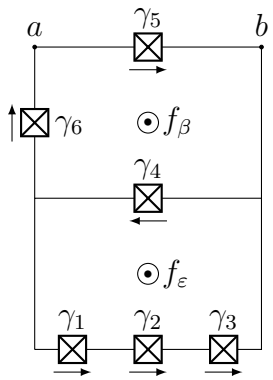


Figure 4.3: Circuit model of the tunable coupler connected to the flux qubit. The tunable coupler connects to the transmission line through the points a and b.

The tunable coupler + flux qubit circuit is quantized by using the following conjugate sets of variables

$$\boldsymbol{\gamma} = \begin{bmatrix} \gamma_1 \\ \gamma_2 \\ \gamma_5 \\ \gamma_6 \end{bmatrix}, \quad \boldsymbol{p} = \hbar \boldsymbol{N} = \hbar \begin{bmatrix} N_1 \\ N_2 \\ N_5 \\ N_6 \end{bmatrix}, \tag{4.14}$$

where the phase degrees of freedom, γ_i, are 2π-periodic. The resulting Hamiltonian of the tunable coupler and the flux qubit is

$$\begin{aligned} \hat{H}_{\text{TC+FQ}} = 2e^2 \hat{\boldsymbol{N}}^\top C^{-1} \hat{\boldsymbol{N}} &- \sum_{i \in \{1,2,5,6\}} E_{J_i} \cos(\hat{\gamma}_i) \\ &- E_{J_3} \cos(\hat{\gamma}_1 + \hat{\gamma}_2 - \hat{\gamma}_5 - \hat{\gamma}_6 + 2\pi f_\varepsilon + 2\pi f_\beta) \\ &- E_{J_4} \cos(\hat{\gamma}_5 + \hat{\gamma}_6 - 2\pi f_\beta), \end{aligned} \tag{4.15}$$

where the C is a matrix of capacitances, the E_{J_i} is the Josephson energy of the i-th junction[1], and the f_ε and f_β are external magnetic fluxes, which can be controlled during the experiment. For a review of the circuit theory for superconducting qubits, which was used to derive this Hamiltonian, see [105].

Notice that $\hat{H}_{\text{TC+FQ}}$ plays the role of the free Hamiltoinan in the usual detector models, and importantly, it has non-linear cosine terms, which come from the Josephson junctions and do not appear in most common detector models, such as qubits or harmonic oscillators. These terms are key to create superconducting qubits and superconducting devices in general. Moreover, the presence of the external magnetic fluxes f_ε and f_β in the non-linear terms is what allows to tune the coupling to the transmission line. However, relating the Hamiltonian of this circuit to the common detector models requires some work that will be done in section 4.2. It is there that we will show how this circuit can be approximated under certain regimes as a variable gap qubit detector.

4.1.3 Coupling the superconducting circuit to the transmission line

Here, we derive the interaction between a superconducting circuit, such as the tunable coupler + flux qubit (TC+FQ) circuit, and the transmission line. To do so, we start from the lumped circuit model depicted in Figure 4.4, which includes both the TC+FQ circuit and the transmission line, and take the limit $\Delta x \to 0$.

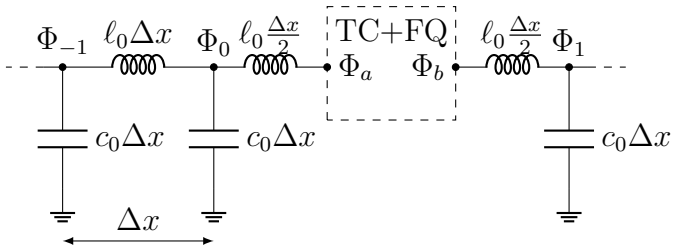


Figure 4.4: Lumped circuit model of a transmission line coupled to the TC+FQ circuit of Figure 4.3, depicted as a dashed box.

[1]Ref. [3] obtained the matrix of capcitances from an electromagnetic simulation of the superconducting circuit. Then, they found the value of the critical currents $I_{c_i} = E_{J_i}/\varphi_0$ by fitting the numerically computed qubit frequencies to their measurements for multiple values of f_β and f_ε. Here, $\varphi_0 = \hbar/(2e)$ denotes the reduced magnetic flux quanta.

The circuit in Figure 4.4 has the following Hamiltonian:

$$\hat{H}_{\Delta x} = \hat{H}_{\text{TC+FQ}} + \sum_i \frac{\hat{q}_i^2}{2c_0\Delta x} + \sum_{i\neq 0} \frac{1}{2\ell_0\Delta x}(\hat{\Phi}_{i+1} - \hat{\Phi}_i)^2 + \frac{1}{\ell_0\Delta x}(\hat{\Phi}_a - \hat{\Phi}_0)^2 + \frac{1}{\ell_0\Delta x}(\hat{\Phi}_1 - \hat{\Phi}_b)^2. \tag{4.16}$$

Here, $\hat{\Phi}_a$ and $\hat{\Phi}_b$ respectively denote the fluxes at the nodes a and b of the TC+FQ circuit depicted in Figure 4.3. These fluxes relate to the branch variable $\hat{\gamma}_5$ as follows, $\hat{\Phi}_b - \hat{\Phi}_a = \varphi_0\hat{\gamma}_5$, with $\varphi_0 = \frac{\hbar}{2e}$ the reduced magnetic flux quanta. Performing the change of variables $\hat{\Phi}_\pm = \hat{\Phi}_b \pm \hat{\Phi}_a$ and a few algebraic manipulations,

$$\begin{aligned}&(\hat{\Phi}_0 - \hat{\Phi}_a)^2 + (\hat{\Phi}_1 - \hat{\Phi}_b)^2 \\ &= \frac{1}{2}(\hat{\Phi}_1 - \hat{\Phi}_0)^2 - (\hat{\Phi}_1 - \hat{\Phi}_0)\hat{\Phi}_- + \frac{\hat{\Phi}_-^2}{2} + \frac{1}{2}(\hat{\Phi}_1 + \hat{\Phi}_0 - \hat{\Phi}_+)^2.\end{aligned} \tag{4.17}$$

Substituting back into $\hat{H}_{\Delta x}$,

$$\hat{H}_{\Delta x} = \hat{H}_{\text{TC+FQ}} + \hat{H}_{\text{TL},\Delta x} - \frac{\hat{\Phi}_1 - \hat{\Phi}_0}{\ell_0\Delta x}\hat{\Phi}_- + \frac{\hat{\Phi}_-^2}{2\ell_0\Delta x} + \frac{(\hat{\Phi}_1 + \hat{\Phi}_0 - \hat{\Phi}_+)^2}{2\ell_0\Delta x}. \tag{4.18}$$

Now, taking $\Delta x \to 0$, the Hamiltonian becomes

$$\begin{aligned}\hat{H} &= \hat{H}_{\text{TC+FQ}} + \hat{H}_{\text{TL}} + \hat{H}_{\text{INT}}, \\ \hat{H}_{\text{INT}} &= -\frac{1}{\ell_0}\hat{\Phi}_-\partial_x\hat{\Phi}(x_{\text{TC+FQ}}).\end{aligned} \tag{4.19}$$

Here, $x_{\text{TC+FQ}}$ is the position of the TC+FQ circuit, which we effectively treat as point-like. This treatment is justified because the field cutoff given in Eq. (4.9) (with scale $\Omega_{\text{cut}}/(2\pi) = 50\,\text{GHz}$) dominates the TC+FQ circuit physical size[2], which is approximately 100 µm in the proposal of [3]. For a more detailed study of how the effects of the cutoff and the superconducting circuit size combine, see [67].

Moreover, we used that $(\hat{\Phi}_1 + \hat{\Phi}_0 - \hat{\Phi}_+)^2/\Delta x \to 0$ when taking $\Delta x \to 0$. This is a consequence of the following inductor relationships,

$$\hat{\Phi}_0 - \hat{\Phi}_a = \frac{\ell_0\Delta x}{2}\hat{I}_{0a}, \quad \hat{\Phi}_b - \hat{\Phi}_1 = \frac{\ell_0\Delta x}{2}\hat{I}_{b1}. \tag{4.20}$$

[2]The cutoff makes it so that distances smaller than $\frac{v}{\Omega_{\text{cut}}} = 0.38\,\text{mm}$ are not resolved by the field.

Here, $\hat{I}_{0a}$ and $\hat{I}_{b1}$ respectively are the currents from nodes 0 to a and from nodes b to 1. Then, from Eq. (4.20) and $\hat{\Phi}_+ = \hat{\Phi}_a + \hat{\Phi}_b$,

$$\frac{(\hat{\Phi}_1 + \hat{\Phi}_0 - \hat{\Phi}_+)^2}{\Delta x} = \frac{\ell_0^2}{4}(\hat{I}_{0a} - \hat{I}_{b1})^2 \Delta x = \mathcal{O}(\Delta x), \tag{4.21}$$

which implies that $(\hat{\Phi}_1 + \hat{\Phi}_0 - \hat{\Phi}_+)^2/\Delta x \to 0$ as $\Delta x \to 0$.[3]

Additionally, to obtain $\hat{H}$, we neglected the renormalization term $\hat{\Phi}_-^2/(2\ell_0 \Delta x)$. This approximation is common for superconducting circuits coupled to transmission lines. The renormalization term diverges in the limit $\Delta x \to 0$. This divergence could be avoided by not fully taking the continuum limit, and instead picking a finite value of Δx. Such a discretized transmission line has a dispersion relation $\omega(k)$ that is linear at small k, but nonlinearities kick in as k approaches $1/\Delta x$, see e.g. [104]. A reasonable choice of Δx would be the one associated to the smallest resolvable length given the measured cutoff, $v/\Omega_{\text{cut}} = 0.38\,\text{mm}$. For this value of Δx, the renormalization term would significantly modify the energy levels of the TC+FQ circuit [4]. Nonetheless, in this work we *do* take the continuum limit, neglecting the renormalization term, for both ease of computation and ease of comparison with common UDW detector models. We do not expect that adding back the renormalization term would change the main conclusions of our work. Notably, $\hat{H}_{\text{INT}}$ remains the same regardless of whether the renormalization term is included. The effect of the renormalization term will be analyzed in future work.

Finally, notice that the interaction term $\hat{H}_{\text{INT}}$ is proportional to the flux jump $\hat{\Phi}_-$ across the TC+FQ circuit, which fulfills $\hat{\Phi}_- = \varphi_0 \hat{\gamma}_5$. Moreover, after replacing $\hat{\Phi}$ by the $\hat{\Phi}_{\text{C}}$ of Eq. (4.8), which includes the cutoff, the final expression for $\hat{H}_{\text{INT}}$ becomes

$$\hat{H}_{\text{INT}} = -\frac{\varphi_0}{\ell_0}\hat{\gamma}_5 \partial_x \hat{\Phi}_{\text{C}}(x_{\text{TC+FQ}}). \tag{4.22}$$

While this interaction Hamiltonian is constant, tunability is achieved by controlling the parameters f_β and f_ε, which change the projection of $\hat{\gamma}_5$ on the qubit subspace (i.e., the

[3] This argument relies on the difference of currents $\hat{I}_{0a} - \hat{I}_{b1}$ tending to a finite value as $\Delta x \to 0$. This difference of currents can be understood as the amount of current flowing into the TC+FQ circuit from the transmission line. For the circuit model of the TC+FQ circuit given in this chapter, $\hat{I}_{0a} - \hat{I}_{b1} = 0$. However, one can consider improving the circuit model by adding a capacitive coupling to the ground, which is present in the actual implementation. Even in that case, we expect the amount of current flowing from the TC+FQ circuit to the ground through a capacitive coupling to remain finite as $\Delta x \to 0$, and thus the same should apply to $\hat{I}_{0a} - \hat{I}_{b1}$.

[4] If we choose $\Delta x = 0.38\,\text{mm}$, then $\ell_0 \Delta x = 0.16\,\text{nH}$, which is comparable to the Josephson inductance of the junction that lies in the transmission line path. This means that the renormalization term would contribute significantly to $\hat{H}_{\text{TC+FQ}}$.

space spanned by the two lowest energy eigenvectors of (4.15)), effectively reducing or increasing the intensity of the interaction.

4.2 A variable gap particle detector as a model of flux qubit and tunable coupler

By means of an adiabatic approximation, we will relate the TC+FQ implementation given in Section 4.1 to a variable gap detector model, which resembles the most common particle detector used in RQI protocols, the UDW detector.

4.2.1 Simplifying the TC+FQ circuit model

Two-level approximation

To reduce the tunable coupler + flux qubit circuit into a qubit, we need to truncate the energy levels, keeping only the two lowest-energy eigenvectors of $\hat{H}_{\text{TC+FQ}}$. Neglecting higher energy levels can be justified when their transition frequencies are large compared to the qubit transition frequency. Then, if the coupling is switched on and off slowly enough, the adiabatic theorem forbids transitions that leave the qubit subspace. The exact conditions under which this adiabatic approximation in the ultra-strong coupling regime is justified are subtle and will be explored elsewhere. Here we will operate under the assumption that they hold, as experimentally validated in cases where the coupling is not too strong [70, 106, 107]. All the quantities of interest for the qubit, such as the energy gap and coupling strength, can be computed from the numerical diagonalization of the Hamiltonian $\hat{H}_{\text{TC+FQ}}$ in a suitably truncated charge basis. In the TC+FQ circuit, for each f_β, the value of f_ε is picked to minimize the qubit transition frequency [3]. This choice corresponds to a coupling between the qubit and the transmission line that best approximates the transverse coupling model in UDW detectors. Then, the only remaining controllable parameter in the qubit Hamiltonian is f_β,

$$\hat{H}_{\text{QB}}(f_\beta) = \hbar\Omega(f_\beta)\,|1_{f_\beta}\rangle\langle 1_{f_\beta}|\,. \tag{4.23}$$

Here, we denoted as $|0_{f_\beta}\rangle$ and $|1_{f_\beta}\rangle$ the ground and first excited states, and as $\hbar\Omega(f_\beta)$ the qubit energy gap. For the qubit approximation it is important to mention that the energy levels do not cross between the different eigenvectors of the TC+FQ system.

Notice that the reduction to two levels is not necessary to connect the UDW model to the TC+FQ system. Indeed UDW detectors with multiple levels are commonplace in the literature, but for convenience and simplicity of this analysis we will keep it as two levels.

Taking the adiabatic approximation on the free qubit evolution

Changing the parameter f_β over time can induce transitions in the qubit and even cause the TC+FQ circuit of Figure 4.3 to leave the qubit subspace. These transitions occur even if the circuit is not connected to the transmission line, and are a consequence of the fact that the energy eigenstates of the TC+FQ circuit change with f_β. To avoid this phenomenon, we assume that f_β is tuned slowly enough to apply the adiabatic theorem to the free qubit evolution.

The adiabatic approximation implies that for a qubit state of the form

$$|\psi_{\text{QB}}(t)\rangle = a_0(t)\,|0_t\rangle + a_1(t)\,|1_t\rangle\,, \tag{4.24}$$

where $|0_t\rangle$ and $|1_t\rangle$ are the ground and first excited state at time t (which are determined by the choice of $f_\beta(t)$), coefficients remain the same under time evolution modulo a relative phase:

$$a_0(t) = e^{\mathrm{i}\theta_0(t)}a_0(0),\;\; a_1(t) = e^{-\mathrm{i}\varphi(t)+\mathrm{i}\theta_1(t)}a_1(0). \tag{4.25}$$

This is a good approximation for the free evolution of the qubit when the Hamiltonian $\hat{H}_{\text{QB}}(t)$ changes slowly enough and the energy gap is non-zero, i.e. $\hbar\Omega(t) \neq 0$. The phases $\varphi(t)$ and $\theta_i(t)$ in Eq. (4.25) is given by

$$\varphi(t) = \int_0^t \mathrm{d}t\,'\Omega(t'),\;\; \theta_i(t) = \mathrm{i}\int_0^t \mathrm{d}t'\;\langle i_{t'}|\partial_{t'}|i_{t'}\rangle,\;\; i \in \{0,1\} \tag{4.26}$$

with $\theta_i(t)$ called the geometric phase. We choose to set $\theta_0(t) = \theta_1(t) = 0$, which can always be done when the Hamiltonian depends on a single parameter, by appropriately changing the basis[5].

In summary, the adiabatic limit ensures that there are no transitions between energy levels due to the free dynamics, since their probabilities $p_i = |a_i|^2$ remain constant. Moreover, we can guarantee that the circuit stays in the qubit subspace during its free evolution by similarly applying the adiabatic theorem to the complete multilevel Hamiltonian given in Eq. (4.15). Therefore, after the adiabatic approximation, the circuit behaves exactly as a qubit with constant energy eigenbasis $\{|0\rangle, |1\rangle\}$ and time-dependent energy gap $\hbar\Omega(t)$.

[5]To impose $\theta_0(t) = \theta_1(t) = 0$, we use that the geometric phase can be rewritten as $\theta_i(f_\beta)$ and absorb it into the definition of the $|i_{f_\beta}\rangle$.

Transversal coupling approximation

The interaction Hamiltonian obtained in Eq. (4.22) shows that the coupling occurs through $\hat{\gamma}_5$. Consider $\hat{\gamma}_5^{\mathrm{QB}}$ to be the restriction of $\hat{\gamma}_5$ onto the qubit subspace. Then, $\hat{\gamma}_5^{\mathrm{QB}}$ can be expressed in as a linear combination of identity and Pauli operators,

$$\hat{\gamma}_5^{\mathrm{QB}} = \gamma_x \hat{\sigma}_x + \gamma_y \hat{\sigma}_y + \gamma_z \hat{\sigma}_z + \gamma_{id} \hat{\mathbb{1}}, \tag{4.27}$$

where $\hat{\sigma}_z = |0_{f_\beta}\rangle\langle 0_{f_\beta}| - |1_{f_\beta}\rangle\langle 1_{f_\beta}|$. Notice that, for simplicity of notation we have omitted writing the dependency of all terms on f_β.

In this paper we are going to assume that the longitudinal coupling γ_z and the term γ_{id} are zero. For f_ϵ such that the qubit transition frequency is minimal, the longitudinal coupling γ_z was shown to be negligible in [3]. Moreover, neglecting γ_z and γ_{id} does not affect entanglement harvesting at leading order in the coupling strength under the following sufficient conditions, which are assumed in the next sections: 1) the qubits are prepared in an eigenstate of their free Hamiltonians, 2) we are under the adiabatic approximation for the free evolution of the qubits (see Chapter 3).

The transversal coupling coefficients γ_x and γ_y as a function of f_β are

$$\gamma_x = \mathrm{Re}\,\langle 1_{f_\beta}|\hat{\gamma}_5|0_{f_\beta}\rangle\,,\ \ \gamma_y = \mathrm{Im}\,\langle 1_{f_\beta}|\hat{\gamma}_5|0_{f_\beta}\rangle\,. \tag{4.28}$$

We obtain the states $|0_{f_\beta}\rangle$ and $|1_{f_\beta}\rangle$, up to an overall phase, by diagonalizing the Hamiltonian in Eq. (4.15). We fix this phase freedom by choosing the energy eigenfunctions to be real in the phase representation[6]. This can be done because $\hat{H}_{\mathrm{TC+FQ}}\,|i_{f_\beta}\rangle = E_i(f_\beta)\,|i_{f_\beta}\rangle$ is a real differential equation in this representation. With this phase choice, the geometric phases automatically vanish, i.e. $\langle i_{f_\beta}|\partial_{f_\beta}|i_{f_\beta}\rangle = 0$. To see why, notice that since the wavefunction of $|i_{f_\beta}\rangle$ is real, then $\langle i_{f_\beta}|\partial_{f_\beta}|i_{f_\beta}\rangle$ must be real. However, the normalization condition $\langle i_{f_\beta}|i_{f_\beta}\rangle = 1$ implies that $\langle i_{f_\beta}|\partial_{f_\beta}|i_{f_\beta}\rangle$ must be imaginary. This only leaves the possibility that $\langle i_{f_\beta}|\partial_{f_\beta}|i_{f_\beta}\rangle = 0$, which means that there is no geometric phase for our choice.

Fixing the phase freedom as described above and using the parameters that match the design proposal of Ref. [3][7], we obtain the following: for $f_\beta \in [0.3, 0.5]$, $\gamma_x(f_\beta) \in [-0.02, 0.22]$ and $\gamma_y(f_\beta) = 0$, with $\gamma_x(f_\beta)$ an increasing function. Therefore, controlling f_β tunes the transversal coupling strength γ_x. The reason for $\gamma_y(f_\beta) = 0$ is that $\langle 1_{f_\beta}|\hat{\gamma}_5|0_{f_\beta}\rangle$

[6] In the phase representation, the states are represented by wavefunctions such as $\psi(\gamma_1, \gamma_2, \gamma_5, \gamma_6)$. For $i \in \{1, 2, 5, 6\}$, the phase operators $\hat{\gamma}_i$ act as a multiplication by γ_i, and the number operators $\hat{N}_i$ act as the partial derivative $-\mathrm{i}\partial_{\gamma_i}$.

[7] Specifically, we use for the critical currents: $I_{c_1} = 0.236\,\mu\mathrm{A}$, $I_{c_2} = 0.131\,\mu\mathrm{A}$, $I_{c_3} = 0.236\,\mu\mathrm{A}$, $I_{c_4} =$

is real. To see this, consider that in the phase representation, $\langle 1_{f_\beta}|\hat{\gamma}_5|0_{f_\beta}\rangle$ is the integral of the product of three real functions. Specifically, the real wavefunctions of $|0_{f_\beta}\rangle$ and $|1_{f_\beta}\rangle$, and the real quantity γ_5.

Approximated linear dependence of the gap on the instantaneous transversal coupling strength

The energy gap of the qubit $\hbar\Omega$ varies with f_β, which can be rewritten as a dependence of Ω on the instantaneous transversal coupling strength γ_x. The exact form of this dependence is also obtained using the numerical diagonalization of the Hamiltonian of the tunable coupler + flux qubit. Using the best fit parameters found in [3] for the Hamiltonian (4.15), results in the data in Figure 4.5.

The figure shows that the dependency $\Omega(\gamma_x)$ is approximately linear, which implies that

$$\Omega(t) \approx \Omega^0 + \Delta\Omega\chi(t). \tag{4.29}$$

Here, we chose $\gamma_x(t) = \gamma\chi(t)$, with $\chi(t)$ a switching function which takes values between zero and one, and γ the maximum value of $\gamma_x(t)$ reached during the interaction. Moreover, $\hbar\Omega^0$ is the energy gap of the free qubit, or in other words, the energy gap when the interaction is turned off. The product $\hbar\Delta\Omega$ determines the strength of the gap variation due to the coupling. Precisely, $\hbar\Delta\Omega$ is equal to the difference between the energy gap with the coupling turned on (when $\chi(t) = 1$) and the coupling turned off (when $\chi(t) = 0$). From Figure 4.5, we estimate

$$\frac{\Omega^0}{2\pi} \approx 7.3\,\text{GHz}, \quad \frac{\Delta\Omega}{2\pi} \approx -23 \cdot \gamma\,\text{GHz}. \tag{4.30}$$

4.2.2 Result of the simplifications of the TC+FQ circuit model

In summary, section 4.2.1 provided the following approximations to simplify the TC+FQ circuit:

$0.411\,\mu\text{A}$, $I_{c_5} = 0.584\,\mu\text{A}$, $I_{c_6} = 0.185\,\mu\text{A}$, and for the inverse capacitance matrix:

$$C^{-1} = \begin{pmatrix} 144. & -81.5 & 2.94 & 18.6 \\ -81.5 & 196. & 6.18 & 24.8 \\ 2.94 & 6.18 & 46.1 & -32.4 \\ 18.6 & 24.8 & -32.4 & 87.7 \end{pmatrix} (\text{pF})^{-1}.$$

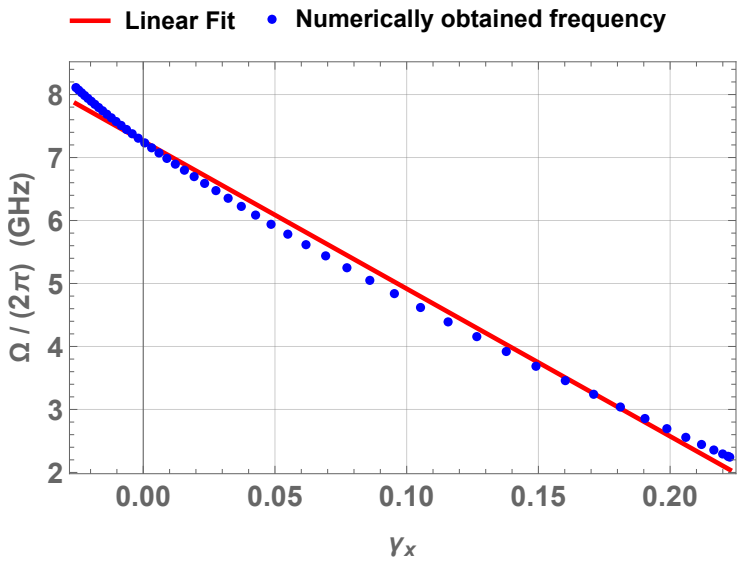


Figure 4.5: The blue dots show the superconducting qubit transition frequency $\Omega/2\pi$ for each transversal coupling strength γ_x. This frequency is computed from the numerical diagonalization of the Hamiltonian (4.15), with parameters chosen to match [3]. The red line is the linear best fit.

1. The two-level approximation.
2. The adiabatic approximation of the free qubit evolution.
3. The transversal coupling assumption, $\gamma_{id} = \gamma_z = 0$.
4. The linear approximation of the dependence of Ω on γ_x.

The resulting simplified model resembles a qubit particle detector with variable gap and spatial derivative coupling. This detector model has the following interaction picture interaction Hamiltonian,

$$\hat{H}_{\text{INT}}(t) = -\frac{\varphi_0}{\ell_0}\gamma\chi(t)\hat{\mu}(t)\partial_x\hat{\Phi}_{\text{C}}(t, x_{\text{D}}). \tag{4.31}$$

Here, remember that $\varphi_0 = \frac{\hbar}{2e}$ is the reduced magnetic flux quanta, ℓ_0 the inductance per unit length of the transmission line, γ the adimensional coupling strength, $\chi(t) \in [0, 1]$ the switching function, and x_{D} the detector position. Moreover, $\hat{\Phi}_{\text{C}}$ is the field with cutoff of

Eq. (4.8), and $\hat{\mu}(t)$ is the monopole moment in the interaction picture, given by

$$\hat{\mu}(t) = e^{\mathrm{i}\varphi(t)}\hat{\sigma}^{+} + \text{H.c.},\ \varphi(t) = \Omega^{0}t + \Delta\Omega \int_{0}^{t} \mathrm{d}t'\chi(t'), \tag{4.32}$$

with $\hbar\Omega^0$ the energy gap of the free qubit, $\hbar\Delta\Omega$ the strength of the energy gap variation due to the coupling, and $\hat{\sigma}^{+} = |1\rangle\langle 0|$, $\hat{\sigma}^{-} = |0\rangle\langle 1|$ the qubit ladder operators.

It is convenient to relate this detector model to the spin-boson model, commonly used to model superconducting qubits coupled to transmission lines, for comparison with other works. Appendix C.1 is devoted to showing this relation. When the interaction is fully switched on ($\chi(t) = 1$), γ relates to the dimensionless spin-boson coupling constant α as follows,

$$\alpha = \frac{R_{\mathrm{K}}}{8\pi^2 Z_0}\gamma^2 \approx 6.54 \cdot \gamma^2, \tag{4.33}$$

where $R_{\mathrm{K}} = \frac{h}{e^2}$ is the von Klitzing constant, and we used $Z_0 \approx 50\,\Omega$ (see Eq. (4.7)).

4.2.3 Comparison of the variable gap detector to UDW detectors

Even with the simplifications of the TC+FQ circuit in Subsection 4.2.2, the resulting detector model (see Eq. (4.31)) has features that have been largely unexplored in the context of RQI. A very usual choice of interaction Hamiltonian for particle detectors in the RQI literature is the simple Unruh-DeWitt model, whose interaction with the field (generating time evolution with respect to the proper time of the detector centre-of-mass) is given by

$$\hat{H}_{\mathrm{UDW}}(t) = \lambda\chi(t)\hat{\mu}_{\mathrm{UDW}}(t) \int \mathrm{d}x\, F(x)\hat{\phi}(t,x). \tag{4.34}$$

Here, λ is the coupling strength, $\chi(t)$ is the switching function, $F(x)$ is the smearing function, $\hat{\phi}(t,x)$ is the field amplitude operator, and the monopole operator is

$$\hat{\mu}_{\mathrm{UDW}}(t) = e^{\mathrm{i}\Omega t}\hat{\sigma}^{+} + \text{H.c.}, \tag{4.35}$$

where the constant qubit energy gap is Ω and typically natural units $\hbar = c = 1$ are chosen.

Notice the similarities with the detector that we provided in Eq. (4.31), which therefore sits in between the full TC+FQ model of the experiment and the simpler UDW model used in RQI theory. The additional features of our proposed intermediate model are:

1. The gap Ω varies over time, with the variation being proportional to $\chi(t)$ (see Eq. (4.29)).

2. The detector couples to the spatial derivative of a 1D real massless scalar quantum field (see Eq. (4.31)).

3. The detector is point-like, but the field has a cutoff (see Eq. (4.8)). This corresponds to effectively having a smearing that fulfills $\widetilde{F}(k) = \mathrm{C}(\omega_k)$, as shown in Eq. (4.11).

These features will impact entanglement harvesting in future experiments that use the TC+FQ circuit design from [3], but they have not yet been studied in detail in the literature on entanglement harvesting. Doing precisely this is the object of the following sections.

4.3 Entanglement Harvesting with detectors of variable gap

This section presents a common protocol to perform entanglement harvesting in RQI, with the modification that we use variable gap detectors with the features highlighted in Section 4.2.2 instead of the usual UDW detectors. We will refer to this model as VGSD detector (variable gap, spatial-derivative coupling). It is useful to write this section with the most generality possible in order to be able to compare with previously existing RQI literature. Therefore, we will work with an arbitrary coupling strength λ and only make the substitutions related to the implementation in superconducting circuits in section 4.5. However, we will still keep full dimensional $\hbar$ and c in the protocol presented below, to make the translation easier.

Consider a massless scalar 1+1D field. The field amplitude operator, expanded in terms of plane waves and including a cutoff function, is

$$\hat{\phi}_{\mathrm{C}}(t,x) = \int \mathrm{d}k \, \frac{\mathrm{C}(\omega_k)}{\sqrt{4\pi|k|}} (e^{\mathrm{i}(\omega_k t - kx)} \hat{a}_k^\dagger + \mathrm{H.c.}) \,. \tag{4.36}$$

Here, $\omega_k = c|k|$, and $\mathrm{C}(\omega_k)$ is the weight function that implements the cutoff.

In order to harvest entanglement, we couple two VGSD detectors to the field, labeled by $\nu \in \{A, B\}$ according to the following interaction Hamiltonian in the interaction picture,

$$\hat{H}_I(t) = \hbar c \sum_\nu \lambda_\nu \chi_\nu(t) \hat{\mu}_\nu(t) \partial_x \hat{\phi}_{\mathrm{C}}(t, x_\nu). \tag{4.37}$$

For the detector ν, λ_ν is the coupling strength, $\chi_\nu(t)$ is the switching function, x_ν is the detector position[8], and $\hat{\mu}_\nu(t)$ is the monopole operator in the interaction picture,

$$\begin{aligned}\hat{\mu}_\nu(t) &= e^{\mathrm{i}\varphi_\nu(t)}\hat{\sigma}_\nu^+ + \text{H.c.},\\ \varphi_\nu(t) &= \int_0^t \mathrm{d}t'\,\Omega_\nu(t'),\end{aligned} \tag{4.38}$$

with $\hat{\sigma}_\nu^+ = |1_\nu\rangle\langle 0_\nu|$, $\hat{\sigma}_\nu^- = |0_\nu\rangle\langle 1_\nu|$ the qubit ladder operators and $\hbar\Omega_\nu(t)$ the variable energy gap.

Using the model above, we compute the final state $\hat{\rho}$. Given an initial state $\hat{\rho}_0$,

$$\hat{\rho} = \hat{U}\hat{\rho}_0\hat{U}^\dagger, \quad \hat{U} = \mathcal{T}e^{-\mathrm{i}\int \mathrm{d}t\,\hat{H}_I(t)}, \tag{4.39}$$

with the $\mathcal{T}$ in the second term is there to denote the time-ordered exponential. We will assume that $\lambda = \lambda_{\mathrm{A}} = \lambda_{\mathrm{B}}$ for simplicity and perform a Dyson expansion of $\hat{U}$ on λ,

$$\hat{U} = \hat{U}^{(0)} + \hat{U}^{(1)} + \hat{U}^{(2)} + \mathcal{O}(\lambda^3), \tag{4.40}$$

$$\begin{aligned}\hat{U}^{(0)} &= \hat{\mathbb{1}},\\ \hat{U}^{(1)} &= -\frac{\mathrm{i}}{\hbar}\int \mathrm{d}t\,\hat{H}_I(t),\\ \hat{U}^{(2)} &= -\frac{1}{\hbar^2}\int_{t>t'} \mathrm{d}t\,\mathrm{d}t'\,\hat{H}_I(t)\hat{H}_I(t').\end{aligned} \tag{4.41}$$

Then, the time-evolved density operator for the state of the detectors and the field is

$$\hat{\rho} = \hat{\rho}_0 + \hat{\rho}^{(1,0)} + \hat{\rho}^{(0,1)} + \hat{\rho}^{(2,0)} + \hat{\rho}^{(1,1)} + \hat{\rho}^{(0,2)} + \mathcal{O}(\lambda^3)\,. \tag{4.42}$$

where the different corrections are

$$\hat{\rho}^{(i,j)} = \hat{U}^{(i)}\hat{\rho}_0\hat{U}^{(j)\dagger}\,. \tag{4.43}$$

For our study, let us assume that the field and detectors start uncorrelated,

$$\hat{\rho}_0 = \hat{\rho}_{\mathrm{AB},0} \otimes \hat{\rho}_{\phi,0}\,. \tag{4.44}$$

[8]Recall that even though we consider the detector to be pointlike, the spatial smearing of the detector can just be reabsorbed in the cutoff function. See [67].

We also assume that the initial field states $\hat{\rho}_{\phi,0}$ have vanishing odd-point functions, that is, $\forall n \in \{0,1,2,\ldots\}$,

$$\mathrm{Tr}\Big(\hat{\rho}_{\phi,0}\hat{\phi}(t_0,x_0)\ldots\hat{\phi}(t_{2n+1},x_{2n+1})\Big) = 0. \tag{4.45}$$

For example, that is the case for the field vacuum, and any Fock states as well as any zero mean Gaussian state such as thermal states, squeezed vacuum, etc. With this assumption, the odd order corrections cancel and the final state for the two detectors (after tracing over the field) becomes

$$\hat{\rho}_{\mathrm{AB}} = \mathrm{Tr}_\phi\,\hat{\rho} = \hat{\rho}_{\mathrm{AB},0} + \hat{\rho}^{(2,0)}_{\mathrm{AB}} + \hat{\rho}^{(1,1)}_{\mathrm{AB}} + \hat{\rho}^{(0,2)}_{\mathrm{AB}} + \mathcal{O}(\lambda^4)\,. \tag{4.46}$$

Finally, we assume that the *detectors start from the ground state*

$$\hat{\rho}_{\mathrm{AB},0} = |0_{\mathrm{A}}0_{\mathrm{B}}\rangle\langle 0_{\mathrm{A}}0_{\mathrm{B}}|\,. \tag{4.47}$$

The final state has the usual form of the final state in a vacuum entanglement harvesting setting (see, e.g., [2]). The details of the calculation are also included in Appendix C.2. The state of the detectors after the interaction, represented in the basis $|0_{\mathrm{A}}0_{\mathrm{B}}\rangle$, $|1_{\mathrm{A}}0_{\mathrm{B}}\rangle$, $|0_{\mathrm{A}}1_{\mathrm{B}}\rangle$, $|1_{\mathrm{A}}1_{\mathrm{B}}\rangle$, is

$$\hat{\rho}_{\mathrm{AB}} = \begin{pmatrix} 1-\mathcal{L}_{\mathrm{AA}}-\mathcal{L}_{\mathrm{BB}} & 0 & 0 & \mathcal{M}^* \\ 0 & \mathcal{L}_{\mathrm{AA}} & \mathcal{L}_{\mathrm{AB}} & 0 \\ 0 & \mathcal{L}_{\mathrm{BA}} & \mathcal{L}_{\mathrm{BB}} & 0 \\ \mathcal{M} & 0 & 0 & 0 \end{pmatrix} + \mathcal{O}(\lambda^4), \tag{4.48}$$

with

$$\begin{aligned} \mathcal{L}_{\mu\nu} &= c^2\lambda^2 \int \mathrm{d}t\,\mathrm{d}t'\,\mathcal{W}_{xx'}(t',x_\nu,t,x_\mu)\chi_{\varphi_\mu}(t)\chi^*_{\varphi_\nu}(t'), \\ \mathcal{M} &= -c^2\lambda^2 \int \mathrm{d}t\,\mathrm{d}t'\,G_{xx'}(t,x_{\mathrm{A}},t',x_{\mathrm{B}})\chi_{\varphi_{\mathrm{A}}}(t)\chi_{\varphi_{\mathrm{B}}}(t'), \\ \chi_{\varphi_\nu}(t) &= e^{\mathrm{i}\varphi_\nu(t)}\chi_\nu(t). \end{aligned} \tag{4.49}$$

The phase $\varphi_\nu(t)$ is given in Eq. (4.38) and

$$\begin{aligned} \mathcal{W}_{xx'}(t,x,t',x') &= \langle \partial_x\hat{\phi}_{\mathrm{C}}(t,x)\partial_{x'}\hat{\phi}_{\mathrm{C}}(t',x')\rangle_{\hat{\rho}_{\phi,0}}, \\ G_{xx'}(t,x,t',x') &= \Theta(t-t')\mathcal{W}_{xx'}(t,x,t',x') + \Theta(t'-t)\mathcal{W}_{xx'}(t',x',t,x)\,, \end{aligned} \tag{4.50}$$

where Θ is the Heaviside step function.

After the interaction the detectors will be generically entangled. As a measure of the entanglement acquired by the detectors we will use the negativity. This quantity is a faithful entanglement monotone for systems of two qubits [87, 88]. The negativity of $\hat{\rho}_{\mathrm{AB}}$ amounts to

$$\begin{aligned}\mathcal{N} &= \max(\eta, 0) + \mathcal{O}(\lambda^4),\\ \eta &= \sqrt{|\mathcal{M}|^2 - \frac{(\mathcal{L}_{\mathrm{AA}} - \mathcal{L}_{\mathrm{BB}})^2}{2}} - \frac{\mathcal{L}_{\mathrm{AA}} + \mathcal{L}_{\mathrm{BB}}}{2}.\end{aligned} \tag{4.51}$$

This expression simplifies, for $\mathcal{L} = \mathcal{L}_{\mathrm{AA}} = \mathcal{L}_{\mathrm{BB}}$, to

$$\mathcal{N} = \max(|\mathcal{M}| - \mathcal{L}, 0) + \mathcal{O}(\lambda^4). \tag{4.52}$$

4.3.1 Harvesting from the vacuum

Let us consider that the quantum field is prepared in the vacuum state, given by

$$\hat{\rho}_{\phi,0} = |0_\phi\rangle\langle 0_\phi| \,. \tag{4.53}$$

For the vacuum, the correlators defined in Eq. (4.50) only depend on $t_- = t - t'$ and $x_- = x - x'$:

$$\begin{aligned}\mathcal{W}^{\mathrm{vac}}_{xx'}(t_-, x_-) &= \frac{1}{2\pi c^2}\int_0^\infty \mathrm{d}\omega\, \omega\, \mathrm{C}(\omega)^2 \cos\left(\omega \frac{x_-}{c}\right) e^{-\mathrm{i}\omega t_-}\,,\\ G^{\mathrm{vac}}_{xx'}(t_-, x_-) &= \mathcal{W}^{\mathrm{vac}}_{xx'}(|t_-|, x_-).\end{aligned} \tag{4.54}$$

Next, we substitute $\mathcal{W}^{\mathrm{vac}}_{xx'}$ and $G^{\mathrm{vac}}_{xx'}$ back into $\mathcal{L}_{\mu\nu}$ and $\mathcal{M}$ and provide two ways to simplify the resulting integrals, each of them helpful in different scenarios.

Integrating over the field modes last

Substituting Eq. (4.54) into Eq. (4.49) leads to

$$\begin{aligned}\mathcal{L}_{\nu\nu} &= \frac{\lambda^2}{2\pi}\int_0^\infty \mathrm{d}\omega\, \omega\, \mathrm{C}(\omega)^2 |\widetilde{\chi_{\varphi_\nu}}(\omega)|^2,\\ \mathcal{L}_{\mathrm{AB}} &= \frac{\lambda^2}{2\pi}\int_0^\infty \mathrm{d}\omega\, \omega\, \mathrm{C}(\omega)^2 \cos(\omega t_d) \widetilde{\chi_{\varphi_{\mathrm{A}}}}(\omega)\widetilde{\chi_{\varphi_{\mathrm{B}}}}(\omega)^*,\\ \mathcal{M} &= -\frac{\lambda^2}{2\pi}\int_0^\infty \mathrm{d}\omega\, \omega\, \mathrm{C}(\omega)^2 \cos(\omega t_d) \int \mathrm{d}t\, \mathrm{d}t'\, e^{-\mathrm{i}\omega|t-t'|}\chi_{\varphi_{\mathrm{A}}}(t)\chi_{\varphi_{\mathrm{B}}}(t').\end{aligned} \tag{4.55}$$

Here, we used the Fourier transform convention stated in Eq. (4.12). Notice that the expression for $\mathcal{L}_{\mathrm{BA}}$ follows from $\mathcal{L}_{\mathrm{BA}} = \mathcal{L}^*_{\mathrm{AB}}$. Moreover, t_d stands for the time it takes for the detectors to send a signal to each other through the field,

$$t_d = \frac{|x_{\mathrm{A}} - x_{\mathrm{B}}|}{c}. \tag{4.56}$$

The expressions for $\mathcal{L}_{\mu\nu}$ and $\mathcal{M}$ in Eq. (4.55) are similar to the ones obtained for UDW detectors in (3+1)D that couple to the field amplitude (see, e.g. [2]), with radially symmetric smearing functions[9] $F(\boldsymbol{x})$.

Integrating over the field modes first

An alternative to Eq. (4.55) and a quite helpful way of evaluating these integrals is to integrate over ω before performing the time integrals. Doing this, $\mathcal{W}^{\mathrm{vac}}_{xx'}$ becomes

$$\begin{aligned}
\mathcal{W}^{\mathrm{vac}}_{xx'}(t_-, x_-) &= \frac{1}{4\pi c^2}\left(\mathcal{J}\left(t_- + \frac{|x_-|}{c}\right) + \mathcal{J}\left(t_- - \frac{|x_-|}{c}\right)\right), \\
\mathcal{J}(t) &= \int_0^\infty \mathrm{d}\omega\, \omega\, \mathrm{C}(\omega)^2 e^{-\mathrm{i}\omega t}.
\end{aligned} \tag{4.57}$$

For the exponential cutoff of Eq. (4.9), $\mathcal{J}(t)$ has the following analytical expression,

$$\mathcal{J}(t) = \frac{\Omega^2_{\mathrm{cut}}}{(1 + \mathrm{i}\Omega_{\mathrm{cut}} t)^2}. \tag{4.58}$$

Substituting Eq. (4.57) back into Eq. (4.49),

$$\begin{aligned}
\mathcal{L}_{\nu\nu} &= \frac{\lambda^2}{2\pi}\int \mathrm{d}t\, \mathrm{d}t'\ \mathrm{Re}\big(\mathcal{J}(t'-t)\chi_{\varphi_\nu}(t)\chi^*_{\varphi_\nu}(t')\big), \\
\mathcal{L}_{\mathrm{AB}} &= \frac{\lambda^2}{2\pi}\int \mathrm{d}t\, \mathrm{d}t'\, \mathcal{I}(t'-t)\chi_{\varphi_{\mathrm{A}}}(t)\chi^*_{\varphi_{\mathrm{B}}}(t'), \\
\mathcal{M} &= -\frac{\lambda^2}{2\pi}\int \mathrm{d}t\, \mathrm{d}t'\, \mathcal{I}(|t-t'|)\chi_{\varphi_{\mathrm{A}}}(t)\chi_{\varphi_{\mathrm{B}}}(t'), \\
\mathcal{I}(t) &= \frac{1}{2}\big(\mathcal{J}(t+t_d) + \mathcal{J}(t-t_d)\big),
\end{aligned} \tag{4.59}$$

[9] To obtain $\mathcal{L}_{\mu\nu}$ and $\mathcal{M}$ for the 3+1D amplitude coupling, radially symmetric UDW model, Eq. (4.55) needs to be modified as follows: 1) replace all $\cos(\omega t_d)$ by $\sin(\omega t_d)/(\omega t_d)$, 2) fix $\hbar\Omega_\nu(t) = \hbar\Omega_\nu$, which implies $\chi_{\varphi_\nu}(t) = e^{\mathrm{i}\Omega_\nu t}\chi_\nu(t)$, 3) replace $\mathrm{C}(\omega)$ by $|\widetilde{F}(\boldsymbol{k})|$ (with the Fourier transform convention of Eq. (4.12)) evaluated at a radius $|\boldsymbol{k}| = \omega/c$, 4) change the overall constants to account for the different model and geometry. For example, for the setup in the reference [2], the constants in front of the equations in (4.55) would be $\frac{\lambda^2}{4\pi^2}$ instead of $\frac{\lambda^2}{2\pi}$.

where we used $\mathcal{J}(-t) = \mathcal{J}^*(t)$ and $t_d = |x_{\rm A} - x_{\rm B}|/c$.

Further simplification of the $\mathcal{L}_{\mu\nu}$ and $\mathcal{M}$ integrals, used to ease the numerical calculations in the next sections, are explored in Appendix C.3.

4.4 Genuine entanglement harvesting

As previously discussed in chapter 2, when two detectors are in causal contact they can acquire entanglement in two different ways: they can communicate by exchanging information via the field, but they can also harvest entanglement at the same time. Here, we provide a reminder of section 2.2, which described how to decompose the entanglement acquired by causally connected detectors into two components: (a) entanglement extracted from preexisting field correlations and (b) entanglement mediated by communication through the field, following [55]. For simplicity in the equations, we denote spacetime points by x in this section.

The decomposition of the acquired entanglement is based on the two-point correlator of the field amplitude $\hat{\phi}$, which for a field state $\hat{\rho}_\phi$ is

$$W(\mathsf{x},\mathsf{x}') = \langle \hat{\phi}(\mathsf{x})\hat{\phi}(\mathsf{x}')\rangle_{\hat{\rho}_\phi}. \tag{4.60}$$

This correlator can be split into symmetric and antisymmetric parts

$$W^{\pm}(\mathsf{x},\mathsf{x}') = \frac{W(\mathsf{x},\mathsf{x}') \pm W(\mathsf{x}',\mathsf{x})}{2}. \tag{4.61}$$

W^+ and W^- respectively are the real and imaginary parts of W, due to $W(\mathsf{x}',\mathsf{x}) = W^*(\mathsf{x},\mathsf{x}')$. Moreover,

$$\begin{aligned} W^+(\mathsf{x},\mathsf{x}') &= \frac{1}{2}\langle\{\hat{\phi}(\mathsf{x}),\hat{\phi}(\mathsf{x}')\}\rangle_{\hat{\rho}_\phi}, \\ W^-(\mathsf{x},\mathsf{x}') &= \frac{1}{2}\langle[\hat{\phi}(\mathsf{x}),\hat{\phi}(\mathsf{x}')]\rangle_{\hat{\rho}_\phi}. \end{aligned} \tag{4.62}$$

The contribution of W^+ to the acquired entanglement can be associated with genuine harvesting, for the reasons described on section 2.2. Then, the term $\mathcal{M}$ in Eq. (4.51) decomposes into two parts associated to preexisting field correlations ($\mathcal{M}^+$) and communication ($\mathcal{M}^-$),

$$\mathcal{M} = \mathcal{M}^+ + \mathcal{M}^-, \tag{4.63}$$

where $\mathcal{M}^{\pm}$ contains only the contribution of $W^{\pm}$. As an estimator of the amount of correlations that are genuinely harvested, in this chapter we use the following ratio,

$$\frac{|\mathcal{M}^{+}|}{|\mathcal{M}^{+}| + |\mathcal{M}^{-}|}, \tag{4.64}$$

which ranges from 0 (correlations from communication) to 1 (correlations from harvesting).

In this article, we explore entanglement harvesting with the variable gap detector models of Eq. (4.37). These detectors do not couple to $\hat{\phi}$, but rather to $\partial_x \hat{\phi}_C$, which incorporates a derivative and the cutoff as prescribed in Eq. (4.36). Nonetheless, the analysis above to separate the communication and genuine harvesting contributions still carries. Furthermore, the current scenario is analogous to the 1+1D derivative coupling case with smearing explored in section 2.3.[10]

4.5 Exploring the effects of the implementation features on entanglement harvesting

In this section, we study entanglement harvesting using the detectors of Eq. (4.31), motivated by the experimental implementation. As shown in Section 4.2, these particular VGSD detectors are designed to emulate the TC+FQ superconducting circuit implementation demonstrated in [3]. Our goal is to evaluate the effect the combined variable gap and derivative coupling features on the ability of the detectors to harvest entanglement. To do so, we will numerically compute the amount of entanglement acquired by VGSD detectors, using the results of Section 4.3. We will do so in a variety of experimentally accessible scenarios, and estimate how much of the entanglement is actually harvested from the field (see Section 4.4).

First of all, we apply the calculations of Section 4.3 to the VGSD detector of Eq. (4.31). This amounts to substituting the speed of light c, the coupling strength λ_ν, and the time dependency of the energy gap $\hbar\Omega_\nu(t)$ by expressions that match the superconducting implementation.

Firstly, the speed of light in the transmission line is not c, but rather a function of its capacitance c_0 and inductance l_0 per unit length: $v = 1/\sqrt{c_0 \ell_0}$. We recall that common values are of the order of $v \approx 0.3\,c$. This modification affects the definition of t_d, which

[10] Remember that having a cutoff is equivalent to having a smeared field, as shown in Eq. (4.10).

now becomes the time required for signals to travel between the detectors through the transmission line,

$$t_d = \frac{|x_{\mathrm{A}} - x_{\mathrm{B}}|}{v}. \tag{4.65}$$

Secondly, to determine λ_ν, we need to relate it with γ_ν. To do so, we compare the particular interaction Hamiltonian of Eq. (4.31) with the general VGSD interaction Hamiltonian of Eq. (4.37). The models match when

$$\lambda_\nu = -\frac{\varphi_0}{\hbar v \ell_0}\gamma_\nu \sqrt{\hbar Z_0} = -\sqrt{\frac{R_{\mathrm{K}}}{8\pi Z_0}}\gamma_\nu \approx -4.53 \cdot \gamma_\nu, \tag{4.66}$$

where we used $\varphi_0 = \hbar/(2e)$, $Z_0 = v\ell_0$, and $R_{\mathrm{K}} = h/e^2$. The numerical value comes from choosing $Z_0 \approx 50\,\Omega$, as in Eq. (4.7). Notably, $\lambda_\nu^2 = \pi\alpha_\nu$, where α_ν is the dimensionless spin-boson coupling constant of Eq. (4.33), for the detector ν (where we recall $\nu \in \{\mathrm{A}, \mathrm{B}\}$).

Finally, we link the dependency $\Omega_\nu(t)$ to the switching on and off of the interactions. Specifically, we use the following simple linear dependence that matches well with the superconducting implementation (see Eq. (4.29)),

$$\Omega_\nu(t) = \Omega_\nu^0 + \Delta\Omega_\nu \chi_\nu(t). \tag{4.67}$$

Therefore,

$$\varphi_\nu(t) = \Omega_\nu^0 t + \Delta\Omega_\nu \int_0^t \mathrm{d}t'\, \chi_\nu(t'). \tag{4.68}$$

4.5.1 Fixed vs tunable parameters

Here, we split the parameters of the particular VGSD model of Eq. (4.31) into two categories: *fixed parameters* that cannot be changed once the superconducting device is fabricated and *tunable parameters* that can be freely changed without requiring any redesign or fabrication of a new device. For simplicity, let us consider that the two detectors are equal: $\lambda = \lambda_{\mathrm{A}} = \lambda_{\mathrm{B}}$, $\Omega^0 = \Omega^0_{\mathrm{A}} = \Omega^0_{\mathrm{B}}$, $\Delta\Omega = \Delta\Omega_{\mathrm{A}} = \Delta\Omega_{\mathrm{B}}$.

We give the following *fixed parameters* experimentally realistic values, which best mimic the implementation demonstrated in [3],

- $\Omega^0/(2\pi) \approx 7.3\,\mathrm{GHz}$ for the transition frequency of the free qubit (see Eq. (4.30)).
- $\Delta\Omega/(2\pi) \approx 5.2 \cdot \lambda\,\mathrm{GHz}$ for the difference between the transition frequency of the qubit when the coupling is fully switched on and $\Omega^0/(2\pi)$ (see Eqs. (4.30) and (4.66)).

- $\Omega_{\text{cut}}/(2\pi) \approx 50\,\text{GHz}$ for the transmission line cutoff frequency, matching [70].
- $Z_0 \approx 50\,\Omega$ for the transmission line impedance, matching [70].
- $v \approx 1.2 \cdot 10^8\,\text{m}\,\text{s}^{-1}$, as measured in [102] for a typical superconducting coplanar waveguide.
- $t_d = \frac{d}{v} = 1\,\text{ns}$ for the time the detectors take to signal to each other. Equivalently, the detectors are separated by $d = 12\,\text{cm}$, which is is feasible with the current fabrication methods [108].

These fixed parameters will be kept the same for all the exploration, except for t_d. Testing different t_d can advise the choice of distance between detectors in future entanglement harvesting experiments.

The following *tunable parameters* will be varied during the following numerical exploration, to understand their effects on entanglement harvesting,

- The coupling strength λ. We test the λ shown in Table 4.1. These values are in the achievable range $\lambda \in [-1, 0.1]$. This range is obtained from combining Eq. (4.66) with the range $\gamma \in [-0.02, 0.22]$ obtained from the numerical simulations outlined in subsection 4.2.1.
- The switching function $\chi_\nu(t)$. Our choices of switching functions are detailed next, in subsection 4.5.2.

Scenario	λ	γ	α	$\frac{\Delta\Omega}{2\pi}$ (GHz)
1	$\to 0$	$\to 0$	$\to 0$	$\to 0$
2	-0.1	0.02	0.003	-0.5
3	-0.3	0.07	0.03	-1.6
4	-0.65	0.14	0.1	-3.4
5	-1	0.22	0.3	-5.2
6	0.1	-0.02	0.003	0.5

Table 4.1: This table depicts the scenarios that will be explored in the present section. The $\to 0$ corresponds to the weak coupling limit. The qubit transition frequency variation follows $\Delta\Omega/(2\pi) \approx 5.2 \cdot \lambda\,\text{GHz}$.

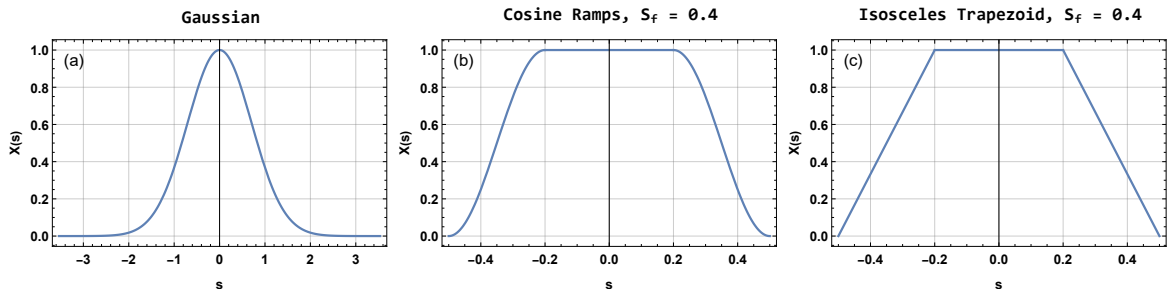


Figure 4.6: (a) Gaussian switching shape, with 5 standard deviations shown. (b) Cosine ramps switching shape with $S_f = 0.4$. (c) Isosceles trapezoid switching shape with $S_f = 0.4$.

4.5.2 Explored switching functions

To simplify our exploration, we will choose switching functions $\chi_\nu(t)$ such that

$$\chi_\nu(t) = X\left(\frac{t - t_\nu}{T}\right), \tag{4.69}$$

where:

- $X(s)$ is a single shape for the switching function of both detectors, which fulfills $X(s) = X(-s)$.
- T is the duration or time-scale of the interaction.
- t_ν controls the time at which the detector ν is switched on and off. In our setup, only the delay $t_\Delta = t_\mathrm{B} - t_\mathrm{A}$ affects the entanglement acquired by the detectors.

The explored switching function shapes $X(s)$ are provided next.

Gaussian Switching Shape

The Gaussian switching is common in the literature of entanglement harvesting and we explore it to ease comparisons with established results. Its shape is

$$X(s) = e^{-s^2}, \tag{4.70}$$

plotted in Figure 4.6(a).

Cosine Ramps Switching Shape

The cosine ramps switching function lasts for a finite time and has a continuous derivative. Its shape is

$$X(s) = \begin{cases} 1 & |s| \leq \frac{S_\mathrm{f}}{2}, \\ \frac{1}{2} + \frac{1}{2}\cos\left(\pi \frac{2|s| - S_\mathrm{f}}{1 - S_\mathrm{f}}\right) & \frac{S_\mathrm{f}}{2} < |s| < \frac{1}{2}, \\ 0 & \frac{1}{2} \leq |s|, \end{cases} \tag{4.71}$$

with an example plotted in Figure 4.6(b). S_f is the portion of time that the interaction remains at its maximum.

Isosceles Trapezoid Switching Shape

The isosceles trapezoid switching function lasts a finite time and is continuous. Its shape is

$$X(s) = \begin{cases} 1 & |s| \leq \frac{S_\mathrm{f}}{2}, \\ \frac{1 - 2|s|}{1 - S_\mathrm{f}} & \frac{S_\mathrm{f}}{2} < |s| < \frac{1}{2}, \\ 0 & \frac{1}{2} \leq |s|, \end{cases} \tag{4.72}$$

with an example plotted in Figure 4.6(c). S_f is the portion of time that the interaction remains at its maximum.

4.5.3 Effect of duration and delay

First, we study the effect of T and t_Δ, which respectively are the interaction duration and the delay between the detector switchings. The fixed parameters are kept as indicated in subsection 4.5.1, and the results for the scenarios of Table 4.1 are respectively shown in Figures 4.7, 4.8, 4.9, 4.10, 4.11, 4.12. The scenarios 1 to 5 and the corresponding Figures 4.7 to 4.11 are presented in order of increasingly negative coupling strength and corresponding larger (negative) gap variation $\Delta\Omega$. Additionally, the scenario 6 and Figure 4.12 show the case of small positive $\Delta\Omega$. Here and from now on, the negativity and the harvesting estimator are numerically computed using the simplified integrals given in Appendix C.3.

First, we observe that the negativity decreases quickly with T for the Gaussian switching, while decreasing much slower with T for the cosine ramps switching and even slower

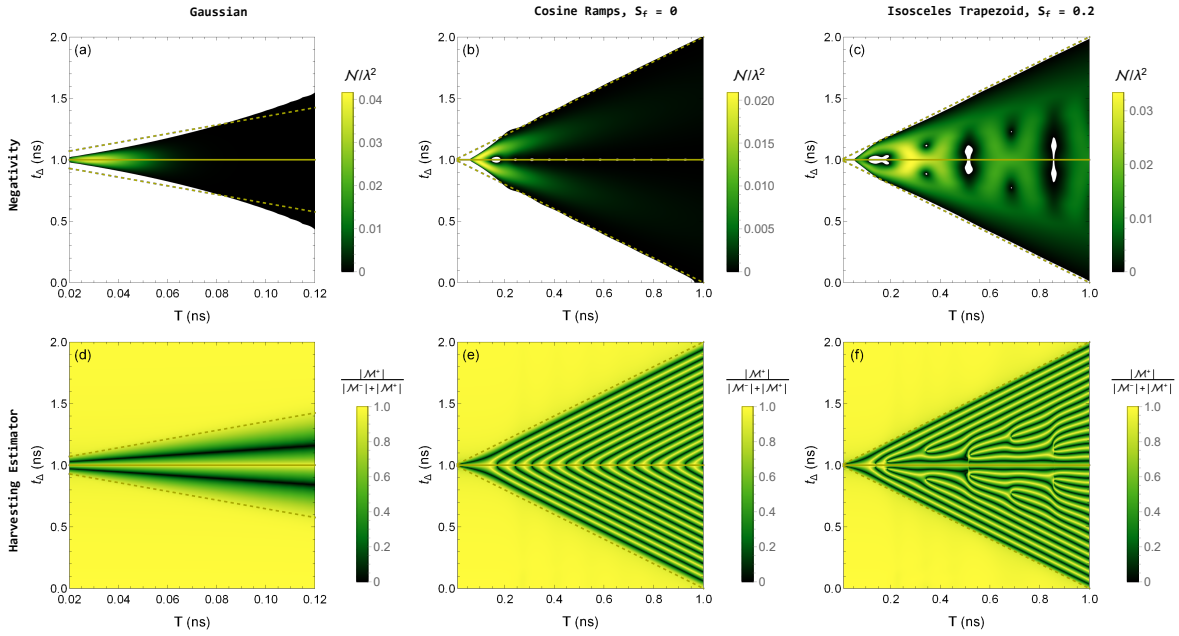


Figure 4.7: Plots for the scenario 1 of Table 4.1: $\lambda \to 0$, $\Delta\Omega \to 0$. **The following applies to Figures 4.7, 4.8, 4.9, 4.10, 4.11 and 4.12:** The first row shows $\mathcal{N}/\lambda^2$, with white indicating $\mathcal{N} = 0$, while darker colors indicate progressively smaller but non-zero $\mathcal{N}$. The second row shows the harvesting estimator $|\mathcal{M}^+|/(|\mathcal{M}^-| + |\mathcal{M}^+|)$, which goes from 0 (all entanglement acquired by communication) to 1 (all entanglement from genuine harvesting). The horizontal axes indicate the switching timescale or duration T and the vertical axes indicate the delay t_Δ between switchings. Each column explores a different switching function, which are, from left to right: Gaussian, cosine ramps with $S_f = 0$, isosceles trapezoid with $S_f = 0.2$. The horizontal solid line indicates full lightlike contact. For the compact switchings, the detectors' interactions are spacelike below the lower dashed lines and timelike above the upper dashed lines. Outside the region enclosed by the dashed yellow lines, only the 5σ tails of the Gaussian switchings overlap.

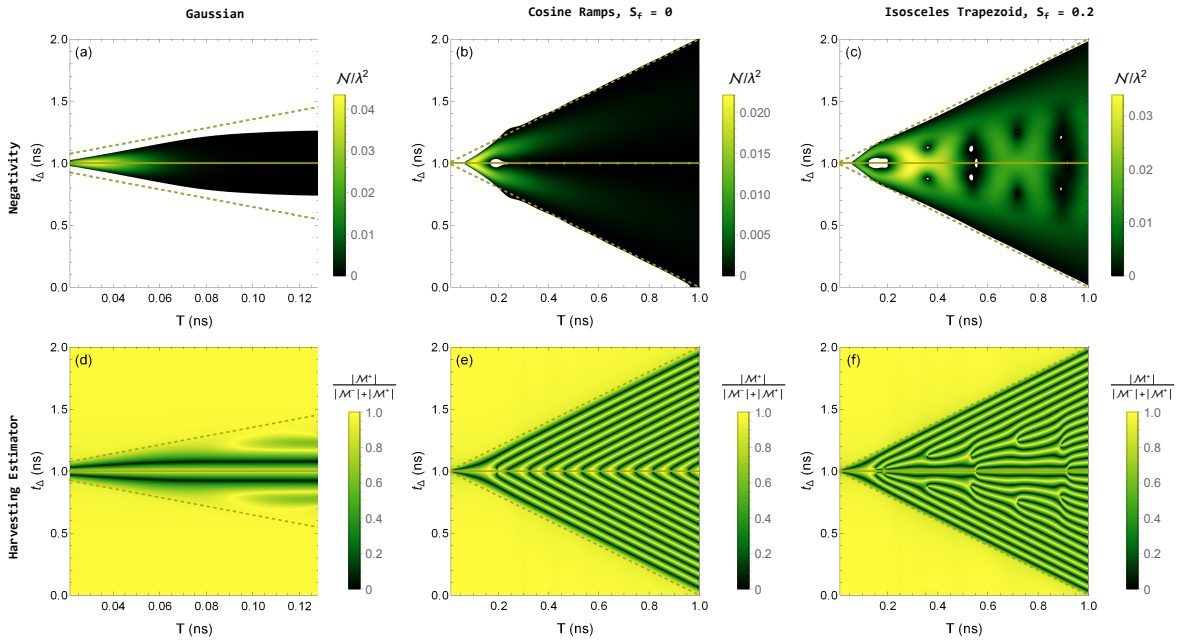


Figure 4.8: Analogous to Figure 4.7, but for scenario 2 of Table 4.1, with $\lambda = -0.1$ and gap variation $\Delta\Omega = -0.5$.

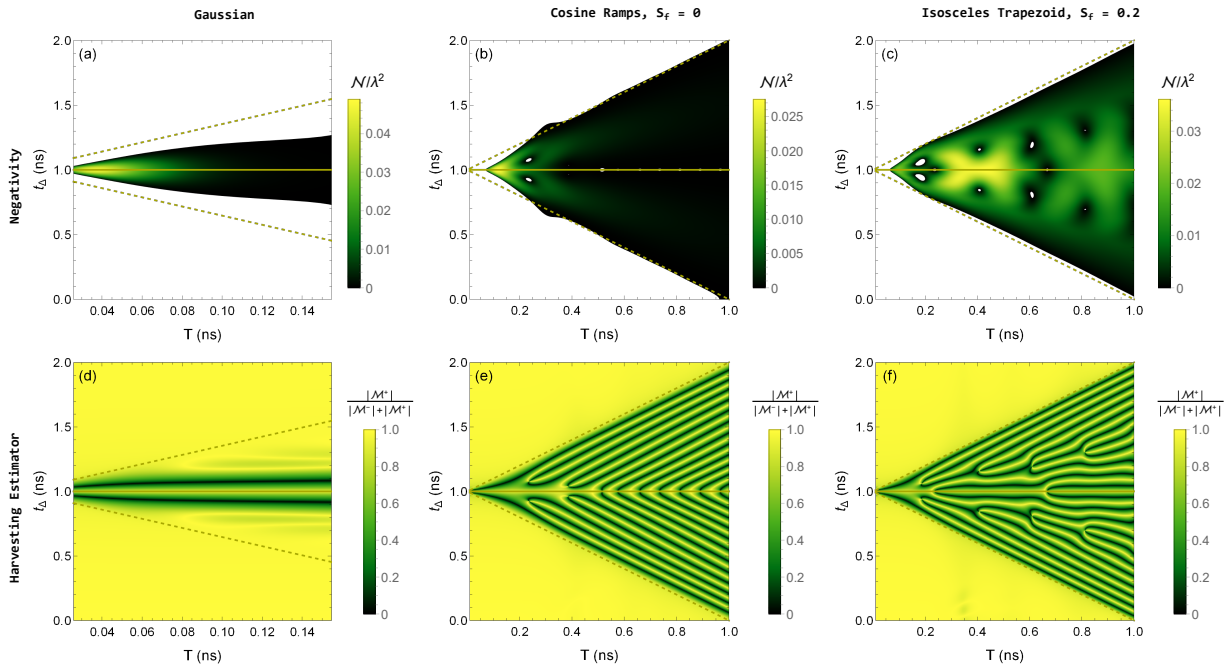


Figure 4.9: Analogous to Figure 4.7, but for scenario 3 of Table 4.1, with $\lambda = -0.3$ and gap variation $\Delta\Omega/(2\pi) = -1.6\,\mathrm{GHz}$.

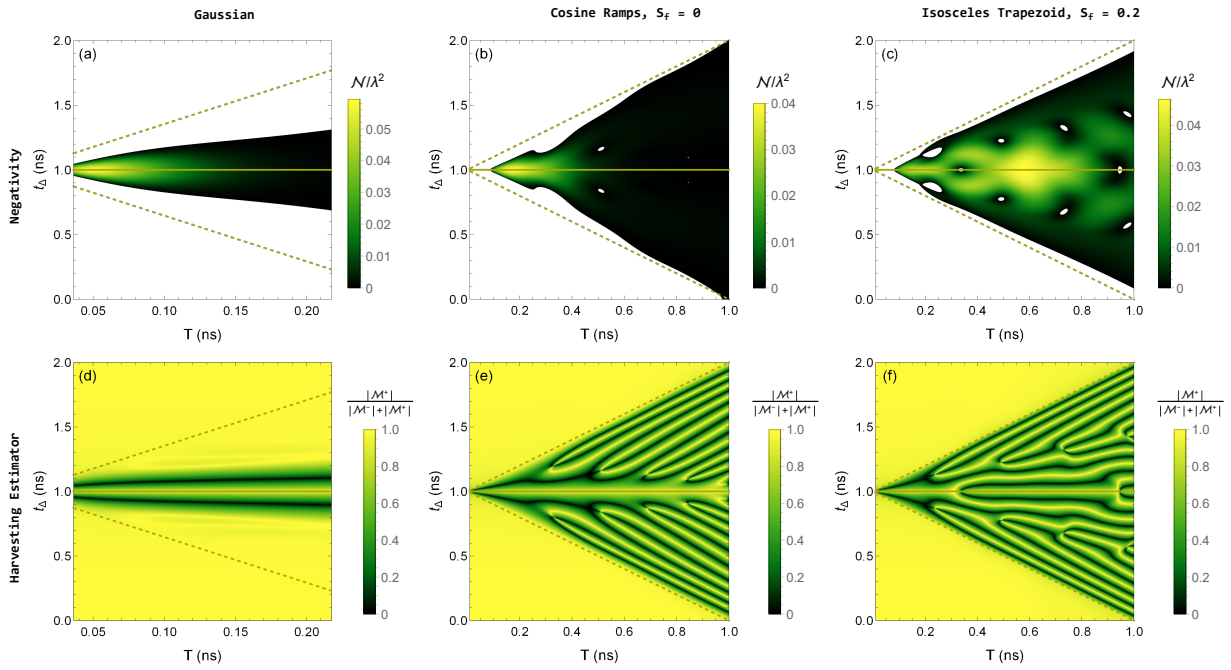


Figure 4.10: Analogous to Figure 4.7, but for scenario 4 of Table 4.1, with $\lambda = -0.65$ and gap variation $\Delta\Omega/(2\pi) = -3.4\,\mathrm{GHz}$.

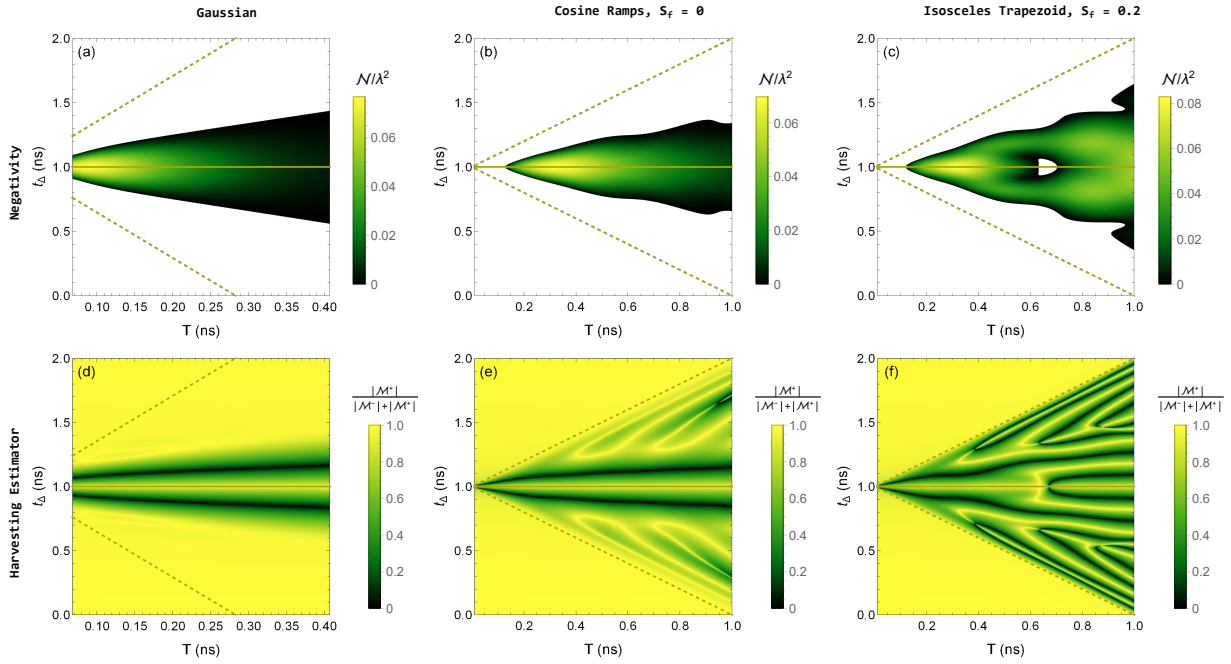


Figure 4.11: Analogous to Figure 4.7, but for scenario 5 of Table 4.1, with $\lambda = -1$ and gap variation $\Delta\Omega/(2\pi) = -5.2\,\mathrm{GHz}$.

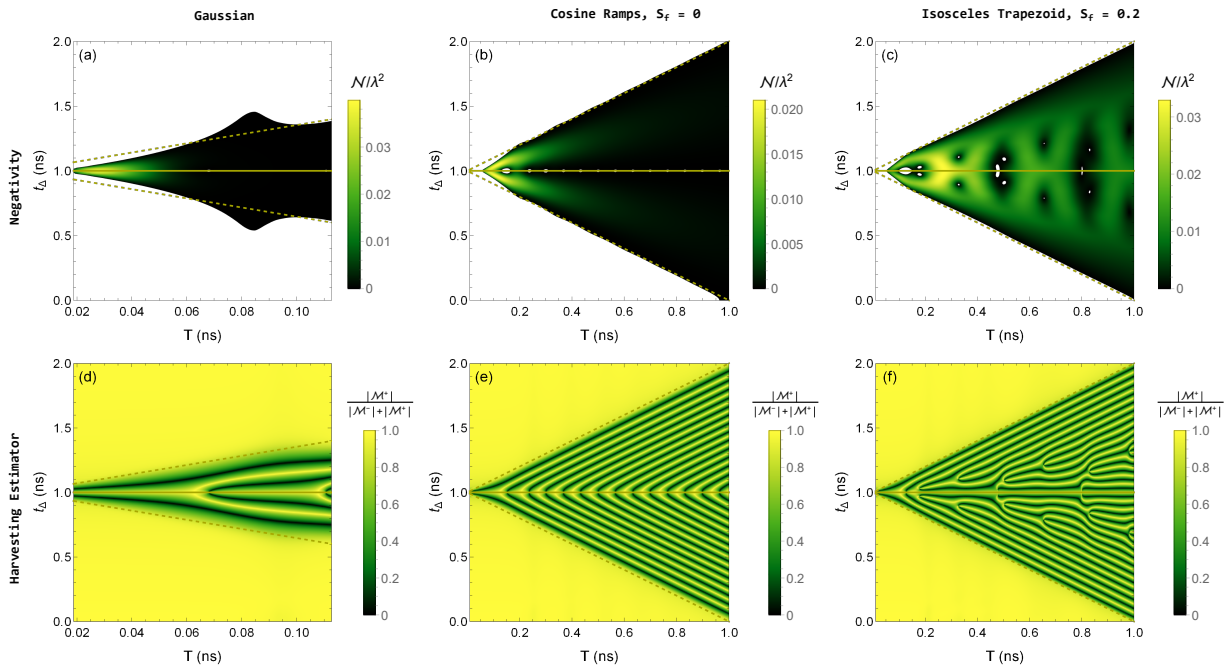


Figure 4.12: Analogous to Figure 4.7, but for scenario 6 of Table 4.1, with $\lambda = 0.1$ and gap variation $\Delta\Omega = 0.5$.

for the isosceles trapezoid switching. This is true regardless of the choice of parameters in the problem.

Let us now focus on Figure 4.7, which shows the acquired negativity in the weak coupling limit $\lambda \to 0$, the case without gap variation. In order to determine the amount of entanglement that is genuinely harvested from the field, we also plot the harvesting estimator from Eq. (4.64). Since the negativity is multiplied by λ^2 at leading order, we plot $\mathcal{N}/\lambda^2$. For switching functions of compact support (cosine ramps and isosceles trapezoid), the detectors acquire negativity mostly when they have partial or full light contact, which is indicated as being inside the dashed yellow lines in the plots. Nonetheless, there is some negativity outside the dashed lines, which indicates that spacelike and timelike harvesting are both possible. Notice that spacelike harvesting is still possible when the cutoff is taken to be infinitely large $\Omega_{\text{cut}} \to \infty$, as depicted in Appendix C.4. Furthermore, looking at the genuine harvesting indicator on the second row of plots, i.e. the subfigures 4.7(d), 4.7(e), 4.7(f), we observe that a significant amount of entanglement harvesting is possible in causal contact. For Gaussian switching, we observe that when the detectors are in full lightlike contact (yellow solid line at $t_\Delta = 1$ ns) all the acquired entanglement is harvested (and not acquired through communication), with two peaks of communication at partial lightlike contact. This is not surprising and matches the results of the previous chapter 2. For the cosine ramps and isosceles trapezoid switchings, the genuine harvesting estimator displays rapidly oscillatory patterns in the regions of causal contact. Nonetheless, this also means that genuine lightlike entanglement harvesting is possible for these finite duration switching functions.

Next, we analyze how varying the energy gap affects entanglement harvesting by comparing the scenarios of Figures 4.7, 4.8, 4.9, 4.10, 4.11, each with progressively larger (negative) gap variations $\Delta\Omega$ driven by making the coupling strength λ more negative. As $\Delta\Omega$ becomes more negative, both spacelike and timelike entanglement harvesting decrease. Conversely, in the region inside the dashed lines, where detectors are in causal contact, negativity increases overall. The change in shape of the negativity and genuine harvesting estimator can partially be intuited from the change in detector gap. Since for negative $\Delta\Omega$ the gap becomes smaller, the T axis in terms of units of Ω^{-1} is effectively rescaled. Specifically, the shape of the plotted quantities 'stretches' in the horizontal axis around $T = 0$ as $\Delta\Omega$ becomes more negative. We also explored one scenario with small positive $\Delta\Omega$, and encountered spacelike harvesting, as shown in Figure 4.12.

4.5.4 Spacelike harvesting for finite duration switchings

We now study harvesting in the regime of strict spacelike separation and, hence, only for the cases of the compactly supported switching functions: the cosine ramps and the isosceles trapezoid. Usually, spacelike detectors acquire more entanglement the closer they are to being in causal contact and the distance at which spacelike separated detectors can harvest entanglement increases with the smoothness of the switching function (see Appendix C.4). Taking this into account, we consider two ways to place the detectors and to switch on the interactions, depicted in Figure 4.13, which maximize the harvested entanglement. These two ways are as follows:

1. Place the detectors at a fixed distance, i.e. with a constant t_d, and pick their switching delay to be $t_\Delta = t_d - T$. The reason for this choice stems from detectors being spacelike as long as $|t_\Delta| \leq t_d - T$. For larger $|t_\Delta|$, detectors would be in lightlike contact, and for even larger $|t_\Delta|$, timelike separated. Therefore, $t_\Delta = t_d - T$ makes the detectors as close as possible to being in causal contact while keeping them spacelike, maximizing the acquired entanglement. This choice is illustrated in a spacetime diagram in subfigure 4.13(a). The acquired negativity is shown in Figure 4.14 for $t_d = 1\,\text{ns}$ and in Figure 4.15 for $t_d = 0.5\,\text{ns}$.

2. Place two simultaneously switched detectors, $t_\Delta = 0$, as close as possible while keeping their interactions spacelike. This is achieved by allowing t_d to take the value $t_d = T$. This choice is illustrated in a spacetime diagram in subfigure 4.13(b) and the acquired negativity is shown in Figure 4.16.

Figures 4.14, 4.15 and 4.16 show the final negativity of the detectors as a function of: 1) the interaction duration T and 2) the switching function parameter S_f, as defined in Eqs. (4.71) and (4.72). Each figure provides plots for the scenarios of Table 4.1 that have some non-zero negativity. We observe that large negative values of $\Delta\Omega$ make spacelike harvesting harder by reducing the range of parameters (T and S_f) where negativity is non-zero. This is consistent with the findings in subsection 4.5.3. On the other hand, increasing λ improves negativity, which has a λ^2 prefactor. However, a stronger coupling is accompanied by larger gap variation, due to $\Delta\Omega/(2\pi) \approx 5.2 \cdot \lambda\,\text{GHz}$. Eventually, the larger negative $\Delta\Omega$ has a stronger negative effect, making spacelike harvesting impossible for strong couplings. For small positive $\Delta\Omega$ (scenario 6), the regions with non-zero negativity are moderately larger compared to when there is no gap variation (scenario 1), but this comes at the cost of a slight decrease in the maximum negativity that can be harvested.

Looking at the differences caused by the positioning of the detectors, one finds that the most entanglement is found when $t_d = T$ and $t_\Delta = 0$, as shown in Figure 4.16. However,

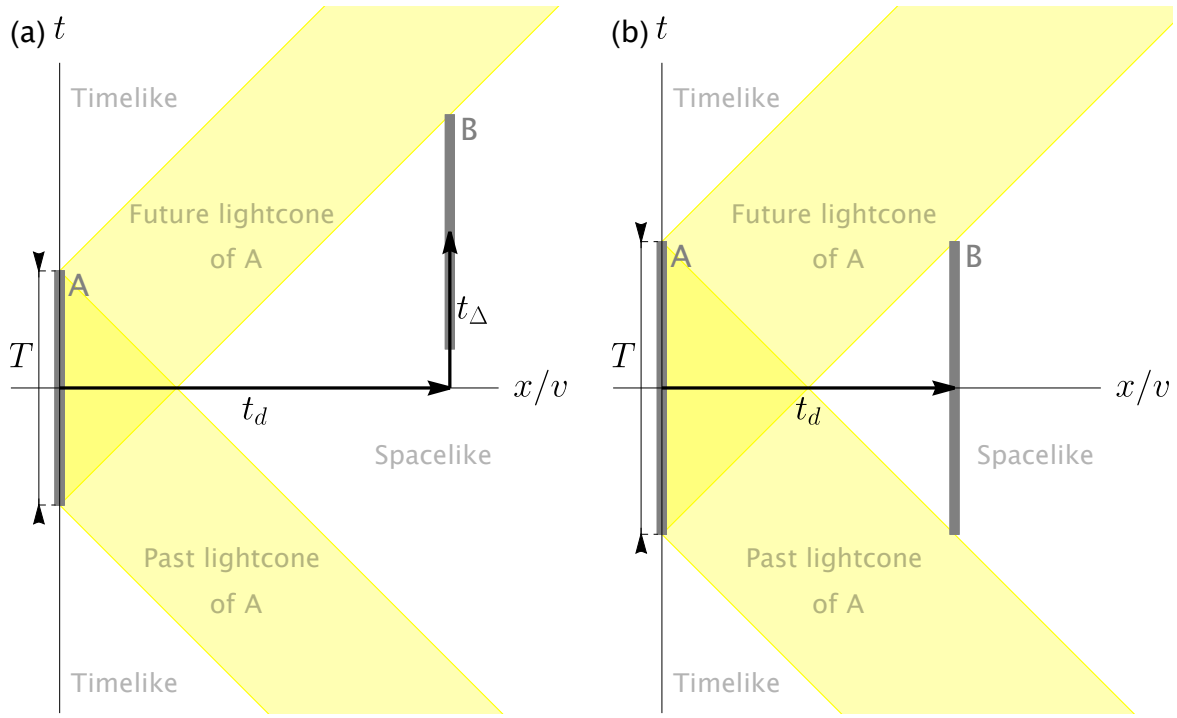


Figure 4.13: Spacetime diagrams with gray rectangles representing the detectors' interactions. (a) Case $t_\Delta = t_d - T$, with t_d fixed. The entanglement harvested in this case is shown in Figure 4.14 ($t_d = 1\,\text{ns}$) and Figure 4.15 ($t_d = 0.5\,\text{ns}$). (b) Case $t_d = T$, $t_\Delta = 0$. The entanglement harvested in this case is shown in in Figure 4.16.

this choice is impractical in an actual setup, because the distance between detectors is fixed after the device is built, and cannot be tuned to match the interaction duration T. This leaves the tuning of t_Δ for a fixed t_d as the way to maximize harvested entanglement for a given T in a superconducting implementation. This method allows to reach the negativities shown in Figures 4.14 and 4.15. Furthermore, by comparing Figure 4.14 (fixed $t_d = 1\,\text{ns}$) and Figure 4.15 (fixed $t_d = 0.5\,\text{ns}$), we observe that reducing t_d has two main effects: 1) reducing the range of values of T for which the interaction can be spacelike, 2) increasing spacelike negativity, but only for $T \approx t_d$. Specifically, for the explored cases, if $T < 0.45\,\text{ns}$, the negativity is the same regardless of wether $t_d = 0.5\,\text{ns}$ or $t_d = 1\,\text{ns}$. The difference appears for $T \in [0.45\,\text{ns}, 0.5\,\text{ns}]$, for which negativity is larger in the case $t_d = 0.5\,\text{ns}$. For $T \in [0.5\,\text{ns}, 1\,\text{ns}]$, only $t_d = 1\,\text{ns}$ allows for the detectors to be spacelike.

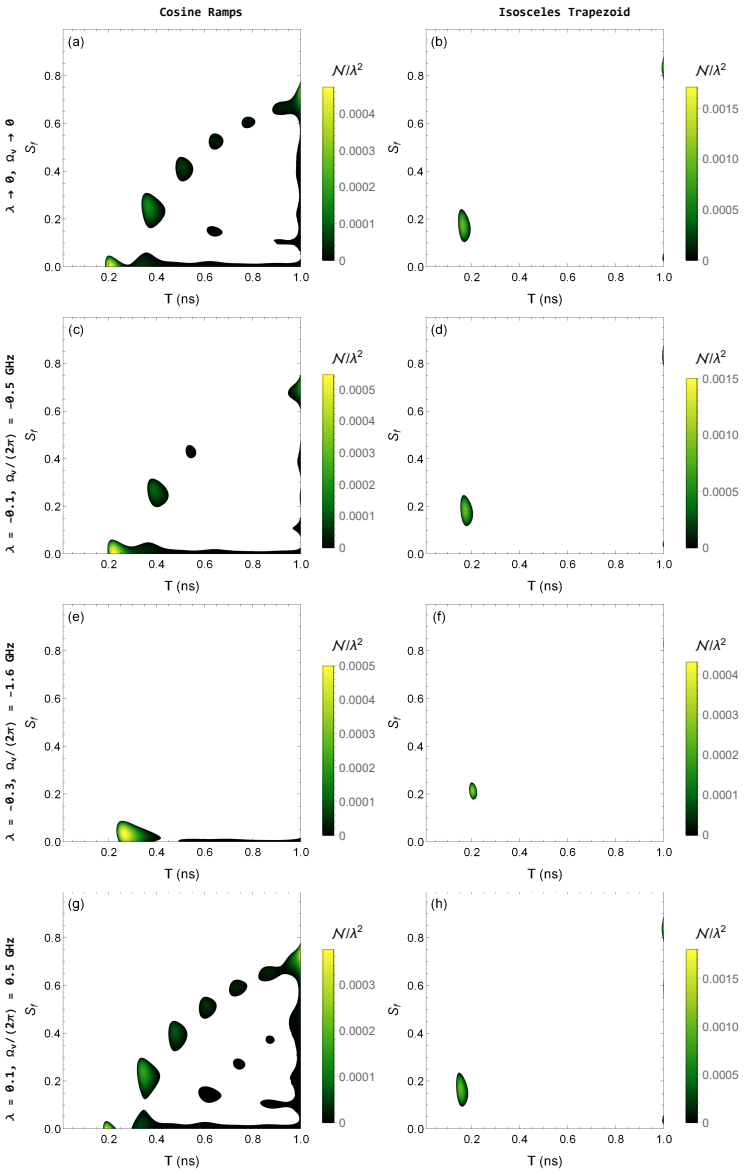


Figure 4.14: Negativity acquired by spacelike detectors. To ensure the negativity is the largest, we explore the boundary where interactions become spacelike, by choosing $t_\Delta = t_d - T$, with $t_d = 1\,\text{ns}$. This arrangement is depicted in the spacetime diagram of Figure 4.13(a). **The following applies to Figures 4.14, 4.15, and 4.16:** The plots' horizontal axes are the switching durations T and the vertical axes are the portion of the switching function that is flat S_f and at full coupling. The switching function for the left column is the cosine ramps and for the right column the isosceles trapezoid. The rows respectively correspond to the scenarios 1, 2, 3 and 6 of Table 4.1.

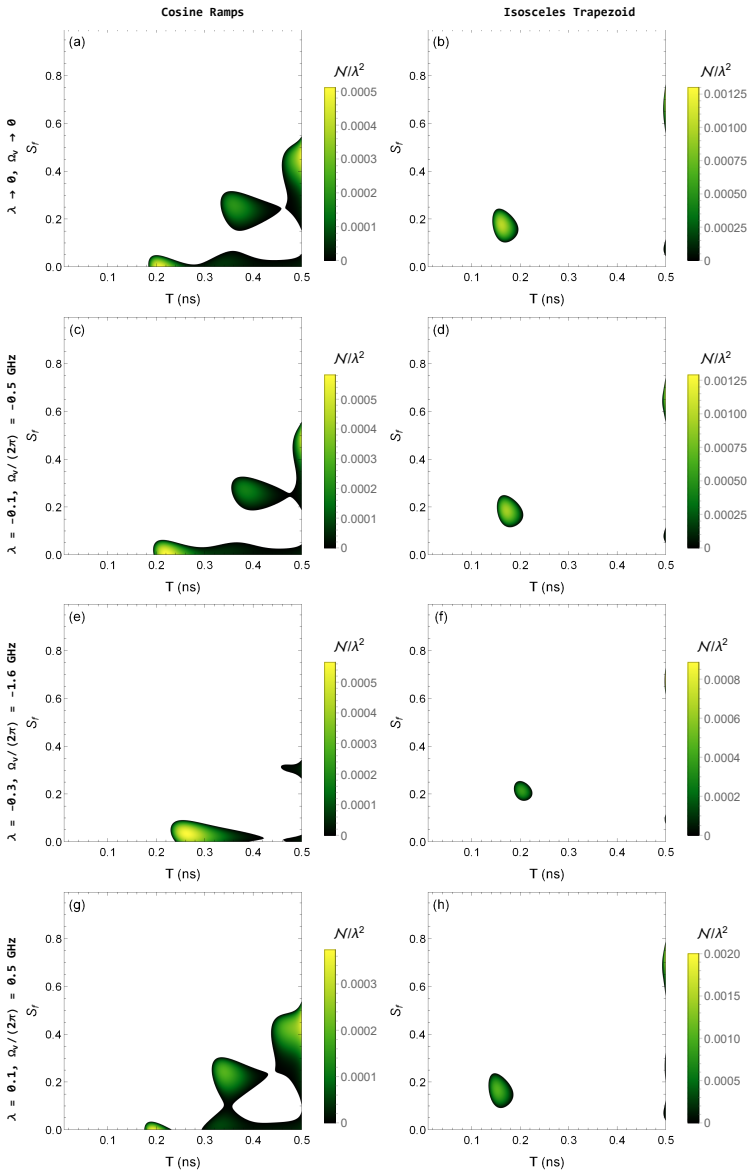


Figure 4.15: Negativity acquired by spacelike detectors. The plots are analogous to Figure 4.14, with the only difference being that the distance between detectors is reduced so that $t_d = 0.5\,\mathrm{ns}$.

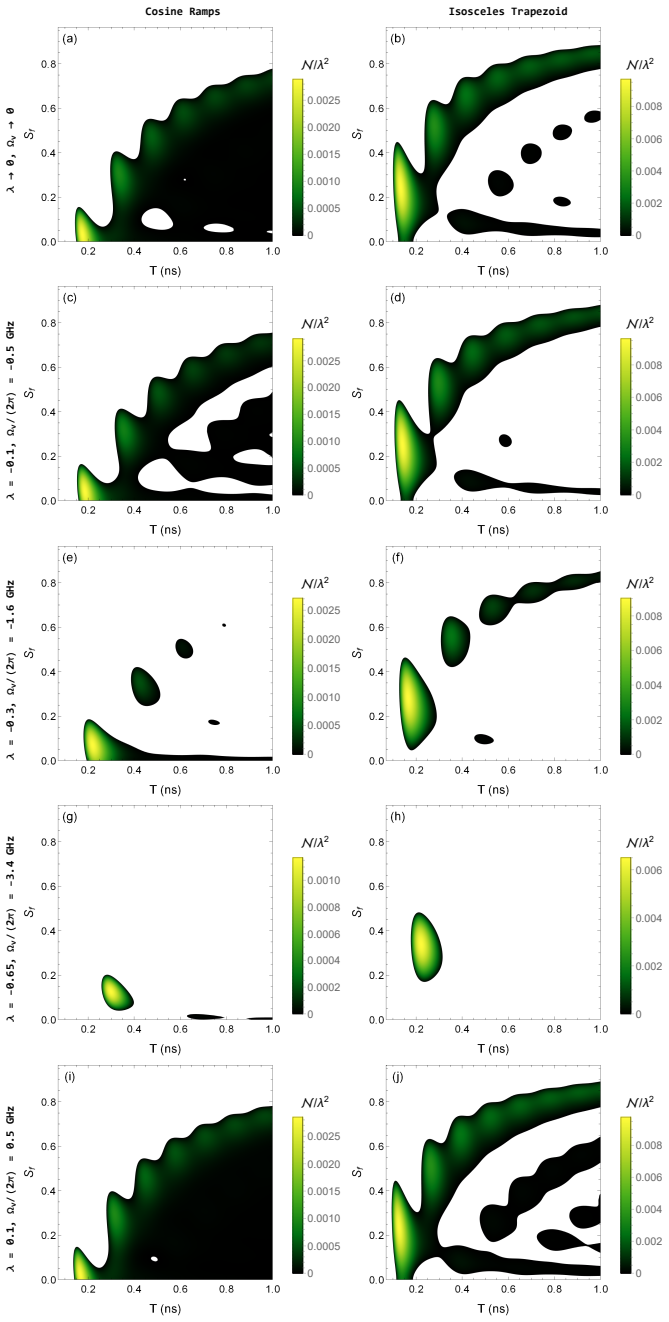


Figure 4.16: Negativity acquired by spacelike detectors. The plots are analogous to Figure 4.14, with the exceptions of fixing $t_\Delta = 0$ and allowing the distance between detectors to vary as $t_d = T$, as depicted in the spacetime diagram of Figure 4.13(b). Moreover, the rows show the scenarios 1, 2, 3, 4 and 6 of Table 4.1.

4.5.5 Effect of the distance between detectors

Here we show how the entanglement acquired by the detectors changes with the distance between them. Finding an optimal distance is important, since it cannot be changed after building the superconducting device.

Now, when plotting the negativity and the genuine harvesting estimator we will use as independent variables t_d and t_Δ. The variable t_d determines the distance between the probes, and the delay t_Δ can compensate the reduction in negativity that occurs when separating the detectors, since the amount of harvested entanglement is ruled by the distance of the detectors' interactions to each other's lightcones. Moreover, t_Δ is easily tunable in the superconducting implementation. We explore the scenarios in Table 4.1. Results for scenarios 1 to 5 are respectively shown in Figures 4.17, 4.18, 4.19, 4.20, 4.21, in order of increasingly negative coupling strength and gap variation. Additionally, results for scenario 6 (small positive gap variation) are shown in Figure 4.22. We explore the three switching function shapes given in subsection 4.5.2. We pick values of T and S_f for scenario 1 ($\Delta\Omega \to 0$) that have considerable spacelike harvesting. For the rest of scenarios, which have different $\Delta\Omega$, we pick T so that the adimensional quantity $T(\Omega^0 + \Delta\Omega)$ stays constant, and we keep a constant S_f.

We observe, consistently with subsections 4.5.3 and 4.5.4, that larger negative $\Delta\Omega$ concentrates the negativity towards the lightcone, reducing the amount of parameters for which spacelike entanglement harvesting occurs. For the explored scenario with largest negative $\Delta\Omega$ (scenario 5 of Table 4.1), there is no spacelike harvesting, as in Figure 4.21. However, negativity in causal contact grows considerably. Moreover, entanglement can still be harvested for all explored $\Delta\Omega$ for detectors in causal contact, according to the genuine harvesting estimator.

The figures show that negativity is higher when the detectors are in causal contact, i.e. $|t_\Delta| \approx t_d$. At the same time, the negativity around $|t_\Delta| \approx t_d$ decreases with increasing t_d. However, this decay slows down and eventually halts. After such point, the negativity only depends on $t_\Delta - t_d$ and is unaffected by further separating the detectors. This parameter $t_\Delta - t_d$ quantifies the distance of the detector B from the lightcone of the detector A.

This behavior is particular of 1+1D fields, and contrasts with the usual entanglement harvesting results in 3+1D, where the negativity along the lightcone always keeps decaying with distance. In 1+1D the decay along the lightcone stops because the two point correlations of the vacuum of the field tend to non-zero values as the distance along the lightcone

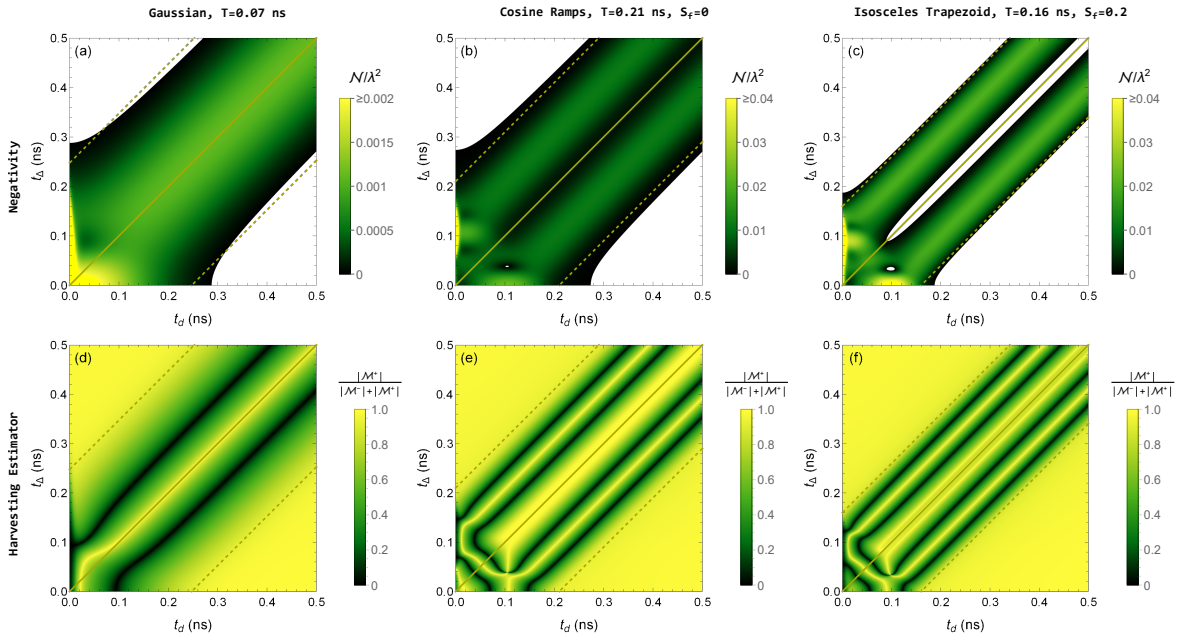


Figure 4.17: Scenario 1 of Table 4.1, with $\lambda \to 0$, $\Delta\Omega \to 0$. **The following applies to Figures 4.17, 4.18, 4.19, 4.20, 4.21 and 4.22:** The first row shows $\mathcal{N}/\lambda^2$, with $\mathcal{N} = 0$ in white. The second row shows $|\mathcal{M}^+|/(|\mathcal{M}^-| + |\mathcal{M}^+|)$, which goes from 0 (all entanglement from communication) to 1 (all entanglement from harvesting). t_d is the signaling time and t_Δ the delay between switchings. The columns use, from left to right, the switching functions: 1) Gaussian, $T = 0.07\,\text{ns}$, 2) cosine ramps, $T = 0.21\,\text{ns}$, $S_f = 0$, 3) isosceles trapezoid, $T = 0.16\,\text{ns}$, $S_f = 0.2$. The diagonal solid lines indicate full lightlike contact. Outside the dashed lines, either there is no light contact (compact switchings) or only the 5σ tails of the Gaussian can interact. To aid visualization, the values of negativity larger than the thresholds indicated in the legend are plotted yellow.

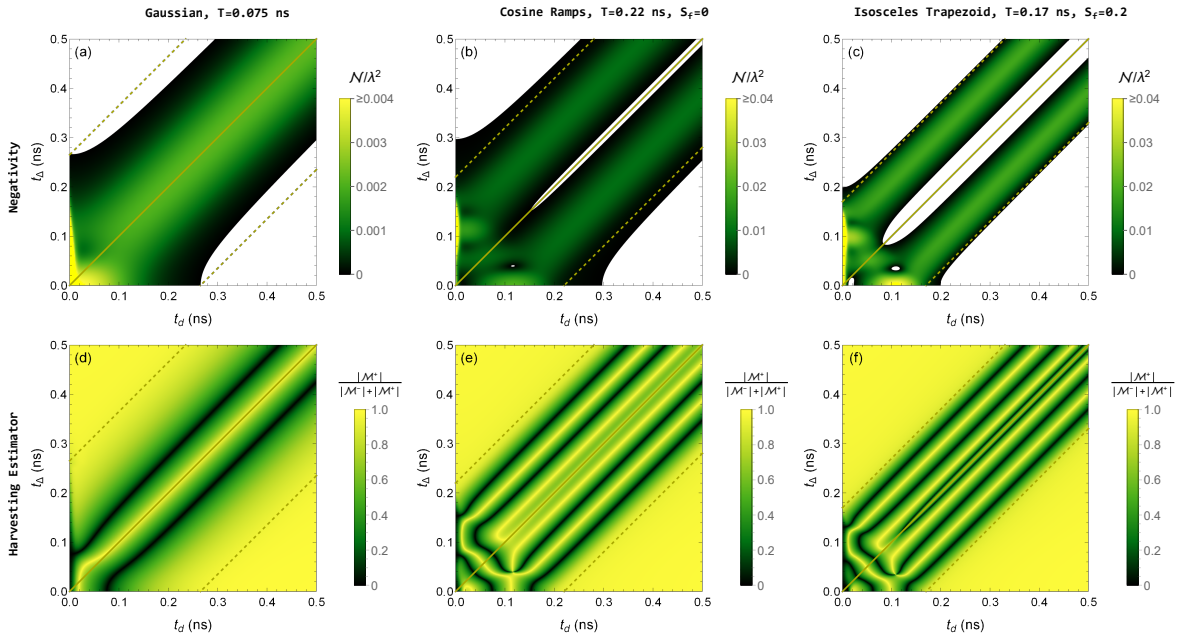


Figure 4.18: Analogous to Figure 4.17, but for scenario 2 of Table 4.1, with $\lambda = -0.1$, $\Delta\Omega/(2\pi) = -0.5\,\mathrm{GHz}$. Moreover, each column of plots uses, from left to right, Gaussian switching with $T = 0.075\,\mathrm{ns}$, cosine ramps switching with $T = 0.22\,\mathrm{ns}$, $S_f = 0$, and isosceles trapezoid switching with $T = 0.17\,\mathrm{ns}$, $S_f = 0.2$.

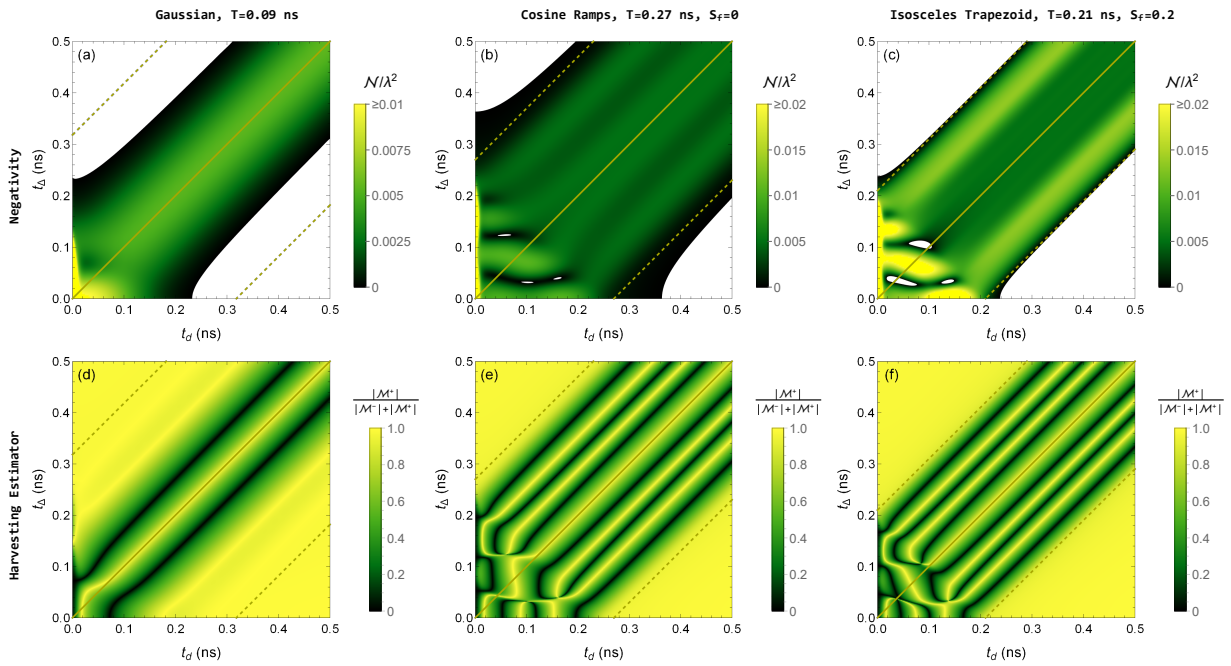


Figure 4.19: Analogous to Figure 4.17, but for scenario 3 of Table 4.1, with $\lambda = -0.3$, $\Delta\Omega/(2\pi) = -1.6\,\mathrm{GHz}$. Moreover, each column of plots uses, from left to right, Gaussian switching with $T = 0.09\,\mathrm{ns}$, cosine ramps switching with $T = 0.27\,\mathrm{ns}$, $S_f = 0$, and isosceles trapezoid switching with $T = 0.21\,\mathrm{ns}$, $S_f = 0.2$.

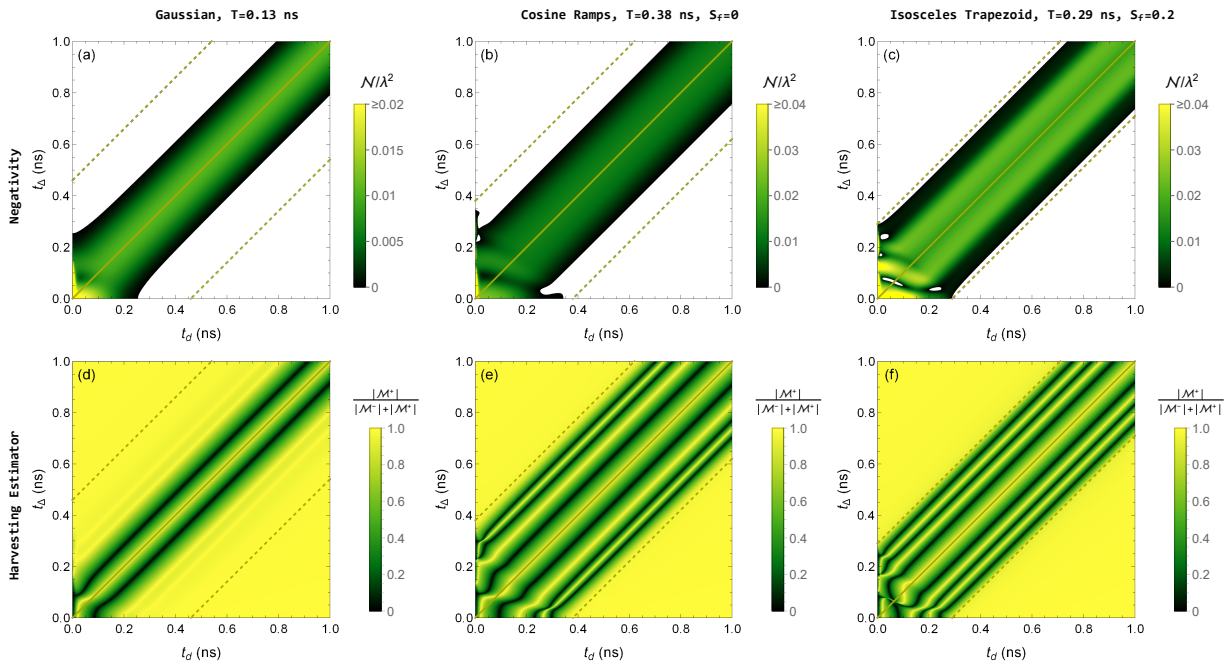


Figure 4.20: Analogous to Figure 4.17, but for scenario 4 of Table 4.1, with $\lambda = -0.65$, $\Delta\Omega/(2\pi) = -3.4\,\mathrm{GHz}$. Moreover, each column of plots uses, from left to right, Gaussian switching with $T = 0.13\,\mathrm{ns}$, cosine ramps switching with $T = 0.38\,\mathrm{ns}$, $S_f = 0$, and isosceles trapezoid switching with $T = 0.29\,\mathrm{ns}$, $S_f = 0.2$.

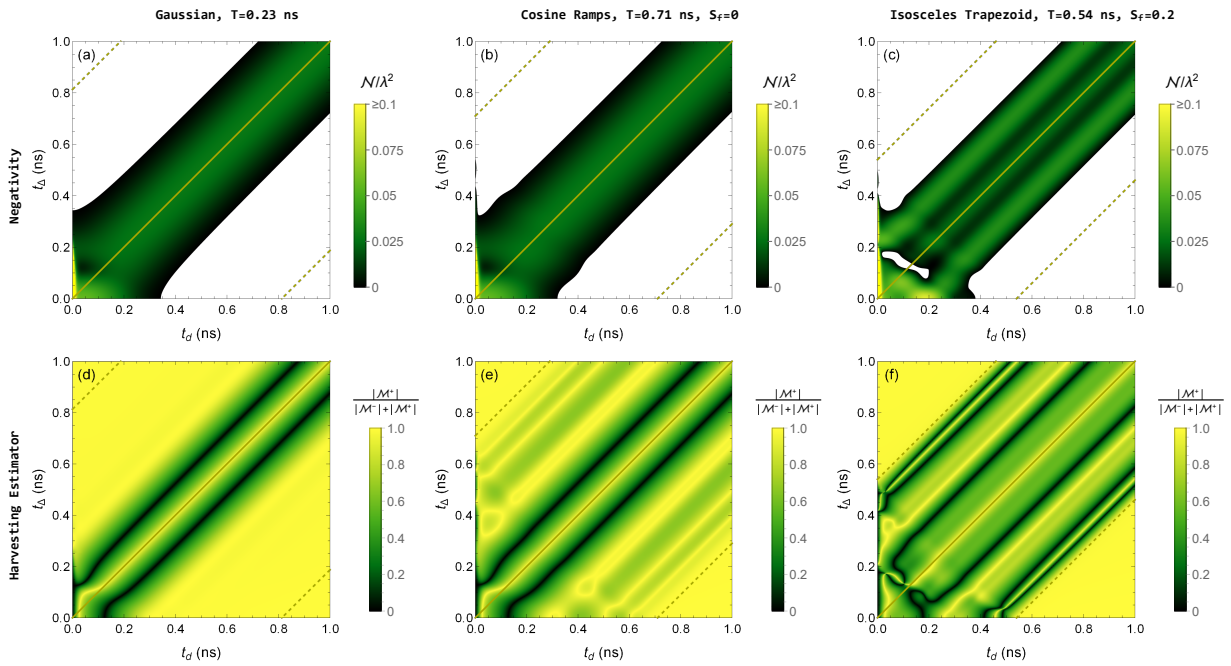


Figure 4.21: Analogous to Figure 4.17, but for scenario 5 of Table 4.1, with $\lambda = -1$, $\Delta\Omega/(2\pi) = -5.2\,\mathrm{GHz}$. Moreover, each column of plots uses, from left to right, Gaussian switching with $T = 0.23\,\mathrm{ns}$, cosine ramps switching with $T = 0.71\,\mathrm{ns}$, $S_f = 0$, and isosceles trapezoid switching with $T = 0.54\,\mathrm{ns}$, $S_f = 0.2$.

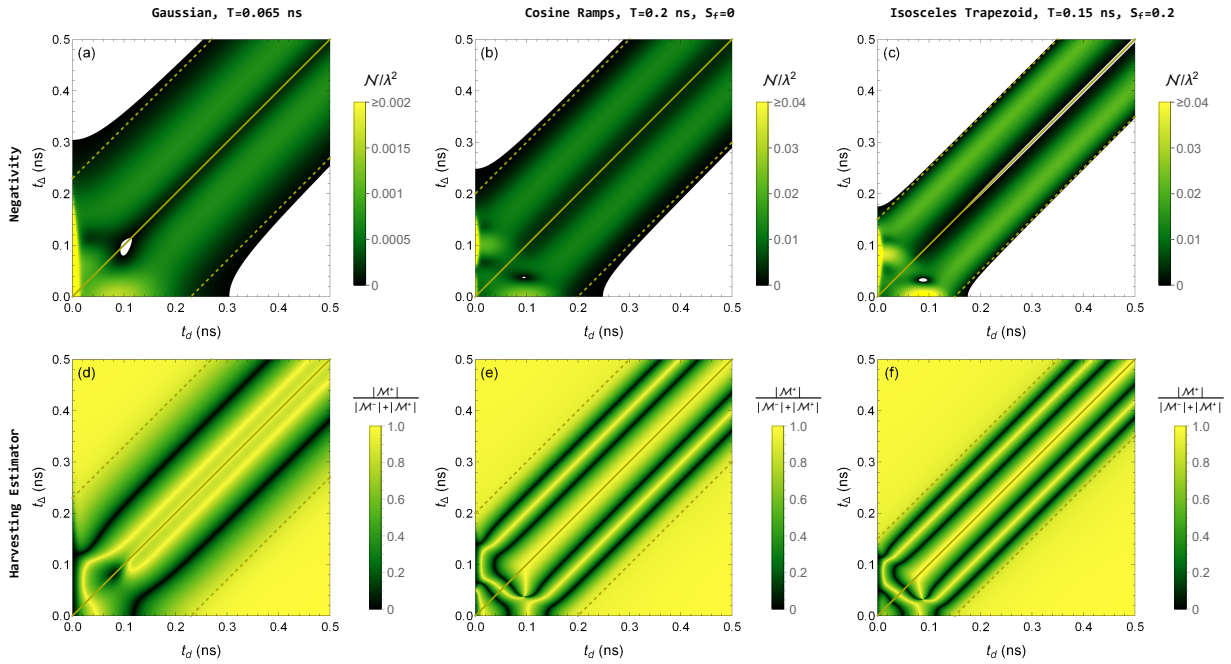


Figure 4.22: Analogous to Figure 4.17, but for scenario 6 of Table 4.1, with $\lambda = 0.1$, $\Delta\Omega/(2\pi) = 0.5\,\mathrm{GHz}$. Moreover, each column of plotss uses, from left to right, Gaussian switching with $T = 0.065\,\mathrm{ns}$, cosine ramps switching with $T = 0.2\,\mathrm{ns}$, $S_f = 0$, and isosceles trapezoid switching with $T = 0.15\,\mathrm{ns}$, $S_f = 0.2$.

increases. This can be seen from Eq. (4.57),

$$\mathcal{W}^{\text{vac}}_{xx'}(t_-, x_-) = \frac{1}{4\pi c^2}\left(\mathcal{J}\left(t_- + \frac{|x_-|}{v}\right) + \mathcal{J}\left(t_- - \frac{|x_-|}{v}\right)\right), \tag{4.73}$$

and defining $u_\pm = |t_-| \pm \frac{|x_-|}{v}$,

$$\lim_{u_+\to\infty} \mathcal{W}^{\text{vac}}_{xx'}(t_-, x_-)\big|_{u_-=\text{ctt.}} = \frac{1}{4\pi c^2}\mathcal{J}\left(|t_-| - \frac{|x_-|}{v}\right), \tag{4.74}$$

which will be non-zero and even large if $|t_-| \approx \frac{|x_-|}{v}$. The negativity exhibits the same limit behavior, but replacing t_- and $|x_-|/v$ by the corresponding t_Δ and t_d. Moreover, if $|t_\Delta| \approx t_d$, the negativity along the lightcone plateaus for $t_d \gg \Omega_{\text{cut}}^{-1}, T$. This can be deduced from the expressions for $\mathcal{L}$ and $\mathcal{M}$ of Eq. (4.59), by taking a change of variables $t \to s + t_{\text{A}}$, $t' \to s' + t_{\text{B}}$.

In 3+1D, there would be a $1/|x_-|$ prefactor in the two point correlator of the field amplitudes in the vacuum, $\mathcal{W}^{\text{vac}}$, which would cause correlations and communication to decay with distance even along the lightcone. However, as already discussed, this decay does not occur in the 1+1D case, which we are interested in due to the the field implementation being superconducting transmission lines. This suggests that detectors in causal contact or close to it can be placed far apart without losing most negativity.

Chapter 5

Conclusions and Outlook

Discussion for chapter 2

The first scenario studied in this thesis considers a pair of particle detectors in causal contact, which get entangled through their interaction with a quantum field. The entanglement between the detectors could generally come from 1) their exchange of information through the field, and 2) from from extracting preexisting entanglement in the field. When the second contribution dominates we can say that the detectors are *harvesting* entanglement from the field. In previous results it was shown than in most common cases in flat spacetime and for massless fields, when the (the interaction regions of the) detectors are in full light contact, the entanglement they acquire is dominated by communication [55] (with interesting exceptions to this rule appearing in spacetimes with caustics [56]).

In contrast, section 2.3 showed that if the particle detectors couple through a massless field in flat spacetimes through the so-called *derivative coupling*, it is possible to have the peak of entanglement between the detectors happening while they are in full light contact, and (more importantly) the source of that entanglement is genuine harvesting and not communication. This is relevant since the derivative coupling is arguably important both from the theoretical and experimental points of view. In the first case, to sidestep IR ambiguity problems and to study problems in reduced dimensions, and in the second, because it adequately models superconducting qubits coupled to transmission lines.

Moreover, we explored the interplay between the two different ways, communication and harvesting, in which two particle detectors can get entangled through their interaction with a quantum field. The analysis demonstrated that, in general entanglement harvesting setups, the contributions are not always additive, but instead they can interfere both destructively and constructively. Then, we provided sufficient conditions for an entanglement

harvesting setup to not display destructive interference between these two contributions. We discuss that the reason this phenomenon was not observed in the past is because these conditions are met in the scenarios commonly explored in the literature, which typically have a lot of symmetry.

Finally, we presented simple examples in Minkowski and cosmological spacetimes using entanglement harvesting setups that violate these conditions and for which the two contributions to harvesting a) combine constructively, amplifying the total amount of entanglement beyond previously observed scenarios and b) interfere destructively, preventing the detectors from getting entangled. For example, whenever the detectors are in causal contact and the switching functions are not time-symmetric, we can see regimes where due to destructive interference the detectors cannot get entangled. This is so even though in these regimes harvesting alone or communication alone would have gotten the detectors entangled.

These results suggest that if one wants to make two detectors entangled through short interactions with a quantum field, one can enhance the amount of entanglement acquired by the detectors by choosing the setup so that the two contributions interfere constructively.

Discussion for chapter 3

At the beginning of this chapter, we introduced the most general entanglement harvesting protocol considered in this thesis. Detectors are modeled as arbitrary quantum systems with a finite or countable basis, and couple to the field via the product of a detector operator and a field operator. The only assumption on the field operator is that it can be expressed as a linear combination of ladder operators. This framework is flexible enough to encompass implementations in superconducting circuits, such as the one discussed in Chapter 4.

Within this framework, we decompose the detector–field interaction into longitudinal (diagonal) and transversal (off-diagonal) components relative to a preferred detector basis. While this basis can be chosen to be the energy basis, the results hold for any choice of basis. A key finding is that entanglement harvesting, as quantified by the negativity, is primarily driven by the part of the coupling that is transversal to the initial state. Specifically, the leading contribution is second order in the transversal coupling strength and zeroth order in the longitudinal one. Thus, longitudinal effects appear only beyond leading order, becoming significant only for sufficiently strong or prolonged longitudinal interactions.

We analyze these higher-order effects using an expression for the negativity that is perturbative in the transversal interaction but non-perturbative in the longitudinal one. As an example, we consider a qubit detector for which entanglement is successfully harvested after smoothly switching on and off the transversal interaction. We then examine how a constant, spurious longitudinal interaction suppresses this entanglement. The suppression grows as the longitudinal coupling strength increases, eventually eliminating harvesting entirely, for the explored case. We also observe that strong longitudinal coupling can lead to the detectors getting more excited during and after the harvesting protocol. The expressions derived here allow to accurately estimate when the longitudinal interaction effects become relevant. This can inform future implementations of entanglement harvesting in superconducting circuits, where longitudinal interactions can occur.

Discussion for chapter 4

In the last chapter before the conclusions, we strengthened the connection of entanglement harvesting in theoretical Relativistic Quantum Information (RQI) to practical experiments in superconducting circuits. We did so by modeling superconducting circuits as Unruh-DeWitt (UDW) detectors with features such as variable energy gaps and derivative coupling to a 1+1D field. While these features had been previously explored separately, here we explore them together and include an explicit mapping of the parameters of the theoretical models to the experimental parameters in superconducting circuit implementations.

A major contribution is the analysis of the effects on entanglement harvesting of the variable gap detector models that mimic superconducting implementations such as the one in [3]. Specifically, the variable gap detectors that we consider have a linear reduction in the energy gap due to the coupling (and thus the switching function). For these models, we numerically explored a wide range of parameters, including strength of the gap variation, detector positions, switching functions, and interaction durations. In the scenarios explored, we observe that increasing the gap variation reduces the entanglement acquired by spacelike detectors but does not completely cancel it. Furthermore, this reduction does not occur for detectors in lightlike contact, for which genuine harvesting (subtracting the contributions from communication between the detectors) can even see an enhancement. Moreover, we also see that increasing the distance between detectors does not significantly impair their ability to become entangled, which is a feature of using 1+1D quantum fields.

In more detail, for detectors in causal contact, we considered the two contributions of the entanglement acquired by the detectors, in line with chapter 2: entanglement due to communicating through the field and entanglement that is actually extracted from preexisting field correlations. Using the tools from [55] to split these two contributions,

we show that having a variable gap does not preclude entanglement harvesting, but rather can even enhance it for detectors in causal contact. This endorses the possibility that this entanglement could be detected in future implementations in those superconducting devices where gap variations cannot be avoided in the ultra-strong coupling regime. Conversely, this work motivates improved implementation designs where the gap variation is reduced or even completely avoided[1] in order to explore spacelike entanglement harvesting.

Outlook

The works in this thesis lead to further research questions to explore in the future, presented below.

Let us start with chapter 2, whose overarching topic is entanglement harvesting for detectors in causal contact. Specifically, we looked at how to split the detectors' entanglement and correlations into a part sourced by communication and a part harvested from the preexisting field correlations. The following list proposes future work related to this topic:

1. Consider that the split into communication and harvesting provided in section 2.2 only works up to second order in perturbation theory (which is the leading order for the entanglement acquired by the detectors). Therefore, it would be of interest to develop a way to split detector entanglement that works for non-perturbative calculations. A possible way to guarantee that there are no communication contributions would be as follows: set the commutator of the field to zero for the terms where both detectors participate, while keeping the rest of the non-perturbative calculation the same. One would expect that the remaining entanglement after this modification would be exclusively harvested. However, the usefulness and adequacy of this hypothetical approach remains as future work.

2. Better understanding the split into communication and harvesting, by replacing the quantum field with a discrete version of it: a chain, or lattice, of coupled harmonic oscillators. In such a model, the entanglement between the harmonic oscillators is well defined. Then, the propagation of entanglement along the harmonic oscillator chain could be studied and related to the discrete versions of the commutator and anticommutator of the field operator.

[1] Furthermore, in principle, spacelike harvesting could be improved in setups where the gap of the detector is fully tunable during the experiment. This could be done by optimizing over all possible functions of time that the gap could be tuned to follow. However, this goes beyond the scenarios explored in this thesis.

3. Exploring how to take advantage of the interference phenomenon between communication and harvesting contributions to entanglement. We are interested in exploring how the parameters can be chosen so that interference can be made constructive, enhancing the entanglement acquired by the detectors.

Secondly, Chapter 3 explored the entanglement harvesting protocol for a very general class of detector models and couplings. Furthermore, it split the evolution into a non-perturbatively computed longitudinal part and a perturbatively computed transversal part. Further research using this work would include:

1. Explore further examples of detectors that include both longitudinal and transversal terms. A motivation to study these would be to choose couplings that better mimic the experimental implementation in superconducting circuits, such as the one studied in Chapter 4. In that chapter, we neglected the longitudinal terms to simplify the analysis, since their effect is of subleading order in perturbation theory. However, a more complete treatment of the interaction, by using the tools of Chapter 3, would be interesting to verify whether it is justified to neglect the longitudinal terms.

2. Optimizing the amount of harvested entanglement by controlling the detector operator that couples to the field. This could be achieved via tuning the free Hamiltonian of the detector, or equivalently, via applying unitary gates to the detectors. This changes the interaction picture operator of the detector that couples to the field. Controlling this operator optimally to harvest the most entanglement is a promising avenue. Importantly, such optimization would be implementable on detectors built in superconducting circuits, since this platform allows applying unitaries to the detectors.

Finally, the context of Chapter 4 is the implementation of detectors and entanglement harvesting in superconducting circuits. Specifically, we focused on improving the RQI theoretical models for detectors so that they better match the superconducting implementation, while remaining simple. However, to better predict experiments, we would want to further improve the accuracy of the modeling, including more elements of the implementation. Such improvements include:

1. Not taking the approximations listed in subsection 4.2.1. This would imply the use of multi-level detectors, with non-trivial free dynamics, and a coupling to the field through more general detector operators.

2. Further examine the continuum limit for the circuit model of the transmission line tunably coupled to the superconducting qubit. This was done in subsection 4.1.3. There, as commonly done in previous literature, we neglected the renormalization term that modifies the detector Hamiltonian and that diverges in the continuum limit. We want to explore the validity of this assumption or, alternatively, to find what corrections need to be included in the model. As mentioned in the same subsection, we plan to do this by comparing the discrete circuit model with finite discretization length Δx and the continuous field model with a cutoff. We expect the cutoff to play a major role, since it also induces a minimum resolution for the field amplitude.

3. The quantization procedure we followed in subsection 4.1.2 assumes that the external magnetic fluxes f_ε and f_β are constant. However, we intend to rapidly change this fluxes during the experiment to quickly turn on and off the interaction with the field. To properly include the effects of time-dependent flux in our model, we plan to follow the recent work in [109, 110, 111].

4. We choose the field cutoff to be exponential, see equation (4.9), since it is simple and has been previously used in the literature. However, a future work would be to design experiments that distinguish between different cutoff shapes. Then, performing such experiments on the detector implementation would allow to find a best fit for the cutoff.

5. For simplicity, we assumed that the detectors and field start in the vacuum state, i.e. a zero temperature state. However, in reality, the expected temperature for the experiment is around 20-30mK. This effect has been preliminarily explored in [101], using a simpler UDW model with parameters that match the experiment. For the case explored there, increasing temperature decreases entanglement harvesting until it no entanglement is harvested for temperatures higher than 30mK. Therefore, it is important to include the effect of the temperature in more accurate models of the implementation.

6. The model used for the transmission line assumes it is infinite and has no boundaries. In such case, waves propagate away to infinity unimpeded. However, in the real implementation, the transmission line is finite, and we expect partial reflections on their boundaries [3]. Including these reflections in the model is relevant to quantify their effect on entanglement harvesting.

The resulting model will be more complex, and need extensive use of numerical calculations to predict the amount of harvested entanglement. However, its higher accuracy will be cru-

cial in determining the setups for which harvesting is largest, facilitating an experimental realization.

References

[1] Adam Teixidó-Bonfill and Eduardo Martín-Martínez. Work in preparation.

[2] Alejandro Pozas-Kerstjens and Eduardo Martín-Martínez. Harvesting correlations from the quantum vacuum. *Phys. Rev. D*, 92:064042, Sep 2015.

[3] Noah Janzen, Xi Dai, Shaun Ren, Jihao Shi, and Adrian Lupascu. Tunable coupler for mediating interactions between a two-level system and a waveguide from a decoupled state to the ultrastrong coupling regime. *Phys. Rev. Res.*, 5:033155, Sep 2023.

[4] Stephen J. Summers and Reinhard F. Werner. The vacuum violates bell's inequalities. *Phys. Lett. A*, 110:257–259, 1985.

[5] Stephen J. Summers and Reinhard Werner. Bell's inequalities and quantum field theory. I. General setting. *J. Math. Phys.*, 28(10):2440–2447, 10 1987.

[6] Michael Redhead. More ado about nothing. *Foundations of Physics*, 25(1):123–137, Jan 1995.

[7] Michael L. G. Redhead and Fabian Wagner. Unified treatment of epr and bell arguments in algebraic quantum field theory. *Foundations of Physics Letters*, 11(2):111–125, Apr 1998.

[8] Rob Clifton, David V. Feldman, Hans Halvorson, Michael L. G. Redhead, and Alexander Wilce. Superentangled states. *Phys. Rev. A*, 58:135–145, Jul 1998.

[9] Benni Reznik, Alex Retzker, and Jonathan Silman. Violating bell's inequalities in vacuum. *Phys. Rev. A*, 71:042104, Apr 2005.

[10] Antony Valentini. Non-local correlations in quantum electrodynamics. *Phys. Lett. A*, 153(6-7):321 – 325, 1991.

[11] Benni Reznik. Entanglement from the vacuum. *Found. Phys.*, 33(1):167–176, 2003.

[12] Greg Ver Steeg and Nicolas C. Menicucci. Entangling power of an expanding universe. *Phys. Rev. D*, 79:044027, Feb 2009.

[13] Laura J. Henderson, Robie A. Hennigar, Robert B. Mann, Alexander R. H. Smith, and Jialin Zhang. Harvesting entanglement from the black hole vacuum. *Class. Quantum Gravity*, 35(21):21LT02, oct 2018.

[14] Alejandro Pozas-Kerstjens and Eduardo Martín-Martínez. Entanglement harvesting from the electromagnetic vacuum with hydrogenlike atoms. *Phys. Rev. D*, 94:064074, Sep 2016.

[15] T. Rick Perche, Boris Ragula, and Eduardo Martín-Martínez. Harvesting entanglement from the gravitational vacuum. *Phys. Rev. D*, 108:085025, Oct 2023.

[16] Kensuke Gallock-Yoshimura, Erickson Tjoa, and Robert B. Mann. Harvesting entanglement with detectors freely falling into a black hole. *Phys. Rev. D*, 104:025001, Jul 2021.

[17] Lana Bozanic, Manar Naeem, Kensuke Gallock-Yoshimura, and Robert B. Mann. Correlation harvesting between particle detectors in uniform motion. *Phys. Rev. D*, 108:105017, Nov 2023.

[18] Jose Trevison, Koji Yamaguchi, and Masahiro Hotta. Pure state entanglement harvesting in quantum field theory. *Prog. Theor. Exp. Phys.*, 2018(10):103A03, 10 2018.

[19] Erickson Tjoa and Robert B. Mann. Harvesting correlations in schwarzschild and collapsing shell spacetimes. *J. High Energy Phys.*, 2020(8):155, Aug 2020.

[20] Wan Cong, Erickson Tjoa, and Robert B. Mann. Entanglement harvesting with moving mirrors. *J. High Energy Phys.*, 2019(6):21, Jun 2019.

[21] Keith K. Ng, Robert B. Mann, and Eduardo Martín-Martínez. Unruh-dewitt detectors and entanglement: The anti–de sitter space. *Phys. Rev. D*, 98:125005, Dec 2018.

[22] Laura J. Henderson, Robie A. Hennigar, Robert B. Mann, Alexander R. H. Smith, and Jialin Zhang. Entangling detectors in anti-de sitter space. *J. High Energy Phys.*, 2019(5):178, May 2019.

[23] Subhajit Barman, Dipankar Barman, and Bibhas Ranjan Majhi. Entanglement harvesting from conformal vacuums between two unruh-dewitt detectors moving along null paths. *J. High Energy Phys.*, 2022(9):106, Sep 2022.

[24] Joshua Foo, Robert B. Mann, and Magdalena Zych. Entanglement amplification between superposed detectors in flat and curved spacetimes. *Phys. Rev. D*, 103:065013, Mar 2021.

[25] Zhihong Liu, Jialin Zhang, and Hongwei Yu. Entanglement harvesting in the presence of a reflecting boundary. *J. High Energy Phys.*, 2021(8):20, Aug 2021.

[26] William G. Unruh. Notes on black-hole evaporation. *Phys. Rev. D*, 14:870–892, Aug 1976.

[27] Bryce DeWitt. *General Relativity; an Einstein Centenary Survey.* Cambridge University Press, Cambridge, UK, 1980.

[28] William G. Unruh and Robert M. Wald. What happens when an accelerating observer detects a rindler particle. *Phys. Rev. D*, 29:1047–1056, Mar 1984.

[29] Sebastian Schlicht. Considerations on the Unruh effect: causality and regularization. *Class. Quantum Gravity*, 21(19):4647–4660, sep 2004.

[30] Jorma Louko and Alejandro Satz. How often does the Unruh-DeWitt detector click? regularization by a spatial profile. *Class. Quantum Gravity*, 23(22):6321–6343, oct 2006.

[31] Eduardo Martín-Martínez, Miguel Montero, and Marco del Rey. Wavepacket detection with the unruh-dewitt model. *Phys. Rev. D*, 87:064038, Mar 2013.

[32] Natalie Klco and Martin J. Savage. Entanglement spheres and a uv-ir connection in effective field theories. *Phys. Rev. Lett.*, 127:211602, Nov 2021.

[33] Natalie Klco, D. H. Beck, and Martin J. Savage. Entanglement structures in quantum field theories: Negativity cores and bound entanglement in the vacuum, 2022.

[34] Natalie Klco and D. H. Beck. Entanglement structures in quantum field theories. ii. distortions of vacuum correlations through the lens of local observers. *Phys. Rev. A*, 108:012429, Jul 2023.

[35] Bruno de S. L. Torres, Kelly Wurtz, José Polo-Gómez, and Eduardo Martín-Martínez. Entanglement structure of quantum fields through local probes. *Journal of High Energy Physics*, 2023(5):58, May 2023.

[36] Ivan Agullo, Béatrice Bonga, Patricia Ribes-Metidieri, Dimitrios Kranas, and Sergi Nadal-Gisbert. How ubiquitous is entanglement in quantum field theory?, 2023.

[37] Boyu Gao and Natalie Klco. Detecting spacelike vacuum entanglement at all distances and promoting negativity to a necessary and sufficient entanglement measure in many-body regimes, 2024.

[38] Ivan Agullo, Béatrice Bonga, Eduardo Martín-Martínez, Sergi Nadal-Gisbert, T. Rick Perche, José Polo-Gómez, Patricia Ribes-Metidieri, and Bruno de S. L. Torres. The multimode nature of spacetime entanglement in qft, 2024.

[39] Eduardo Martín-Martínez, Eric G. Brown, William Donnelly, and Achim Kempf. Sustainable entanglement production from a quantum field. *Phys. Rev. A*, 88:052310, Nov 2013.

[40] Alex Retzker, Juan I. Cirac, and Benni Reznik. Detecting vacuum entanglement in a linear ion trap. *Phys. Rev. Lett.*, 94(5):050504, 2005.

[41] Carlos Sabín, Juan José García-Ripoll, Enrique Solano, and Juan León. Dynamics of entanglement via propagating microwave photons. *Phys. Rev. B*, 81:184501, May 2010.

[42] Carlos Sabín, Marco del Rey, Juan José García-Ripoll, and Juan León. Fermi problem with artificial atoms in circuit qed. *Phys. Rev. Lett.*, 107:150402, Oct 2011.

[43] Carlos Sabín, Borja Peropadre, Marco del Rey, and Eduardo Martín-Martínez. Extracting Past-Future Vacuum Correlations Using Circuit QED. *Phys. Rev. Lett.*, 109:033602, Jul 2012.

[44] Juan Sebastián Ardenghi. Entanglement harvesting in double-layer graphene by vacuum fluctuations in a microcavity. *Phys. Rev. D*, 98:045006, Aug 2018.

[45] Cisco Gooding, Steffen Biermann, Sebastian Erne, Jorma Louko, William G. Unruh, Jörg Schmiedmayer, and Silke Weinfurtner. Interferometric unruh detectors for bose-einstein condensates. *Phys. Rev. Lett.*, 125:213603, Nov 2020.

[46] Cisco Gooding, Allison Sachs, Robert B. Mann, and Silke Weinfurtner. Vacuum entanglement probes for ultra-cold atom systems, 2023.

[47] Frieder Lindel, Robert Bennett, and Stefan Yoshi Buhmann. Theory of polaritonic quantum-vacuum detection. *Phys. Rev. A*, 102:041701, Oct 2020.

[48] Francesca Fabiana Settembrini, Frieder Lindel, Alexa Marina Herter, Stefan Yoshi Buhmann, and Jérôme Faist. Detection of quantum-vacuum field correlations outside the light cone. *Nature Communications*, 13(1):3383, Jun 2022.

[49] Frieder Lindel, Alexa Herter, Jérôme Faist, and Stefan Yoshi Buhmann. Probing vacuum field fluctuations and source radiation separately in space and time, 2023.

[50] Frieder Lindel, Alexa Herter, Valentin Gebhart, Jérôme Faist, and Stefan Y. Buhmann. Entanglement harvesting from electromagnetic quantum fields, 2023.

[51] Robert H. Jonsson, Eduardo Martín-Martínez, and Achim Kempf. Quantum signaling in cavity qed. *Phys. Rev. A*, 89:022330, Feb 2014.

[52] Robert H. Jonsson, Eduardo Martín-Martínez, and Achim Kempf. Information transmission without energy exchange. *Phys. Rev. Lett.*, 114:110505, Mar 2015.

[53] Eduardo Martín-Martínez. Causality issues of particle detector models in qft and quantum optics. *Phys. Rev. D*, 92:104019, Nov 2015.

[54] José de Ramón, Maria Papageorgiou, and Eduardo Martín-Martínez. Causality and signalling in noncompact detector-field interactions. *Phys. Rev. D*, 108:045015, Aug 2023.

[55] Erickson Tjoa and Eduardo Martín-Martínez. When entanglement harvesting is not really harvesting. *Phys. Rev. D*, 104:125005, Dec 2021.

[56] João G. A. Caribé, Robert H. Jonsson, Marc Casals, Achim Kempf, and Eduardo Martín-Martínez. Lensing of vacuum entanglement near schwarzschild black holes. *Phys. Rev. D*, 108:025016, Jul 2023.

[57] Derek J. Raine, Dennis William Sciama, and P. G. Grove. Does a uniformly accelerated quantum oscillator radiate? *Proc. R. Soc. A*, 435(1893):205–215, 1991.

[58] Alpan Raval, Bei-Lok Hu, and James Anglin. Stochastic theory of accelerated detectors in a quantum field. *Phys. Rev. D*, 53:7003–7019, Jun 1996.

[59] Eduardo Martín-Martínez and Jorma Louko. Particle detectors and the zero mode of a quantum field. *Phys. Rev. D*, 90:024015, Jul 2014.

[60] Benito A. Juárez-Aubry and Jorma Louko. Onset and decay of the 1 + 1 hawking–unruh effect: what the derivative-coupling detector saw. *Class. Quantum Gravity*, 31(24):245007, nov 2014.

[61] Qingdi Wang and William G. Unruh. Motion of a mirror under infinitely fluctuating quantum vacuum stress. *Phys. Rev. D*, 89:085009, Apr 2014.

[62] Benito A. Juárez-Aubry and Jorma Louko. Quantum fields during black hole formation: how good an approximation is the unruh state? *J. High Energy Phys.*, 2018(5):140, May 2018.

[63] Benito A. Juárez-Aubry and Jorma Louko. Quantum kicks near a Cauchy horizon. *AVS Quantum Sci.*, 4(1):013201, 02 2022.

[64] Cameron R D Bunney and Jorma Louko. Circular motion analogue unruh effect in a 2+1 thermal bath: robbing from the rich and giving to the poor. *Class. Quantum Gravity*, 40(15):155001, jun 2023.

[65] T. Rick Perche and Matheus H. Zambianco. Duality between amplitude and derivative coupled particle detectors in the limit of large energy gaps. *Phys. Rev. D*, 108:045017, Aug 2023.

[66] Richard Lopp and Eduardo Martín-Martínez. Quantum delocalization, gauge, and quantum optics: Light-matter interaction in relativistic quantum information. *Phys. Rev. A*, 103:013703, Jan 2021.

[67] Emma McKay, Adrian Lupascu, and Eduardo Martín-Martínez. Finite sizes and smooth cutoffs in superconducting circuits. *Phys. Rev. A*, 96:052325, Nov 2017.

[68] Anthony J. Leggett, Sudip Chakravarty, Alan T. Dorsey, Matthew P. A. Fisher, Anupam Garg, and Wilhelm Zwerger. Dynamics of the dissipative two-state system. *Rev. Mod. Phys.*, 59:1–85, Jan 1987.

[69] Borja Peropadre, David Zueco, Diego Porras, and Juan José García-Ripoll. Nonequilibrium and nonperturbative dynamics of ultrastrong coupling in open lines. *Phys. Rev. Lett.*, 111:243602, Dec 2013.

[70] Pol Forn-Díaz, Juan José García-Ripoll, Borja Peropadre, Jean-Luc Orgiazzi, Muhammet A. Yurtalan, Ron Belyansky, Cristopher M. Wilson, and Adrian Lupascu. Ultrastrong coupling of a single artificial atom to an electromagnetic continuum in the nonperturbative regime. *Nat. Phys.*, 13(1):39–43, Jan 2017.

[71] Laura J. Henderson, Su Yu Ding, and Robert B. Mann. Entanglement harvesting with a twist. *AVS Quantum Sci.*, 4(1):014402, 2022.

[72] Héctor Maeso-García, T. Rick Perche, and Eduardo Martín-Martínez. Entanglement harvesting: Detector gap and field mass optimization. *Phys. Rev. D*, 106:045014, Aug 2022.

[73] Nadine Stritzelberger, Laura J. Henderson, Valentina Baccetti, Nicolas C. Menicucci, and Achim Kempf. Entanglement harvesting with coherently delocalized matter. *Phys. Rev. D*, 103:016007, Jan 2021.

[74] Laura J. Henderson and Nicolas C. Menicucci. Bandlimited entanglement harvesting. *Phys. Rev. D*, 102:125026, Dec 2020.

[75] Keith K. Ng, Robert B. Mann, and Eduardo Martín-Martínez. New techniques for entanglement harvesting in flat and curved spacetimes. *Phys. Rev. D*, 97:125011, Jun 2018.

[76] Allison Sachs, Robert B. Mann, and Eduardo Martín-Martínez. Entanglement harvesting and divergences in quadratic unruh-dewitt detector pairs. *Phys. Rev. D*, 96:085012, Oct 2017.

[77] Dyuman Bhattacharya, Kensuke Gallock-Yoshimura, Laura J. Henderson, and Robert B. Mann. Extraction of entanglement from quantum fields with entangled particle detectors. *Phys. Rev. D*, 107:105008, May 2023.

[78] Shahnewaz Ahmed, Mir Mehedi Faruk, and Muktadir Rahman. Accelerated paths and unruh effect: finite time detector response in (anti) de sitter spacetime and huygen's principle. *Eur. Phys. J. C*, 83(11):1087, Nov 2023.

[79] S. Jay Olson and Timothy C. Ralph. Entanglement between the future and the past in the quantum vacuum. *Phys. Rev. Lett.*, 106:110404, Mar 2011.

[80] S. Jay Olson and Timothy C. Ralph. Extraction of timelike entanglement from the quantum vacuum. *Phys. Rev. A*, 85:012306, Jan 2012.

[81] Anton Frisk Kockum, Adam Miranowicz, Simone De Liberato, Salvatore Savasta, and Franco Nori. Ultrastrong coupling between light and matter. *Nature Reviews Physics*, 1(1):19–40, Jan 2019.

[82] Pol Forn-Díaz, Lucas Lamata, Enrique Rico, Junichiro Kono, and Enrique Solano. Ultrastrong coupling regimes of light-matter interaction. *Rev. Mod. Phys.*, 91:025005, Jun 2019.

[83] Edwin T. Jaynes and Fred W. Cummings. Comparison of quantum and semiclassical radiation theories with application to the beam maser. *Proceedings of the IEEE*, 51(1):89–109, 1963.

[84] Borja Peropadre, Pol Forn-Díaz, Enrique Solano, and Juan José García-Ripoll. Switchable ultrastrong coupling in circuit qed. *Phys. Rev. Lett.*, 105:023601, Jul 2010.

[85] Guillermo Romero, D. Ballester, Yimin M. Wang, Valerio Scarani, and Enrique Solano. Ultrafast Quantum Gates in Circuit QED. *Phys. Rev. Lett.*, 108:120501, Mar 2012.

[86] Karol Życzkowski, Paweł Horodecki, Anna Sanpera, and Maciej Lewenstein. Volume of the set of separable states. *Phys. Rev. A*, 58:883–892, Aug 1998.

[87] Guifré Vidal and Reinhard F. Werner. Computable measure of entanglement. *Phys. Rev. A*, 65:032314, Feb 2002.

[88] Martin B. Plenio. Logarithmic negativity: A full entanglement monotone that is not convex. *Phys. Rev. Lett.*, 95:090503, Aug 2005.

[89] T. Rick Perche and Eduardo Martín-Martínez. Role of quantum degrees of freedom of relativistic fields in quantum information protocols. *Phys. Rev. A*, 107:042612, Apr 2023.

[90] Eduardo Martín-Martínez, T. Rick Perche, and Bruno de S. L. Torres. General relativistic quantum optics: Finite-size particle detector models in curved spacetimes. *Phys. Rev. D*, 101:045017, Feb 2020.

[91] Eduardo Martín-Martínez, T. Rick Perche, and Bruno de S. L. Torres. Broken covariance of particle detector models in relativistic quantum information. *Phys. Rev. D*, 103:025007, Jan 2021.

[92] Shin Takagi. Vacuum Noise and Stress Induced by Uniform Acceleration: Hawking-Unruh Effect in Rindler Manifold of Arbitrary Dimension. *Progress of Theoretical Physics Supplement*, 88:1–142, 03 1986.

[93] Robert Manuel Wald. *Quantum Field Theory in Curved Spacetime and Black Hole Thermodynamics*. The University of Chicago Press, 1994.

[94] S. Jay Olson and Timothy C. Ralph. Entanglement between the future and the past in the quantum vacuum. *Phys. Rev. Lett.*, 106:110404, Mar 2011.

[95] S. Jay Olson and Timothy C. Ralph. Extraction of timelike entanglement from the quantum vacuum. *Phys. Rev. A*, 85:012306, Jan 2012.

[96] Héctor Maeso-García, José Polo-Gómez, and Eduardo Martín-Martínez. Entanglement harvesting: State dependence and covariance. *Phys. Rev. D*, 106:105001, Nov 2022.

[97] Adelchi Azzalini. A class of distributions which includes the normal ones. *Scand. J. Stat.*, 12(2):171–178, 1985.

[98] Ana Blasco, Luis J. Garay, Mercedes Martín-Benito, and Eduardo Martín-Martínez. Timelike information broadcasting in cosmology. *Phys. Rev. D*, 93:024055, Jan 2016.

[99] Eduardo Martín-Martínez and Nicolas C Menicucci. Cosmological quantum entanglement. *Class. Quantum Gravity*, 29(22):224003, oct 2012.

[100] Jiahao Shi. Fast switchable ultrastrong coupling between superconducting artificial atoms and electromagnetic fields. Master's thesis, University of Waterloo, 2019.

[101] Shaun Ren. Design and implementation of an entanglement harvesting experiment with superconducting flux qubits. Master's thesis, University of Waterloo, 2022.

[102] Martin Göppl, Andreas Fragner, Matthias Baur, Romeo Bianchetti, Stefan Filipp, Johannes M. Fink, Peter J. Leek, G. Puebla, Lars Steffen, and Andreas Wallraff. Coplanar waveguide resonators for circuit quantum electrodynamics. *Journal of Applied Physics*, 104(11):113904, 12 2008.

[103] D. H. Douglass Jr. and R. Meservey. Energy gap measurements by tunneling between superconducting films. i. temperature dependence. *Phys. Rev.*, 135:A19–A23, Jul 1964.

[104] Guillermo Díaz-Camacho, Alejandro Bermudez, and Juan José García-Ripoll. Dynamical polaron Ansatz: A theoretical tool for the ultrastrong-coupling regime of circuit QED. *Phys. Rev. A*, 93:043843, Apr 2016.

[105] Uri Vool and Michel Devoret. Introduction to quantum electromagnetic circuits. *International Journal of Circuit Theory and Applications*, 45(7):897–934, 2017.

[106] Fumiki Yoshihara, Tomoko Fuse, Sahel Ashhab, Kosuke Kakuyanagi, Shiro Saito, and Kouichi Semba. Superconducting qubit–oscillator circuit beyond the ultrastrong-coupling regime. *Nat. Phys.*, 13(1):44–47, Jan 2017.

[107] Oleg Astafiev, Alexandre M. Zagoskin, A. A. Abdumalikov Jr., Yuri A. Pashkin, Tsuyoshi Yamamoto, Kunihiro Inomata, Yasunobu Nakamura, and Jaw S. Tsai. Resonance fluorescence of a single artificial atom. *Science*, 327(5967):840–843, 2010.

[108] Noah Janzen. Demonstration of a tunable coupler suitable for investigating ultrastrong coupling light-matter interactions in superconducting devices. Master's thesis, University of Waterloo, 2022. Available at http://hdl.handle.net/10012/18213.

[109] Xinyuan You, James Avery Sauls, and Jens Koch. Circuit quantization in the presence of time-dependent external flux. *Phys. Rev. B*, 99:174512, May 2019.

[110] Roman-Pascal Riwar and David P. DiVincenzo. Circuit quantization with time-dependent magnetic fields for realistic geometries. *npj Quantum Information*, 8(1):36, Mar 2022.

[111] Jacob Bryon, Daniel K. Weiss, Xinyuan You, Sara Sussman, Xanthe Croot, Ziwen Huang, Jens Koch, and Andrew A. Houck. Time-dependent magnetic flux in devices for circuit quantum electrodynamics. *Phys. Rev. Appl.*, 19:034031, Mar 2023.

[112] T. Rick Perche, José Polo-Gómez, Bruno de S. L. Torres, and Eduardo Martín-Martínez. Fully relativistic entanglement harvesting. *Phys. Rev. D*, 109:045018, Feb 2024.

[113] Robert Manuel Wald. *General Relativity*. The University of Chicago Press, 1984.

[114] T. Rick Perche, Caroline Lima, and Eduardo Martín-Martínez. Harvesting entanglement from complex scalar and fermionic fields with linearly coupled particle detectors. *Phys. Rev. D*, 105:065016, Mar 2022.

[115] José de Ramón and Eduardo Martín-Martínez. A non-perturbative analysis of spin-boson interactions using the Weyl relations, 2020.

APPENDICES

Appendix A

Appendices for Chapter 2

A.1 Communication at leading order through a mediating system

Here we provide an quick review on how to compute estimator for the ability of a system A to send a signal to a system B, through a mediating system C, at leading perturbative order. This scenario generalizes the case of a pair of detectors communicating through a quantum field. For a more thorough analysis see [53, 54].

To quantify communication from A to B, it is useful to distinguish between the full time evolution $\hat{U}$, and the time evolution if we only allow the system $\nu \in \{\mathrm{A}, \mathrm{B}\}$ and C to interact, which we denote as $\hat{U}_\nu$. Then, all the conributions to the final state of B coming from the existence of A, i.e. how A influences the final state of B, can be expressed as

$$\hat{\rho}_{\mathrm{B}}^{\mathrm{signal}} = \mathrm{Tr}_{\mathrm{AC}}(\hat{U}\hat{\rho}_0\hat{U}^\dagger - \hat{U}_{\mathrm{B}}\hat{\rho}_0\hat{U}_{\mathrm{B}}^\dagger), \tag{A.1}$$

for any initial state $\hat{\rho}_0$.

For simplicity, we restrict ourselves to interaction Hamiltonians (in the interaction picture) of the form

$$\begin{aligned} \hat{H}_{\mathrm{I}}(t) &= \hat{H}_{\mathrm{A}}(t) + \hat{H}_{\mathrm{B}}(t), \\ \hat{H}_\nu(t) &= \hat{O}_\nu(t)\hat{C}_\nu(t). \end{aligned} \tag{A.2}$$

Here, $\hat{O}_{\mathrm{A}}(t)$ and $\hat{O}_{\mathrm{B}}(t)$ are observables of the system A and B respectively. The operators $\hat{C}_{\mathrm{A}}(t)$ and $\hat{C}_{\mathrm{B}}(t)$ are observables of the mediating system C.

To further showcase the role of $[\hat{C}_{\mathrm{A}}(t), \hat{C}_{\mathrm{B}}(t')]$ in communication we explicitly compute $\hat{\rho}_{\mathrm{B}}^{\mathrm{signal}}$ to the leading order in a perturbative expansion. Using the Dyson series for the time evolution generated by $\hat{H}_{\mathrm{I}}$,

$$\begin{aligned}\hat{\rho}_{\mathrm{B}}^{\mathrm{signal}} = \mathrm{Tr}_{\mathrm{AC}}\Big(\hat{U}_{\mathrm{B}}^{(1)}\hat{\rho}_0\hat{U}_{\mathrm{A}}^{\dagger(1)} + \big(\hat{U}_{\mathrm{AB}}^{(2)} + \hat{U}_{\mathrm{BA}}^{(2)}\big)\hat{\rho}_0 + \mathrm{H.c.}\Big) \\ + \mathcal{O}\big(\hat{O}_{\mathrm{A}}^m\hat{O}_{\mathrm{B}}^l\big),\end{aligned} \tag{A.3}$$

where $m, l \geq 1$, $m + l \geq 3$ and we defined

$$\begin{aligned}\hat{U}_{\nu}^{(1)} &= -\mathrm{i}\int \mathrm{d}t\, \hat{H}_{\nu}(t), \\ \hat{U}_{\mu\nu}^{(2)} &= -\int \mathrm{d}t \int^{t} \mathrm{d}t'\, \hat{H}_{\mu}(t)\hat{H}_{\nu}(t').\end{aligned} \tag{A.4}$$

Then, using the properties of the trace, and that observables from different systems commute,

$$\begin{aligned}&\mathrm{Tr}_{\mathrm{AC}}\big(\hat{U}_{\mathrm{B}}^{(1)}\hat{\rho}_0\hat{U}_{\mathrm{A}}^{\dagger(1)}\big) \\ &= \int \mathrm{d}t\, \mathrm{d}t'\, \hat{O}_{\mathrm{B}}(t)\, \mathrm{Tr}_{\mathrm{AC}}\big(\hat{\rho}_0\hat{O}_{\mathrm{A}}(t')\hat{C}_{\mathrm{A}}(t')\hat{C}_{\mathrm{B}}(t)\big),\end{aligned} \tag{A.5}$$

$$\begin{aligned}&\mathrm{Tr}_{\mathrm{AC}}\big((\hat{U}_{\mathrm{AB}}^{(2)} + \hat{U}_{\mathrm{BA}}^{(2)})\hat{\rho}_0\big) \\ &= -\int \mathrm{d}t\, \mathrm{d}t'\, \hat{O}_{\mathrm{B}}(t)\, \mathrm{Tr}_{\mathrm{AC}}\Big(\hat{\rho}_0\hat{O}_{\mathrm{A}}(t') \\ &\quad \times \big(\,\Theta(t'-t)\hat{C}_{\mathrm{A}}(t')\hat{C}_{\mathrm{B}}(t) + \Theta(t-t')\hat{C}_{\mathrm{B}}(t)\hat{C}_{\mathrm{A}}(t')\big)\Big),\end{aligned} \tag{A.6}$$

where Θ is the Heaviside step function. Substituting back into $\hat{\rho}_{\mathrm{B}}^{\mathrm{signal}}$,

$$\begin{aligned}\hat{\rho}_{\mathrm{B}}^{\mathrm{signal}} = \int \mathrm{d}t \int_t \mathrm{d}t'\, [\hat{O}_{\mathrm{B}}(t'), \mathrm{Tr}_{\mathrm{AC}}\big(\hat{\rho}_0\hat{O}_{\mathrm{A}}(t)[\hat{C}_{\mathrm{A}}(t), \hat{C}_{\mathrm{B}}(t')]\big)] \\ + \mathcal{O}\big(\hat{O}_{\mathrm{A}}^m\hat{O}_{\mathrm{B}}^l\big),\end{aligned} \tag{A.7}$$

with $m, l \geq 1$, $m + l \geq 3$. Therefore, at leading order, the communication is mediated solely by the commutator $[\hat{C}_{\mathrm{A}}(t), \hat{C}_{\mathrm{B}}(t')]$, as we wanted to show. Notice that $[\hat{C}_{\mathrm{A}}(t), \hat{C}_{\mathrm{B}}(t')]$ only contributes for $t' \geq t$, i.e. A can only message B through $\hat{C}_{\mathrm{B}}(t')$ after A has coupled to $\hat{C}_{\mathrm{A}}(t)$, as would be expected. This order adequately reverses if we consider communication from B to A.

Non-perturbative case: Remarkably, communication is impossible if the observables of system C in Eq. (A.2) commute, i.e. if $[\hat{C}_{\rm A}(t), \hat{C}_{\rm B}(t')] = 0$, then $\hat{\rho}_{\rm B}^{\rm signal} = 0$. This follows from noticing that, under this assumption, $[\hat{H}_{\rm A}(t), \hat{H}_{\rm B}(t')] = 0$, and thus $\hat{U} = \hat{U}_{\rm A}\hat{U}_{\rm B} = \hat{U}_{\rm B}\hat{U}_{\rm A}$, which after substituting in Eq. (A.1) and using the cyclic property of the trace together with $\hat{U}_{\rm A}\hat{U}_{\rm A}^\dagger = \hat{\mathbb{1}}$ shows that $\hat{\rho}_{\rm B}^{\rm signal} = 0$. In other words, communicating through C requires coupling to non-commuting interaction picture observables of C. Notice that the same is not necessarily true for gaining correlations. A and B can get correlated even if they couple to commuting interaction picture observables of C, by extracting preexisting correlations in C.

A.2 Inequality between negativity and its communication and harvesting contributions

Here, we would like to show that the assumption

$$|\mathcal{M}| = \sqrt{|\mathcal{M}^+|^2 + |\mathcal{M}^-|^2} \tag{A.8}$$

implies the following relation between the negativity and its contributions:

$$\mathcal{N} \geq \sqrt{(\mathcal{N}^+)^2 + (\mathcal{N}^-)^2}. \tag{A.9}$$

Let us prove this statement by considering different cases.

- **Case 1:** $\mathcal{N}^+ = 0$.

  The relation (A.9) becomes equivalent to $\mathcal{N} \geq \mathcal{N}^-$, which is directly verified using $|\mathcal{M}| \geq |\mathcal{M}^-|$ in the definition of negativity and its associated components, namely Eqs. (2.60) and (2.64).

- **Case 2:** $\mathcal{N}^- = 0$.

  The argument is analogous to case 1.

- **Case 3**: $\mathcal{N}^+ \neq 0$ and $\mathcal{N}^- \neq 0$.

  Here, we have $\mathcal{N}^\pm = \mathcal{V}^\pm > 0$. Let us define

$$\mathcal{L}_\pm = \frac{|\mathcal{L}_{\rm AA} \pm \mathcal{L}_{\rm BB}|}{2}. \tag{A.10}$$

In this way, we can write

$$\begin{aligned}\mathcal{V} &= \sqrt{|\mathcal{M}|^2 + \mathcal{L}_-^2} - \mathcal{L}_+, \\ \mathcal{V}^\pm &= \sqrt{|\mathcal{M}^\pm|^2 + \mathcal{L}_-^2} - \mathcal{L}_+.\end{aligned} \tag{A.11}$$

Then, using Eq. (A.8), we can cast the statement of Eq. (A.9) into

$$\begin{aligned}0 &\leq \mathcal{V}^2 - (\mathcal{V}^+)^2 - (\mathcal{V}^-)^2 \\ &= -\mathcal{L}_-^2 + 3\mathcal{L}_+^2 + 2\mathcal{L}_+\left(\mathcal{V}^+ + \mathcal{V}^- - \sqrt{|\mathcal{M}|^2 + \mathcal{L}_-^2}\right),\end{aligned} \tag{A.12}$$

Next, we get rid of the square root by moving it to the other side of the inequality and then taking the square on both sides. Further manipulation allows us to rewrite the inequality as

$$8\mathcal{L}_+^2\mathcal{V}^+\mathcal{V}^- + 4\mathcal{L}_+(\mathcal{L}_+^2 - \mathcal{L}_-^2)(\mathcal{V}^+ + \mathcal{V}^-) + (\mathcal{L}_+^2 - \mathcal{L}_-^2)^2 \geq 0. \tag{A.13}$$

Finally, this statement is true because because of $\mathcal{L}_+ \geq 0$, $\mathcal{L}_+^2 \geq \mathcal{L}_-^2$ and the assumption $\mathcal{V}^\pm > 0$. Therefore, we conclude that given the relation (A.8), the statement (A.9) is true.

A.3 Examples of symmetries that satisfy Corollary 1

Here, we focus on examples of maps $\boldsymbol{T}$ constructed to satisfy the hypotheses of Corollary 1. In particular, we provide sufficient conditions for the harvesting setups so that all the Corollary hypotheses are fulfilled. Moreover, these examples are later used to prove Propositions 3 and 4 of the main text.

Symmetry 1. *Time reversal around the value t_{R} of a time coordinate in an arbitrary coordinate system $(t, \boldsymbol{x})$:*

$$\begin{aligned}\boldsymbol{T}(\mathsf{x}, \mathsf{x}') &= (T_{\mathrm{R}}(\mathsf{x}), T_{\mathrm{R}}(\mathsf{x}')), \\ T_{\mathrm{R}}(t_{\mathrm{R}} + t, \boldsymbol{x}) &= (t_{\mathrm{R}} - t, \boldsymbol{x}).\end{aligned} \tag{A.14}$$

The hypotheses of Corollary 1 are satisfied if the following assumptions hold:

1. $g(t_{\mathrm{R}} + t, \boldsymbol{x}) = g(t_{\mathrm{R}} - t, \boldsymbol{x})$,
2. $G_F(t_{\mathrm{R}} + t, \boldsymbol{x}, t_{\mathrm{R}} + t', \boldsymbol{x}') = G_F(t_{\mathrm{R}} - t, \boldsymbol{x}, t_{\mathrm{R}} - t', \boldsymbol{x}')$,

3. $\Lambda_\nu(t_{\mathrm{R}}+t,\boldsymbol{x})=\Lambda_\nu(t_{\mathrm{R}}-t,\boldsymbol{x})$,

4. *For some constant* θ_ν,

$$\langle\zeta_\nu|\hat{\mu}_\nu\big(\tau_\nu(t_{\mathrm{R}}+t,\boldsymbol{x})\big)|\psi_\nu\rangle=e^{\mathrm{i}\theta_\nu}\,\langle\psi_\nu|\hat{\mu}_\nu\big(\tau_\nu(t_{\mathrm{R}}-t,\boldsymbol{x})\big)|\zeta_\nu\rangle\,.$$

Here, we recall that g *is the determinant of the metric,* G_{F} *is the Feynman propagator,* $\{\Lambda_\nu\}$ *are the spacetime smearing functions, and* $|\zeta_\nu\rangle$ *are the states orthogonal to the initial states* $|\psi_\nu\rangle$ *as defined in Eq. (2.51).*

Symmetry 2. *Time reversal around* t_{R} *in the arbitrary coordinates* $(t,\boldsymbol{x})$ *& swap of spacetime points:*

$$\begin{aligned}&\boldsymbol{T}(\mathsf{x},\mathsf{x}')=(T_{\mathrm{R}}(\mathsf{x}'),T_{\mathrm{R}}(\mathsf{x})),\\&T_{\mathrm{R}}(t_{\mathrm{R}}+t,\boldsymbol{x})=(t_{\mathrm{R}}-t,\boldsymbol{x}).\end{aligned}\tag{A.15}$$

The hypotheses of Corollary 1 are satisfied if the following assumptions hold:

1. $g(t_{\mathrm{R}}+t,\boldsymbol{x})=g(t_{\mathrm{R}}-t,\boldsymbol{x})$,

2. $G_F(t_{\mathrm{R}}+t',\boldsymbol{x}',t_{\mathrm{R}}+t,\boldsymbol{x})=G_F(t_{\mathrm{R}}-t,\boldsymbol{x},t_{\mathrm{R}}-t',\boldsymbol{x}')$,

3. $\Lambda_{\mathrm{A}}(t_{\mathrm{R}}+t,\boldsymbol{x})=\Lambda_{\mathrm{B}}(t_{\mathrm{R}}-t,\boldsymbol{x})$,

4. *For some constant* θ,

$$\langle\zeta_{\mathrm{A}}|\hat{\mu}_{\mathrm{A}}\big(\tau_{\mathrm{A}}(t_{\mathrm{R}}+t,\boldsymbol{x})\big)|\psi_{\mathrm{A}}\rangle=e^{\mathrm{i}\theta}\,\langle\psi_{\mathrm{B}}|\hat{\mu}_{\mathrm{B}}\big(\tau_{\mathrm{B}}(t_{\mathrm{R}}-t,\boldsymbol{x})\big)|\zeta_{\mathrm{B}}\rangle\,.$$

Symmetry 3. *Time reversal around* t_{R} *in the arbitrary coordinates* $(t,\boldsymbol{x})$*, reflection about* $\boldsymbol{x}_0$ *in* $(t,\boldsymbol{x})$ *& swap of spacetime points:*

$$\begin{aligned}&\boldsymbol{T}(\mathsf{x},\mathsf{x}')=(T_{\mathrm{RR}}(\mathsf{x}'),T_{\mathrm{RR}}(\mathsf{x})),\\&T_{\mathrm{RR}}(t_{\mathrm{R}}+t,\boldsymbol{x}_0+\boldsymbol{x})=(t_{\mathrm{R}}-t,\boldsymbol{x}_0-\boldsymbol{x}).\end{aligned}\tag{A.16}$$

The hypotheses of Corollary 1 are satisfied if the following assumptions hold:

1. $g(t_{\mathrm{R}}+t,\boldsymbol{x}_0+\boldsymbol{x})=g(t_{\mathrm{R}}-t,\boldsymbol{x}_0-\boldsymbol{x})$,

2. $G_F(t_{\mathrm{R}}+t',\boldsymbol{x}_0+\boldsymbol{x}',t_{\mathrm{R}}+t,\boldsymbol{x}_0+\boldsymbol{x})$
$=G_F(t_{\mathrm{R}}-t,\boldsymbol{x}_0-\boldsymbol{x},t_{\mathrm{R}}-t',\boldsymbol{x}_0-\boldsymbol{x}')$,

3. $\Lambda_{\mathrm{A}}(t_{\mathrm{R}}+t,\boldsymbol{x}_0+\boldsymbol{x})=\Lambda_{\mathrm{B}}(t_{\mathrm{R}}-t,\boldsymbol{x}_0-\boldsymbol{x})$,

4. *For some constant* θ,

$$\begin{aligned}&\langle\zeta_{\mathrm{A}}|\hat{\mu}_{\mathrm{A}}\big(\tau_{\mathrm{A}}(t_{\mathrm{R}}+t,\boldsymbol{x}_0+\boldsymbol{x})\big)|\psi_{\mathrm{A}}\rangle\\&=e^{\mathrm{i}\theta}\,\langle\psi_{\mathrm{B}}|\hat{\mu}_{\mathrm{B}}\big(\tau_{\mathrm{B}}(t_{\mathrm{R}}-t,\boldsymbol{x}_0-\boldsymbol{x})\big)|\zeta_{\mathrm{B}}\rangle\,.\end{aligned}$$

Notice that in this symmetry the distance between the detectors at time t_{R} can be adjusted by changing $\boldsymbol{x}_0$, in contrast to Symmetry 2, where the detectors must be at the same place at time t_{R}.

Symmetry 4. *Proper time swap and reversal around* $\upsilon_{\mathrm{R}}/2$. *To better describe this symmetry, we use the coordinates* $(\tau_\nu,\widetilde{\boldsymbol{x}}_\nu)$ *where* $\Lambda_\nu(\tau_\nu,\widetilde{\boldsymbol{x}}_\nu)=\chi_\nu(\tau_\nu)F_\nu(\widetilde{\boldsymbol{x}}_\nu)$ *and where* τ_ν *are the proper times of the detectors.*[1]

Now we can express this symmetry as

$$\boldsymbol{T}(\tau_{\mathrm{A}},\widetilde{\boldsymbol{x}}_{\mathrm{A}},\tau_{\mathrm{B}},\widetilde{\boldsymbol{x}}_{\mathrm{B}})=(\upsilon_{\mathrm{R}}-\tau_{\mathrm{B}},\widetilde{\boldsymbol{x}}_{\mathrm{A}},\upsilon_{\mathrm{R}}-\tau_{\mathrm{A}},\widetilde{\boldsymbol{x}}_{\mathrm{B}}),\tag{A.17}$$

where pairs of spacetime points are expressed in the joint coordinates $(\tau_{\mathrm{A}},\widetilde{\boldsymbol{x}}_{\mathrm{A}},\tau_{\mathrm{B}},\widetilde{\boldsymbol{x}}_{\mathrm{B}})$. *The hypotheses of Corollary 1 are satisfied if the following assumptions hold:*

1. $g_{\mathrm{A}}(\tau_{\mathrm{A}},\widetilde{\boldsymbol{x}}_{\mathrm{A}})g_{\mathrm{B}}(\tau_{\mathrm{B}},\widetilde{\boldsymbol{x}}_{\mathrm{B}})=g_{\mathrm{A}}(\upsilon_{\mathrm{R}}-\tau_{\mathrm{B}},\widetilde{\boldsymbol{x}}_{\mathrm{A}})g_{\mathrm{B}}(\upsilon_{\mathrm{R}}-\tau_{\mathrm{A}},\widetilde{\boldsymbol{x}}_{\mathrm{B}})$.

2. $G_F(\tau_{\mathrm{A}},\widetilde{\boldsymbol{x}}_{\mathrm{A}},\tau_{\mathrm{B}},\widetilde{\boldsymbol{x}}_{\mathrm{B}})=G_F(\upsilon_{\mathrm{R}}-\tau_{\mathrm{B}},\widetilde{\boldsymbol{x}}_{\mathrm{A}},\upsilon_{\mathrm{R}}-\tau_{\mathrm{A}},\widetilde{\boldsymbol{x}}_{\mathrm{B}})$,

3. $\chi_{\mathrm{A}}(\tau)=\chi_{\mathrm{B}}(\upsilon_{\mathrm{R}}-\tau)$,

4. $\Omega_{\mathrm{A}}=\Omega_{\mathrm{B}}=\Omega$,

5. $\beta_{\mathrm{A}}+\beta_{\mathrm{B}}=\Omega\upsilon_{\mathrm{R}}$,

6. $|\cos\alpha_{\mathrm{A}}|=|\cos\alpha_{\mathrm{B}}|$, $|\sin\alpha_{\mathrm{A}}|=|\sin\alpha_{\mathrm{B}}|$.

Here, the g_ν *are the determinant of the metric in* $(\tau_\nu,\widetilde{\boldsymbol{x}}_\nu)$ *coordinates, and the detectors' initial states are*

$$|\psi_\nu\rangle=\cos\alpha_\nu\,|g_\nu\rangle+\sin\alpha_\nu e^{\mathrm{i}\beta_\nu}\,|e_\nu\rangle\,.\tag{A.18}$$

[1] In the usual prescription for detectors, $(\tau_\nu,\widetilde{\boldsymbol{x}}_\nu)$ will be chosen to be the Fermi normal coordinates associated to the detectors' trajectories. However, the result given here holds regardless of whether $(\tau_\nu,\widetilde{\boldsymbol{x}}_\nu)$ are chosen to be the Fermi normal coordinates.

Notice that assumptions 4, 5, and 6 appear because they are sufficient to show that

$$\langle\zeta_{\mathrm{A}}|\hat{\mu}_{\mathrm{A}}(\tau)|\psi_{\mathrm{A}}\rangle = e^{\mathrm{i}\Omega\upsilon_{\mathrm{R}}}\,\langle\zeta_{\mathrm{B}}|\hat{\mu}_{\mathrm{B}}(\upsilon_{\mathrm{R}}-\tau)|\psi_{\mathrm{B}}\rangle\,, \tag{A.19}$$

with $|\zeta_\nu\rangle$ the states orthogonal to $|\psi_\nu\rangle$ as defined in Eq. (2.51).

In order for this $\boldsymbol{T}$ to satisfy Corollary 1, first notice that $|J(\tau_{\mathrm{A}},\widetilde{\boldsymbol{x}}_{\mathrm{A}},\tau_{\mathrm{B}},\widetilde{\boldsymbol{x}}_{\mathrm{B}})| = 1$. Then, the symmetry assumptions 1 and 2 directly translate to the conditions required by Eq. (2.92). It only remains to show that Eq. (2.93) is fulfilled. This condition asks that for some constant angle θ,

$$P^*_{\mathrm{A}}\big(T_1(\mathsf{x},\mathsf{x}')\big)P^*_{\mathrm{B}}\big(T_2(\mathsf{x},\mathsf{x}')\big) = e^{\mathrm{i}\theta}P_{\mathrm{A}}(\mathsf{x})P_{\mathrm{B}}(\mathsf{x}'). \tag{A.20}$$

Substituting the definition of P_ν,

$$P_\nu(\mathsf{x}) = \Lambda_\nu(\mathsf{x})\,\langle\zeta_\nu|\hat{\mu}_\nu(\tau_\nu(\mathsf{x}))|\psi_\nu\rangle\,, \tag{A.21}$$

and using $\Lambda_\nu(\tau_\nu,\widetilde{\boldsymbol{x}}_\nu) = \chi_\nu(\tau_\nu)F_\nu(\widetilde{\boldsymbol{x}}_\nu)$, one sees that to satisfy Eq. (A.20) the following conditions are enough:

$$\chi_{\mathrm{A}}(\tau) = \chi_{\mathrm{B}}(\upsilon_{\mathrm{R}}-\tau), \tag{A.22}$$

$$\langle\zeta_{\mathrm{A}}|\hat{\mu}_{\mathrm{A}}(\tau)|\psi_{\mathrm{A}}\rangle = e^{\mathrm{i}\theta/2}\,\langle\psi_{\mathrm{B}}|\hat{\mu}_{\mathrm{B}}(\upsilon_{\mathrm{R}}-\tau)|\zeta_{\mathrm{B}}\rangle\,. \tag{A.23}$$

The condition over the monopole operators $\hat{\mu}_\nu$ simplifies by using the identity

$$\langle\zeta_\nu|\hat{\mu}_\nu(\tau_\nu)|\psi_\nu\rangle = e^{\mathrm{i}\beta_\nu}\big(c_\nu e^{\mathrm{i}(\Omega_\nu\tau_\nu-\beta_\nu)} - s_\nu e^{-\mathrm{i}(\Omega_\nu\tau_\nu-\beta_\nu)}\big), \tag{A.24}$$

where we denote $s_\nu = \sin^2\alpha_\nu$, $c_\nu = \cos^2\alpha_\nu$. Together with the hypotheses $\Omega_{\mathrm{A}} = \Omega_{\mathrm{B}} = \Omega$, $\beta_{\mathrm{A}} = -\beta_{\mathrm{B}} + \Omega\upsilon_{\mathrm{R}}$, $c_{\mathrm{A}} = c_{\mathrm{B}}$, $s_{\mathrm{A}} = s_{\mathrm{B}}$,

$$\begin{aligned}
&\langle\zeta_{\mathrm{A}}|\hat{\mu}_{\mathrm{A}}(\tau)|\psi_{\mathrm{A}}\rangle\\
&= e^{\mathrm{i}\beta_{\mathrm{A}}}\big(c_{\mathrm{A}}e^{\mathrm{i}(\Omega\tau-\beta_{\mathrm{A}})} - s_{\mathrm{A}}e^{-\mathrm{i}(\Omega\tau-\beta_{\mathrm{A}})}\big)\\
&= e^{\mathrm{i}\beta_{\mathrm{A}}}\big(c_{\mathrm{B}}e^{-\mathrm{i}(\Omega(\upsilon_{\mathrm{R}}-\tau)-\beta_{\mathrm{B}})} - s_{\mathrm{B}}e^{\mathrm{i}(\Omega(\upsilon_{\mathrm{R}}-\tau)-\beta_{\mathrm{B}})}\big)\\
&= e^{\mathrm{i}\Omega\upsilon_{\mathrm{R}}}\,\langle\psi_{\mathrm{B}}|\hat{\mu}_{\mathrm{B}}(\upsilon_{\mathrm{R}}-\tau)|\zeta_{\mathrm{B}}\rangle\,.
\end{aligned} \tag{A.25}$$

Therefore, Eq. (A.23) is fulfilled with $\theta = 2\Omega\upsilon_{\mathrm{R}}$. This completes proving that the assumptions in the statement of Symmetry 4 are enough to fulfill Corollary 1.

Summary: Corollary 1 holds for harvesting setups that meet the conditions described in any of the symmetries presented in this section. We recall that for such symmetric setups, $\cos\Delta\gamma = 0$, i.e.

$$|\mathcal{M}| = \sqrt{|\mathcal{M}^+|^2 + |\mathcal{M}^-|^2}, \tag{A.26}$$

which precludes any destructive interference between $\mathcal{M}^+$ and $\mathcal{M}^-$.

As a final remark, a common extension of the UDW detector model includes complex spacetime smearings, i.e. $\Lambda_\nu^* \neq \Lambda_\nu$. All the results presented in this section can be generalized to account for complex spacetime smearings, but we have restricted our results to real smearings for simplicity. For complex smearings, the Hamiltonian interaction density for each detector in the interaction picture becomes $\hat{h}_{\mathrm{I},\nu}(\mathsf{x}) = \lambda\Lambda_\nu(\mathsf{x})e^{\mathrm{i}\Omega_\nu\tau_\nu}\hat{\sigma}_\nu^+ + \mathrm{H.c.}$, with H.c. denoting the Hermitian conjugate. Therefore, the expression for $\mathcal{M}$ also changes (see, e.g., [114]). Nonetheless, the requirements specified for each symmetry only need a modification of the conditions of Λ_ν (or χ_ν). Specifically, whenever an equality between smearing or switching functions appears, one of the sides has to be conjugated, and the equality only needs to be fulfilled up to a constant complex phase.

A.4 Further simplifications of the hypotheses of Corollary 1

In this appendix, we introduce several lemmas that simplify the conditions 3 and 4 of Symmetries 1, 2 and 3 respectively.

Lemma 1. *Consider the two sets of coordinates $(\tau_\nu, \widetilde{\boldsymbol{x}}_\nu)$ with $\nu \in \{A, B\}$, where $\Lambda_\nu(\tau_\nu, \widetilde{\boldsymbol{x}}_\nu) = \chi_\nu(\tau_\nu)F_\nu(\widetilde{\boldsymbol{x}}_\nu)$. Given coordinates $(t, \boldsymbol{x})$, the time reversal around t_{R} is $T_{\mathrm{R}}(t_{\mathrm{R}} + t, \boldsymbol{x}) = (t_{\mathrm{R}} - t, \boldsymbol{x})$. Assume that*

1. *Given $\tau_{\mathrm{R},\nu} = \tau_\nu(t_{\mathrm{R}}, \boldsymbol{0})$,*

$$\begin{aligned} \tau_\nu(\mathsf{x}) &= 2\tau_{\mathrm{R},\nu} - \tau_\nu\big(T_{\mathrm{R}}(\mathsf{x})\big), \\ \widetilde{\boldsymbol{x}}_\nu(\mathsf{x}) &= \widetilde{\boldsymbol{x}}_\nu\big(T_{\mathrm{R}}(\mathsf{x})\big). \end{aligned} \tag{A.27}$$

2. $\chi_\nu(\tau) = \chi_\nu(2\tau_{\mathrm{R},\nu} - \tau)$.

3. $\beta_\nu = \Omega_\nu\tau_{\mathrm{R},\nu}$.

Recall that β_ν is the relative phase in the detectors' initial states $|\psi_\nu\rangle = \cos\alpha_\nu\,|g_\nu\rangle + \sin\alpha_\nu e^{\mathrm{i}\beta_\nu}\,|e_\nu\rangle$.

Under these assumptions, the conditions 3 and 4 of Symmetry 1 are fulfilled.

Proof. We prove the condition 3 first, to do so, keep in mind that

$$\Lambda_\nu(t,\boldsymbol{x}) = \chi_\nu\big(\tau_\nu(t,\boldsymbol{x})\big)F_\nu\big(\widetilde{\boldsymbol{x}}_\nu(t,\boldsymbol{x})\big). \tag{A.28}$$

Then, using the time reversibility condition over χ_ν,

$$\begin{aligned}\chi_\nu\big(\tau_\nu(t_{\mathrm{R}}-t,\boldsymbol{x})\big) &= \chi_\nu\big(2\tau_{\mathrm{R},\nu}-\tau_\nu(t_{\mathrm{R}}-t,\boldsymbol{x})\big)\\ &= \chi_\nu\big(\tau_\nu(t_{\mathrm{R}}+t,\boldsymbol{x})\big).\end{aligned} \tag{A.29}$$

Substituting back into the first equation shows condition 3 of Symmetry 1,

$$\begin{aligned}\Lambda_\nu(t_{\mathrm{R}}-t,\boldsymbol{x}) &= \chi_\nu\big(\tau_\nu(t_{\mathrm{R}}-t,\boldsymbol{x})\big)F_\nu\big(\widetilde{\boldsymbol{x}}_\nu(t_{\mathrm{R}}-t,\boldsymbol{x})\big)\\ &= \chi_\nu\big(\tau_\nu(t_{\mathrm{R}}+t,\boldsymbol{x})\big)F_\nu\big(\widetilde{\boldsymbol{x}}_\nu(t_{\mathrm{R}}+t,\boldsymbol{x})\big)\\ &= \Lambda_\nu(t_{\mathrm{R}}+t,\boldsymbol{x}).\end{aligned} \tag{A.30}$$

To prove the condition 4 of Symmetry 1, let us use the identity

$$\langle\zeta_\nu|\hat{\mu}_\nu(\tau_\nu)|\psi_\nu\rangle = e^{\mathrm{i}\beta_\nu}\big(c_\nu e^{\mathrm{i}(\Omega_\nu\tau_\nu-\beta_\nu)} - s_\nu e^{-\mathrm{i}(\Omega_\nu\tau_\nu-\beta_\nu)}\big), \tag{A.31}$$

where $s_\nu = \sin^2\alpha_\nu$, $c_\nu = \cos^2\alpha_\nu$ and we recall that $|\zeta_\nu\rangle$ are the states orthogonal to the initial state $|\psi_\nu\rangle$ as defined in Eq. (2.51). Substituting into the following expression,

$$\begin{aligned}&\langle\zeta_\nu|\hat{\mu}_\nu\big(\tau_\nu(t_{\mathrm{R}}-t,\boldsymbol{x})\big)|\psi_\nu\rangle\\ &= e^{\mathrm{i}\Omega_\nu\tau_{\mathrm{R},\nu}}\Big(c_\nu e^{\mathrm{i}\left(\Omega_\nu\tau_\nu(t_{\mathrm{R}}-t,\boldsymbol{x})-\Omega_\nu\tau_{\mathrm{R},\nu}\right)}\\ &\qquad\qquad - s_\nu e^{-\mathrm{i}\left(\Omega_\nu\tau_\nu(t_{\mathrm{R}}-t,\boldsymbol{x})-\Omega_\nu\tau_{\mathrm{R},\nu}\right)}\Big)\\ &= e^{\mathrm{i}\Omega_\nu\tau_{\mathrm{R},\nu}}\Big(c_\nu e^{-\mathrm{i}\left(\Omega_\nu\tau_\nu(t_{\mathrm{R}}+t,\boldsymbol{x})-\Omega_\nu\tau_{\mathrm{R},\nu}\right)}\\ &\qquad\qquad - s_\nu e^{\mathrm{i}\left(\Omega_\nu\tau_\nu(t_{\mathrm{R}}+t,\boldsymbol{x})-\Omega_\nu\tau_{\mathrm{R},\nu}\right)}\Big)\\ &= e^{2\mathrm{i}\Omega_\nu\tau_{\mathrm{R},\nu}}\,\langle\psi_\nu|\hat{\mu}_\nu\big(\tau_\nu(t_{\mathrm{R}}+t,\boldsymbol{x})\big)|\zeta_\nu\rangle\,,\end{aligned} \tag{A.32}$$

where the condition over τ_ν given by Eq. (A.27), and that $\beta_\nu = \Omega_\nu\tau_{\mathrm{R},\nu}$, finishing the proof. □

Lemma 2. *Consider the two sets of coordinates $(\tau_\nu,\widetilde{\boldsymbol{x}}_\nu)$ with $\nu\in\{A,B\}$, where $\Lambda_\nu(\tau_\nu,\widetilde{\boldsymbol{x}}_\nu) = \chi_\nu(\tau_\nu)F_\nu(\widetilde{\boldsymbol{x}}_\nu)$. Given coordinates $(t,\boldsymbol{x})$, the time reversal around t_{R} is $T_{\mathrm{R}}(t_{\mathrm{R}}+t,\boldsymbol{x}) = (t_{\mathrm{R}}-t,\boldsymbol{x})$. Assume that*

1. *Given* $\upsilon_{\mathrm{R}} = \tau_{\mathrm{A}}(t_{\mathrm{R}}, \mathbf{0}) + \tau_{\mathrm{B}}(t_{\mathrm{R}}, \mathbf{0})$,

$$\begin{aligned} \tau_{\mathrm{A}}(\mathsf{x}) &= \upsilon_{\mathrm{R}} - \tau_{\mathrm{B}}\big(T_{\mathrm{R}}(\mathsf{x})\big), \\ \widetilde{\boldsymbol{x}}_{\mathrm{A}}(\mathsf{x}) &= \widetilde{\boldsymbol{x}}_{\mathrm{B}}\big(T_{\mathrm{R}}(\mathsf{x})\big). \end{aligned} \tag{A.33}$$

2. $F_{\mathrm{A}}(\widetilde{\boldsymbol{x}}) = F_{\mathrm{B}}(\widetilde{\boldsymbol{x}})$.

3. $\chi_{\mathrm{A}}(\tau) = \chi_{\mathrm{B}}(\upsilon_{\mathrm{R}} - \tau)$.

4. $\Omega_{\mathrm{A}} = \Omega_{\mathrm{B}} = \Omega$.

5. $\beta_{\mathrm{A}} + \beta_{\mathrm{B}} = \Omega\upsilon_{\mathrm{R}}$.

6. $|\cos\alpha_{\mathrm{A}}| = |\cos\alpha_{\mathrm{B}}|$, $|\sin\alpha_{\mathrm{A}}| = |\sin\alpha_{\mathrm{B}}|$,

where we recall that the detectors' initial states are $|\psi_\nu\rangle = \cos\alpha_\nu\,|g_\nu\rangle + \sin\alpha_\nu e^{\mathrm{i}\beta_\nu}\,|e_\nu\rangle$.

Under these assumptions, conditions 3 and 4 of Symmetry 2 are fulfilled.

Proof. We prove condition 3 first, to do so, keep in mind that

$$\Lambda_\nu(t, \boldsymbol{x}) = \chi_\nu\big(\tau_\nu(t, \boldsymbol{x})\big) F_\nu\big(\widetilde{\boldsymbol{x}}_\nu(t, \boldsymbol{x})\big). \tag{A.34}$$

Then, using the time reversibility condition over the χ_ν,

$$\begin{aligned} \chi_{\mathrm{A}}\big(\tau_{\mathrm{A}}(t_{\mathrm{R}} - t, \boldsymbol{x})\big) &= \chi_{\mathrm{B}}\big(\upsilon_{\mathrm{R}} - \tau_{\mathrm{A}}(t_{\mathrm{R}} - t, \boldsymbol{x})\big) \\ &= \chi_{\mathrm{B}}\big(\tau_{\mathrm{B}}(t_{\mathrm{R}} + t, \boldsymbol{x})\big), \end{aligned} \tag{A.35}$$

and similarly,

$$F_{\mathrm{A}}\big(\widetilde{\boldsymbol{x}}_{\mathrm{A}}(t_{\mathrm{R}} - t, \boldsymbol{x})\big) = F_{\mathrm{B}}\big(\widetilde{\boldsymbol{x}}_{\mathrm{B}}(t_{\mathrm{R}} + t, \boldsymbol{x})\big). \tag{A.36}$$

Substituting these back into the first equation completes the first half of the proof,

$$\begin{aligned} \Lambda_{\mathrm{A}}(t_{\mathrm{R}} - t, \boldsymbol{x}) &= \chi_{\mathrm{A}}\big(\tau_{\mathrm{A}}(t_{\mathrm{R}} - t, \boldsymbol{x})\big) F_{\mathrm{A}}\big(\widetilde{\boldsymbol{x}}_{\mathrm{A}}(t_{\mathrm{R}} - t, \boldsymbol{x})\big) \\ &= \chi_{\mathrm{B}}\big(\tau_{\mathrm{B}}(t_{\mathrm{R}} + t, \boldsymbol{x})\big) F_{\mathrm{B}}\big(\widetilde{\boldsymbol{x}}_\nu(t_{\mathrm{R}} + t, \boldsymbol{x})\big) \\ &= \Lambda_{\mathrm{B}}(t_{\mathrm{R}} + t, \boldsymbol{x}). \end{aligned} \tag{A.37}$$

To prove the condition 4 of Symmetry 2, let us use the identity

$$\langle\zeta_\nu|\hat{\mu}_\nu(\tau_\nu)|\psi_\nu\rangle = e^{\mathrm{i}\beta_\nu}\big(c_\nu e^{\mathrm{i}(\Omega_\nu\tau_\nu - \beta_\nu)} - s_\nu e^{-\mathrm{i}(\Omega_\nu\tau_\nu - \beta_\nu)}\big), \tag{A.38}$$

where $s_\nu = \sin^2\alpha_\nu$, $c_\nu = \cos^2\alpha_\nu$ and we recall that $|\zeta_\nu\rangle$ are the states orthogonal to the initial state $|\psi_\nu\rangle$ as defined in Eq. (2.51). The proof finishes by combining this identity with the hypotheses $c_{\mathrm{A}} = c_{\mathrm{B}}$, $s_{\mathrm{A}} = s_{\mathrm{B}}$, $\Omega_{\mathrm{A}} = \Omega_{\mathrm{B}} = \Omega$, $\beta_{\mathrm{A}} = -\beta_{\mathrm{B}} + \Omega\upsilon_{\mathrm{R}}$, and with the assumption over the τ_ν,

$$\begin{aligned}
&\langle\zeta_{\mathrm{A}}|\hat{\mu}_{\mathrm{A}}\big(\tau_{\mathrm{A}}(t_{\mathrm{R}}-t,\boldsymbol{x})\big)|\psi_{\mathrm{A}}\rangle \\
&= e^{\mathrm{i}\beta_{\mathrm{A}}}\big(c_{\mathrm{A}}e^{\mathrm{i}(\Omega\tau_{\mathrm{A}}(t_{\mathrm{R}}-t,\boldsymbol{x})-\beta_{\mathrm{A}})} - s_{\mathrm{A}}e^{-\mathrm{i}(\Omega\tau_{\mathrm{A}}(t_{\mathrm{R}}-t,\boldsymbol{x})-\beta_{\mathrm{A}})}\big) \\
&= e^{\mathrm{i}\beta_{\mathrm{A}}}\big(c_{\mathrm{B}}e^{-\mathrm{i}(\Omega\tau_{\mathrm{B}}(t_{\mathrm{R}}+t,\boldsymbol{x})-\beta_{\mathrm{B}})} - s_{\mathrm{B}}e^{\mathrm{i}(\Omega\tau_{\mathrm{B}}(t_{\mathrm{R}}+t,\boldsymbol{x})-\beta_{\mathrm{B}})}\big) \\
&= e^{\mathrm{i}\Omega\upsilon_{\mathrm{R}}}\,\langle\psi_{\mathrm{B}}|\hat{\mu}_{\mathrm{B}}\big(\tau_{\mathrm{B}}(t_{\mathrm{R}}+t,\boldsymbol{x})\big)|\zeta_{\mathrm{B}}\rangle\,. \qquad \text{(A.39)}
\end{aligned}$$

□

Lemma 3. *Consider the two sets of coordinates $(\tau_\nu, \widetilde{\boldsymbol{x}}_\nu)$ with $\nu \in \{A, B\}$, where $\Lambda_\nu(\tau_\nu, \widetilde{\boldsymbol{x}}_\nu) = \chi_\nu(\tau_\nu)F_\nu(\widetilde{\boldsymbol{x}}_\nu)$. Given coordinates $(t, \boldsymbol{x})$, the time reversal around t_{R} and reflection around $\boldsymbol{x}_0$ is $T_{\mathrm{RR}}(t, \boldsymbol{x}) = (2t_{\mathrm{R}} - t, 2\boldsymbol{x}_0 - \boldsymbol{x})$. Assume that*

1. *Given $\upsilon_{\mathrm{R}} = \tau_{\mathrm{A}}(t_{\mathrm{R}}, \mathbf{0}) + \tau_{\mathrm{B}}(t_{\mathrm{R}}, \mathbf{0})$,*

$$\begin{aligned}
\tau_{\mathrm{A}}(\mathsf{x}) &= \upsilon_{\mathrm{R}} - \tau_{\mathrm{B}}\big(T_{\mathrm{RR}}(\mathsf{x})\big), \\
\widetilde{\boldsymbol{x}}_{\mathrm{A}}(\mathsf{x}) &= \widetilde{\boldsymbol{x}}_{\mathrm{B}}\big(T_{\mathrm{RR}}(\mathsf{x})\big). \qquad \text{(A.40)}
\end{aligned}$$

2. *$F_{\mathrm{A}}(\widetilde{\boldsymbol{x}}) = F_{\mathrm{B}}(\widetilde{\boldsymbol{x}})$.*
3. *$\chi_{\mathrm{A}}(\tau) = \chi_{\mathrm{B}}(\upsilon_{\mathrm{R}} - \tau)$.*
4. *$\Omega_{\mathrm{A}} = \Omega_{\mathrm{B}} = \Omega$.*
5. *$\beta_{\mathrm{A}} + \beta_{\mathrm{B}} = \Omega\upsilon_{\mathrm{R}}$.*
6. *$|\cos\alpha_{\mathrm{A}}| = |\cos\alpha_{\mathrm{B}}|$, $|\sin\alpha_{\mathrm{A}}| = |\sin\alpha_{\mathrm{B}}|$.*

where we recall that the detectors' initial states are $|\psi_\nu\rangle = \cos\alpha_\nu\,|g_\nu\rangle + \sin\alpha_\nu e^{\mathrm{i}\beta_\nu}\,|e_\nu\rangle$.

Under these assumptions, the conditions 3 and 4 of Symmetry 3 are fulfilled.

This lemma is proven analogously to the previous Lemma 2. Notice the following apparent incompatibility: the lemma asks the smearing functions F_ν to be equal, while the assumptions of Symmetry 3 ask spacetime smearings Λ_ν to be related by a spatial reflection and a time reversal. However, the equality between F_ν is actually expected because the spatial smearing functions F_ν are defined in their corresponding prescription coordinates $(\tau_\nu, \widetilde{\boldsymbol{x}}_\nu)$, which we assumed to be related by a time reflection and a space reflection, as in Eq. (A.40).

A.5 Simplifying the symmetries for the most common entanglement harvesting scenarios

Many of the scenarios analyzed in the literature of entanglement harvesting already restrict themselves to very symmetric particular setups. While this is done for different reasons (mainly simplifying the math) this yields important simplifications of the conditions required for each of the $\boldsymbol{T}$ maps described in Appendix A.3 to be symmetries that fulfill the assumptions of Corollary 1.

In particular, we will show how the usual assumptions in the literature for harvesting in flat spacetime and FRW yield Propositions 3 and 4 of the main text.

A.5.1 Sufficient symmetries for harvesting and communication collaboration in Minkowski spacetime

This Subappendix proves Proposition 3 of the main text. This proof consists of showing that the conditions for the symmetries provided in Appendix A.3 are fulfilled in Minkowski spacetime, for fields that are prepared in the vacuum and inertial, comoving, symmetrically switched detectors that are prepared both in the ground state or both in the excited state.

Lemma 4. *Assume that*

1. *The spacetime is flat.*
2. *The field starts in the Minkowski vacuum.*

This implies that f any inertial coordinate system $(t, \boldsymbol{x})$ *and any constants* t_{R} *and* $\boldsymbol{x}_0$*, the Feynmann propagator* G_F *fulfills*

$$\begin{aligned} G_F(t, \boldsymbol{x}, t', \boldsymbol{x}') &= G_F(2t_{\mathrm{R}} - t', 2\boldsymbol{x}_0 - \boldsymbol{x}', 2t_{\mathrm{R}} - t, 2\boldsymbol{x}_0 - \boldsymbol{x}) \\ &= G_F(2t_{\mathrm{R}} - t', \boldsymbol{x}', 2t_{\mathrm{R}} - t, \boldsymbol{x}) \\ &= G_F(2t_{\mathrm{R}} - t, \boldsymbol{x}, 2t_{\mathrm{R}} - t', \boldsymbol{x}'). \end{aligned} \tag{A.41}$$

And therefore, these relations fulfill the condition 2 for the Symmetries 1, 2, 3. Moreover, since $g(t, \boldsymbol{x}) = -1$*, the condition 1 of all these symmetries is also fulfilled.*

Proof. The Wightman of the Minkowski vacuum for a scalar field is

$$W(t,\boldsymbol{x},t',\boldsymbol{x}') = \frac{1}{(2\pi)^n}\int \frac{\mathrm{d}^n\boldsymbol{k}}{2\omega_{\boldsymbol{k}}} e^{\mathrm{i}\boldsymbol{k}\cdot(\boldsymbol{x}-\boldsymbol{x}')} e^{-\mathrm{i}\omega_{\boldsymbol{k}}(t-t')}, \tag{A.42}$$

with $\omega_{\boldsymbol{k}} = \sqrt{\boldsymbol{k}^2+m^2}$. The Minkowski vacuum Wightman function fulfills

$$W(t,\boldsymbol{x},t',\boldsymbol{x}') = W(\Delta t, |\Delta\boldsymbol{x}|), \tag{A.43}$$

where we denoted $W(\Delta t,|\Delta\boldsymbol{x}|) = W(\Delta t,|\Delta\boldsymbol{x}|,0,\boldsymbol{0})$ and $\Delta t = t-t'$, $\Delta\boldsymbol{x} = \boldsymbol{x}-\boldsymbol{x}'$. Then, from the definition of G_{F} in Eq. (2.58), we have

$$\begin{aligned} &G_{\mathrm{F}}(t,\boldsymbol{x},t',\boldsymbol{x}') \\ &= \Theta(\Delta t)W(\Delta t,|\Delta\boldsymbol{x}|) + \Theta(-\Delta t)W(-\Delta t,|\Delta\boldsymbol{x}|) \\ &= W(|\Delta t|,|\Delta\boldsymbol{x}|). \end{aligned} \tag{A.44}$$

Therefore, Eq. (A.41) is fulfilled because all of the equated expressions for G_{F} have the same values of $|\Delta t|$ and $|\Delta\boldsymbol{x}|$. □

Lemma 5. *Assume that, for a given constant t_{R},*

1. *The spacetime is flat.*
2. *The field starts in the Minkowski vacuum.*
3. *The detectors start both in their ground state or both in their excited state.*
4. *The detectors are inertial and comoving.*
5. *In the comoving frame $(t,\boldsymbol{x})$, the spacetime smearing factorizes $\Lambda_\nu(t,\boldsymbol{x}) = \chi_\nu(t)F_\nu(\boldsymbol{x})$.*
6. *$\chi_\nu(t) = \chi_\nu(2t_{\mathrm{R}}-t)$.*

Then, the conditions of Symmetry 1 are fulfilled.

Proof. First, conditions 1 and 2 of Symmetry 1 hold because of Lemma 4.

To prove the conditions 3 and 4 of Symmetry 1, we show next that the assumptions of Lemma 1 hold. First, choose both coordinate systems $(\tau_{\mathrm{A}},\widetilde{\boldsymbol{x}}_{\mathrm{A}})$ and $(\tau_{\mathrm{B}},\widetilde{\boldsymbol{x}}_{\mathrm{B}})$ to be $(t,\boldsymbol{x})$. Then, the assumption 1 of Lemma 1 holds. The assumption 2 holds because of $\chi_\nu(t) = \chi_\nu(2t_{\mathrm{R}}-t)$ and $t_{\mathrm{R}} = \tau_{\mathrm{R},\nu}$. Finally, the assumption 3 upon the relative phases β_ν is trivially satisfied because both initial states are either $|\psi_\nu\rangle = |g_\nu\rangle$ or $|\psi_\nu\rangle = |e_\nu\rangle$.

□

Lemma 6. *Assume that, for a given constant* t_{R}*,*

1. *The spacetime is flat.*
2. *The field starts in the Minkowski vacuum.*
3. *The detectors start both in their ground state or both in their excited state.*
4. *The detectors are inertial and comoving.*
5. *In the comoving frame* $(t, \boldsymbol{x})$*, the spacetime smearing factorizes* $\Lambda_\nu(t, \boldsymbol{x}) = \chi_\nu(t) F_\nu(\boldsymbol{x})$*.*
6. $\Omega_{\mathrm{A}} = \Omega_{\mathrm{B}}$*.*
7. $\chi_{\mathrm{A}}(t) = \chi_{\mathrm{B}}(2t_{\mathrm{R}} - t)$*.*
8. $F_{\mathrm{A}}(\boldsymbol{x}) = F_{\mathrm{B}}(\boldsymbol{x})$*.*

Then, the conditions of Symmetry 2 are fulfilled.

Proof. Shown analogously to Lemma 5, using Lemma 2 instead of Lemma 1. Additionally, $|\cos\alpha_{\mathrm{A}}| = |\cos\alpha_{\mathrm{B}}|$ and $|\sin\alpha_{\mathrm{A}}| = |\sin\alpha_{\mathrm{B}}|$ hold because of restricting the initial states of the detectors to be both ground or both excited. □

Lemma 7. *Assume that, for a given constant* t_{R}*,*

1. *The spacetime is flat.*
2. *The field starts in the Minkowski vacuum.*
3. *The detectors start both in their ground state or both in their excited state.*
4. *The detectors are inertial and comoving.*
5. *In the comoving frame* $(t, \boldsymbol{x})$*, the spacetime smearing factorizes* $\Lambda_\nu(t, \boldsymbol{x}) = \chi_\nu(t) F_\nu(\boldsymbol{x})$*.*
6. $\Omega_{\mathrm{A}} = \Omega_{\mathrm{B}}$*.*
7. $\chi_{\mathrm{A}}(t) = \chi_{\mathrm{B}}(2t_{\mathrm{R}} - t)$*.*
8. $F_{\mathrm{A}}(\boldsymbol{x}) = F_{\mathrm{B}}(2\boldsymbol{x}_0 - \boldsymbol{x})$*.*

Then, the conditions of Symmetry 3 are fulfilled.

Proof. Shown analogously to Lemma 5, using Lemma 3 instead of Lemma 1. The major difference is that while we still choose the coordinate system $(\tau_{\mathrm{A}}, \widetilde{\boldsymbol{x}}_{\mathrm{A}})$ to be $(t, \boldsymbol{x})$, here we choose $(\tau_{\mathrm{B}}, \widetilde{\boldsymbol{x}}_{\mathrm{B}})$ to be instead

$$\tau_{\mathrm{B}}(t, \boldsymbol{x}) = t, \;\; \widetilde{\boldsymbol{x}}_{\mathrm{B}}(t, \boldsymbol{x}) = 2\boldsymbol{x}_0 - \boldsymbol{x}. \tag{A.45}$$

□

Lemma 8. *Assume that, for a given constant* t_{R}*,*

1. *The spacetime is flat.*
2. *The field starts in the Minkowski vacuum.*
3. *The detectors start both in their ground state or both in their excited state.*
4. *The detectors are inertial and comoving.*
5. *In the comoving frame* $(t, \boldsymbol{x})$*, the spacetime smearing factorizes* $\Lambda_\nu(t, \boldsymbol{x}) = \chi_\nu(t) F_\nu(\boldsymbol{x})$*.*
6. $\Omega_{\mathrm{A}} = \Omega_{\mathrm{B}}$*.*
7. $\chi_{\mathrm{A}}(t) = \chi_{\mathrm{B}}(2t_{\mathrm{R}} - t)$*.*

Then, the conditions of Symmetry 4 are fulfilled, by picking both coordinate systems $(\tau_\nu, \widetilde{\boldsymbol{x}}_\nu)$ *to be* $(t, \boldsymbol{x})$*.*

Proof. Since we picked both $(\tau_\nu, \widetilde{\boldsymbol{x}}_\nu)$ to be the inertial comoving frame $(t, \boldsymbol{x})$, then the determinants of the metric in coordinates $(\tau_\nu, \widetilde{\boldsymbol{x}}_\nu)$ satisfy $g_{\mathrm{A}} = g_{\mathrm{B}} = -1$ under the given assumptions, hence fulfilling the condition 1 of Symmetry 4. The condition 2 over G_{F} becomes the following: for a given constant $t_{\mathrm{R}} = \upsilon_{\mathrm{R}}/2$,

$$G_{\mathrm{F}}(t, \boldsymbol{x}, t', \boldsymbol{x}') = G_{\mathrm{F}}(2t_{\mathrm{R}} - t, \boldsymbol{x}, 2t_{\mathrm{R}} - t', \boldsymbol{x}'), \tag{A.46}$$

which is true regardless of t_{R} for the Minkowski vacuum, as shown in Lemma 4.

The conditions 3 and 4 of Symmetry 4 are the assumptions 6 and 7 of the current lemma, using the relationship $t_{\mathrm{R}} = \upsilon_{\mathrm{R}}/2$.

Finally, condition 5 upon the relative phases β_ν is trivially satisfied because of the initial states of the detectors are either both the ground or both the excited state, and condition 6 ($|\cos\alpha_{\mathrm{A}}| = |\cos\alpha_{\mathrm{B}}|$, $|\sin\alpha_{\mathrm{A}}| = |\sin\alpha_{\mathrm{B}}|$) is fulfilled as well for the same reason. □

Finally, Proposition 3 of the main text follows from combining the assumptions of the Lemmas 5, 6, 7, 8. Specifically, fulfilling any of these lemmas is enough to have the corresponding symmetry and thus for Corollary 1 to hold. It is worth noticing that although we included one lemma per symmetry of Appendix A.3 for completion, Lemmas 6 and 7 become redundant after Lemma 8, because whenever Lemmas 6 or 7 hold, then Lemma 8 also holds. This explains why no condition upon $F_\nu(\boldsymbol{x})$ needs to be checked in Proposition 3. Thus the assumptions of Proposition 3 result from solely combining the assumptions of Lemmas 5 and 8. Moreover, we take $\Omega_{\mathrm{A}} = \Omega_{\mathrm{B}}$ to be a condition of Proposition 3 for simplicity, even though this condition is not needed to satisfy Lemma 5. In general, the conditions 5 and 6 of the Proposition 3 can be replaced by the following less restrictive combined condition: in the comoving frame, for some time t_{R}, it is satified that either

$$\chi_\nu(t+t_{\mathrm{R}}) = \chi_\nu(t_{\mathrm{R}}-t),\ \ \nu = A, B, \tag{A.47}$$

$$\text{or}\ \ \chi_{\mathrm{A}}(t+t_{\mathrm{R}}) = \chi_{\mathrm{B}}(t-t_{\mathrm{R}})\ \text{and}\ \Omega_{\mathrm{A}} = \Omega_{\mathrm{B}}. \tag{A.48}$$

For future convenience, we point out that, in the scenarios where Proposition 3 applies and both detectors start in the ground state, $\mathcal{M}$ simplifies to

$$\begin{aligned}\mathcal{M} = -\lambda^2 \int \mathrm{d}t\, \mathrm{d}t'\, \mathrm{d}\boldsymbol{x}\, \mathrm{d}\boldsymbol{x}'\, e^{\mathrm{i}\Omega(t+t')}\chi_{\mathrm{A}}(t)\chi_{\mathrm{B}}(t') \\ \times F_{\mathrm{A}}(\boldsymbol{x})F_{\mathrm{B}}(\boldsymbol{x}')G_{\mathrm{F}}(t,\boldsymbol{x},t',\boldsymbol{x}').\end{aligned} \tag{A.49}$$

If both detectors start in the excited state, Ω in the expression above picks up a negative sign.

A.5.2 Sufficient symmetries for constructive interference between harvesting and communication in FRW spacetimes

Here, we show that Proposition 4 for FRW spacetimes holds for the entanglement harvesting scenarios prescribed in the subsection 2.6.2. The proof arises from the fact that $\mathcal{M}$ can be rewritten to have an analogous form to the $\mathcal{M}$ term of setups where Proposition 3 applies. Concretely, the only changes are the replacement given in Eq. (2.122) and the substitution of t by $\eta(t)$ in G_{F}. Moreover, using the assumption $\Lambda_\nu(t,\boldsymbol{x}) = \mathfrak{T}_\nu(t)\mathfrak{X}_\nu(\boldsymbol{x})$ results in

$$\begin{aligned}\mathcal{M} = -\lambda^2 \int \mathrm{d}t\, \mathrm{d}t'\, \mathrm{d}\boldsymbol{x}\, \mathrm{d}\boldsymbol{x}'\, e^{\mathrm{i}\Omega(t+t')}\mathfrak{T}_{\mathrm{A}}(t)\mathfrak{T}_{\mathrm{B}}(t') \\ \times \mathfrak{X}_{\mathrm{A}}(\boldsymbol{x})\mathfrak{X}_{\mathrm{B}}(\boldsymbol{x}')\frac{G_{\mathrm{F}}\big(\eta(t),\boldsymbol{x},\eta(t'),\boldsymbol{x}'\big)}{a(t)a(t')}.\end{aligned} \tag{A.50}$$

Here, G_{F} is the usual expression in inertial coordinates of the Feynmann propagator for the Minkowski vacuum, as given in the proof of Lemma 4. Notice that this expression for $\mathcal{M}$ assumes that both detectors start in the ground state. The case where both detectors are prepared in the excited state amounts to considering $\Omega < 0$. Therefore, this case is automatically included in Eq. (A.50), and in the current proof.

Notice that if we define

$$\widetilde{G}_{\text{F}}(t, \boldsymbol{x}, t, \boldsymbol{x}') = \frac{G_{\text{F}}\big(\eta(t), \boldsymbol{x}, \eta(t'), \boldsymbol{x}'\big)}{a(t)a(t')}, \tag{A.51}$$

then the expression for $\mathcal{M}$ becomes the same as for the scenarios of Proposition 3 (see Eq. (A.49)), but with $\widetilde{G}_{\text{F}}$, $\mathfrak{T}_\nu(t)$, $\mathfrak{X}_\nu(\boldsymbol{x})$ instead of G_{F}, $\chi_\nu(t)$, $F_\nu(\boldsymbol{x})$. Therefore, to get the analogous Proposition 4, we need $\widetilde{G}_{\text{F}}$ and $\mathfrak{T}_\nu(t)$ to fulfill the corresponding conditions specified in the Symmetries 1 and 4, which were the ones used to derive Proposition 3. Notice that now, to define the Symmetry 4, we need to use the comoving coordinates $(t, \boldsymbol{x})$ as prescription coordinates for the detectors. This is a consequence of assuming that the split $\Lambda_\nu(t, \boldsymbol{x}) = \mathfrak{T}_\nu(t)\mathfrak{X}_\nu(\boldsymbol{x})$ happens in the comoving coordinates, and that the detectors' proper times coincide with the comoving time t.

The conditions over $\mathfrak{T}_\nu(t)$ are directly stated in Proposition 4 and are the same as for $\chi_\nu(t)$ in Proposition 3. Furthermore, since condition 2 of Symmetries 1 and 4 was needed to prove Proposition 3, here we also need to verify whether $\widetilde{G}_{\text{F}}$ satisfies to the same condition. Namely, we would like to show that

$$\begin{aligned}\widetilde{G}_{\text{F}}(t, \boldsymbol{x}, t', \boldsymbol{x}') &= \widetilde{G}_{\text{F}}(2t_R - t, \boldsymbol{x}, 2t_R - t', \boldsymbol{x}'),\\ &= \widetilde{G}_{\text{F}}(2t_R - t', \boldsymbol{x}, 2t_R - t, \boldsymbol{x}').\end{aligned} \tag{A.52}$$

To show that this relation is indeed fulfilled, first notice that the second equal sign can be readily checked by substituting the definition of $\widetilde{G}_{\text{F}}$ and using that G_{F} fulfills the same equality, as shown in Lemma 4. Second, we need to show that $\widetilde{G}_{\text{F}}$ is time symmetric around t_{R}. For this proof, we start with the hypothesis of Proposition 4 that $a(t) = a(2t_{\text{R}} - t)$. Then, the conformal time (as defined in Eq. (2.117)) fulfills

$$\eta(t) = 2\eta(t_{\text{R}}) - \eta(2t_{\text{R}} - t), \tag{A.53}$$

which can be readily verified by taking the derivative with respect to t. Then,

$$\begin{aligned}
&\widetilde{G}_{\mathrm{F}}(t,\boldsymbol{x},t',\boldsymbol{x}')\\
&=\frac{G_{\mathrm{F}}\big(\eta(t),\boldsymbol{x},\eta(t'),\boldsymbol{x}'\big)}{a(t)a(t')}\\
&=\frac{G_{\mathrm{F}}\big(2\eta(t_{\mathrm{R}})-\eta(2t_{\mathrm{R}}-t),\boldsymbol{x},2\eta(t_{\mathrm{R}})-\eta(2t_{\mathrm{R}}-t'),\boldsymbol{x}'\big)}{a(2t_{\mathrm{R}}-t)a(2t_{\mathrm{R}}-t')}\\
&=\frac{G_{\mathrm{F}}\big(\eta(2t_{\mathrm{R}}-t),\boldsymbol{x},\eta(2t_{\mathrm{R}}-t'),\boldsymbol{x}'\big)}{a(2t_{\mathrm{R}}-t)a(2t_{\mathrm{R}}-t')}\\
&=\widetilde{G}_{\mathrm{F}}(2t_{\mathrm{R}}-t,\boldsymbol{x},2t_{\mathrm{R}}-t',\boldsymbol{x}'),
\end{aligned}\tag{A.54}$$

where we used the first line of Eq. (A.41) for the Minkowski vacuum G_{F}. This completes the proof that Eq. (A.52) holds under the hypothesis that $a(t)=a(2t_{\mathrm{R}}-t)$. Bringing everything together, an analogous version of Proposition 3 holds for FRW spacetimes, resulting in Proposition 4.

A.6 Alternative symmetry conditions for detectors prescribed in Fermi normal coordinates

A.6.1 Conditions for the time reversibility and spatial reflection symmetry of Fermi normal coordinates

Here we shall study how pairs of Fermi normal coordinates are related by a time reversal or a time reversal combined with a spatial reflection. Knowing the symmetries respected by the Fermi normal coordinates is instrumental in determining the symmetries of the entanglement harvesting setup. This is the case when the harvesting setup uses the usual covariant prescription for the Unruh-DeWitt detector [90] which is based on the Fermi normal coordinates adapted to the detector trajectory $\mathsf{z}(\tau)$. Concretely, given an arbitrary coordinate system $(t,\boldsymbol{x})$, we will consider the transformations:

$$T_{\mathrm{R}}(t,\boldsymbol{x})=(2t_{\mathrm{R}}-t,\boldsymbol{x}),\ T_{\mathrm{RR}}(t,\boldsymbol{x})=(2t_{\mathrm{R}}-t,2\boldsymbol{x}_0-\boldsymbol{x}),\tag{A.55}$$

where time reversals are performed around the time t_{R}, and the spatial reflection is performed about the point $\boldsymbol{x}_0$. The lemmas in this appendix provide the conditions on the metric and trajectories for the pair of Fermi normal coordinates to be related either by T_{R} or by T_{RR}, which will be later used in Appendix A.6.2.

First, we recall how to construct the Fermi normal coordinates $(\tau, \boldsymbol{X})$ adapted to a timelike curve $\mathsf{z}(\tau)$, where τ is the curve's proper time. Choose a fixed proper time τ_0, and pick an orthonormal basis $\{\mathsf{e}_\rho(\tau_0)\}$ in the tangent space to $\mathsf{z}(\tau_0)$, such that $\mathsf{e}_0 = \dot{\mathsf{z}}(\tau_0)$. This basis extends to the whole curve, $\{\mathsf{e}_\rho(\tau)\}$, by imposing that the basis vectors are Fermi-Walker (FW) transported along the curve. A vector field v^α on the curve is FW transported if

$$\frac{\mathrm{D}v^\alpha}{\mathrm{d}\tau} + (a^\alpha u^\beta - u^\alpha a^\beta)v_\beta = 0, \tag{A.56}$$

where u^α and a^α are the components of $\mathsf{u} = \mathrm{d}\mathsf{z}/\mathrm{d}\tau$ and $\mathsf{a} = \mathrm{D}\mathsf{u}/\mathrm{d}\tau$, the four-velocity and four-acceleration of the curve, respectively. Moreover, we use $\mathrm{D}/\mathrm{d}\tau$ to denote the directional covariant derivative along $\mathsf{z}(\tau)$, which for a vector $\mathsf{v} = v^\alpha \partial_\alpha$ is

$$\frac{\mathrm{D}v^\alpha}{\mathrm{d}\tau} = \frac{\mathrm{d}v^\alpha}{\mathrm{d}\tau} + \Gamma^\alpha_{\beta\gamma} v^\beta u^\gamma. \tag{A.57}$$

Notably, u is always FW transported, therefore $\mathsf{e}_0(\tau) = \mathsf{u}(\tau)$. Moreover, $\{\mathsf{e}_\rho(\tau)\}$ remains an orthonormal basis for each point of the curve. The idea behind the definition of the FW transport is to generalize the parallel transport to account for the possible change in orientation introduced by the acceleration of the trajectory. That is, we would like to transport the frame $\{\mathsf{e}_\rho(\tau)\}$ in a way that it does not rotate with respect to the curve. To see this concretely, consider coordinates where $u^\rho = (u^0, 0, 0, 0)$, and define the two-form $\omega_{\alpha\beta} = 2a_{[\alpha}u_{\beta]}$. In this case, the only non-vanishing components of $\omega_{\alpha\beta}$ are $\omega_{i0} = -\omega_{0i}$, $i = 1, 2, 3$, since $a^\rho u_\rho = 0$. Thus, the second term in Eq. (A.56) is essentially describing the projection of v^ρ along the 3-vector $n^i = \omega^{i0}$, which describes the rotation of the orthonormal "spatial" frame e_i along the trajectory.

Now, we define the Fermi normal coordinates as follows. Let $\mathcal{N}_\mathsf{p}$ be the normal neighborhood of p, which is the set of points that are connected to p by a unique geodesic. For each τ, denote with Σ_τ the space-like hypersurface orthogonal to $\mathsf{u}(\tau)$. This hypersurface consists of all the points in $\mathcal{N}_{\mathsf{z}(\tau)}$ that can be reached by geodesics that start from $\mathsf{z}(\tau)$ and start with tangent vectors orthogonal to $\mathsf{u}(\tau)$. These hypersurfaces Σ_τ constitute rest spaces around $\mathsf{z}(\tau)$, and locally define a foliation of spacetime. Then, the coordinates $(\tau, \boldsymbol{X})$ are assigned to the point $\exp_{\mathsf{z}(\tau)}\left(X^a \mathsf{e}_a(\tau)\right) \in \Sigma_\tau$. Here, we use the convention that latin indices run over spatial components, $a = 1, \ldots, n$. The exponential map is defined as

$$\exp_\mathsf{p}\left(\mathsf{v}\right) = \gamma_\mathsf{v}(1), \tag{A.58}$$

where $\gamma_\mathsf{v}(s)$ is a geodesic that fulfills $\gamma_\mathsf{v}(0) = \mathsf{p}$, $\dot{\gamma}_\mathsf{v}(0) = \mathsf{v}$. Notice that in this prescription $\mathsf{z}(\tau)$ has coordinates $(\tau, \mathbf{0})$, and its proper distance to a point with coordinates $(\tau, \boldsymbol{X})$ is $|\boldsymbol{X}| = \sqrt{\sum_a (X^a)^2}$.

Lemma 9. *Choose arbitrary $(t, \boldsymbol{x})$ coordinates, in which the metric components are $g_{\rho\sigma}$. Consider a pair of time-like curves $\mathsf{z}_\nu(\tau_\nu)$, $\nu = A, B$, parametrized by their proper times τ_ν. Denote the coordinates of the curves' points as $\big(t, \boldsymbol{z}_\nu(t)\big)$. Assume that for some $t_{\rm R}$,*

1. $g_{\rho\sigma}(t_{\rm R} + t, \boldsymbol{x}) = s(\rho, \sigma) g_{\rho\sigma}(t_{\rm R} - t, \boldsymbol{x})$,
2. $\boldsymbol{z}_{\rm A}(t_{\rm R} + t) = \boldsymbol{z}_{\rm B}(t_{\rm R} - t)$,

Here, $s(\rho_1, \rho_2, \ldots, \rho_n) = 1$ if the number of zeros among the set of arguments $\rho_1, \ldots, \rho_n$ is even and $s(\rho_1, \rho_2, \ldots, \rho_n) = -1$ otherwise. Then, there exist Fermi normal coordinates $(\tau_\nu, \widetilde{\boldsymbol{x}}_\nu)$ adapted to the trajectories $\mathsf{z}_\nu(\tau_\nu)$ that are related by

$$\begin{aligned} \tau_{\rm A}(t_{\rm R} + t, \boldsymbol{x}) &= \upsilon_{\rm R} - \tau_{\rm B}(t_{\rm R} - t, \boldsymbol{x}), \\ \widetilde{\boldsymbol{x}}_{\rm A}(t_{\rm R} + t, \boldsymbol{x}) &= \widetilde{\boldsymbol{x}}_{\rm B}(t_{\rm R} - t, \boldsymbol{x}), \end{aligned} \tag{A.59}$$

with $\upsilon_{\rm R} = \tau_{\rm R,A} + \tau_{\rm R,B}$, where $\tau_{{\rm R},\nu}$ are the proper times that fulfill $t_{\rm R} = z^0_\nu(\tau_{{\rm R},\nu})$.

Proof. Let us start defining a convenient notation: for any function $f(t)$, let

$$[f(t)]_{\rm R} = f(2t_{\rm R} - t). \tag{A.60}$$

Then, the assumptions of the lemma can be simply rewritten as

$$[g_{\rho\sigma}]_{\rm R} = s(\rho, \sigma) g_{\rho\sigma}, \;\; [\boldsymbol{z}_{\rm A}]_{\rm R} = [\boldsymbol{z}_{\rm B}]_{\rm R}. \tag{A.61}$$

Next, let us show that these assumptions imply that

i) $[g^{\rho\sigma}]_{\rm R} = s(\rho, \sigma) g^{\rho\sigma}$,

ii) $[\partial_\lambda g_{\rho\sigma}]_{\rm R} = s(\rho, \sigma, \lambda) \partial_\lambda g_{\rho\sigma}$,

iii) $[\Gamma^\lambda_{\rho\sigma}]_{\rm R} = s(\rho, \sigma, \lambda) \Gamma^\lambda_{\rho\sigma}$,

iv) $[u^\rho_{\rm A}]_{\rm R} = -s(\rho) u^\rho_{\rm B}$,

v) $[a^\rho_{\rm A}]_{\rm R} = s(\rho) a^\rho_{\rm B}$.

Showing that $s(\rho, \sigma) g^{\rho\sigma}$ is the inverse of $[g_{\rho\sigma}]_{\rm R}$ is enough for i),

$$s(\rho, \sigma) g^{\rho\sigma} [g_{\sigma\lambda}]_{\rm R} = s(\rho, \lambda) g^{\rho\sigma} g_{\sigma\lambda} = \delta^\lambda_\rho. \tag{A.62}$$

For ii), it is enough to use i) and to notice that for a general function $h(t, \boldsymbol{x})$,

$$\partial_0[h]_{\mathrm{R}} = -[\partial_0 h]_{\mathrm{R}},\ \partial_a[h]_{\mathrm{R}} = [\partial_a h]_{\mathrm{R}}. \tag{A.63}$$

Relation iii) follows from combining i) and ii) with the formula for the Christoffel symbols, namely

$$\Gamma^{\lambda}_{\rho\sigma} = \frac{1}{2} g^{\lambda\epsilon} \left(\partial_\sigma g_{\epsilon\rho} + \partial_\rho g_{\epsilon\sigma} - \partial_\epsilon g_{\rho\sigma}\right). \tag{A.64}$$

Proving iv) starts from taking the derivative on the trajectory condition, to obtain $[\dot{\boldsymbol{z}}_{\mathrm{A}}]_{\mathrm{R}} = -\dot{\boldsymbol{z}}_{\mathrm{B}}$. Then, using

$$u^0_\nu = \frac{\mathrm{d}t}{\mathrm{d}\tau_\nu},\ u^a_\nu = \frac{\mathrm{d}t}{\mathrm{d}\tau_\nu}\dot{\boldsymbol{z}}^a_\nu, \tag{A.65}$$

together with $g_{\rho\sigma}u^\rho_\nu u^\sigma_\nu = -1$, implies

$$\frac{\mathrm{d}t}{\mathrm{d}\tau_\nu} = \sqrt{-g_{00} - 2g_{a0}\dot{\boldsymbol{z}}^a_\nu - g_{ab}\dot{\boldsymbol{z}}^a_\nu \dot{\boldsymbol{z}}^b_\nu}. \tag{A.66}$$

Therefore, using $[\dot{\boldsymbol{z}}_{\mathrm{A}}]_{\mathrm{R}} = -\dot{\boldsymbol{z}}_{\mathrm{B}}$ and ii), we get

$$\left[\frac{\mathrm{d}t}{\mathrm{d}\tau_{\mathrm{A}}}\right]_{\mathrm{R}} = \frac{\mathrm{d}t}{\mathrm{d}\tau_{\mathrm{B}}}. \tag{A.67}$$

Then, substituting back on Eq. (A.65) allows showing iv). Finally, to prove v), combine

$$a^\alpha_\nu = \frac{\mathrm{d}t}{\mathrm{d}\tau_\nu}\frac{\mathrm{d}u^\alpha_\nu}{\mathrm{d}t} + \Gamma^\alpha_{\beta\gamma} u^\beta_\nu u^\gamma_\nu \tag{A.68}$$

with Eqs. (A.63), (A.67), and relations iii), iv).

Next, we prove that the FW transported orthonormal bases along the curves can be related by a time reversal transformation. Consider an orthonormal basis $\{\mathsf{e}_\rho(t)\}$ that is FW transported along z_{A} and fulfills $\mathsf{e}_0 = \mathsf{u}_{\mathrm{A}}$. Define f_ρ such that

$$(\mathsf{f}_\rho)^\alpha = s(\rho, \alpha)[(\mathsf{e}_\rho)^\alpha]_{\mathrm{R}}. \tag{A.69}$$

We now will show that this basis is FW transported along z_{B}. Let us start reversing the FW transport equation that the $\{\mathsf{e}_\rho\}$ fulfill,

$$\begin{aligned} 0 &= \left[\frac{\mathrm{D}(\mathsf{e}_\rho)^\alpha}{\mathrm{d}\tau_{\mathrm{A}}} + (a^\alpha_{\mathrm{A}} u^\beta_{\mathrm{A}} - u^\alpha_{\mathrm{A}} a^\beta_{\mathrm{A}}) g_{\beta\gamma}(\mathsf{e}_\rho)^\gamma\right]_{\mathrm{R}} \\ &= -s(\rho,\alpha)\left(\frac{\mathrm{D}(\mathsf{f}_\rho)^\alpha}{\mathrm{d}\tau_{\mathrm{B}}} + (a^\alpha_{\mathrm{B}} u^\beta_{\mathrm{B}} - u^\alpha_{\mathrm{B}} a^\beta_{\mathrm{B}}) g_{\beta\gamma}(\mathsf{f}_\rho)^\gamma\right), \end{aligned} \tag{A.70}$$

where we used the relations ii), iv), v), and also

$$\left[\frac{\mathrm{D}(\mathsf{e}_\rho)^\alpha}{\mathrm{d}\tau_{\mathrm{A}}}\right]_{\mathrm{R}} = \left[\frac{\mathrm{d}t}{\mathrm{d}\tau_{\mathrm{A}}}\frac{\mathrm{d}(\mathsf{e}_\rho)^\alpha}{\mathrm{d}t} + \Gamma^\alpha_{\beta\gamma}(\mathsf{e}_\rho)^\beta u^\gamma_{\mathrm{A}}\right]_{\mathrm{R}}$$
$$= -s(\rho,\alpha)\frac{\mathrm{D}(\mathsf{f}_\rho)^\alpha}{\mathrm{d}\tau_{\mathrm{B}}}, \tag{A.71}$$

which used Eqs. (A.63), (A.67), (A.69), and relations iii), iv). Therefore, the $\{\mathsf{f}_\rho\}$, as defined in Eq. (A.69) are FW transported along z_{B}. Moreover, the $\{\mathsf{f}_\rho\}$ are orthonormal because

$$(\mathsf{f}_\rho)^\alpha(\mathsf{f}_\sigma)^\beta g_{\alpha\beta} = \left[(\mathsf{e}_\rho)^\alpha(\mathsf{e}_\sigma)^\beta g_{\alpha\beta}\right]_{\mathrm{R}} = \eta_{\rho\sigma}, \tag{A.72}$$

where $\eta_{\rho\sigma}$ is the Minkowski metric. Lastly, $\mathsf{f}_0 = \mathsf{u}_{\mathrm{B}}$, because

$$(\mathsf{f}_0)^\alpha = -s(\alpha)[(\mathsf{e}_0)^\alpha]_{\mathrm{R}} = -s(\alpha)\,[u^\alpha_{\mathrm{A}}]_{\mathrm{R}} = u^\alpha_{\mathrm{B}}. \tag{A.73}$$

All these results guarantee that the orthonormal basis $\{\mathsf{f}_\rho(t)\}$ can be used to define the Fermi normal coordinates along z_{B}. From now on, let us use $\{\mathsf{e}_\rho\}$ and $\{\mathsf{f}_\rho\}$ to respectively define the Fermi normal coordinates $(\tau_{\mathrm{A}}, \widetilde{\boldsymbol{x}}_{\mathrm{A}})$ around $\mathsf{z}_{\mathrm{A}}(\tau_{\mathrm{A}})$ and $(\tau_{\mathrm{B}}, \widetilde{\boldsymbol{x}}_{\mathrm{B}})$ around $\mathsf{z}_{\mathrm{B}}(\tau_{\mathrm{B}})$.

Next, we check the relationships in Eq. (A.59) between $(\tau_{\mathrm{A}}, \widetilde{\boldsymbol{x}}_{\mathrm{A}})$ and $(\tau_{\mathrm{B}}, \widetilde{\boldsymbol{x}}_{\mathrm{B}})$. For any spacetime point p_{A}, we define p_{B} as follows. We denote the Fermi normal coordinates j of the point p_ν as

$$\tau_{\mathsf{p}_\nu} = \tau_\nu(\mathsf{p}_\nu),\ \ \widetilde{\boldsymbol{x}}_{\mathsf{p}_\nu} = \widetilde{\boldsymbol{x}}_\nu(\mathsf{p}_\nu). \tag{A.74}$$

Then, p_{B} is chosen so that the coordinates of p_{A} and p_{B} are related by

$$\tau_{\mathsf{p}_{\mathrm{A}}} = \upsilon_{\mathrm{R}} - \tau_{\mathsf{p}_{\mathrm{B}}},\ \ \widetilde{\boldsymbol{x}}_{\mathsf{p}_{\mathrm{A}}} = \widetilde{\boldsymbol{x}}_{\mathsf{p}_{\mathrm{B}}}, \tag{A.75}$$

with $\upsilon_{\mathrm{R}} = \tau_{\mathrm{R,A}} + \tau_{\mathrm{R,B}}$, where $\tau_{\mathrm{R},\nu}$ are the proper times that fulfill $t_{\mathrm{R}} = z^0_\nu(\tau_{\mathrm{R},\nu})$. By expressing the points p_ν in the coordinate system $(t, \boldsymbol{x})$ on Eqs. (A.74) and (A.75), one can see that the Eq. (A.59) that we want to prove is equivalent to showing $T_{\mathrm{R}}(\mathsf{p}_{\mathrm{A}}) = \mathsf{p}_{\mathrm{B}}$, with T_{R} as defined in (A.55). Therefore, to complete the proof, it will be enough to show that $T_{\mathrm{R}}(\mathsf{p}_{\mathrm{A}}) = \mathsf{p}_{\mathrm{B}}$ is true, as is done next.

Consider a geodesic $\gamma_{\mathrm{A}}(\lambda)$ such that

$$\gamma_{\mathrm{A}}(0) = \mathsf{z}_{\mathrm{A}}(\tau_{\mathsf{p}_{\mathrm{A}}}),\ \ \dot\gamma_{\mathrm{A}}(0) = \widetilde{x}^a_{\mathsf{p}_{\mathrm{A}}}\mathsf{e}_a\big(z^0_{\mathrm{A}}(\tau_{\mathsf{p}_{\mathrm{A}}})\big). \tag{A.76}$$

Notice that, by the definition of the Fermi normal coordinates, we have $\gamma_{\mathrm{A}}(1) = \mathsf{p}_{\mathrm{A}}$. Next, define $\gamma_{\mathrm{B}}(\lambda)$ as

$$\gamma_{\mathrm{B}}(\lambda) = T_{\mathrm{R}}(\gamma_{\mathrm{A}}(\lambda)). \tag{A.77}$$

The next steps are to show that such $\gamma_{\text{B}}(\lambda)$ is a geodesic that fulfills

$$\gamma_{\text{B}}(0) = \mathsf{z}_{\text{B}}(\tau_{\mathsf{p}_{\text{B}}}),\ \dot{\gamma}_{\text{B}}(0) = \widetilde{x}^a_{\mathsf{p}_{\text{B}}} \mathsf{f}_a\big(z^0_{\text{B}}(\tau_{\mathsf{p}_{\text{B}}})\big). \tag{A.78}$$

We start checking the first identity in the equation above by computing

$$\frac{\mathrm{d}}{\mathrm{d}\tau}\Big(\big(\mathsf{z}^0_{\text{B}}\big)^{-1}\big(2t_{\text{R}} - z^0_{\text{A}}(\tau)\big)\Big) = -\frac{u^0_{\text{A}}\big(z^0_{\text{A}}(\tau)\big)}{u^0_{\text{B}}\big(2t_{\text{R}} - z^0_{\text{A}}(\tau)\big)} = -1, \tag{A.79}$$

where we used the statement iv) that we proved at the start of the proof. Therefore, for some constant τ_0,

$$z^0_{\text{B}}(\tau_0 - \tau) = 2t_{\text{R}} - z^0_{\text{A}}(\tau). \tag{A.80}$$

To find τ_0, choose $\tau = \tau_{\text{R,A}}$, so that

$$z^0_{\text{B}}(\tau_0 - \tau_{\text{R,A}}) = 2t_{\text{R}} - z^0_{\text{A}}(\tau_{\text{R,A}}) = t_{\text{R}}, \tag{A.81}$$

which means $\tau_0 - \tau_{\text{R,A}} = \tau_{\text{R,B}}$, and thus $\tau_0 = \upsilon_{\text{R}}$. Substituting back to Eq. (A.80), and using $\tau_{\mathsf{p}_{\text{A}}} = \upsilon_{\text{R}} - \tau_{\mathsf{p}_{\text{B}}}$,

$$z^0_{\text{B}}(\tau_{\mathsf{p}_{\text{B}}}) = 2t_{\text{R}} - z^0_{\text{A}}(\tau_{\mathsf{p}_{\text{A}}}), \tag{A.82}$$

and therefore, $\gamma^0_{\text{B}}(0) = z^0_{\text{B}}(\tau_{\mathsf{p}_{\text{B}}})$. Moreover, we have $\gamma^a_{\text{B}}(0) = z^a_{\text{B}}(\tau_{\mathsf{p}_{\text{B}}})$ because $\gamma^a_{\text{B}}(0) = z^a_{\text{A}}(\tau_{\mathsf{p}_{\text{A}}})$ and

$$\boldsymbol{z}_{\text{A}}\big(z^0_{\text{A}}(\tau_{\mathsf{p}_{\text{A}}})\big) = \boldsymbol{z}_{\text{B}}\big(2t_{\text{R}} - z^0_{\text{A}}(\tau_{\mathsf{p}_{\text{A}}})\big) = \boldsymbol{z}_{\text{B}}\big(z^0_{\text{B}}(\tau_{\mathsf{p}_{\text{B}}})\big), \tag{A.83}$$

where we used the assumption $\boldsymbol{z}_{\text{A}}(t) = \boldsymbol{z}_{\text{B}}(2t_{\text{R}} - t)$. This completes showing the claim from Eq. (A.78) that $\gamma_{\text{B}}(0) = \mathsf{z}_{\text{B}}(\tau_{\mathsf{p}_{\text{B}}})$.

To get the identity for $\dot{\gamma}_{\text{B}}(0)$ in Eq. (A.78), we start from the definition of γ_{B} given in Eq. (A.77). Expressing this definition in $(t, \boldsymbol{x})$ coordinates gives

$$\gamma^0_{\text{B}}(\lambda) = 2t_{\text{R}} - \gamma^0_{\text{A}}(\lambda),\ \gamma^a_{\text{B}}(\lambda) = \gamma^a_{\text{A}}(\lambda). \tag{A.84}$$

Then, taking derivatives w.r.t. λ, we get

$$\dot{\gamma}^\alpha_{\text{B}}(\lambda) = s(\alpha)\dot{\gamma}^\alpha_{\text{A}}(\lambda). \tag{A.85}$$

Combining this result with Eqs. (A.69), (A.75) and (A.82) leads to

$$\begin{aligned}
\dot{\gamma}^\alpha_{\text{B}}(0) &= s(\alpha)\dot{\gamma}^\alpha_{\text{A}}(0) \\
&= s(\alpha)\widetilde{x}^a_{\mathsf{p}_{\text{A}}}(\mathsf{e}_a)^\alpha\big(z^0_{\text{A}}(\tau_{\mathsf{p}_{\text{A}}})\big) \\
&= \widetilde{x}^a_{\mathsf{p}_{\text{B}}}(\mathsf{f}_a)^\alpha\big(z^0_{\text{B}}(\tau_{\mathsf{p}_{\text{B}}})\big),
\end{aligned} \tag{A.86}$$

which, as we wanted to show, is the expression for $\dot{\gamma}_{\mathrm{B}}(0)$ in Eq. (A.78).

Finally, let us show that γ_{B} is a geodesic. Taking the derivative w.r.t. λ in Eq. (A.85),

$$\dot{\gamma}^{\alpha}_{\mathrm{B}}(\lambda) = s(\alpha)\dot{\gamma}^{\alpha}_{\mathrm{A}}(\lambda),\ \ddot{\gamma}^{\alpha}_{\mathrm{B}}(\lambda) = s(\alpha)\ddot{\gamma}^{\alpha}_{\mathrm{A}}(\lambda). \tag{A.87}$$

Then, substituting these expressions into the geodesic equation which γ_{A} fulfills,

$$\begin{aligned}
\ddot{\gamma}^{\alpha}_{\mathrm{A}} &= -\Gamma^{\alpha}_{\beta\gamma}\big(\gamma^{0}_{\mathrm{A}}, \gamma^{a}_{\mathrm{A}}\big)\,\dot{\gamma}^{\beta}_{\mathrm{A}}\dot{\gamma}^{\gamma}_{\mathrm{A}}, \\
s(\alpha)\ddot{\gamma}^{\alpha}_{\mathrm{B}} &= -s(\alpha)\Gamma^{\alpha}_{\beta\gamma}\big(2t_{\mathrm{R}} - \gamma^{0}_{\mathrm{A}}, \gamma^{a}_{\mathrm{A}}\big)\,\dot{\gamma}^{\beta}_{\mathrm{B}}\dot{\gamma}^{\gamma}_{\mathrm{B}}, \\
\ddot{\gamma}^{\alpha}_{\mathrm{B}} &= -\Gamma^{\alpha}_{\beta\gamma}\big(\gamma^{0}_{\mathrm{B}}, \gamma^{a}_{\mathrm{B}}\big)\,\dot{\gamma}^{\beta}_{\mathrm{B}}\dot{\gamma}^{\gamma}_{\mathrm{B}},
\end{aligned} \tag{A.88}$$

where we also used the statement iii) and Eq. (A.77). The last line is, as we wanted, the geodesic equation for γ_{B}.

Therefore, γ_{B} matches the requirements of the exponential map definition and thus $\mathsf{p}_{\mathrm{B}} = \gamma_{\mathrm{B}}(1)$. Now, remember that $T_{\mathrm{R}}(\gamma_{\mathrm{A}}(\lambda)) = \gamma_{\mathrm{B}}(\lambda)$. Then, choosing $\lambda = 1$, $T_{\mathrm{R}}(\mathsf{p}_{\mathrm{A}}) = \mathsf{p}_{\mathrm{B}}$. This finally completes the proof that

$$\begin{aligned}
\tau_{\mathrm{A}}(t_{\mathrm{R}} + t, \boldsymbol{x}) &= \upsilon_{\mathrm{R}} - \tau_{\mathrm{B}}(t_{\mathrm{R}} - t, \boldsymbol{x}), \\
\widetilde{\boldsymbol{x}}_{\mathrm{A}}(t_{\mathrm{R}} + t, \boldsymbol{x}) &= \widetilde{\boldsymbol{x}}_{\mathrm{B}}(t_{\mathrm{R}} - t, \boldsymbol{x}).
\end{aligned} \tag{A.89}$$

□

Lemma 10. *Choose arbitrary coordinates $(t, \boldsymbol{x})$, in which the metric components are $g_{\rho\sigma}$. Consider a time-like curve $\mathsf{z}(\tau)$, parametrized by its proper time τ. Denote the coordinates of the curve's points as $\big(t, \boldsymbol{z}(t)\big)$. Assume that for some t_{R},*

1. $g_{\rho\sigma}(t_{\mathrm{R}} + t, \boldsymbol{x}) = s(\rho, \sigma) g_{\rho\sigma}(t_{\mathrm{R}} - t, \boldsymbol{x})$,
2. $\boldsymbol{z}(t_{\mathrm{R}} + t) = \boldsymbol{z}(t_{\mathrm{R}} - t)$,

Here, $s(\rho_1, \rho_2, \ldots, \rho_n) = 1$ if the number of zeros among the set of arguments $\rho_1, \ldots, \rho_n$ is even and $s(\rho_1, \rho_2, \ldots, \rho_n) = -1$ otherwise. Then, the Fermi normal coordinates $(\tau, \widetilde{\boldsymbol{x}})$ adapted to the trajectory $\mathsf{z}(\tau)$ fulfill

$$\begin{aligned}
\tau(t_{\mathrm{R}} + t, \boldsymbol{x}) &= 2\tau_{\mathrm{R}} - \tau(t_{\mathrm{R}} - t, \boldsymbol{x}), \\
\widetilde{\boldsymbol{x}}(t_{\mathrm{R}} + t, \boldsymbol{x}) &= \widetilde{\boldsymbol{x}}(t_{\mathrm{R}} - t, \boldsymbol{x}),
\end{aligned} \tag{A.90}$$

where τ_{R} is the proper time that fulfills $t_{\mathrm{R}} = z^0(\tau_{\mathrm{R}})$.

Proof. The assumptions of this lemma fulfill the hypotheses of Lemma 9 for the case $\mathsf{z}(\tau) = \mathsf{z}_{\mathrm{A}}(\tau) = \mathsf{z}_{\mathrm{B}}(\tau)$. Then, Lemma 9 provides two coordinate systems $(\tau_{\mathrm{A}}, \widetilde{\boldsymbol{x}}_{\mathrm{A}})$ and $(\tau_{\mathrm{B}}, \widetilde{\boldsymbol{x}}_{\mathrm{B}})$ adapted to $\mathsf{z}(\tau)$, which are related by the Eq. (A.59). A priori, these two coordinate systems could be different, because there is freedom in the choice of orthonormal basis that defines any Fermi normal coordinates adapted to $\mathsf{z}(\tau)$. However, Eq. (A.59) implies that

$$\widetilde{\boldsymbol{x}}_{\mathrm{A}}(t_{\mathrm{R}}, \boldsymbol{x}) = \widetilde{\boldsymbol{x}}_{\mathrm{B}}(t_{\mathrm{R}}, \boldsymbol{x}), \tag{A.91}$$

which means that there is a spatial surface where both Fermi normal coordinates $(\tau_{\mathrm{A}}, \widetilde{\boldsymbol{x}}_{\mathrm{A}})$ and $(\tau_{\mathrm{B}}, \widetilde{\boldsymbol{x}}_{\mathrm{B}})$ adapted to $\mathsf{z}(\tau)$ are the same. This can only happen if $(\tau_{\mathrm{A}}, \widetilde{\boldsymbol{x}}_{\mathrm{A}})$ and $(\tau_{\mathrm{B}}, \widetilde{\boldsymbol{x}}_{\mathrm{B}})$ are the same coordinate systems, thus proving that there are Fermi normal coordinates adapted to $\mathsf{z}(\tau)$ that fulfill Eq. (A.90), finishing the proof.

□

Lemma 11. *Choose arbitrary coordinates $(t, \boldsymbol{x})$, in which the metric components are $g_{\rho\sigma}$. Consider a pair of time-like curves $\mathsf{z}_\nu(\tau_\nu)$, $\nu = A, B$, parametrized by their proper times τ_ν. Denote the coordinates of the curves' points as $\big(t, \boldsymbol{z}_\nu(t)\big)$. Assume that for some t_{R},*

1. $g_{\rho\sigma}(t_{\mathrm{R}} + t, \boldsymbol{x}_0 + \boldsymbol{x}) = g_{\rho\sigma}(t_{\mathrm{R}} - t, \boldsymbol{x}_0 - \boldsymbol{x})$,
2. $\boldsymbol{z}_{\mathrm{A}}(t_{\mathrm{R}} + t) = 2\boldsymbol{x}_0 - \boldsymbol{z}_{\mathrm{B}}(t_{\mathrm{R}} - t)$.

Then, there exist Fermi normal coordinates $(\tau_\nu, \widetilde{\boldsymbol{x}}_\nu)$ adapted to the trajectories $\boldsymbol{z}_\nu(t)$ that are related by

$$\begin{aligned} \tau_{\mathrm{A}}(t_{\mathrm{R}} + t, \boldsymbol{x}_0 + \boldsymbol{x}) &= \upsilon_{\mathrm{R}} - \tau_{\mathrm{B}}(t_{\mathrm{R}} - t, \boldsymbol{x}_0 - \boldsymbol{x}), \\ \widetilde{\boldsymbol{x}}_{\mathrm{A}}(t_{\mathrm{R}} + t, \boldsymbol{x}_0 + \boldsymbol{x}) &= \widetilde{\boldsymbol{x}}_{\mathrm{B}}(t_{\mathrm{R}} - t, \boldsymbol{x}_0 - \boldsymbol{x}), \end{aligned} \tag{A.92}$$

with $\upsilon_{\mathrm{R}} = \tau_{\mathrm{R,A}} + \tau_{\mathrm{R,B}}$, where $\tau_{\mathrm{R},\nu}$ are the proper times that fulfill $t_{\mathrm{R}} = z^0_\nu(\tau_{\mathrm{R},\nu})$.

Proof. This lemma is proven analogously to Lemma 9, so we will only point out the differences. Here, it is convenient to instead use the following notation for any functions $f(t)$, $h(t, \boldsymbol{x})$,

$$\begin{aligned} [f(t)]_{\mathrm{R}} &= f(2t_{\mathrm{R}} - t), \\ [h(t, \boldsymbol{x})]_{\mathrm{RR}} &= h(2t_{\mathrm{R}} - t, 2\boldsymbol{x}_0 - \boldsymbol{x}). \end{aligned} \tag{A.93}$$

Then, following similar steps to the previous proof,

i) $[g_{\rho\sigma}]_{\rm R} = g_{\rho\sigma}$,

ii) $[\partial_\lambda g_{\rho\sigma}]_{\rm RR} = -\partial_\lambda g_{\rho\sigma}$,

iii) $[\Gamma^\lambda_{\rho\sigma}]_{\rm RR} = -\Gamma^\lambda_{\rho\sigma}$,

iv) $[u^\rho_{\rm A}]_{\rm R} = u^\rho_{\rm B}$,

v) $[a^\rho_{\rm A}]_{\rm R} = -a^\rho_{\rm B}$.

Notice that these relations are useful because the trajectories transform into one another when performing a time reversal and a spatial reflection. These relations can be used to find a pair of orthonormal basis $\{\mathsf{e}_\rho(t)\}$ and $\{\mathsf{f}_\rho(t)\}$, which respectively are FW transported along $\mathsf{z}_{\rm A}(\tau_{\rm A})$ and $\mathsf{z}_{\rm B}(\tau_{\rm B})$, and that fulfill

$$[(\mathsf{e}_\rho)^\alpha]_{\rm R} = (\mathsf{f}_\rho)^\alpha. \tag{A.94}$$

Then, we again pick $\{\mathsf{e}_\rho(t)\}$ and $\{\mathsf{f}_\rho(t)\}$ to respectively define the Fermi normal coordinates adapted to $\mathsf{z}_{\rm A}(\tau_{\rm A})$ and $\mathsf{z}_{\rm B}(\tau_{\rm B})$. The final part of the proof is also analogous to Lemma 9, but changing Eq. (A.77) to relate $\gamma_{\rm A}$ and $\gamma_{\rm B}$ by $T_{\rm RR}$ instead of $T_{\rm R}$. □

A.6.2 Simplified conditions to satisfy Corollary 1 when detectors are prescribed in the Fermi normal coordinates

Here we combine the results obtained in the previous Subappendix with the results of the Appendices A.3 and A.4 to get simplified propositions that guarantee no destructive interference between harvesting and communication. This section assumes that we follow the covariant UDW detector prescription of [90], where the detector ν is prescribed in the Fermi normal coordinates $(\tau_\nu, \widetilde{\boldsymbol{x}}_\nu)$ adapted to its trajectory $\mathsf{z}_\nu(\tau_\nu)$. These coordinates are valid locally around the trajectory and factorize the smearing function, $\Lambda_\nu(\tau_\nu, \widetilde{\boldsymbol{x}}_\nu) = \chi_\nu(\tau_\nu)F_\nu(\widetilde{\boldsymbol{x}}_\nu)$. Moreover, τ_ν are the proper times of the detectors.

Proposition 5. *Let $g_{\rho\sigma}$ be the metric components in an arbitrary coordinate system $(t, \boldsymbol{x})$, $\boldsymbol{z}_\nu(t)$ the spatial components of the detectors' trajectories and $(\tau_\nu, \widetilde{\boldsymbol{x}}_\nu)$ the Fermi normal coordinates adapted to $\boldsymbol{z}_\nu(t)$. Assume that*

1. $g_{\rho\sigma}(t_{\rm R} - t, \boldsymbol{x}) = s(\rho,\sigma)g_{\rho\sigma}(t_{\rm R} + t, \boldsymbol{x})$,
2. $G_F(t_{\rm R} - t, \boldsymbol{x}, t_{\rm R} - t', \boldsymbol{x}') = G_F(t_{\rm R} + t, \boldsymbol{x}, t_{\rm R} + t', \boldsymbol{x}')$,

3. $\boldsymbol{z}_\nu(t_{\mathrm{R}} - t) = \boldsymbol{z}_\nu(t_{\mathrm{R}} + t)$,

4. $\Lambda_\nu(\tau_\nu, \widetilde{\boldsymbol{x}}_\nu) = \chi_\nu(\tau_\nu) F_\nu(\widetilde{\boldsymbol{x}}_\nu)$,

5. $\chi_\nu(\tau_{\mathrm{R},\nu} - \tau_\nu) = \chi_\nu(\tau_{\mathrm{R},\nu} + \tau_\nu)$,

6. $\beta_\nu = \Omega_\nu \tau_{\mathrm{R},\nu}$,

where $\tau_{\mathrm{R},\nu} = \tau_\nu(t_{\mathrm{R}}, \boldsymbol{z}_\nu(t_{\mathrm{R}}))$, *and* $s(\rho, \sigma)$ *is the sign function defined in Lemma 10. Moreover, recall that the detectors' initial states are* $|\psi_\nu\rangle = \cos\alpha_\nu |g_\nu\rangle + \sin\alpha_\nu e^{\mathrm{i}\beta_\nu} |e_\nu\rangle$.

These assumptions are sufficient to fulfill the conditions given in Symmetry 1, thus fulfilling Corollary 1.

This proposition follows from fulfilling the hypotheses of Lemma 10 in order to get the time reversibility condition over the Fermi normal coordinates in Eq. (A.27) of Lemma 1 and, in turn, fulfill conditions 3 and 4 of Symmetry 1. Moreover, notice that condition 1 of Symmetry 1, i.e., $g(t_{\mathrm{R}} - t, \boldsymbol{x}) = g(t_{\mathrm{R}} + t, \boldsymbol{x})$, is fulfilled due to the assumption of the proposition on the components $g_{\rho\sigma}$.

Proposition 6. *Let* $g_{\rho\sigma}$ *be the metric components in an arbitrary coordinate system* $(t, \boldsymbol{x})$, $\boldsymbol{z}_\nu(t)$ *the spatial components of the detectors' trajectories and* $(\tau_\nu, \widetilde{\boldsymbol{x}}_\nu)$ *the Fermi normal coordinates adapted to* $\boldsymbol{z}_\nu(t)$. *Assume that*

1. $g_{\rho\sigma}(t_{\mathrm{R}} - t, \boldsymbol{x}) = s(\rho, \sigma) g_{\rho\sigma}(t_{\mathrm{R}} + t, \boldsymbol{x})$,

2. $G_F(t_{\mathrm{R}} - t, \boldsymbol{x}, t_{\mathrm{R}} - t', \boldsymbol{x}') = G_F(t_{\mathrm{R}} + t', \boldsymbol{x}', t_{\mathrm{R}} + t, \boldsymbol{x})$,

3. $\boldsymbol{z}_{\mathrm{A}}(t_{\mathrm{R}} - t) = \boldsymbol{z}_{\mathrm{B}}(t_{\mathrm{R}} + t)$,

4. $\widetilde{\boldsymbol{x}}_{\mathrm{A}}(t_{\mathrm{R}}, \boldsymbol{x}) = \widetilde{\boldsymbol{x}}_{\mathrm{B}}(t_{\mathrm{R}}, \boldsymbol{x})$,

5. $\Lambda_\nu(\tau_\nu, \widetilde{\boldsymbol{x}}_\nu) = \chi_\nu(\tau_\nu) F_\nu(\widetilde{\boldsymbol{x}}_\nu)$,

6. $\chi_{\mathrm{A}}(\tau) = \chi_{\mathrm{B}}(\upsilon_{\mathrm{R}} - \tau)$,

7. $F_{\mathrm{A}}(\widetilde{\boldsymbol{x}}) = F_{\mathrm{B}}(\widetilde{\boldsymbol{x}})$,

8. $\Omega_{\mathrm{A}} = \Omega_{\mathrm{B}} = \Omega$,

9. $\beta_{\mathrm{A}} + \beta_{\mathrm{B}} = \Omega \upsilon_{\mathrm{R}}$,

10. $|\cos\alpha_{\mathrm{A}}| = |\cos\alpha_{\mathrm{B}}|$, $|\sin\alpha_{\mathrm{A}}| = |\sin\alpha_{\mathrm{B}}|$,

where $\upsilon_{\mathrm{R}} = \tau_{\mathrm{A}}(t_{\mathrm{R}}, \boldsymbol{z}_{\mathrm{A}}(t_{\mathrm{R}})) + \tau_{\mathrm{B}}(t_{\mathrm{R}}, \boldsymbol{z}_{\mathrm{B}}(t_{\mathrm{R}}))$ *and* $s(\rho, \sigma)$ *is the sign function defined in Lemma 9. Moreover, recall that the detectors' initial states are expressed as* $|\psi_\nu\rangle = \cos\alpha_\nu |g_\nu\rangle + \sin\alpha_\nu e^{\mathrm{i}\beta_\nu} |e_\nu\rangle$.

These assumptions are sufficient to fulfill the conditions given in Symmetry 2, thus fulfilling Corollary 1.

This proposition follows analogously to the previous one, by combining the conditions in Symmetry 2 and the Lemmas 2 and 9.

Proposition 7. *Let* $g_{\rho\sigma}$ *be the metric components in an arbitrary coordinate system* $(t, \boldsymbol{x})$, $\boldsymbol{z}_\nu(t)$ *the spatial components of the detectors' trajectories and* $(\tau_\nu, \widetilde{\boldsymbol{x}}_\nu)$ *the Fermi normal coordinates adapted to* $\boldsymbol{z}_\nu(t)$. *Assume that*

1. $g_{\rho\sigma}(t_{\mathrm{R}} - t, \boldsymbol{x}_0 - \boldsymbol{x}) = g_{\rho\sigma}(t_{\mathrm{R}} + t, \boldsymbol{x}_0 + \boldsymbol{x})$,
2. $G_F(t_{\mathrm{R}} - t, \boldsymbol{x}_0 - \boldsymbol{x}, t_{\mathrm{R}} - t', \boldsymbol{x}_0 - \boldsymbol{x}')$
   $= G_F(t_{\mathrm{R}} + t', \boldsymbol{x}_0 + \boldsymbol{x}', t_{\mathrm{R}} + t, \boldsymbol{x}_0 + \boldsymbol{x})$,
3. $\boldsymbol{z}_{\mathrm{A}}(t_{\mathrm{R}} - t) = 2\boldsymbol{x}_0 - \boldsymbol{z}_{\mathrm{B}}(t_{\mathrm{R}} + t)$,
4. $\widetilde{\boldsymbol{x}}_{\mathrm{A}}(t_{\mathrm{R}}, \boldsymbol{x}_0 - \boldsymbol{x}) = \widetilde{\boldsymbol{x}}_{\mathrm{B}}(t_{\mathrm{R}}, \boldsymbol{x}_0 + \boldsymbol{x})$,
5. $\Lambda_\nu(\tau_\nu, \widetilde{\boldsymbol{x}}_\nu) = \chi_\nu(\tau_\nu) F_\nu(\widetilde{\boldsymbol{x}}_\nu)$,
6. $\chi_{\mathrm{A}}(\tau) = \chi_{\mathrm{B}}(\upsilon_{\mathrm{R}} - \tau)$,
7. $F_{\mathrm{A}}(\widetilde{\boldsymbol{x}}) = F_{\mathrm{B}}(\widetilde{\boldsymbol{x}})$,
8. $\Omega_{\mathrm{A}} = \Omega_{\mathrm{B}} = \Omega$,
9. $\beta_{\mathrm{A}} + \beta_{\mathrm{B}} = \Omega\upsilon_{\mathrm{R}}$,
10. $|\cos\alpha_{\mathrm{A}}| = |\cos\alpha_{\mathrm{B}}|$, $|\sin\alpha_{\mathrm{A}}| = |\sin\alpha_{\mathrm{B}}|$,

where $\upsilon_{\mathrm{R}} = \tau_{\mathrm{A}}(t_{\mathrm{R}}, \boldsymbol{x}_0 + \boldsymbol{z}_{\mathrm{A}}(t_{\mathrm{R}})) + \tau_{\mathrm{B}}(t_{\mathrm{R}}, \boldsymbol{x}_0 - \boldsymbol{z}_{\mathrm{B}}(t_{\mathrm{R}}))$. *Moreover, recall that the detectors' initial states are expressed as* $|\psi_\nu\rangle = \cos\alpha_\nu |g_\nu\rangle + \sin\alpha_\nu e^{\mathrm{i}\beta_\nu} |e_\nu\rangle$.

These assumptions are sufficient to fulfill the conditions given in Symmetry 3, thus fulfilling Corollary 1.

This following proposition follows analogously to the previous ones, by combining the conditions in Symmetry 3 and the Lemmas 3 and 11.

A.7 Additional symmetries when swapping the times at which the detectors are switched

In the numerical results of figures 2.4 and 2.6 we have observed symmetries with respect to changing the sign of $\Delta t = t_{\mathrm{B}} - t_{\mathrm{A}}$. Here we show why these symmetries are expected.

Proposition 8. *Assume that*

1. *The spacetime is flat.*
2. *The detectors are inertial and comoving, and start in the ground state.*
3. $G_F(t, \boldsymbol{x}, t', \boldsymbol{x}') = G_F(t', \boldsymbol{x}, t, \boldsymbol{x}')$*, in the comoving frame of reference.*
4. *The switching functions are equal besides a time shift,* $\chi_\nu(t) = \chi(t - t_\nu)$ *(in the comoving frame of reference, where* $\Lambda_\nu(t, \boldsymbol{x}) = \chi_\nu(t) F_\nu(\boldsymbol{x})$*).*
5. *Equal gaps,* $\Omega_{\mathrm{A}} = \Omega_{\mathrm{B}}$*.*

Then,

$$\mathcal{M} = \mathcal{M}_{\mathrm{S}}, \quad \mathcal{M}^{\pm} = \mathcal{M}^{\pm}_{\mathrm{S}}, \tag{A.95}$$

where S *denotes swapping* t_{A} *and* t_{B}*.*

Proof. Using the assumptions to simplify the Eqs. (2.54) and (2.56), and defining $\Omega = \Omega_{\mathrm{A}} = \Omega_{\mathrm{B}}$,

$$\begin{aligned} \mathcal{M} &= -\lambda^2 \int \mathrm{d}t\, \mathrm{d}\boldsymbol{x}\, \mathrm{d}t'\, \mathrm{d}\boldsymbol{x}'\, e^{\mathrm{i}\Omega(t+t')} \chi(t - t_{\mathrm{A}}) \chi(t' - t_{\mathrm{B}}) \\ &\qquad \times F_{\mathrm{A}}(\boldsymbol{x}) F_{\mathrm{B}}(\boldsymbol{x}') G_{\mathrm{F}}(t, \boldsymbol{x}, t', \boldsymbol{x}') \\ &= \mathcal{M}_{\mathrm{S}}, \end{aligned} \tag{A.96}$$

where, to obtain the last equality, we performed a change of variables $t \to t'$, $t' \to t$ and used the hypotheses over and G_{F}.

The same result holds for $\mathcal{M}^{\pm}$, because the only difference is using $G^{\pm}_{\mathrm{F}}$, which have the same symmetries as G_{F}. □

This Proposition 8 implies that the quantities in the plots of Figure 2.4 must be even functions along the Δt axis, which is exactly the case. The condition over G_{F} is automatically fulfilled for the vacuum of Minkowski, as seen in Lemma 4.

Finally, the following proposition applies to the scenario of Figure 2.6, causing the odd symmetry that can be seen in the plot of the relative phase (after adding $\pi/2$ to the relative phase). In such plot, the swap indicated by S in what will be Eqs. (A.97) is equivalent to changing the sign of $\Delta t = t_{\mathrm{B}} - t_{\mathrm{A}}$. The condition over G_{F} is automatically fulfilled for the vacuum of Minkowski, as seen in Lemma 4.

Proposition 9. *Assume that*

1. *The spacetime is flat.*
2. *The detectors are inertial and comoving, and start in the ground state.*
3. $\Lambda_\nu(t, \boldsymbol{x}) = \chi_\nu(t) F_\nu(\boldsymbol{x})$ *in the comoving frame* $(t, \boldsymbol{x})$.
4. $\chi_\nu(t_\nu + t) = \chi_\nu(t_\nu - t)$.
5. $G_F(t, \boldsymbol{x}, t', \boldsymbol{x}') = G_F(t_{\mathrm{A}} + t_{\mathrm{B}} - t, \boldsymbol{x}, t_{\mathrm{A}} + t_{\mathrm{B}} - t', \boldsymbol{x}')$.

Then,

$$|\mathcal{M}^{\pm}| = |\mathcal{M}^{\pm}_{\mathrm{S}}|, \;\; \cos\Delta\gamma = -\cos\left(\Delta\gamma\right)_{\mathrm{S}}, \tag{A.97}$$

where S *indicates swapping* t_{A}, t_{B}, *and* $\Delta\gamma$ *the relative phase between* $\mathcal{M}^{+}$ *and* $\mathcal{M}^{-}$.

Proof. Using the assumptions to simplify the Eqs. (2.54) and (2.56), the definition of $\mathcal{M}^{\pm}$, and that switching t_{A} and t_{B} changes $\chi_{\mathrm{A}}(t)$ into $\chi_{\mathrm{A}}(t+t_{\mathrm{A}}-t_{\mathrm{B}})$ and $\chi_{\mathrm{B}}(t)$ into $\chi_{\mathrm{B}}(t+t_{\mathrm{B}}-t_{\mathrm{A}})$,

$$\begin{aligned}
\mathcal{M}^{\pm}_{\mathrm{S}} &= -\lambda^2 \int \mathrm{d}t\, \mathrm{d}\boldsymbol{x}\, \mathrm{d}t'\, \mathrm{d}\boldsymbol{x}'\, e^{\mathrm{i}(\Omega_{\mathrm{A}} t + \Omega_{\mathrm{B}} t')} G^{\pm}_{\mathrm{F}}(t, \boldsymbol{x}, t', \boldsymbol{x}') \\
&\qquad \times \chi_{\mathrm{A}}(t + t_{\mathrm{A}} - t_{\mathrm{B}}) \chi_{\mathrm{B}}(t' + t_{\mathrm{B}} - t_{\mathrm{A}}) F_{\mathrm{A}}(\boldsymbol{x}) F_{\mathrm{B}}(\boldsymbol{x}') \\
&= -\lambda^2 e^{\mathrm{i}(\Omega_{\mathrm{A}} + \Omega_{\mathrm{B}})(t_{\mathrm{A}} + t_{\mathrm{B}})} \int \mathrm{d}t\, \mathrm{d}\boldsymbol{x}\, \mathrm{d}t'\, \mathrm{d}\boldsymbol{x}'\, e^{-\mathrm{i}(\Omega_{\mathrm{A}} t + \Omega_{\mathrm{B}} t')} \\
&\qquad \times \chi_{\mathrm{A}}(t) \chi_{\mathrm{B}}(t') F_{\mathrm{A}}(\boldsymbol{x}) F_{\mathrm{B}}(\boldsymbol{x}') G^{\pm}_{\mathrm{F}}(t, \boldsymbol{x}, t', \boldsymbol{x}') \\
&= e^{\mathrm{i}(\Omega_{\mathrm{A}} + \Omega_{\mathrm{B}})(t_{\mathrm{A}} + t_{\mathrm{B}})} \mathcal{M}^{\pm}(-\Omega_{\mathrm{A}}, -\Omega_{\mathrm{B}}).
\end{aligned} \tag{A.98}$$

Here, to get the second equality, we performed the change of variables $t \to t_{\mathrm{A}} + t_{\mathrm{B}} - t$, $t' \to t_{\mathrm{A}} + t_{\mathrm{B}} - t'$ and used the hypotheses upon χ_ν and G_{F}.

Finally, we get the Eq. (A.97) by applying Proposition 1 for the case where the initial states of the detector are the ground states, and thus $\mathcal{M}^{\pm}(-\Omega_{\mathrm{A}}, -\Omega_{\mathrm{B}}) = \widetilde{\mathcal{M}}^{\pm}$. □

Appendix B

Appendices for Chapter 3

B.1 Computing the transversal picture Hamiltonian

This appendix derives the expression for $\hat{H}_{\mathrm{T}}$ of Eq. (3.31), via computing the transversal picture of $\hat{\lambda}_{\perp}^{\nu}$ and $\hat{\phi}^{\alpha^{\nu}}$,

$$\hat{\lambda}_{\mathrm{T}}^{\nu} = \hat{U}^{\parallel\dagger}\hat{\lambda}_{\perp}^{\nu}\hat{U}^{\parallel}, \quad \hat{\phi}_{\mathrm{T}}^{\alpha^{\nu}} = \hat{U}^{\parallel\dagger}\hat{\phi}^{\alpha^{\nu}}\hat{U}^{\parallel}. \tag{B.1}$$

First, let us show that

$$\begin{aligned}\hat{U}^{\parallel}(t) &= e^{\hat{\Omega}^{\mathrm{AA}}(t)+\hat{\Omega}^{\mathrm{BB}}(t)+2\hat{\Omega}^{\mathrm{BA}}(t)}\hat{D}_{\hat{\beta}^{\mathrm{A}}(t)}\hat{D}_{\hat{\beta}^{\mathrm{B}}(t)} \\ &= e^{\hat{\Omega}^{\mathrm{AA}}(t)+\hat{\Omega}^{\mathrm{BB}}(t)+2\hat{\Omega}^{\mathrm{AB}}(t)}\hat{D}_{\hat{\beta}^{\mathrm{B}}(t)}\hat{D}_{\hat{\beta}^{\mathrm{A}}(t)},\end{aligned} \tag{B.2}$$

by substituting into Eq. (3.19) the following expressions,

$$\begin{aligned}\hat{D}_{\hat{\beta}^{\mathrm{A}}(t)+\hat{\beta}^{\mathrm{B}}(t)} &= e^{-\mathrm{i}\hat{\phi}^{\hat{\beta}^{\mathrm{A}}(t)}-\mathrm{i}\hat{\phi}^{\hat{\beta}^{\mathrm{B}}(t)}} \\ &= e^{-\mathrm{i}\hat{\phi}^{\hat{\beta}^{\mathrm{A}}(t)}}e^{-\mathrm{i}\hat{\phi}^{\hat{\beta}^{\mathrm{B}}(t)}}e^{\hat{\Omega}^{\mathrm{BA}}(t)-\hat{\Omega}^{\mathrm{AB}}(t)} \\ &= e^{-\mathrm{i}\hat{\phi}^{\hat{\beta}^{\mathrm{B}}(t)}}e^{-\mathrm{i}\hat{\phi}^{\hat{\beta}^{\mathrm{A}}(t)}}e^{\hat{\Omega}^{\mathrm{AB}}(t)-\hat{\Omega}^{\mathrm{BA}}(t)}.\end{aligned} \tag{B.3}$$

Here, we used the Baker-Campbell-Hausdorff formula, $[\hat{\beta}^{\mu}, \hat{\beta}^{\nu}] = 0$, and that

$$\frac{1}{2}[\hat{\phi}^{\hat{\beta}^{\mathrm{A}}(t)}, \hat{\phi}^{\hat{\beta}^{\mathrm{B}}(t)}] = \hat{\Omega}^{\mathrm{BA}}(t) - \hat{\Omega}^{\mathrm{AB}}(t). \tag{B.4}$$

Then, substituting Eq. (B.2) into Eq. (B.1),

$$\begin{aligned}\hat{\lambda}^{\mathrm{A}}_{\mathrm{T}} &= e^{-2\hat{\Omega}^{\mathrm{AB}}}\hat{\Gamma}^{\mathrm{A}}_{\perp}e^{2\hat{\Omega}^{\mathrm{AB}}},\\ \hat{\lambda}^{\mathrm{B}}_{\mathrm{T}} &= e^{-2\hat{\Omega}^{\mathrm{BA}}}\hat{\Gamma}^{\mathrm{B}}_{\perp}e^{2\hat{\Omega}^{\mathrm{BA}}},\\ \hat{\Gamma}^{\nu}_{\perp} &= e^{-\hat{\Omega}^{\nu\nu}}\hat{D}^{\dagger}_{\hat{\beta}^{\nu}}\hat{\lambda}^{\nu}_{\perp}\hat{D}_{\hat{\beta}^{\nu}}e^{\hat{\Omega}^{\nu\nu}}.\end{aligned} \tag{B.5}$$

Here, $\hat{\Gamma}^{\nu}_{\perp}$ is an operator of the field and a transversal operator for the detector ν. Remember that $\hat{\beta}^{\nu}$ and $\hat{\Omega}^{\mu\nu}$ were defined in Eq. (3.16) and $\hat{D}_{\hat{\beta}}$ in Eq. (3.20). In order to obtain the expressions in Eq. (B.5) we used the fact that $\hat{D}_{\hat{\beta}^{\mathrm{B}}}$ and $e^{\hat{\Omega}^{\mathrm{BB}}}$ commute with $\hat{\lambda}^{\mathrm{A}}_{\perp}$, and the analogous statement swapping A and B.

Let us now find the components of $\hat{\Gamma}^{\nu}_{\perp}$ in the basis $\{|i_\nu\rangle\}$,

$$\langle i_\nu|\hat{\Gamma}^{\nu}_{\perp}|i'_\nu\rangle = \langle i_\nu|\hat{\lambda}^{\nu}_{\perp}|i'_\nu\rangle\, e^{\vartheta^{\nu\nu-+}_{ii'ii'}}\hat{D}_{-\beta^{\nu-}_{ii'}}. \tag{B.6}$$

Here, we defined

$$\begin{aligned}\vartheta^{\mu\nu-+}_{ii'jj'}(t) &= \int_{t_\parallel}^{t}\mathrm{d}t_1\int_{t_\parallel}^{t_1}\mathrm{d}t_2\,\lambda^{\mu-}_{\parallel,ii'}(t_1)\lambda^{\nu+}_{\parallel,jj'}(t_2)W^{\mu\nu-}(t_1,t_2),\\ \beta^{\nu-}_{ii'}(t,\boldsymbol{k}) &= \int_{t_\parallel}^{t}\mathrm{d}t_1\,\lambda^{\nu-}_{\parallel,ii'}(t_1)\alpha^{\nu}(t_1,\boldsymbol{k}),\\ \lambda^{\nu\pm}_{\parallel,ii'} &= \lambda^{\nu}_{\parallel,i}\pm\lambda^{\nu}_{\parallel,i'}.\end{aligned} \tag{B.7}$$

In order to find Eq. (B.6), we used the Baker-Campbell-Hausdorff formula to get

$$\begin{aligned}\hat{D}^{\dagger}_{\beta^{\nu}_{i}}\hat{D}_{\beta^{\nu}_{i'}} &= e^{\mathrm{i}\hat{\phi}^{\beta^{\nu}_{i}}}e^{-\mathrm{i}\hat{\phi}^{\beta^{\nu}_{i'}}}\\ &= e^{\mathrm{i}\hat{\phi}^{\beta^{\nu}_{i}}-\mathrm{i}\hat{\phi}^{\beta^{\nu}_{i'}}}e^{\frac{1}{2}[\hat{\phi}^{\beta^{\nu}_{i}},\hat{\phi}^{\beta^{\nu}_{i'}}]}\\ &= e^{\vartheta^{\nu\nu}_{ii'}-\vartheta^{\nu\nu}_{i'i}}\hat{D}_{-\beta^{\nu-}_{ii'}},\end{aligned} \tag{B.8}$$

where $\vartheta^{\mu\nu}_{ij}$ was defined in Eq. (3.26). We also used that

$$\vartheta^{\nu\nu-+}_{ii'ii'} = \vartheta^{\nu\nu}_{ii} - \vartheta^{\nu\nu}_{i'i} + \vartheta^{\nu\nu}_{ii'} - \vartheta^{\nu\nu}_{i'i'}. \tag{B.9}$$

Next, using $\hat{U}^{\parallel}$ from Eq. (3.19),

$$\begin{aligned}\hat{\phi}^{\alpha^{\nu}}_{\mathrm{T}} &= \hat{D}^{\dagger}_{\hat{\beta}^{\mathrm{A}}+\hat{\beta}^{\mathrm{B}}}e^{-\hat{\Omega}_2}\hat{\phi}^{\alpha^{\nu}}e^{\hat{\Omega}_2}\hat{D}_{\hat{\beta}^{\mathrm{A}}+\hat{\beta}^{\mathrm{B}}}\\ &= \hat{D}^{\dagger}_{\hat{\beta}^{\mathrm{A}}+\hat{\beta}^{\mathrm{B}}}\hat{\phi}^{\alpha^{\nu}}\hat{D}_{\hat{\beta}^{\mathrm{A}}+\hat{\beta}^{\mathrm{B}}}\\ &= \hat{\phi}^{\alpha^{\nu}} + \mathrm{i}[\hat{\phi}^{\hat{\beta}^{\mathrm{A}}+\hat{\beta}^{\mathrm{B}}},\hat{\phi}^{\alpha^{\nu}}]\\ &= \hat{\phi}^{\alpha^{\nu}} + \hat{m}^{\mathrm{A}^{\nu}}_{\parallel} + \hat{m}^{\mathrm{B}^{\nu}}_{\parallel},\end{aligned} \tag{B.10}$$

Here, we used that

$$\hat{D}^{\dagger}_{\hat{\beta}}\hat{\phi}^{\alpha}\hat{D}_{\hat{\beta}} = \hat{\phi}^{\alpha} + \mathrm{i}[\hat{\phi}^{\hat{\beta}}, \hat{\phi}^{\alpha}]. \tag{B.11}$$

This equality can be derived from the Campbell identity,

$$e^{\hat{X}}\hat{Y}e^{-\hat{X}} = \hat{Y} + \big[\hat{X}, \hat{Y}\big] + \frac{1}{2!}\big[\hat{X}, \big[\hat{X}, \hat{Y}\big]\big] + \ldots, \tag{B.12}$$

by using that the nested commutators of $\hat{\phi}^{\hat{\beta}}$ and $\hat{\phi}^{\alpha}$ go to zero. This is true because the $\hat{\beta}(\boldsymbol{k})$ commute among themselves and with $\hat{a}_{\boldsymbol{k}}$, and $[\hat{a}_{\boldsymbol{k}}, \hat{a}^{\dagger}_{\boldsymbol{k}'}] = \delta(\boldsymbol{k} - \boldsymbol{k}')\hat{\mathbb{1}}$. Moreover, we defined

$$\begin{aligned}\hat{m}_{\parallel}^{\mu^{\nu}}(t) &= \mathrm{i}[\hat{\phi}^{\hat{\beta}^{\mu}}(t), \hat{\phi}^{\alpha^{\nu}}(t)], \\ &= 2\mathrm{i}\int_{t_{\parallel}}^{t} \mathrm{d}t_1\, \hat{\lambda}^{\mu}_{\parallel}(t_1) W^{\mu\nu-}(t_1, t),\end{aligned} \tag{B.13}$$

which are longitudinal operators of the detector μ. To find the explicit expression for the commutator in the second line, we used Eqs. (3.15), (3.18), and that $\hat{\lambda}^{\mu}_{\parallel}$ is Hermitian.

Finally, combining the results above, one finds that

$$\hat{H}_{\mathrm{T}} = \sum_{\nu} \hat{\lambda}^{\nu}_{\mathrm{T}}(\hat{\phi}^{\alpha^{\nu}} + \hat{m}_{\parallel}^{\mathrm{A}^{\nu}} + \hat{m}_{\parallel}^{\mathrm{B}^{\nu}}), \tag{B.14}$$

with $\hat{\lambda}^{\nu}_{\mathrm{T}}$ from Eq. (B.5) and $\hat{m}_{\parallel}^{\mu^{\nu}}$ from Eq. (B.13). Here it becomes apparent that the field is mediating an interaction between the detectors, since $\hat{H}_{\mathrm{T}}$ contains terms such as $\hat{\lambda}^{\mathrm{A}}_{\mathrm{T}}\hat{m}_{\parallel}^{\mathrm{B}^{\mathrm{A}}}$ and $\hat{\lambda}^{\mathrm{B}}_{\mathrm{T}}\hat{m}_{\parallel}^{\mathrm{A}^{\mathrm{B}}}$, which involve both detectors.

B.2 Perturbative expansion of the longitudinal evolution

As a check, we recover the Dyson expansion for $\hat{U}(t)$ from the expression we obtained in Eq. (3.39) which includes the non-perturbative longitudinal interaction and the perturbative transversal interaction.

The expression for $\hat{U}(t)$ is

$$\hat{U}(t) = \mathcal{T}\exp\left(-\mathrm{i}\int_{t_0}^{t} \mathrm{d}t_1\, \hat{H}_{\mathrm{I}}(t_1)\right). \tag{B.15}$$

Therefore, we aim to recover the following Dyson expansion,

$$\hat{U}(t) = \hat{U}^{(0)}(t) + \hat{U}^{(1)}(t) + \hat{U}^{(2)}(t) + \mathcal{O}(\hat{H}_{\mathrm{I}}^3), \tag{B.16}$$

$$\begin{aligned}
\hat{U}^{(0)}(t) &= \hat{\mathbb{1}}, \\
\hat{U}^{(1)}(t) &= -\mathrm{i}\int_{t_0}^{t} \mathrm{d}t_1\, \hat{H}_{\mathrm{I}}(t_1), \\
\hat{U}^{(2)}(t) &= -\int_{t_0}^{t} \mathrm{d}t_1 \int_{t_0}^{t_1} \mathrm{d}t_2\, \hat{H}_{\mathrm{I}}(t_1)\hat{H}_{\mathrm{I}}(t_2),
\end{aligned} \tag{B.17}$$

by performing an expansion of Eq. (3.39) up to second order on the longitudinal interaction $\hat{H}_{\parallel}$, and its corresponding parameter, $\lambda_{\parallel}$.

First, let us expand $\hat{U}^{\parallel}$ from Eq. (3.19),

$$\begin{aligned}
\hat{U}^{\parallel}(t) &= e^{\hat{\Omega}_2(t)} e^{-\mathrm{i}\hat{\phi}^{\hat{\beta}^{\mathrm{A}}(t)+\hat{\beta}^{\mathrm{B}}(t)}} \\
&= \Big(\hat{\mathbb{1}} + \hat{\Omega}_2(t) + \mathcal{O}\big(\lambda_{\parallel}^4\big)\Big)\Big(\hat{\mathbb{1}} - \mathrm{i}\hat{\phi}^{\hat{\beta}^{\mathrm{A}}(t)+\hat{\beta}^{\mathrm{B}}(t)} \\
&\quad - \frac{1}{2}\big(\hat{\phi}^{\hat{\beta}^{\mathrm{A}}(t)+\hat{\beta}^{\mathrm{B}}(t)}\big)^2 + \mathcal{O}\big(\lambda_{\parallel}^3\big)\Big) \\
&= \hat{\mathbb{1}} - \mathrm{i}\hat{\phi}^{\hat{\beta}^{\mathrm{A}}(t)+\hat{\beta}^{\mathrm{B}}(t)} + \hat{\Omega}_2(t) - \frac{1}{2}\big(\hat{\phi}^{\hat{\beta}^{\mathrm{A}}(t)+\hat{\beta}^{\mathrm{B}}(t)}\big)^2 \\
&\quad + \mathcal{O}\big(\lambda_{\parallel}^3\big),
\end{aligned} \tag{B.18}$$

Here, we can identify

$$\hat{U}^{\parallel}(t) = \hat{U}^{\parallel(0)}(t) + \hat{U}^{\parallel(1)}(t) + \hat{U}^{\parallel(2)}(t) + \mathcal{O}\big(\lambda_{\parallel}^3\big), \tag{B.19}$$

$$
\begin{aligned}
\hat{U}^{\parallel(0)}(t) &= \hat{\mathbb{1}}, \\
\hat{U}^{\parallel(1)}(t) &= -\mathrm{i}\hat{\phi}^{\hat{\beta}^{\mathrm{A}}(t)+\hat{\beta}^{\mathrm{B}}(t)} \\
&= -\mathrm{i}\int_{t_\parallel}^{t} \mathrm{d}t_1\, \hat{H}_\parallel(t_1), \\
\hat{U}^{\parallel(2)}(t) &= \hat{\Omega}_2(t) - \left(\hat{\phi}^{\hat{\beta}^{\mathrm{A}}(t)+\hat{\beta}^{\mathrm{B}}(t)}\right)^2 \\
&= -\frac{1}{2}\int_{t_\parallel}^{t} \mathrm{d}t_1 \int_{t_\parallel}^{t_1} \mathrm{d}t_2\, [\hat{H}_\parallel(t_1), \hat{H}_\parallel(t_2)] \\
&\quad - \frac{1}{2}\int_{t_\parallel}^{t} \mathrm{d}t_1 \int_{t_\parallel}^{t} \mathrm{d}t_2\, \hat{H}_\parallel(t_1)\hat{H}_\parallel(t_2) \\
&= -\int_{t_\parallel}^{t} \mathrm{d}t_1 \int_{t_\parallel}^{t_1} \mathrm{d}t_2\, \hat{H}_\parallel(t_1)\hat{H}_\parallel(t_2),
\end{aligned}
\tag{B.20}
$$

which is the result that we would have expected if we computed $\hat{U}^{\parallel}$ via a Dyson expansion instead of analytically.

On what follows, for simplicity, we take the choice $t_\parallel = t_0$. Then, using the expansion for $\hat{U}^{\parallel}$, Eq. (3.38) becomes

$$
\begin{aligned}
\hat{U} &= \left(\hat{U}^{\parallel(0)} + \hat{U}^{\parallel(1)} + \hat{U}^{\parallel(2)} + \mathcal{O}\big(\lambda_\parallel^3\big)\right) \\
&\quad \times \left(\hat{\mathcal{U}}^{(0)} + \hat{\mathcal{U}}^{(1)} + \hat{\mathcal{U}}^{(2)} + \mathcal{O}\big(\hat{H}_\perp^3\big)\right) \\
&= \hat{\mathbb{1}} + \hat{U}^{\parallel(1)} + \hat{\mathcal{U}}^{(1)} + \hat{U}^{\parallel(2)} + \hat{U}^{\parallel(1)}\hat{\mathcal{U}}^{(1)} + \hat{\mathcal{U}}^{(2)} + \mathcal{O}(\hat{H}_{\mathrm{I}}^3),
\end{aligned}
\tag{B.21}
$$

where $\mathcal{O}(\hat{H}_{\mathrm{I}}^3)$ includes any terms of order $\lambda_\parallel^3$, $\lambda_\parallel^2\lambda_\perp$, $\lambda_\parallel\lambda_\perp^2$, $\lambda_\perp^3$ or higher.

Now, let us also take a perturbative expansion of the $\hat{\mathcal{U}}^{(1)}$ and $\hat{\mathcal{U}}^{(2)}$ from Eq. (3.33),

$$
\begin{aligned}
\hat{\mathcal{U}}^{(1)}(t) &= -\mathrm{i}\int_{t_0}^{t} \mathrm{d}t_1\, \hat{H}_\perp(t_1) \\
&\quad - \int_{t_0}^{t} \mathrm{d}t_1 \int_{t_0}^{t_1} \mathrm{d}t_2\, [\hat{H}_\perp(t_1), \hat{H}_\parallel(t_2)] + \mathcal{O}\big(\lambda_\parallel^2\lambda_\perp\big), \\
\hat{\mathcal{U}}^{(2)}(t) &= -\int_{t_0}^{t} \mathrm{d}t_1 \int_{t_0}^{t_1} \mathrm{d}t_2\, \hat{H}_\perp(t_1)\hat{H}_\perp(t_2) + \mathcal{O}\big(\lambda_\parallel\lambda_\perp^2\big),
\end{aligned}
\tag{B.22}
$$

where we used Eq. (B.20) with the choice $t_\parallel = t_0$, and that

$$\begin{aligned}\hat{H}_{\scriptscriptstyle T} &= \hat{U}^{\parallel\dagger}\hat{H}_\perp\hat{U}^{\parallel} \\ &= \hat{H}_\perp + \hat{U}^{\parallel(1)\dagger}\hat{H}_\perp + \hat{H}_\perp\hat{U}^{\parallel(1)} + \mathcal{O}\big(\lambda_\parallel^2\lambda_\perp\big).\end{aligned} \tag{B.23}$$

Now, combining Eqs. (B.21) and (B.22), and grouping terms of the same order in $\hat{H}_{\rm I} = \hat{H}_\parallel + \hat{H}_\perp$, we find that

$$\begin{aligned}\hat{U}^{(0)}(t) &= \hat{\mathbb{1}}, \\ \hat{U}^{(1)}(t) &= \hat{U}^{\parallel(1)} - \mathrm{i}\int_{t_0}^{t}\mathrm{d}t_1\,\hat{H}_\perp(t_1) \\ &= -\mathrm{i}\int_{t_0}^{t}\mathrm{d}t_1\,\hat{H}_{\rm I}(t_1),\end{aligned} \tag{B.24}$$

$$\begin{aligned}\hat{U}^{(2)}(t) &= -\int_{t_0}^{t}\mathrm{d}t_1\int_{t_0}^{t}\mathrm{d}t_2\,\hat{H}_\parallel(t_1)\hat{H}_\perp(t_2) \\ &\quad -\int_{t_0}^{t}\mathrm{d}t_1\int_{t_0}^{t_1}\mathrm{d}t_2\,\Big(\hat{H}_\parallel(t_1)\hat{H}_\parallel(t_2) \\ &\qquad + [\hat{H}_\perp(t_1),\hat{H}_\parallel(t_2)] + \hat{H}_\perp(t_1)\hat{H}_\perp(t_2)\Big) \\ &= -\int_{t_0}^{t}\mathrm{d}t_1\int_{t_0}^{t_1}\mathrm{d}t_2\,\hat{H}_\parallel(t_1)\hat{H}_\parallel(t_2).\end{aligned} \tag{B.25}$$

These results match the Dyson expansion of $\hat{U}$ provided in (B.17), showing that taking a perturbative expansion with respect to the longitudinal interaction in the expression for $\hat{U}$ of Eq. (3.39) recovers the expected result.

B.3 Interaction picture state in the longitudinal basis

Here, we provide $\hat{\rho}(t)$ in the chosen detector bases $\{|i_{\rm A}\rangle\}$ and $\{|j_{\rm B}\rangle\}$. Remember that $\hat{\rho}(t)$ is the state of the field and detectors for which we performed the entanglement harvesting protocol, and the detector bases are the ones used to define longitudinal and transversal. Specifically, we will give expressions for the field operators $\langle i_{\rm A}j_{\rm B}|\hat{\rho}(t)|i'_{\rm A}j'_{\rm B}\rangle$, which can be used to reconstruct the state of the detectors and the field at any time,

$$\hat{\rho}(t) = \sum_{iji'j'}|i_{\rm A}j_{\rm B}\rangle\langle i'_{\rm A}j'_{\rm B}|\otimes\langle i_{\rm A}j_{\rm B}|\hat{\rho}(t)|i'_{\rm A}j'_{\rm B}\rangle\,. \tag{B.26}$$

In order to organize the expression for $\hat{\rho}(t)$, let us define

$$\begin{aligned}
&\hat{H}^{\nu}_{\mathrm{T}} = \hat{\lambda}^{\nu}_{\mathrm{T}}\hat{\phi}^{\alpha^{\nu}}_{\mathrm{T}},\\
&\hat{\mathcal{U}}^{\nu}(t) = -\mathrm{i}\int_{t_0}^{t}\mathrm{d}t_1\,\hat{H}^{\nu}_{\mathrm{T}}(t_1),\\
&\hat{\mathcal{U}}^{\mu\nu}(t) = -\int_{t_0}^{t}\mathrm{d}t_1\int_{t_0}^{t_1}\mathrm{d}t_2\,\hat{H}^{\mu}_{\mathrm{T}}(t_1)\hat{H}^{\nu}_{\mathrm{T}}(t_2),
\end{aligned} \tag{B.27}$$

so that

$$\hat{H}_{\mathrm{T}} = \sum_{\nu}\hat{H}^{\nu}_{\mathrm{T}},\ \hat{\mathcal{U}}^{(1)} = \sum_{\nu}\hat{\mathcal{U}}^{\nu},\ \hat{\mathcal{U}}^{(2)} = \sum_{\mu\nu}\hat{\mathcal{U}}^{\mu\nu}. \tag{B.28}$$

Moreover, taking $t_{\parallel} = t_0$ for simplicity, define

$$\begin{aligned}
&\hat{\rho}^{(\nu,0)} = \hat{U}^{\parallel}\hat{\mathcal{U}}^{\nu}\hat{\rho}_0\hat{U}^{\parallel\dagger} = \hat{\rho}^{(0,\nu)\dagger},\\
&\hat{\rho}^{(\mu,\nu)} = \hat{U}^{\parallel}\hat{\mathcal{U}}^{\mu}\hat{\rho}_0\hat{\mathcal{U}}^{\nu\dagger}\hat{U}^{\parallel\dagger} = \hat{\rho}^{(\nu,\mu)\dagger},\\
&\hat{\rho}^{(\mu\nu,0)} = \hat{U}^{\parallel}\hat{\mathcal{U}}^{\mu\nu}\hat{\rho}_0\hat{U}^{\parallel\dagger} = \hat{\rho}^{(0,\mu\nu)\dagger},
\end{aligned} \tag{B.29}$$

so that

$$\hat{\rho}^{(1,0)} = \sum_{\nu}\hat{\rho}^{(\nu,0)},\ \hat{\rho}^{(1,1)} = \sum_{\mu\nu}\hat{\rho}^{(\mu,\nu)},\ \hat{\rho}^{(2,0)} = \sum_{\mu\nu}\hat{\rho}^{(\mu\nu,0)}. \tag{B.30}$$

Considering the above together with

$$\begin{aligned}
\langle i_{\mathrm{A}}j_{\mathrm{B}}|\hat{\rho}|i'_{\mathrm{A}}j'_{\mathrm{B}}\rangle = \langle i_{\mathrm{A}}j_{\mathrm{B}}|\,\big(&\hat{\rho}^{(0,0)} + \hat{\rho}^{(1,0)} + \hat{\rho}^{(0,1)} + \hat{\rho}^{(1,1)}\\
&+ \hat{\rho}^{(2,0)} + \hat{\rho}^{(0,2)}\big)\,|i'_{\mathrm{A}}j'_{\mathrm{B}}\rangle + \mathcal{O}\big(\lambda_{\perp}^{3}\big),
\end{aligned} \tag{B.31}$$

and $\hat{\rho}^{(0,1)} = \hat{\rho}^{(1,0)\dagger}$, $\hat{\rho}^{(0,2)} = \hat{\rho}^{(2,0)\dagger}$, we see that it is enough to provide expressions for

$$\begin{aligned}
&\langle i_{\mathrm{A}}j_{\mathrm{B}}|\hat{\rho}^{(0,0)}|i'_{\mathrm{A}}j'_{\mathrm{B}}\rangle\,,\ \ \langle i_{\mathrm{A}}j_{\mathrm{B}}|\hat{\rho}^{(\nu,0)}|i'_{\mathrm{A}}j'_{\mathrm{B}}\rangle\,,\\
&\langle i_{\mathrm{A}}j_{\mathrm{B}}|\hat{\rho}^{(\mu,\nu)}|i'_{\mathrm{A}}j'_{\mathrm{B}}\rangle\,,\ \ \langle i_{\mathrm{A}}j_{\mathrm{B}}|\hat{\rho}^{(\mu\nu,0)}|i'_{\mathrm{A}}j'_{\mathrm{B}}\rangle\,,
\end{aligned} \tag{B.32}$$

for $\mu,\nu \in \{\mathrm{A},\mathrm{B}\}$, as done next.

$$\langle i_{\mathrm{A}}j_{\mathrm{B}}|\hat{\rho}^{(0,0)}|i'_{\mathrm{A}}j'_{\mathrm{B}}\rangle = \hat{U}^{\parallel}_{ij}\,\langle i_{\mathrm{A}}j_{\mathrm{B}}|\hat{\rho}_0|i'_{\mathrm{A}}j'_{\mathrm{B}}\rangle\,\hat{U}^{\parallel\dagger}_{i'j'}, \tag{B.33}$$

$$
\begin{aligned}
\langle i_{\mathrm{A}} j_{\mathrm{B}}|\hat{\rho}^{(\mathrm{A},0)}|i'_{\mathrm{A}} j'_{\mathrm{B}}\rangle &= \hat{U}^{\parallel}_{ij} \sum_{k\neq i} \hat{\mathcal{U}}^{\mathrm{A}}_{ijkj} \langle k_{\mathrm{A}} j_{\mathrm{B}}|\hat{\rho}_0|i'_{\mathrm{A}} j'_{\mathrm{B}}\rangle \hat{U}^{\parallel\dagger}_{i'j'}, \\
\langle i_{\mathrm{A}} j_{\mathrm{B}}|\hat{\rho}^{(\mathrm{B},0)}|i'_{\mathrm{A}} j'_{\mathrm{B}}\rangle &= \hat{U}^{\parallel}_{ij} \sum_{l\neq j} \hat{\mathcal{U}}^{\mathrm{B}}_{ijil} \langle i_{\mathrm{A}} l_{\mathrm{B}}|\hat{\rho}_0|i'_{\mathrm{A}} j'_{\mathrm{B}}\rangle \hat{U}^{\parallel\dagger}_{i'j'},
\end{aligned}
\tag{B.34}
$$

$$
\begin{aligned}
&\langle i_{\mathrm{A}} j_{\mathrm{B}}|\hat{\rho}^{(\mathrm{A},\mathrm{A})}|i'_{\mathrm{A}} j'_{\mathrm{B}}\rangle \\
&= \hat{U}^{\parallel}_{ij} \sum_{k\neq i} \sum_{k'\neq i'} \hat{\mathcal{U}}^{\mathrm{A}}_{ijkj} \langle k_{\mathrm{A}} j_{\mathrm{B}}|\hat{\rho}_0|k'_{\mathrm{A}} j'_{\mathrm{B}}\rangle \left(\hat{\mathcal{U}}^{\mathrm{A}}_{i'j'k'j'}\right)^{\dagger} \hat{U}^{\parallel\dagger}_{i'j'}, \\
&\langle i_{\mathrm{A}} j_{\mathrm{B}}|\hat{\rho}^{(\mathrm{A},\mathrm{B})}|i'_{\mathrm{A}} j'_{\mathrm{B}}\rangle \\
&= \hat{U}^{\parallel}_{ij} \sum_{k\neq i} \sum_{l'\neq j'} \hat{\mathcal{U}}^{\mathrm{A}}_{ijkj} \langle k_{\mathrm{A}} j_{\mathrm{B}}|\hat{\rho}_0|i'_{\mathrm{A}} l'_{\mathrm{B}}\rangle \left(\hat{\mathcal{U}}^{\mathrm{B}}_{i'j'i'l'}\right)^{\dagger} \hat{U}^{\parallel\dagger}_{i'j'}, \\
&\langle i_{\mathrm{A}} j_{\mathrm{B}}|\hat{\rho}^{(\mathrm{B},\mathrm{A})}|i'_{\mathrm{A}} j'_{\mathrm{B}}\rangle \\
&= \hat{U}^{\parallel}_{ij} \sum_{l\neq j} \sum_{l'\neq j'} \hat{\mathcal{U}}^{\mathrm{B}}_{ijil} \langle i_{\mathrm{A}} l_{\mathrm{B}}|\hat{\rho}_0|k'_{\mathrm{A}} j'_{\mathrm{B}}\rangle \left(\hat{\mathcal{U}}^{\mathrm{A}}_{i'j'k'j'}\right)^{\dagger} \hat{U}^{\parallel\dagger}_{i'j'}, \\
&\langle i_{\mathrm{A}} j_{\mathrm{B}}|\hat{\rho}^{(\mathrm{B},\mathrm{B})}|i'_{\mathrm{A}} j'_{\mathrm{B}}\rangle \\
&= \hat{U}^{\parallel}_{ij} \sum_{l\neq j} \sum_{l'\neq j'} \hat{\mathcal{U}}^{\mathrm{B}}_{ijil} \langle i_{\mathrm{A}} l_{\mathrm{B}}|\hat{\rho}_0|i'_{\mathrm{A}} l'_{\mathrm{B}}\rangle \left(\hat{\mathcal{U}}^{\mathrm{B}}_{i'j'i'l'}\right)^{\dagger} \hat{U}^{\parallel\dagger}_{i'j'},
\end{aligned}
\tag{B.35}
$$

$$
\begin{aligned}
\langle i_{\mathrm{A}} j_{\mathrm{B}}|\hat{\rho}^{(\mathrm{AA},0)}|i'_{\mathrm{A}} j'_{\mathrm{B}}\rangle &= \hat{U}^{\parallel}_{ij} \sum_{k} \hat{\mathcal{U}}^{\mathrm{AA}}_{ijkj} \langle k_{\mathrm{A}} j_{\mathrm{B}}|\hat{\rho}_0|i'_{\mathrm{A}} j'_{\mathrm{B}}\rangle \hat{U}^{\parallel\dagger}_{i'j'}, \\
\langle i_{\mathrm{A}} j_{\mathrm{B}}|\hat{\rho}^{(\mathrm{AB},0)}|i'_{\mathrm{A}} j'_{\mathrm{B}}\rangle &= \hat{U}^{\parallel}_{ij} \sum_{k\neq i} \sum_{l\neq j} \hat{\mathcal{U}}^{\mathrm{AB}}_{ijkl} \langle k_{\mathrm{A}} l_{\mathrm{B}}|\hat{\rho}_0|i'_{\mathrm{A}} j'_{\mathrm{B}}\rangle \hat{U}^{\parallel\dagger}_{i'j'}, \\
\langle i_{\mathrm{A}} j_{\mathrm{B}}|\hat{\rho}^{(\mathrm{BA},0)}|i'_{\mathrm{A}} j'_{\mathrm{B}}\rangle &= \hat{U}^{\parallel}_{ij} \sum_{k\neq i} \sum_{l\neq j} \hat{\mathcal{U}}^{\mathrm{BA}}_{ijkl} \langle k_{\mathrm{A}} l_{\mathrm{B}}|\hat{\rho}_0|i'_{\mathrm{A}} j'_{\mathrm{B}}\rangle \hat{U}^{\parallel\dagger}_{i'j'}, \\
\langle i_{\mathrm{A}} j_{\mathrm{B}}|\hat{\rho}^{(\mathrm{BB},0)}|i'_{\mathrm{A}} j'_{\mathrm{B}}\rangle &= \hat{U}^{\parallel}_{ij} \sum_{l} \hat{\mathcal{U}}^{\mathrm{BB}}_{ijil} \langle i_{\mathrm{A}} l_{\mathrm{B}}|\hat{\rho}_0|i'_{\mathrm{A}} j'_{\mathrm{B}}\rangle \hat{U}^{\parallel\dagger}_{i'j'}.
\end{aligned}
\tag{B.36}
$$

Here, we denoted

$$
\begin{aligned}
\hat{U}^{\parallel}_{ij} &= \langle i_{\mathrm{A}} j_{\mathrm{B}}|\hat{U}^{\parallel}|i_{\mathrm{A}} j_{\mathrm{B}}\rangle, \\
\hat{\mathcal{U}}^{\nu}_{iji'j'} &= \langle i_{\mathrm{A}} j_{\mathrm{B}}|\, \hat{\mathcal{U}}^{\nu}\, |i'_{\mathrm{A}} j'_{\mathrm{B}}\rangle, \\
\hat{\mathcal{U}}^{\mu\nu}_{iji'j'} &= \langle i_{\mathrm{A}} j_{\mathrm{B}}|\, \hat{\mathcal{U}}^{\mu\nu}\, |i'_{\mathrm{A}} j'_{\mathrm{B}}\rangle.
\end{aligned}
\tag{B.37}
$$

Moreover, to derive the equations above, we used that $\hat{U}^{\parallel}$ is longitudinal and thus diagonal with respect to $\{|i_{\mathrm{A}}\rangle\}$ and $\{|j_{\mathrm{B}}\rangle\}$, while $\hat{\mathcal{U}}^{\mathrm{A}}$ is transversal with respect to $\{|i_{\mathrm{A}}\rangle\}$ and longitudinal with respect to $\{|j_{\mathrm{B}}\rangle\}$. Additionally, $\hat{\mathcal{U}}^{\mathrm{AB}}$ is transversal with respect to both $\{|i_{\mathrm{A}}\rangle\}$ and $\{|j_{\mathrm{B}}\rangle\}$, and $\hat{\mathcal{U}}^{\mathrm{AA}}$ is longitudinal with respect to $\{|j_{\mathrm{B}}\rangle\}$. All these statements are also true upon swapping the detector labels.

Next, we provide explicit expressions for the field operators $\hat{U}^{\parallel}_{ij}$, $\hat{\mathcal{U}}^{\nu}_{iji'j'}$, $\hat{\mathcal{U}}^{\mu\nu}_{iji'j'}$, defined in Eq. (B.37).

First, using Eq. (3.27),

$$\hat{U}^{\parallel}_{ij} = e^{\Omega_{2,ij}}\, \hat{D}_{\beta^{\mathrm{A}}_i + \beta^{\mathrm{B}}_j}, \tag{B.38}$$

where $\hat{D}_{\beta^{\mathrm{A}}_i + \beta^{\mathrm{B}}_j}$ is a displacement (see Eq. (3.21)). Moreover,

$$\begin{aligned}
&\Omega_{2,ij} = -\vartheta^{\mathrm{AA}}_{ii} - \vartheta^{\mathrm{BB}}_{jj} - \vartheta^{\mathrm{AB}}_{ij} - \vartheta^{\mathrm{BA}}_{ji}\,,\\
&\vartheta^{\mu\nu}_{ij}(t) = \int_{t_{\parallel}}^{t} \mathrm{d}t_1 \int_{t_{\parallel}}^{t_1} \mathrm{d}t_2\, \lambda^{\mu}_{\parallel,i}(t_1)\lambda^{\nu}_{\parallel,j}(t_2) W^{\mu\nu -}(t_1,t_2),\\
&\beta^{\nu}_i(t,\boldsymbol{k}) = \int_{t_{\parallel}}^{t} \mathrm{d}t_1\, \lambda^{\nu}_{\parallel,i}(t_1)\alpha^{\nu}(t_1,\boldsymbol{k}),\\
&\lambda^{\nu}_{\parallel,i} = \langle i_\nu|\, \hat{\lambda}^{\nu}_{\parallel}\, |i_\nu\rangle\,,
\end{aligned} \tag{B.39}$$

with $W^{\mu\nu -}$ from Eq. (3.14), and α^{ν} from Eq. (3.1). Here, remember that we picked $t_{\parallel} = t_0$.

Second,

$$\begin{aligned}
\hat{\mathcal{U}}^{\mathrm{A}}_{iji'j'}(t) &= -\mathrm{i}\delta_{jj'} \int_{t_0}^{t} \mathrm{d}t_1\, \hat{\lambda}^{\mathrm{A}}_{\mathrm{T},iji'j'}(t_1)\hat{\phi}^{\alpha^{\mathrm{A}}}_{\mathrm{T},i'j'}(t_1),\\
\hat{\mathcal{U}}^{\mathrm{B}}_{iji'j'}(t) &= -\mathrm{i}\delta_{ii'} \int_{t_0}^{t} \mathrm{d}t_1\, \hat{\lambda}^{\mathrm{B}}_{\mathrm{T},i'ji'j'}(t_1)\hat{\phi}^{\alpha^{\mathrm{B}}}_{\mathrm{T},i'j'}(t_1),
\end{aligned} \tag{B.40}$$

$$
\begin{aligned}
\hat{\mathcal{U}}^{\mathrm{AA}}_{ijj'i'j'}(t) &= -\delta_{jj'}\int_{t_0}^{t}\mathrm{d}t_1\int_{t_0}^{t_1}\mathrm{d}t_2\sum_{k\neq i,i'}\hat{\lambda}^{\mathrm{A}}_{\mathrm{T},ij'kj'}(t_1)\\
&\quad\times\hat{\lambda}^{\mathrm{A}}_{\mathrm{T},kj'i'j'}(t_2)\hat{\phi}^{\alpha^{\mathrm{A}}}_{\mathrm{T},i'j'}(t_1)\hat{\phi}^{\alpha^{\mathrm{A}}}_{\mathrm{T},i'j'}(t_2),\\
\hat{\mathcal{U}}^{\mathrm{BB}}_{ijj'i'j'}(t) &= -\delta_{ii'}\int_{t_0}^{t}\mathrm{d}t_1\int_{t_0}^{t_1}\mathrm{d}t_2\sum_{l\neq j,j'}\hat{\lambda}^{\mathrm{B}}_{\mathrm{T},i'jli'l}(t_1)\\
&\quad\times\hat{\lambda}^{\mathrm{B}}_{\mathrm{T},i'li'j'}(t_2)\hat{\phi}^{\alpha^{\mathrm{B}}}_{\mathrm{T},i'j'}(t_1)\hat{\phi}^{\alpha^{\mathrm{B}}}_{\mathrm{T},i'j'}(t_2),\\
\hat{\mathcal{U}}^{\mathrm{AB}}_{ijj'i'j'}(t) &= -\int_{t_0}^{t}\mathrm{d}t_1\int_{t_0}^{t_1}\mathrm{d}t_2\,\hat{\lambda}^{\mathrm{A}}_{\mathrm{T},ijj'i'j}(t_1)\\
&\quad\times\hat{\lambda}^{\mathrm{B}}_{\mathrm{T},i'jj'i'j'}(t_2)\hat{\phi}^{\alpha^{\mathrm{A}}}_{\mathrm{T},i'j'}(t_1)\hat{\phi}^{\alpha^{\mathrm{B}}}_{\mathrm{T},i'j'}(t_2),\\
\hat{\mathcal{U}}^{\mathrm{BA}}_{ijj'i'j'}(t) &= -\int_{t_0}^{t}\mathrm{d}t_1\int_{t_0}^{t_1}\mathrm{d}t_2\,\hat{\lambda}^{\mathrm{B}}_{\mathrm{T},ijij'}(t_1)\\
&\quad\times\hat{\lambda}^{\mathrm{A}}_{\mathrm{T},ij'i'j'}(t_2)\hat{\phi}^{\alpha^{\mathrm{B}}}_{\mathrm{T},i'j'}(t_1)\hat{\phi}^{\alpha^{\mathrm{A}}}_{\mathrm{T},i'j'}(t_2),
\end{aligned}
\tag{B.41}
$$

where by $\sum_{k\neq i,i'}$ we mean summing over all the possible values of the index k, except for the cases when k equals to i or i'. Moreover,

$$
\begin{aligned}
\hat{\phi}^{\alpha^{\nu}}_{\mathrm{T},ij} &= \langle i_{\mathrm{A}}j_{\mathrm{B}}|\hat{\phi}^{\alpha^{\nu}}_{\mathrm{T}}|i_{\mathrm{A}}j_{\mathrm{B}}\rangle\,,\\
\hat{\lambda}^{\nu}_{\mathrm{T},iji'j'} &= \langle i_{\mathrm{A}}j_{\mathrm{B}}|\,\hat{\lambda}^{\nu}_{\mathrm{T}}\,|i'_{\mathrm{A}}j'_{\mathrm{B}}\rangle\,,
\end{aligned}
\tag{B.42}
$$

and using Appendix B.1,

$$
\begin{aligned}
&\hat{\phi}^{\alpha^{\nu}}_{\mathrm{T},ij} = \hat{\phi}^{\alpha^{\nu}} + \big(m^{\mathrm{A}^{\nu}}_{\parallel,i} + m^{\mathrm{B}^{\nu}}_{\parallel,j}\big)\hat{\mathbb{1}},\\
&m^{\mu^{\nu}}_{\parallel,i}(t) = \langle i_{\mu}|\hat{m}^{\mu^{\nu}}_{\parallel}(t)|i_{\mu}\rangle = 2\mathrm{i}\int_{t_{\parallel}}^{t}\mathrm{d}t_1\,\lambda^{\mu}_{\parallel,i}(t_1)W^{\mu\nu-}(t_1,t),\\
&\hat{\lambda}^{\mathrm{A}}_{\mathrm{T},iji'j'} = \delta_{jj'}\,\langle i_{\mathrm{A}}|\hat{\lambda}^{\mathrm{A}}_{\perp}|i'_{\mathrm{A}}\rangle\,e^{2\vartheta^{\mathrm{AB}}_{ij}-2\vartheta^{\mathrm{AB}}_{i'j}+\vartheta^{\mathrm{AA}-+}_{ii'ii'}}\hat{D}_{-\beta^{\mathrm{A}-}_{ii'}},\\
&\hat{\lambda}^{\mathrm{B}}_{\mathrm{T},iji'j'} = \delta_{ii'}\,\langle j_{\mathrm{B}}|\hat{\lambda}^{\mathrm{B}}_{\perp}|j'_{\mathrm{B}}\rangle\,e^{2\vartheta^{\mathrm{BA}}_{ji}-2\vartheta^{\mathrm{BA}}_{j'i}+\vartheta^{\mathrm{BB}-+}_{jj'jj'}}\hat{D}_{-\beta^{\mathrm{B}-}_{jj'}},\\
&\vartheta^{\mu\nu-+}_{ii'jj'} = \vartheta^{\mu\nu}_{ij} - \vartheta^{\mu\nu}_{i'j} + \vartheta^{\mu\nu}_{ij'} - \vartheta^{\mu\nu}_{i'j'},\\
&\beta^{\mu-}_{ii'} = \beta^{\mu}_{i} - \beta^{\mu}_{i'}.
\end{aligned}
\tag{B.43}
$$

We also provide an alternative expression for $\hat{\lambda}^{\mu}_{\mathrm{T},iji'j'}$ that works for both $\mu\in\{A,B\}$,

$$
\begin{aligned}
\hat{\lambda}^{\mu}_{\mathrm{T},iji'j'} &= \langle i_{\mathrm{A}}j_{\mathrm{B}}|\hat{\lambda}^{\mu}_{\perp}|i'_{\mathrm{A}}j'_{\mathrm{B}}\rangle\,e^{\vartheta_{iji'j'}}\hat{D}_{-\beta^{\mathrm{A}-}_{ii'}-\beta^{\mathrm{B}-}_{jj'}},\\
\vartheta_{iji'j'} &= \vartheta^{\mathrm{AA}-+}_{ii'ii'} + \vartheta^{\mathrm{AB}-+}_{ii'jj'} + \vartheta^{\mathrm{BA}-+}_{jj'ii'} + \vartheta^{\mathrm{BB}-+}_{jj'jj'}.
\end{aligned}
\tag{B.44}
$$

To find this, consider

$$\hat{\lambda}^{\mu}_{\mathrm{T},ijj'i'} = \langle i_{\mathrm{A}} j_{\mathrm{B}} | \hat{\lambda}^{\mu}_{\perp} | i'_{\mathrm{A}} j'_{\mathrm{B}} \rangle \, \hat{U}^{\parallel\dagger}_{ij} \hat{U}^{\parallel}_{i'j'}, \tag{B.45}$$

$$\begin{aligned} \hat{U}^{\parallel\dagger}_{ij} \hat{U}^{\parallel}_{i'j'} &= e^{\Omega_{2,i'j'} - \Omega_{2,ij}} \hat{D}^{\dagger}_{\beta^{\mathrm{A}}_{i} + \beta^{\mathrm{B}}_{j}} \hat{D}_{\beta^{\mathrm{A}}_{i'} + \beta^{\mathrm{B}}_{j'}} \\ &= e^{\vartheta_{iji'j'}} \hat{D}_{-\beta^{\mathrm{A}-}_{ii'} - \beta^{\mathrm{B}-}_{jj'}}, \end{aligned} \tag{B.46}$$

$$\vartheta_{iji'j'} = \Omega_{2,i'j'} - \Omega_{2,ij} + \frac{1}{2} \Big[\hat{\phi}^{\beta^{\mathrm{A}}_{i} + \beta^{\mathrm{B}}_{j}}, \hat{\phi}^{\beta^{\mathrm{A}}_{i'} + \beta^{\mathrm{B}}_{j'}} \Big]. \tag{B.47}$$

Here, we used Eq. (B.38), $\hat{D}^{\dagger}_{\alpha} = \hat{D}_{-\alpha}$, and applied the Baker-Campbell-Hausdorff formula to combine the displacement operators as follows,

$$\begin{aligned} \hat{D}_{\alpha} \hat{D}_{\beta} &= e^{-\mathrm{i}\hat{\phi}^{\alpha}} e^{-\mathrm{i}\hat{\phi}^{\beta}} \\ &= e^{-\frac{1}{2}[\hat{\phi}^{\alpha}, \hat{\phi}^{\beta}]} e^{-\mathrm{i}\hat{\phi}^{\alpha} - \mathrm{i}\hat{\phi}^{\beta}} \\ &= e^{-\frac{1}{2}[\hat{\phi}^{\alpha}, \hat{\phi}^{\beta}]} \hat{D}_{\alpha+\beta}. \end{aligned} \tag{B.48}$$

Then, by considering

$$\begin{aligned} &\frac{1}{2} \Big[\hat{\phi}^{\beta^{\mu}_{i}}(t), \hat{\phi}^{\beta^{\nu}_{j}}(t) \Big] \\ &= \int_{t_{\parallel}}^{t} \mathrm{d}t_1 \int_{t_{\parallel}}^{t} \mathrm{d}t_2 \, \lambda^{\mu}_{\parallel,i}(t_1) \lambda^{\nu}_{\parallel,j}(t_2) W^{\mu\nu-}(t_1, t_2) \\ &= \vartheta^{\mu\nu}_{ij}(t) - \vartheta^{\nu\mu}_{ji}(t) \end{aligned} \tag{B.49}$$

and

$$\begin{aligned} \Omega_{2,ij} &= -\vartheta^{\mathrm{AA}}_{ii} - \vartheta^{\mathrm{BB}}_{jj} - \vartheta^{\mathrm{AB}}_{ij} - \vartheta^{\mathrm{BA}}_{ji}, \\ \vartheta^{\mu\nu-+}_{ii'jj'} &= \vartheta^{\mu\nu}_{ij} - \vartheta^{\mu\nu}_{i'j} + \vartheta^{\mu\nu}_{ij'} - \vartheta^{\mu\nu}_{i'j'}, \end{aligned} \tag{B.50}$$

one can show that

$$\vartheta_{iji'j'} = \vartheta^{\mathrm{AA}-+}_{ii'ii'} + \vartheta^{\mathrm{AB}-+}_{ii'jj'} + \vartheta^{\mathrm{BA}-+}_{jj'ii'} + \vartheta^{\mathrm{BB}-+}_{jj'jj'}. \tag{B.51}$$

B.4 Evolution of the state of the detectors

The state of the detectors in the interaction picture is obtained from $\hat{\rho}(t)$ by tracing over the field,

$$\hat{\rho}_{\mathrm{AB}}(t) = \mathrm{Tr}_{\phi}\, \hat{\rho}(t). \tag{B.52}$$

We are going to find the components in the $\{|i_{\mathrm{A}} j_{\mathrm{B}}\rangle\}$ basis of the following expression for $\hat{\rho}_{\mathrm{AB}}$, which includes the transversal coupling perturbatively,

$$\begin{aligned}\hat{\rho}_{\mathrm{AB}} = \hat{\rho}_{\mathrm{AB}}^{(0,0)} + \hat{\rho}_{\mathrm{AB}}^{(1,0)} + \hat{\rho}_{\mathrm{AB}}^{(0,1)} + \hat{\rho}_{\mathrm{AB}}^{(1,1)} \\ + \hat{\rho}_{\mathrm{AB}}^{(2,0)} + \hat{\rho}_{\mathrm{AB}}^{(0,2)} + \mathcal{O}\big(\lambda_{\perp}^{3}\big).\end{aligned} \tag{B.53}$$

Analogously to Appendix B.3, we split these perturbative contributions further,

$$\hat{\rho}_{\mathrm{AB}}^{(1,0)} = \sum_{\nu} \hat{\rho}_{\mathrm{AB}}^{(\nu,0)},\ \ \hat{\rho}_{\mathrm{AB}}^{(1,1)} = \sum_{\mu\nu} \hat{\rho}_{\mathrm{AB}}^{(\mu,\nu)},\ \ \hat{\rho}_{\mathrm{AB}}^{(2,0)} = \sum_{\mu\nu} \hat{\rho}_{\mathrm{AB}}^{(\mu\nu,0)}. \tag{B.54}$$

Here,

$$\begin{aligned}\hat{\rho}_{\mathrm{AB}}^{(\nu,0)} &= \mathrm{Tr}_{\phi}\, \hat{\rho}^{(\nu,0)} = \hat{\rho}_{\mathrm{AB}}^{(0,\nu)\dagger}, \\ \hat{\rho}_{\mathrm{AB}}^{(\mu,\nu)} &= \mathrm{Tr}_{\phi}\, \hat{\rho}^{(\mu,\nu)} = \hat{\rho}_{\mathrm{AB}}^{(\nu,\mu)\dagger}, \\ \hat{\rho}_{\mathrm{AB}}^{(\mu\nu,0)} &= \mathrm{Tr}_{\phi}\, \hat{\rho}^{(\mu\nu,0)} = \hat{\rho}_{\mathrm{AB}}^{(0,\mu\nu)\dagger},\end{aligned} \tag{B.55}$$

with $\hat{\rho}^{(\nu,0)}$, $\hat{\rho}^{(\mu,\nu)}$, $\hat{\rho}^{(\mu\nu,0)}$ defined in Eq. (B.29).

Then, in the $\{|i_{\mathrm{A}} j_{\mathrm{B}}\rangle\}$ basis, and for any possible indices x, y,

$$\langle i_{\mathrm{A}} j_{\mathrm{B}}|\hat{\rho}_{\mathrm{AB}}^{(x,y)}|i'_{\mathrm{A}} j'_{\mathrm{B}}\rangle = \mathrm{Tr}_{\phi}\left(\langle i_{\mathrm{A}} j_{\mathrm{B}}|\hat{\rho}^{(x,y)}|i'_{\mathrm{A}} j'_{\mathrm{B}}\rangle\right). \tag{B.56}$$

Analogously to Appendix B.3, in order to find the compontents of all the perturbative terms in Eq. (B.53), it is enough to provide expressions for

$$\begin{aligned}&\mathrm{Tr}_{\phi}\left(\langle i_{\mathrm{A}} j_{\mathrm{B}}|\hat{\rho}^{(0,0)}|i'_{\mathrm{A}} j'_{\mathrm{B}}\rangle\right),\ \ \mathrm{Tr}_{\phi}\left(\langle i_{\mathrm{A}} j_{\mathrm{B}}|\hat{\rho}^{(\nu,0)}|i'_{\mathrm{A}} j'_{\mathrm{B}}\rangle\right), \\ &\mathrm{Tr}_{\phi}\left(\langle i_{\mathrm{A}} j_{\mathrm{B}}|\hat{\rho}^{(\mu,\nu)}|i'_{\mathrm{A}} j'_{\mathrm{B}}\rangle\right),\ \ \mathrm{Tr}_{\phi}\left(\langle i_{\mathrm{A}} j_{\mathrm{B}}|\hat{\rho}^{(\mu\nu,0)}|i'_{\mathrm{A}} j'_{\mathrm{B}}\rangle\right),\end{aligned} \tag{B.57}$$

for $\mu, \nu \in \{\mathrm{A}, \mathrm{B}\}$, as done next. These expressions will be enough thanks to the fact that $\hat{\rho}_{\mathrm{AB}}^{(0,1)} = \hat{\rho}_{\mathrm{AB}}^{(1,0)\dagger}$, $\hat{\rho}_{\mathrm{AB}}^{(0,2)} = \hat{\rho}_{\mathrm{AB}}^{(2,0)\dagger}$. Moreover, since we will be using Appendix B.3, we are under the choice $t_{\parallel} = t_0$.

First, using Eq. (B.33),

$$\begin{aligned}
&\langle i_{\mathrm{A}} j_{\mathrm{B}}|\hat{\rho}^{(0,0)}_{\mathrm{AB}}(t)|i'_{\mathrm{A}} j'_{\mathrm{B}}\rangle \\
&= \mathrm{Tr}_\phi\, \hat{U}^{\parallel\dagger}_{i'j'}(t)\hat{U}^{\parallel}_{ij}(t)\, \langle i_{\mathrm{A}} j_{\mathrm{B}}|\hat{\rho}_0|i'_{\mathrm{A}} j'_{\mathrm{B}}\rangle \\
&= e^{-\vartheta_{iji'j'}(t)}\, \mathrm{Tr}_\phi\, \hat{D}_{\beta^{\mathrm{A}-}_{ii'}(t)+\beta^{\mathrm{B}-}_{jj'}(t)}\, \langle i_{\mathrm{A}} j_{\mathrm{B}}|\hat{\rho}_0|i'_{\mathrm{A}} j'_{\mathrm{B}}\rangle\,,
\end{aligned} \tag{B.58}$$

where we were able to use the cyclicity of the trace because $\hat{U}^{\parallel\dagger}_{i'j'}$ is an operator of the field. Moreover, we used Eq. (B.46), together with $\vartheta_{i'j'ij} = -\vartheta_{iji'j'}$ and $\beta^{\mu-}_{i'i} = -\beta^{\mu-}_{ii'}$.

Next, from Eq. (B.34),

$$\begin{aligned}
\langle i_{\mathrm{A}} j_{\mathrm{B}}|\hat{\rho}^{(\mathrm{A},0)}_{\mathrm{AB}}|i'_{\mathrm{A}} j'_{\mathrm{B}}\rangle &= \sum_{k\neq i} \mathrm{Tr}_\phi\, \hat{U}^{\parallel\dagger}_{i'j'}\hat{U}^{\parallel}_{ij}\hat{\mathcal{U}}^{\mathrm{A}}_{ijkj}\, \langle k_{\mathrm{A}} j_{\mathrm{B}}|\hat{\rho}_0|i'_{\mathrm{A}} j'_{\mathrm{B}}\rangle\,, \\
\langle i_{\mathrm{A}} j_{\mathrm{B}}|\hat{\rho}^{(\mathrm{B},0)}_{\mathrm{AB}}|i'_{\mathrm{A}} j'_{\mathrm{B}}\rangle &= \sum_{l\neq j} \mathrm{Tr}_\phi\, \hat{U}^{\parallel\dagger}_{i'j'}\hat{U}^{\parallel}_{ij}\hat{\mathcal{U}}^{\mathrm{B}}_{ijil}\, \langle i_{\mathrm{A}} l_{\mathrm{B}}|\hat{\rho}_0|i'_{\mathrm{A}} j'_{\mathrm{B}}\rangle\,,
\end{aligned} \tag{B.59}$$

Substituting the expressions for $\hat{\mathcal{U}}^{\mu}_{ijkj}$ given in Eq. (B.40),

$$\begin{aligned}
&\hat{U}^{\parallel\dagger}_{i'j'}(t)\hat{U}^{\parallel}_{ij}(t)\hat{\mathcal{U}}^{\mathrm{A}}_{ijkj}(t) \\
&= -\mathrm{i}\int_{t_0}^{t} \mathrm{d}t_1\, \hat{U}^{\parallel\dagger}_{i'j'}(t)\hat{U}^{\parallel}_{ij}(t)\hat{\lambda}^{\mathrm{A}}_{\mathrm{T},ijkj}(t_1)\hat{\phi}^{\alpha^{\mathrm{A}}}_{\mathrm{T},kj}(t_1), \\
&\hat{U}^{\parallel\dagger}_{i'j'}(t)\hat{U}^{\parallel}_{ij}(t)\hat{\mathcal{U}}^{\mathrm{B}}_{ijil}(t) \\
&= -\mathrm{i}\int_{t_0}^{t} \mathrm{d}t_1\, \hat{U}^{\parallel\dagger}_{i'j'}(t)\hat{U}^{\parallel}_{ij}(t)\hat{\lambda}^{\mathrm{B}}_{\mathrm{T},ijil}(t_1)\hat{\phi}^{\alpha^{\mathrm{B}}}_{\mathrm{T},il}(t_1).
\end{aligned} \tag{B.60}$$

Moreover, using Eqs. (B.43), (B.44) and (B.46) and the property $\hat{D}_\alpha\hat{D}_\beta = e^{-\frac{1}{2}[\hat{\phi}^\alpha,\hat{\phi}^\beta]}\hat{D}_{\alpha+\beta}$ shown in Eq (B.48),

$$\begin{aligned}
&\hat{U}^{\parallel\dagger}_{i'j'}(t)\hat{U}^{\parallel}_{ij}(t)\hat{\lambda}^{\mathrm{A}}_{\mathrm{T},ijkj}(t_1) \\
&= e^{\zeta^{(\mathrm{A},0)}_{ijki'j'}(t,t_1)}\, \langle i_{\mathrm{A}}|\hat{\lambda}^{\mathrm{A}}_{\perp}(t_1)|k_{\mathrm{A}}\rangle\, \hat{D}_{\beta^{\mathrm{A}-}_{ii'}(t)+\beta^{\mathrm{B}-}_{jj'}(t)-\beta^{\mathrm{A}-}_{ik}(t_1)}, \\
&\hat{U}^{\parallel\dagger}_{i'j'}(t)\hat{U}^{\parallel}_{ij}(t)\hat{\lambda}^{\mathrm{B}}_{\mathrm{T},ijil}(t_1) \\
&= e^{\zeta^{(\mathrm{B},0)}_{ijli'j'}(t,t_1)}\, \langle j_{\mathrm{B}}|\hat{\lambda}^{\mathrm{B}}_{\perp}(t_1)|l_{\mathrm{B}}\rangle\, \hat{D}_{\beta^{\mathrm{A}-}_{ii'}(t)+\beta^{\mathrm{B}-}_{jj'}(t)-\beta^{\mathrm{B}-}_{jl}(t_1)},
\end{aligned} \tag{B.61}$$

$$
\begin{aligned}
&\zeta^{(\mathrm{A},0)}_{ijki'j'}(t,t_1)\\
&= -\vartheta_{iji'j'}(t) + \vartheta_{ijkj}(t_1) + C^{\mathrm{AA}}_{ii'ik}(t,t_1) + C^{\mathrm{BA}}_{jj'ik}(t,t_1),\\
&\zeta^{(\mathrm{B},0)}_{ijli'j'}(t,t_1)\\
&= -\vartheta_{iji'j'}(t) + \vartheta_{ijil}(t_1) + C^{\mathrm{AB}}_{ii'jl}(t,t_1) + C^{\mathrm{BB}}_{jj'jl}(t,t_1).
\end{aligned}
\tag{B.62}
$$

Here, we defined

$$
\begin{aligned}
&C^{\mu\nu}_{ii'jj'}(t,t')\\
&= \frac{1}{2}\left[\hat{\phi}^{\beta^{\mu-}_{ii'}}(t), \hat{\phi}^{\beta^{\nu-}_{jj'}}(t')\right]\\
&= \int_{t_\parallel}^{t} \mathrm{d}t_1 \int_{t_\parallel}^{t'} \mathrm{d}t_2\, \lambda^{\mu-}_{\parallel,ii'}(t_1)\lambda^{\nu-}_{\parallel,jj'}(t_2) W^{\mu\nu-}(t_1,t_2),
\end{aligned}
\tag{B.63}
$$

with $\lambda^{\mu-}_{\parallel,ii'}$ as defined in Eq. (B.7),

$$
\lambda^{\nu-}_{\parallel,ii'} = \lambda^{\nu}_{\parallel,i} - \lambda^{\nu}_{\parallel,i'}. \tag{B.64}
$$

Moreover, remember that, as stated in Eqs. (B.43) and (B.44),

$$
\begin{aligned}
\vartheta_{iji'j'} &= \vartheta^{\mathrm{AA}-+}_{ii'ii'} + \vartheta^{\mathrm{AB}-+}_{ii'jj'} + \vartheta^{\mathrm{BA}-+}_{jj'ii'} + \vartheta^{\mathrm{BB}-+}_{jj'jj'},\\
\vartheta^{\mu\nu-+}_{ii'jj'} &= \vartheta^{\mu\nu}_{ij} - \vartheta^{\mu\nu}_{i'j} + \vartheta^{\mu\nu}_{ij'} - \vartheta^{\mu\nu}_{i'j'},\\
\beta^{\mu-}_{ii'} &= \beta^{\mu}_{i} - \beta^{\mu}_{i'}.
\end{aligned}
\tag{B.65}
$$

In conclusion, $\hat{U}^{\parallel\dagger}_{i'j'}(t)\hat{U}^{\parallel}_{ij}(t)\hat{\lambda}^{\mu}_{\mathrm{T},ijkl}(t_1)$ is proportional to a displacement operator. Therefore, $\langle i_{\mathrm{A}} j_{\mathrm{B}}|\hat{\rho}^{(\mu,0)}_{\mathrm{AB}}|i'_{\mathrm{A}} j'_{\mathrm{B}}\rangle$ only contains integrals with their integrand comprised of one displacement operator, times a field operator in the transversal picture, which is of the form

$$
\hat{\phi}^{\alpha^\nu}_{\mathrm{T},ij}(t_1) = \hat{\phi}^{\alpha^\nu}(t_1) + \left(m^{\mathrm{A}^\nu}_{\parallel,i}(t_1) + m^{\mathrm{B}^\nu}_{\parallel,j}(t_1)\right)\hat{\mathbb{1}}, \tag{B.66}
$$

as given in Eq. (B.43).

Next, from Eq. (B.35),

$$
\begin{aligned}
&\langle i_{\mathrm{A}} j_{\mathrm{B}}|\hat{\rho}_{\mathrm{AB}}^{(\mathrm{A},\mathrm{A})}|i'_{\mathrm{A}} j'_{\mathrm{B}}\rangle \\
&= \sum_{k\neq i}\sum_{k'\neq i'} \mathrm{Tr}_\phi\left(\hat{\mathcal{U}}^{\mathrm{A}}_{i'j'k'j'}\right)^\dagger \hat{U}^{\parallel\dagger}_{i'j'}\hat{U}^{\parallel}_{ij}\hat{\mathcal{U}}^{\mathrm{A}}_{ijkj}\,\langle k_{\mathrm{A}} j_{\mathrm{B}}|\hat{\rho}_0|k'_{\mathrm{A}} j'_{\mathrm{B}}\rangle\,, \\
&\langle i_{\mathrm{A}} j_{\mathrm{B}}|\hat{\rho}_{\mathrm{AB}}^{(\mathrm{A},\mathrm{B})}|i'_{\mathrm{A}} j'_{\mathrm{B}}\rangle \\
&= \sum_{k\neq i}\sum_{l'\neq j'} \mathrm{Tr}_\phi\left(\hat{\mathcal{U}}^{\mathrm{B}}_{i'j'i'l'}\right)^\dagger \hat{U}^{\parallel\dagger}_{i'j'}\hat{U}^{\parallel}_{ij}\hat{\mathcal{U}}^{\mathrm{A}}_{ijkj}\,\langle k_{\mathrm{A}} j_{\mathrm{B}}|\hat{\rho}_0|i'_{\mathrm{A}} l'_{\mathrm{B}}\rangle\,, \\
&\langle i_{\mathrm{A}} j_{\mathrm{B}}|\hat{\rho}_{\mathrm{AB}}^{(\mathrm{B},\mathrm{A})}|i'_{\mathrm{A}} j'_{\mathrm{B}}\rangle \\
&= \sum_{l\neq j}\sum_{l'\neq j'} \mathrm{Tr}_\phi\left(\hat{\mathcal{U}}^{\mathrm{A}}_{i'j'k'j'}\right)^\dagger \hat{U}^{\parallel\dagger}_{i'j'}\hat{U}^{\parallel}_{ij}\hat{\mathcal{U}}^{\mathrm{B}}_{ijil}\,\langle i_{\mathrm{A}} l_{\mathrm{B}}|\hat{\rho}_0|k'_{\mathrm{A}} j'_{\mathrm{B}}\rangle\,, \\
&\langle i_{\mathrm{A}} j_{\mathrm{B}}|\hat{\rho}_{\mathrm{AB}}^{(\mathrm{B},\mathrm{B})}|i'_{\mathrm{A}} j'_{\mathrm{B}}\rangle \\
&= \sum_{l\neq j}\sum_{l'\neq j'} \mathrm{Tr}_\phi\left(\hat{\mathcal{U}}^{\mathrm{B}}_{i'j'i'l'}\right)^\dagger \hat{U}^{\parallel\dagger}_{i'j'}\hat{U}^{\parallel}_{ij}\hat{\mathcal{U}}^{\mathrm{B}}_{ijil}\,\langle i_{\mathrm{A}} l_{\mathrm{B}}|\hat{\rho}_0|i'_{\mathrm{A}} l'_{\mathrm{B}}\rangle\,.
\end{aligned}
\tag{B.67}
$$

Then,

$$
\begin{aligned}
&\left(\hat{\mathcal{U}}^{\mu}_{i'j'k'l'}(t)\right)^\dagger \hat{U}^{\parallel\dagger}_{i'j'}(t)\hat{U}^{\parallel}_{ij}(t)\hat{\mathcal{U}}^{\nu}_{ijkl}(t) \\
&= \int_{t_0}^{t}\mathrm{d}t_1 \int_{t_0}^{t}\mathrm{d}t_2\, \hat{\phi}^{\alpha^\mu}_{\mathrm{T},k'l'}(t_2)\big(\hat{\lambda}^{\mu}_{\mathrm{T},i'j'k'l'}(t_2)\big)^\dagger \\
&\quad\times \hat{U}^{\parallel\dagger}_{i'j'}(t)\hat{U}^{\parallel}_{ij}(t)\hat{\lambda}^{\nu}_{\mathrm{T},ijkl}(t_1)\hat{\phi}^{\alpha^\nu}_{\mathrm{T},kl}(t_1).
\end{aligned}
\tag{B.68}
$$

which is a consequence of

$$
\hat{\mathcal{U}}^{\mu}_{ijkl}(t) = -\mathrm{i}\int_{t_0}^{t}\mathrm{d}t_1\,\hat{\lambda}^{\mu}_{\mathrm{T},ijkl}(t_1)\hat{\phi}^{\alpha^{\mathrm{A}}}_{\mathrm{T},kl}(t_1),
\tag{B.69}
$$

which can be found similarly to Eq. (B.40). Moreover, we used that $\big(\hat{\phi}^{\alpha^\mu}_{\mathrm{T},kl}(t_1)\big)^\dagger = \hat{\phi}^{\alpha^\mu}_{\mathrm{T},kl}(t_1)$.

We now intend to group together all the displacement operators that appear implicitly in Eq. (B.68). These displacements are all in the following part of the integrands,

$$
\big(\hat{\lambda}^{\mu}_{\mathrm{T},i'j'k'l'}(t_2)\big)^\dagger \hat{U}^{\parallel\dagger}_{i'j'}(t)\hat{U}^{\parallel}_{ij}(t)\hat{\lambda}^{\nu}_{\mathrm{T},ijkl}(t_1).
\tag{B.70}
$$

We will now treat each value of $\mu, \nu \in \{A, B\}$ separately,

$$\begin{aligned}
&\big(\hat{\lambda}^{\mathrm{A}}_{\mathrm{T},i'j'k'l'}(t_2)\big)^\dagger \hat{U}^{\parallel\dagger}_{i'j'}(t)\hat{U}^{\parallel}_{ij}(t)\hat{\lambda}^{\mathrm{A}}_{\mathrm{T},ijkl}(t_1) \\
&= \delta_{jl}\delta_{j'l'}\,\langle i_{\mathrm{A}}|\hat{\lambda}^{\mathrm{A}}_{\perp}(t_1)|k_{\mathrm{A}}\rangle\;\langle k'_{\mathrm{A}}|\hat{\lambda}^{\mathrm{A}}_{\perp}(t_2)|i'_{\mathrm{A}}\rangle\, e^{\zeta^{(\mathrm{A},\mathrm{A})}_{ijki'j'k'}(t,t_1,t_2)} \\
&\quad\times \hat{D}_{\beta^{\mathrm{A}-}_{ii'}(t)+\beta^{\mathrm{B}-}_{jj'}(t)-\beta^{\mathrm{A}-}_{ik}(t_1)+\beta^{\mathrm{A}-}_{i'k'}(t_2)},
\end{aligned} \tag{B.71}$$

$$\begin{aligned}
&\zeta^{(\mathrm{A},\mathrm{A})}_{ijki'j'k'}(t,t_1,t_2) \\
&= -\vartheta_{iji'j'}(t) + C^{\mathrm{AA}}_{ii'ik}(t,t_1) + C^{\mathrm{BA}}_{jj'ik}(t,t_1) - C^{\mathrm{AA}}_{iki'k'}(t_1,t_2) \\
&\quad + \vartheta_{ijkj}(t_1) - \vartheta_{i'j'k'j'}(t_2) + C^{\mathrm{AA}}_{ii'i'k'}(t,t_2) + C^{\mathrm{BA}}_{jj'i'k'}(t,t_2),
\end{aligned} \tag{B.72}$$

$$\begin{aligned}
&\big(\hat{\lambda}^{\mathrm{B}}_{\mathrm{T},i'j'k'l'}(t_2)\big)^\dagger \hat{U}^{\parallel\dagger}_{i'j'}(t)\hat{U}^{\parallel}_{ij}(t)\hat{\lambda}^{\mathrm{A}}_{\mathrm{T},ijkl}(t_1) \\
&= \delta_{jl}\delta_{i'k'}\,\langle i_{\mathrm{A}}|\hat{\lambda}^{\mathrm{A}}_{\perp}(t_1)|k_{\mathrm{A}}\rangle\;\langle l'_{\mathrm{B}}|\hat{\lambda}^{\mathrm{B}}_{\perp}(t_2)|j'_{\mathrm{B}}\rangle\, e^{\zeta^{(\mathrm{A},\mathrm{B})}_{ijki'j'l'}(t,t_1,t_2)} \\
&\quad\times \hat{D}_{\beta^{\mathrm{A}-}_{ii'}(t)+\beta^{\mathrm{B}-}_{jj'}(t)-\beta^{\mathrm{A}-}_{ik}(t_1)+\beta^{\mathrm{B}-}_{j'l'}(t_2)},
\end{aligned} \tag{B.73}$$

$$\begin{aligned}
&\zeta^{(\mathrm{A},\mathrm{B})}_{ijki'j'l'}(t,t_1,t_2) \\
&= -\vartheta_{iji'j'}(t) + C^{\mathrm{AA}}_{ii'ik}(t,t_1) + C^{\mathrm{BA}}_{jj'ik}(t,t_1) - C^{\mathrm{AB}}_{ikj'l'}(t_1,t_2) \\
&\quad + \vartheta_{ijkj}(t_1) - \vartheta_{i'j'i'l'}(t_2) + C^{\mathrm{AB}}_{ii'j'l'}(t,t_2) + C^{\mathrm{BB}}_{jj'j'l'}(t,t_2),
\end{aligned} \tag{B.74}$$

$$\begin{aligned}
&\big(\hat{\lambda}^{\mathrm{A}}_{\mathrm{T},i'j'k'l'}(t_2)\big)^\dagger \hat{U}^{\parallel\dagger}_{i'j'}(t)\hat{U}^{\parallel}_{ij}(t)\hat{\lambda}^{\mathrm{B}}_{\mathrm{T},ijkl}(t_1) \\
&= \delta_{ik}\delta_{j'l'}\,\langle j_{\mathrm{B}}|\hat{\lambda}^{\mathrm{B}}_{\perp}(t_1)|l_{\mathrm{B}}\rangle\;\langle k'_{\mathrm{A}}|\hat{\lambda}^{\mathrm{A}}_{\perp}(t_2)|i'_{\mathrm{A}}\rangle\, e^{\zeta^{(\mathrm{B},\mathrm{A})}_{ijli'j'k'}(t,t_1,t_2)} \\
&\quad\times \hat{D}_{\beta^{\mathrm{A}-}_{ii'}(t)+\beta^{\mathrm{B}-}_{jj'}(t)-\beta^{\mathrm{B}-}_{jl}(t_1)+\beta^{\mathrm{A}-}_{i'k'}(t_2)},
\end{aligned} \tag{B.75}$$

$$\begin{aligned}
&\zeta^{(\mathrm{B},\mathrm{A})}_{ijli'j'k'}(t,t_1,t_2) \\
&= -\vartheta_{iji'j'}(t) + C^{\mathrm{AB}}_{ii'jl}(t,t_1) + C^{\mathrm{BB}}_{jj'jl}(t,t_1) - C^{\mathrm{BA}}_{jli'k'}(t_1,t_2) \\
&\quad + \vartheta_{ijil}(t_1) - \vartheta_{i'j'k'j'}(t_2) + C^{\mathrm{AA}}_{ii'i'k'}(t,t_2) + C^{\mathrm{BA}}_{jj'i'k'}(t,t_2),
\end{aligned} \tag{B.76}$$

$$
\begin{aligned}
&\big(\hat{\lambda}^{\mathrm{B}}_{\mathrm{T},i'j'k'l'}(t_2)\big)^{\dagger}\hat{U}^{\parallel\dagger}_{i'j'}(t)\hat{U}^{\parallel}_{ij}(t)\hat{\lambda}^{\mathrm{B}}_{\mathrm{T},ijkl}(t_1)\\
&= \delta_{jl}\delta_{i'k'}\,\langle i_{\mathrm{B}}|\hat{\lambda}^{\mathrm{B}}_{\perp}(t_1)|k_{\mathrm{B}}\rangle\;\langle l'_{\mathrm{B}}|\hat{\lambda}^{\mathrm{B}}_{\perp}(t_2)|j'_{\mathrm{B}}\rangle\, e^{\zeta^{(\mathrm{B},\mathrm{B})}_{ijli'j'l'}(t,t_1,t_2)}\\
&\quad\times \hat{D}_{\beta^{\mathrm{A}-}_{ii'}(t)+\beta^{\mathrm{B}-}_{jj'}(t)-\beta^{\mathrm{B}-}_{jl}(t_1)+\beta^{\mathrm{B}-}_{j'l'}(t_2)},
\end{aligned}
\tag{B.77}
$$

$$
\begin{aligned}
&\zeta^{(\mathrm{B},\mathrm{B})}_{ijli'j'l'}(t,t_1,t_2)\\
&= -\vartheta_{iji'j'}(t) + C^{\mathrm{AB}}_{ii'jl}(t,t_1) + C^{\mathrm{BB}}_{jj'jl}(t,t_1) - C^{\mathrm{BB}}_{jlj'l'}(t_1,t_2)\\
&\quad + \vartheta_{ijil}(t_1) - \vartheta_{i'j'i'l'}(t_2) + C^{\mathrm{AB}}_{ii'j'l'}(t,t_2) + C^{\mathrm{BB}}_{jj'j'l'}(t,t_2).
\end{aligned}
\tag{B.78}
$$

Here, $C^{\mu\nu}_{ii'jj'}(t,t')$ is defined in Eq. (B.63), we used $\hat{D}_{\alpha}\hat{D}_{\beta} = e^{-\frac{1}{2}[\hat{\phi}^{\alpha},\hat{\phi}^{\beta}]}\hat{D}_{\alpha+\beta}$, Eqs. (B.43), (B.44) and that

$$
\begin{aligned}
\big(\hat{\lambda}^{\mathrm{A}}_{\mathrm{T},i'j'k'l'}\big)^{\dagger} &= \delta_{j'l'}\,\langle k'_{\mathrm{A}}|\hat{\lambda}^{\mathrm{A}}_{\perp}|i'_{\mathrm{A}}\rangle\, e^{-\vartheta_{i'j'k'j'}}\hat{D}_{\beta^{\mathrm{A}-}_{i'k'}},\\
\big(\hat{\lambda}^{\mathrm{B}}_{\mathrm{T},i'j'k'l'}\big)^{\dagger} &= \delta_{i'k'}\,\langle l'_{\mathrm{B}}|\hat{\lambda}^{\mathrm{B}}_{\perp}|j'_{\mathrm{B}}\rangle\, e^{-\vartheta_{i'j'i'l'}}\hat{D}_{\beta^{\mathrm{B}-}_{j'l'}}.
\end{aligned}
\tag{B.79}
$$

Next, starting from Eq. (B.36),

$$
\begin{aligned}
\langle i_{\mathrm{A}}j_{\mathrm{B}}|\hat{\rho}^{(\mathrm{AA},0)}_{\mathrm{AB}}|i'_{\mathrm{A}}j'_{\mathrm{B}}\rangle &= \sum_{k}\mathrm{Tr}_{\phi}\,\hat{U}^{\parallel\dagger}_{i'j'}\hat{U}^{\parallel}_{ij}\hat{\mathcal{U}}^{\mathrm{AA}}_{ijkj}\,\langle k_{\mathrm{A}}j_{\mathrm{B}}|\hat{\rho}_0|i'_{\mathrm{A}}j'_{\mathrm{B}}\rangle\,,\\
\langle i_{\mathrm{A}}j_{\mathrm{B}}|\hat{\rho}^{(\mathrm{BB},0)}_{\mathrm{AB}}|i'_{\mathrm{A}}j'_{\mathrm{B}}\rangle &= \sum_{l}\mathrm{Tr}_{\phi}\,\hat{U}^{\parallel\dagger}_{i'j'}\hat{U}^{\parallel}_{ij}\hat{\mathcal{U}}^{\mathrm{BB}}_{ijil}\,\langle i_{\mathrm{A}}l_{\mathrm{B}}|\hat{\rho}_0|i'_{\mathrm{A}}j'_{\mathrm{B}}\rangle\,,\\
\langle i_{\mathrm{A}}j_{\mathrm{B}}|\hat{\rho}^{(\mathrm{AB},0)}_{\mathrm{AB}}|i'_{\mathrm{A}}j'_{\mathrm{B}}\rangle &= \sum_{k\neq i}\sum_{l\neq j}\mathrm{Tr}_{\phi}\,\hat{U}^{\parallel\dagger}_{i'j'}\hat{U}^{\parallel}_{ij}\hat{\mathcal{U}}^{\mathrm{AB}}_{ijkl}\,\langle k_{\mathrm{A}}l_{\mathrm{B}}|\hat{\rho}_0|i'_{\mathrm{A}}j'_{\mathrm{B}}\rangle\,,\\
\langle i_{\mathrm{A}}j_{\mathrm{B}}|\hat{\rho}^{(\mathrm{BA},0)}_{\mathrm{AB}}|i'_{\mathrm{A}}j'_{\mathrm{B}}\rangle &= \sum_{k\neq i}\sum_{l\neq j}\mathrm{Tr}_{\phi}\,\hat{U}^{\parallel\dagger}_{i'j'}\hat{U}^{\parallel}_{ij}\hat{\mathcal{U}}^{\mathrm{BA}}_{ijkl}\,\langle k_{\mathrm{A}}l_{\mathrm{B}}|\hat{\rho}_0|i'_{\mathrm{A}}j'_{\mathrm{B}}\rangle\,.
\end{aligned}
\tag{B.80}
$$

Then, from Eq. (B.41),

$$
\begin{aligned}
&\hat{U}^{\parallel\dagger}_{i'j'}(t)\hat{U}^{\parallel}_{ij}(t)\hat{\mathcal{U}}^{\mathrm{AA}}_{ijkj}(t)\\
&= -\int_{t_0}^{t}\mathrm{d}t_1\int_{t_0}^{t_1}\mathrm{d}t_2\sum_{s\neq i,k}\hat{U}^{\parallel\dagger}_{i'j'}(t)\hat{U}^{\parallel}_{ij}(t)\\
&\quad\times\hat{\lambda}^{\mathrm{A}}_{\mathrm{T},ijsj}(t_1)\hat{\lambda}^{\mathrm{A}}_{\mathrm{T},sjkj}(t_2)\hat{\phi}^{\alpha^{\mathrm{A}}}_{\mathrm{T},kj}(t_1)\hat{\phi}^{\alpha^{\mathrm{A}}}_{\mathrm{T},kj}(t_2),
\end{aligned}
\tag{B.81}
$$

$$
\begin{aligned}
&\hat{U}^{\parallel\dagger}_{i'j'}(t)\hat{U}^{\parallel}_{ij}(t)\hat{\mathcal{U}}^{\mathrm{BB}}_{ijil}(t)\\
&= -\int_{t_0}^{t}\mathrm{d}t_1\int_{t_0}^{t_1}\mathrm{d}t_2\sum_{s\neq j,l}\hat{U}^{\parallel\dagger}_{i'j'}(t)\hat{U}^{\parallel}_{ij}(t)\\
&\quad\times\hat{\lambda}^{\mathrm{B}}_{\mathrm{T},ijis}(t_1)\hat{\lambda}^{\mathrm{B}}_{\mathrm{T},isil}(t_2)\hat{\phi}^{\alpha^{\mathrm{B}}}_{\mathrm{T},il}(t_1)\hat{\phi}^{\alpha^{\mathrm{B}}}_{\mathrm{T},il}(t_2),
\end{aligned}
\tag{B.82}
$$

$$
\begin{aligned}
&\hat{U}^{\parallel\dagger}_{i'j'}(t)\hat{U}^{\parallel}_{ij}(t)\hat{\mathcal{U}}^{\mathrm{AB}}_{ijkl}(t)\\
&= -\int_{t_0}^{t}\mathrm{d}t_1\int_{t_0}^{t_1}\mathrm{d}t_2\,\hat{U}^{\parallel\dagger}_{i'j'}(t)\hat{U}^{\parallel}_{ij}(t)\\
&\quad\times\hat{\lambda}^{\mathrm{A}}_{\mathrm{T},ijkj}(t_1)\hat{\lambda}^{\mathrm{B}}_{\mathrm{T},kjkl}(t_2)\hat{\phi}^{\alpha^{\mathrm{A}}}_{\mathrm{T},kl}(t_1)\hat{\phi}^{\alpha^{\mathrm{B}}}_{\mathrm{T},kl}(t_2),
\end{aligned}
\tag{B.83}
$$

$$
\begin{aligned}
&\hat{U}^{\parallel\dagger}_{i'j'}(t)\hat{U}^{\parallel}_{ij}(t)\hat{\mathcal{U}}^{\mathrm{BA}}_{ijkl}(t)\\
&= -\int_{t_0}^{t}\mathrm{d}t_1\int_{t_0}^{t_1}\mathrm{d}t_2\,\hat{U}^{\parallel\dagger}_{i'j'}(t)\hat{U}^{\parallel}_{ij}(t)\\
&\quad\times\hat{\lambda}^{\mathrm{B}}_{\mathrm{T},ijil}(t_1)\hat{\lambda}^{\mathrm{A}}_{\mathrm{T},ilkl}(t_2)\hat{\phi}^{\alpha^{\mathrm{B}}}_{\mathrm{T},kl}(t_1)\hat{\phi}^{\alpha^{\mathrm{A}}}_{\mathrm{T},kl}(t_2),
\end{aligned}
\tag{B.84}
$$

Now we combine all the displacement operators implicitly appearing in the equations above, analogously to previous calculations,

$$
\begin{aligned}
&\hat{U}^{\parallel\dagger}_{i'j'}(t)\hat{U}^{\parallel}_{ij}\hat{\lambda}^{\mathrm{A}}_{\mathrm{T},ijsj}(t_1)\hat{\lambda}^{\mathrm{A}}_{\mathrm{T},sjkj}(t_2)\\
&=\langle i_{\mathrm{A}}|\hat{\lambda}^{\mathrm{A}}_{\perp}(t_1)|s_{\mathrm{A}}\rangle\,\langle s_{\mathrm{A}}|\hat{\lambda}^{\mathrm{A}}_{\perp}(t_2)|k_{\mathrm{A}}\rangle\,e^{\zeta^{(\mathrm{AA},0)}_{ijski'j'}(t,t_1,t_2)}\\
&\quad\times\hat{D}_{\beta^{\mathrm{A}-}_{ii'}(t)+\beta^{\mathrm{B}-}_{jj'}(t)-\beta^{\mathrm{A}-}_{is}(t_1)-\beta^{\mathrm{A}-}_{sk}(t_2)},
\end{aligned}
\tag{B.85}
$$

$$
\begin{aligned}
\zeta^{(\mathrm{AA},0)}_{ijski'j'}(t,t_1,t_2) = &-\vartheta_{iji'j'}(t)+C^{\mathrm{AA}}_{ii'is}(t,t_1)+C^{\mathrm{BA}}_{jj'is}(t,t_1)\\
&+C^{\mathrm{AA}}_{ii'sk}(t,t_2)+C^{\mathrm{BA}}_{jj'sk}(t,t_2)\\
&-C^{\mathrm{AA}}_{issk}(t_1,t_2)+\vartheta_{ijsj}(t_1)+\vartheta_{sjkj}(t_2),
\end{aligned}
\tag{B.86}
$$

$$
\begin{aligned}
&\hat{U}^{\parallel\dagger}_{i'j'}(t)\hat{U}^{\parallel}_{ij}\hat{\lambda}^{\mathrm{B}}_{\mathrm{T},ijis}(t_1)\hat{\lambda}^{\mathrm{B}}_{\mathrm{T},isil}(t_2)\\
&=\langle j_{\mathrm{B}}|\hat{\lambda}^{\mathrm{B}}_{\perp}(t_1)|s_{\mathrm{B}}\rangle\,\langle s_{\mathrm{B}}|\hat{\lambda}^{\mathrm{B}}_{\perp}(t_2)|l_{\mathrm{B}}\rangle\,e^{\zeta^{(\mathrm{BB},0)}_{ijsli'j'}(t,t_1,t_2)}\\
&\quad\times\hat{D}_{\beta^{\mathrm{A}-}_{ii'}(t)+\beta^{\mathrm{B}-}_{jj'}(t)-\beta^{\mathrm{B}-}_{js}(t_1)-\beta^{\mathrm{B}-}_{sl}(t_2)},
\end{aligned}
\tag{B.87}
$$

$$\zeta^{(\mathrm{BB},0)}_{ijsli'j'}(t,t_1,t_2) = -\vartheta_{iji'j'}(t) + C^{\mathrm{AB}}_{ii'js}(t,t_1) + C^{\mathrm{BB}}_{jj'js}(t,t_1) + C^{\mathrm{AB}}_{ii'sl}(t,t_2) + C^{\mathrm{BB}}_{jj'sl}(t,t_2) - C^{\mathrm{BB}}_{jssl}(t_1,t_2) + \vartheta_{ijis}(t_1) + \vartheta_{isil}(t_2), \tag{B.88}$$

$$\begin{aligned}&\hat{U}^{\parallel\dagger}_{i'j'}(t)\hat{U}^{\parallel}_{ij}\hat{\lambda}^{\mathrm{A}}_{\mathrm{T},ijkj}(t_1)\hat{\lambda}^{\mathrm{B}}_{\mathrm{T},kjkl}(t_2)\\ &= \langle i_{\mathrm{A}}|\hat{\lambda}^{\mathrm{A}}_{\perp}(t_1)|k_{\mathrm{A}}\rangle\ \langle j_{\mathrm{B}}|\hat{\lambda}^{\mathrm{B}}_{\perp}(t_2)|l_{\mathrm{B}}\rangle\, e^{\zeta^{(\mathrm{AB},0)}_{ijkli'j'}(t,t_1,t_2)}\\ &\quad\times \hat{D}_{\beta^{\mathrm{A}-}_{ii'}(t)+\beta^{\mathrm{B}-}_{jj'}(t)-\beta^{\mathrm{A}-}_{ik}(t_1)-\beta^{\mathrm{B}-}_{jl}(t_2)},\end{aligned} \tag{B.89}$$

$$\zeta^{(\mathrm{AB},0)}_{ijkli'j'}(t,t_1,t_2) = -\vartheta_{iji'j'}(t) + C^{\mathrm{AA}}_{ii'ik}(t,t_1) + C^{\mathrm{BA}}_{jj'ik}(t,t_1) + C^{\mathrm{AB}}_{ii'jl}(t,t_2) + C^{\mathrm{BB}}_{jj'jl}(t,t_2) - C^{\mathrm{AB}}_{ikjl}(t_1,t_2) + \vartheta_{ijkj}(t_1) + \vartheta_{kjkl}(t_2), \tag{B.90}$$

$$\begin{aligned}&\hat{U}^{\parallel\dagger}_{i'j'}(t)\hat{U}^{\parallel}_{ij}\hat{\lambda}^{\mathrm{B}}_{\mathrm{T},ijil}(t_1)\hat{\lambda}^{\mathrm{A}}_{\mathrm{T},ilkl}(t_2)\\ &= \langle j_{\mathrm{B}}|\hat{\lambda}^{\mathrm{B}}_{\perp}(t_1)|l_{\mathrm{B}}\rangle\ \langle i_{\mathrm{A}}|\hat{\lambda}^{\mathrm{A}}_{\perp}(t_2)|k_{\mathrm{A}}\rangle\, e^{\zeta^{(\mathrm{BA},0)}_{ijlki'j'}(t,t_1,t_2)}\\ &\quad\times \hat{D}_{\beta^{\mathrm{A}-}_{ii'}(t)+\beta^{\mathrm{B}-}_{jj'}(t)-\beta^{\mathrm{B}-}_{jl}(t_1)-\beta^{\mathrm{A}-}_{ik}(t_2)},\end{aligned} \tag{B.91}$$

$$\zeta^{(\mathrm{BA},0)}_{ijlki'j'}(t,t_1,t_2) = -\vartheta_{iji'j'}(t) + C^{\mathrm{AB}}_{ii'jl}(t,t_1) + C^{\mathrm{BB}}_{jj'jl}(t,t_1) + C^{\mathrm{AA}}_{ii'ik}(t,t_2) + C^{\mathrm{BA}}_{jj'ik}(t,t_2) - C^{\mathrm{BA}}_{jlik}(t_1,t_2) + \vartheta_{ijil}(t_1) + \vartheta_{ilkl}(t_2). \tag{B.92}$$

B.4.1 Summary of components of the detectors' state

Finally, we summarize the expressions found above for the components $\langle i_{\mathrm{A}} j_{\mathrm{B}}|\hat{\rho}_{\mathrm{AB}}|i'_{\mathrm{A}} j'_{\mathrm{B}}\rangle$, in terms of its expansion,

$$\hat{\rho}_{\mathrm{AB}} = \hat{\rho}^{(0,0)}_{\mathrm{AB}} + \hat{\rho}^{(1,0)}_{\mathrm{AB}} + \hat{\rho}^{(0,1)}_{\mathrm{AB}} + \hat{\rho}^{(1,1)}_{\mathrm{AB}} + \hat{\rho}^{(2,0)}_{\mathrm{AB}} + \hat{\rho}^{(0,2)}_{\mathrm{AB}} + \mathcal{O}\big(\lambda^3_{\perp}\big). \tag{B.93}$$

Remember that the expressions provided below only hold for the choice $t_\parallel = t_0$. Moreover, we will be using the following set of definitions throughout this summary,

$$\begin{aligned}
&\vartheta_{iji'j'} = \vartheta^{\mathrm{AA}-+}_{ii'ii'} + \vartheta^{\mathrm{AB}-+}_{ii'jj'} + \vartheta^{\mathrm{BA}-+}_{jj'ii'} + \vartheta^{\mathrm{BB}-+}_{jj'jj'},\\
&\vartheta^{\mu\nu-+}_{ii'jj'}(t) = \int_{t_\parallel}^{t} \mathrm{d}t_1 \int_{t_\parallel}^{t_1} \mathrm{d}t_2\, \lambda^{\mu-}_{\parallel,ii'}(t_1)\lambda^{\nu+}_{\parallel,jj'}(t_2) W^{\mu\nu-}(t_1,t_2),\\
&\beta^{\nu-}_{ii'}(t,\boldsymbol{k}) = \int_{t_\parallel}^{t} \mathrm{d}t_1\, \lambda^{\nu-}_{\parallel,ii'}(t_1)\alpha^{\nu}(t_1,\boldsymbol{k}),\\
&\lambda^{\nu\pm}_{\parallel,ii'} = \lambda^{\nu}_{\parallel,i} \pm \lambda^{\nu}_{\parallel,i'},\\
&\lambda^{\nu}_{\parallel,i} = \langle i_\nu|\hat{\lambda}^{\nu}_{\parallel}|i_\nu\rangle\,,\\
&\lambda^{\nu}_{\perp,ii'} = \langle i_\nu|\hat{\lambda}^{\nu}_{\perp}|i'_\nu\rangle\,,
\end{aligned} \tag{B.94}$$

with $W^{\mu\nu-}$ from Eq. (3.14), and α^ν matching Eq. (3.1).

$$\begin{aligned}
&\hat{\phi}^{\alpha^\nu}_{\mathrm{T},ij} = \hat{\phi}^{\alpha^\nu} + \big(m^{\mathrm{A}^\nu}_{\parallel,i} + m^{\mathrm{B}^\nu}_{\parallel,j}\big)\hat{\mathbb{1}},\\
&m^{\mu^\nu}_{\parallel,i}(t) = 2\mathrm{i}\int_{t_\parallel}^{t} \mathrm{d}t_1\, \lambda^{\mu}_{\parallel,i}(t_1) W^{\mu\nu-}(t_1,t),
\end{aligned} \tag{B.95}$$

$$\begin{aligned}
&C^{\mu\nu}_{ii'jj'}(t,t')\\
&= \int_{t_\parallel}^{t} \mathrm{d}t_1 \int_{t_\parallel}^{t'} \mathrm{d}t_2\, \lambda^{\mu-}_{\parallel,ii'}(t_1)\lambda^{\nu-}_{\parallel,jj'}(t_2) W^{\mu\nu-}(t_1,t_2).
\end{aligned} \tag{B.96}$$

Starting with the zeroth order in $\lambda_\perp$,

$$\begin{aligned}
&\langle i_{\mathrm{A}} j_{\mathrm{B}}|\hat{\rho}^{(0,0)}_{\mathrm{AB}}(t)|i'_{\mathrm{A}} j'_{\mathrm{B}}\rangle\\
&= e^{-\vartheta_{iji'j'}(t)}\,\mathrm{Tr}_\phi\left(\hat{D}_{\beta^{\mathrm{A}-}_{ii'}(t)+\beta^{\mathrm{B}-}_{jj'}(t)}\,\langle i_{\mathrm{A}} j_{\mathrm{B}}|\hat{\rho}_0|i'_{\mathrm{A}} j'_{\mathrm{B}}\rangle\right),
\end{aligned} \tag{B.97}$$

Continuing with the first order,

$$\begin{aligned}
&\langle i_{\mathrm{A}} j_{\mathrm{B}}|\hat{\rho}^{(1,0)}_{\mathrm{AB}}|i'_{\mathrm{A}} j'_{\mathrm{B}}\rangle = \sum_\nu \langle i_{\mathrm{A}} j_{\mathrm{B}}|\hat{\rho}^{(\nu,0)}_{\mathrm{AB}}|i'_{\mathrm{A}} j'_{\mathrm{B}}\rangle\,,\\
&\langle i_{\mathrm{A}} j_{\mathrm{B}}|\hat{\rho}^{(0,1)}_{\mathrm{AB}}|i'_{\mathrm{A}} j'_{\mathrm{B}}\rangle = \langle i'_{\mathrm{A}} j'_{\mathrm{B}}|\hat{\rho}^{(1,0)}_{\mathrm{AB}}|i_{\mathrm{A}} j_{\mathrm{B}}\rangle^*\,,
\end{aligned} \tag{B.98}$$

due to $\hat{\rho}^{(0,1)}_{\rm AB} = \hat{\rho}^{(1,0)\dagger}_{\rm AB}$. Here,

$$\begin{aligned}
&\langle i_{\rm A} j_{\rm B}|\hat{\rho}^{({\rm A},0)}_{\rm AB}(t)|i'_{\rm A} j'_{\rm B}\rangle \\
&= -{\rm i}\sum_{k\neq i}\int_{t_0}^{t} {\rm d}t_1\, e^{\zeta^{({\rm A},0)}_{ijki'j'}(t,t_1)}\lambda^{\rm A}_{\perp,ik}(t_1) \\
&\quad\times {\rm Tr}_\phi\left(\hat{D}_{\beta^{{\rm A}-}_{ii'}(t)+\beta^{{\rm B}-}_{jj'}(t)-\beta^{{\rm A}-}_{ik}(t_1)}\hat{\phi}^{\alpha^{\rm A}}_{{\rm T},kj}(t_1)\,\langle k_{\rm A} j_{\rm B}|\hat{\rho}_0|i'_{\rm A} j'_{\rm B}\rangle\right),
\end{aligned} \tag{B.99}$$

$$\begin{aligned}
&\langle i_{\rm A} j_{\rm B}|\hat{\rho}^{({\rm B},0)}_{\rm AB}(t)|i'_{\rm A} j'_{\rm B}\rangle \\
&= -{\rm i}\sum_{l\neq j}\int_{t_0}^{t} {\rm d}t_1\, e^{\zeta^{({\rm B},0)}_{ijli'j'}(t,t_1)}\lambda^{\rm B}_{\perp,jl}(t_1) \\
&\quad\times {\rm Tr}_\phi\left(\hat{D}_{\beta^{{\rm A}-}_{ii'}(t)+\beta^{{\rm B}-}_{jj'}(t)-\beta^{{\rm B}-}_{jl}(t_1)}\hat{\phi}^{\alpha^{\rm B}}_{{\rm T},il}(t_1)\,\langle i_{\rm A} l_{\rm B}|\hat{\rho}_0|i'_{\rm A} j'_{\rm B}\rangle\right),
\end{aligned} \tag{B.100}$$

$$\begin{aligned}
&\zeta^{({\rm A},0)}_{ijki'j'}(t,t_1) \\
&= -\vartheta_{iji'j'}(t) + \vartheta_{ijkj}(t_1) + C^{\rm AA}_{ii'ik}(t,t_1) + C^{\rm BA}_{jj'ik}(t,t_1), \\
&\zeta^{({\rm B},0)}_{ijli'j'}(t,t_1) \\
&= -\vartheta_{iji'j'}(t) + \vartheta_{ijil}(t_1) + C^{\rm AB}_{ii'jl}(t,t_1) + C^{\rm BB}_{jj'jl}(t,t_1),
\end{aligned} \tag{B.101}$$

For the second order, there are three contributions,

$$\begin{aligned}
\langle i_{\rm A} j_{\rm B}|\hat{\rho}^{(1,1)}_{\rm AB}|i'_{\rm A} j'_{\rm B}\rangle &= \sum_{\mu\nu}\,\langle i_{\rm A} j_{\rm B}|\hat{\rho}^{(\mu,\nu)}_{\rm AB}|i'_{\rm A} j'_{\rm B}\rangle\,, \\
\langle i_{\rm A} j_{\rm B}|\hat{\rho}^{(2,0)}_{\rm AB}|i'_{\rm A} j'_{\rm B}\rangle &= \sum_{\mu\nu}\,\langle i_{\rm A} j_{\rm B}|\hat{\rho}^{(\mu\nu,0)}_{\rm AB}|i'_{\rm A} j'_{\rm B}\rangle\,, \\
\langle i_{\rm A} j_{\rm B}|\hat{\rho}^{(0,2)}_{\rm AB}|i'_{\rm A} j'_{\rm B}\rangle &= \,\langle i'_{\rm A} j'_{\rm B}|\hat{\rho}^{(2,0)}_{\rm AB}|i_{\rm A} j_{\rm B}\rangle^*\,,
\end{aligned} \tag{B.102}$$

$$\begin{aligned}
&\langle i_{\rm A} j_{\rm B}|\hat{\rho}^{({\rm A},{\rm A})}_{\rm AB}(t)|i'_{\rm A} j'_{\rm B}\rangle \\
&= \sum_{k\neq i}\sum_{k'\neq i'}\int_{t_0}^{t}{\rm d}t_1\int_{t_0}^{t}{\rm d}t_2\,\lambda^{\rm A}_{\perp,ik}(t_1)\lambda^{\rm A}_{\perp,k'i'}(t_2) \\
&\quad\times {\rm Tr}_\phi\Big(\hat{D}_{\beta^{{\rm A}-}_{ii'}(t)+\beta^{{\rm B}-}_{jj'}(t)-\beta^{{\rm A}-}_{ik}(t_1)+\beta^{{\rm A}-}_{i'k'}(t_2)} \\
&\quad\times \hat{\phi}^{\alpha^{\rm A}}_{{\rm T},kj}(t_1)\,\langle k_{\rm A} j_{\rm B}|\hat{\rho}_0|k'_{\rm A} j'_{\rm B}\rangle\,\hat{\phi}^{\alpha^{\rm A}}_{{\rm T},k'j'}(t_2)\Big) e^{\zeta^{({\rm A},{\rm A})}_{ijki'j'k'}(t,t_1,t_2)},
\end{aligned} \tag{B.103}$$

$$
\begin{aligned}
&\langle i_{\mathrm{A}} j_{\mathrm{B}}|\hat{\rho}_{\mathrm{AB}}^{(\mathrm{A,B})}(t)|i'_{\mathrm{A}} j'_{\mathrm{B}}\rangle \\
&= \sum_{k\neq i}\sum_{l'\neq j'}\int_{t_0}^{t}\mathrm{d}t_1\int_{t_0}^{t}\mathrm{d}t_2\,\lambda^{\mathrm{A}}_{\perp,ik}(t_1)\lambda^{\mathrm{B}}_{\perp,l'j'}(t_2) \\
&\quad\times \mathrm{Tr}_{\phi}\Big(\hat{D}_{\beta^{\mathrm{A}-}_{ii'}(t)+\beta^{\mathrm{B}-}_{jj'}(t)-\beta^{\mathrm{A}-}_{ik}(t_1)+\beta^{\mathrm{B}-}_{j'l'}(t_2)} \\
&\quad\times \hat{\phi}^{\alpha^{\mathrm{A}}}_{\mathrm{T},kj}(t_1)\,\langle k_{\mathrm{A}} j_{\mathrm{B}}|\hat{\rho}_0|i'_{\mathrm{A}} l'_{\mathrm{B}}\rangle\,\hat{\phi}^{\alpha^{\mathrm{B}}}_{\mathrm{T},i'l'}(t_2)\Big)e^{\zeta^{(\mathrm{A,B})}_{ijki'j'l'}(t,t_1,t_2)},
\end{aligned}
\tag{B.104}
$$

$$
\begin{aligned}
&\langle i_{\mathrm{A}} j_{\mathrm{B}}|\hat{\rho}_{\mathrm{AB}}^{(\mathrm{B,A})}(t)|i'_{\mathrm{A}} j'_{\mathrm{B}}\rangle \\
&= \sum_{l\neq j}\sum_{k'\neq i'}\int_{t_0}^{t}\mathrm{d}t_1\int_{t_0}^{t}\mathrm{d}t_2\,\lambda^{\mathrm{B}}_{\perp,jl}(t_1)\lambda^{\mathrm{A}}_{\perp,k'i'}(t_2) \\
&\quad\times \mathrm{Tr}_{\phi}\Big(\hat{D}_{\beta^{\mathrm{A}-}_{ii'}(t)+\beta^{\mathrm{B}-}_{jj'}(t)-\beta^{\mathrm{B}-}_{jl}(t_1)+\beta^{\mathrm{A}-}_{i'k'}(t_2)} \\
&\quad\times \hat{\phi}^{\alpha^{\mathrm{B}}}_{\mathrm{T},il}(t_1)\,\langle i_{\mathrm{A}} l_{\mathrm{B}}|\hat{\rho}_0|k'_{\mathrm{A}} j'_{\mathrm{B}}\rangle\,\hat{\phi}^{\alpha^{\mathrm{A}}}_{\mathrm{T},k'j'}(t_2)\Big)e^{\zeta^{(\mathrm{B,A})}_{ijli'j'k'}(t,t_1,t_2)},
\end{aligned}
\tag{B.105}
$$

$$
\begin{aligned}
&\langle i_{\mathrm{A}} j_{\mathrm{B}}|\hat{\rho}_{\mathrm{AB}}^{(\mathrm{B,B})}(t)|i'_{\mathrm{A}} j'_{\mathrm{B}}\rangle \\
&= \sum_{l\neq j}\sum_{l'\neq j'}\int_{t_0}^{t}\mathrm{d}t_1\int_{t_0}^{t}\mathrm{d}t_2\,\lambda^{\mathrm{B}}_{\perp,jl}(t_1)\lambda^{\mathrm{B}}_{\perp,l'j'}(t_2) \\
&\quad\times \mathrm{Tr}_{\phi}\Big(\hat{D}_{\beta^{\mathrm{A}-}_{ii'}(t)+\beta^{\mathrm{B}-}_{jj'}(t)-\beta^{\mathrm{B}-}_{jl}(t_1)+\beta^{\mathrm{B}-}_{j'l'}(t_2)} \\
&\quad\times \hat{\phi}^{\alpha^{\mathrm{B}}}_{\mathrm{T},il}(t_1)\,\langle i_{\mathrm{A}} l_{\mathrm{B}}|\hat{\rho}_0|i'_{\mathrm{A}} l'_{\mathrm{B}}\rangle\,\hat{\phi}^{\alpha^{\mathrm{B}}}_{\mathrm{T},i'l'}(t_2)\Big)e^{\zeta^{(\mathrm{B,B})}_{ijli'j'l'}(t,t_1,t_2)},
\end{aligned}
\tag{B.106}
$$

$$
\begin{aligned}
&\zeta^{(\mathrm{A},\mathrm{A})}_{ijki'j'k'}(t,t_1,t_2)\\
&= -\vartheta_{iji'j'}(t) + C^{\mathrm{AA}}_{ii'ik}(t,t_1) + C^{\mathrm{BA}}_{jj'ik}(t,t_1) - C^{\mathrm{AA}}_{iki'k'}(t_1,t_2)\\
&\quad + \vartheta_{ijkj}(t_1) - \vartheta_{i'j'k'j'}(t_2) + C^{\mathrm{AA}}_{ii'i'k'}(t,t_2) + C^{\mathrm{BA}}_{jj'i'k'}(t,t_2),\\
&\zeta^{(\mathrm{A},\mathrm{B})}_{ijki'j'l'}(t,t_1,t_2)\\
&= -\vartheta_{iji'j'}(t) + C^{\mathrm{AA}}_{ii'ik}(t,t_1) + C^{\mathrm{BA}}_{jj'ik}(t,t_1) - C^{\mathrm{AB}}_{ikj'l'}(t_1,t_2)\\
&\quad + \vartheta_{ijkj}(t_1) - \vartheta_{i'j'i'l'}(t_2) + C^{\mathrm{AB}}_{ii'j'l'}(t,t_2) + C^{\mathrm{BB}}_{jj'j'l'}(t,t_2),\\
&\zeta^{(\mathrm{B},\mathrm{A})}_{ijli'j'k'}(t,t_1,t_2)\\
&= -\vartheta_{iji'j'}(t) + C^{\mathrm{AB}}_{ii'jl}(t,t_1) + C^{\mathrm{BB}}_{jj'jl}(t,t_1) - C^{\mathrm{BA}}_{jli'k'}(t_1,t_2)\\
&\quad + \vartheta_{ijil}(t_1) - \vartheta_{i'j'k'j'}(t_2) + C^{\mathrm{AA}}_{ii'i'k'}(t,t_2) + C^{\mathrm{BA}}_{jj'i'k'}(t,t_2),\\
&\zeta^{(\mathrm{B},\mathrm{B})}_{ijli'j'l'}(t,t_1,t_2)\\
&= -\vartheta_{iji'j'}(t) + C^{\mathrm{AB}}_{ii'jl}(t,t_1) + C^{\mathrm{BB}}_{jj'jl}(t,t_1) - C^{\mathrm{BB}}_{jlj'l'}(t_1,t_2)\\
&\quad + \vartheta_{ijil}(t_1) - \vartheta_{i'j'i'l'}(t_2) + C^{\mathrm{AB}}_{ii'j'l'}(t,t_2) + C^{\mathrm{BB}}_{jj'j'l'}(t,t_2).
\end{aligned}
\tag{B.107}
$$

$$
\begin{aligned}
&\langle i_{\mathrm{A}} j_{\mathrm{B}}|\hat{\rho}^{(\mathrm{AA},0)}_{\mathrm{AB}}(t)|i'_{\mathrm{A}} j'_{\mathrm{B}}\rangle\\
&= -\sum_k \sum_{s\neq i,k} \int_{t_0}^{t} \mathrm{d}t_1 \int_{t_0}^{t_1} \mathrm{d}t_2\, \lambda^{\mathrm{A}}_{\perp,is}(t_1)\lambda^{\mathrm{A}}_{\perp,sk}(t_2)\\
&\quad \times \mathrm{Tr}_\phi \Big(\hat{D}_{\beta^{\mathrm{A}-}_{ii'}(t)+\beta^{\mathrm{B}-}_{jj'}(t)-\beta^{\mathrm{A}-}_{is}(t_1)-\beta^{\mathrm{A}-}_{sk}(t_2)}\\
&\quad \times \hat{\phi}^{\alpha^{\mathrm{A}}}_{\mathrm{T},kj}(t_1)\hat{\phi}^{\alpha^{\mathrm{A}}}_{\mathrm{T},kj}(t_2)\, \langle k_{\mathrm{A}} j_{\mathrm{B}}|\hat{\rho}_0|i'_{\mathrm{A}} j'_{\mathrm{B}}\rangle \Big) e^{\zeta^{(\mathrm{AA},0)}_{ijski'j'}(t,t_1,t_2)},
\end{aligned}
\tag{B.108}
$$

$$
\begin{aligned}
&\langle i_{\mathrm{A}} j_{\mathrm{B}}|\hat{\rho}^{(\mathrm{BB},0)}_{\mathrm{AB}}(t)|i'_{\mathrm{A}} j'_{\mathrm{B}}\rangle\\
&= -\sum_l \sum_{s\neq j,l} \int_{t_0}^{t} \mathrm{d}t_1 \int_{t_0}^{t_1} \mathrm{d}t_2\, \lambda^{\mathrm{B}}_{\perp,js}(t_1)\lambda^{\mathrm{B}}_{\perp,sl}(t_2)\\
&\quad \times \mathrm{Tr}_\phi \Big(\hat{D}_{\beta^{\mathrm{A}-}_{ii'}(t)+\beta^{\mathrm{B}-}_{jj'}(t)-\beta^{\mathrm{B}-}_{js}(t_1)-\beta^{\mathrm{B}-}_{sl}(t_2)}\\
&\quad \times \hat{\phi}^{\alpha^{\mathrm{B}}}_{\mathrm{T},il}(t_1)\hat{\phi}^{\alpha^{\mathrm{B}}}_{\mathrm{T},il}(t_2)\, \langle i_{\mathrm{A}} l_{\mathrm{B}}|\hat{\rho}_0|i'_{\mathrm{A}} j'_{\mathrm{B}}\rangle \Big) e^{\zeta^{(\mathrm{BB},0)}_{ijsli'j'}(t,t_1,t_2)},
\end{aligned}
\tag{B.109}
$$

$$
\begin{aligned}
&\langle i_{\mathrm{A}} j_{\mathrm{B}}|\hat{\rho}_{\mathrm{AB}}^{(\mathrm{AB},0)}(t)|i'_{\mathrm{A}} j'_{\mathrm{B}}\rangle \\
&= \sum_{k\neq i}\sum_{l\neq j}\int_{t_0}^{t}\mathrm{d}t_1\int_{t_0}^{t_1}\mathrm{d}t_2\,\lambda^{\mathrm{A}}_{\perp,ik}(t_1)\lambda^{\mathrm{B}}_{\perp,jl}(t_2) \\
&\quad\times \mathrm{Tr}_\phi\Big(\hat{D}_{\beta^{\mathrm{A}-}_{ii'}(t)+\beta^{\mathrm{B}-}_{jj'}(t)-\beta^{\mathrm{A}-}_{ik}(t_1)-\beta^{\mathrm{B}-}_{jl}(t_2)} \\
&\quad\times \hat{\phi}^{\alpha^{\mathrm{A}}}_{\mathrm{T},kl}(t_1)\hat{\phi}^{\alpha^{\mathrm{B}}}_{\mathrm{T},kl}(t_2)\,\langle k_{\mathrm{A}} l_{\mathrm{B}}|\hat{\rho}_0|i'_{\mathrm{A}} j'_{\mathrm{B}}\rangle\Big)e^{\zeta^{(\mathrm{AB},0)}_{ijkli'j'}(t,t_1,t_2)},
\end{aligned}
\tag{B.110}
$$

$$
\begin{aligned}
&\langle i_{\mathrm{A}} j_{\mathrm{B}}|\hat{\rho}_{\mathrm{AB}}^{(\mathrm{BA},0)}(t)|i'_{\mathrm{A}} j'_{\mathrm{B}}\rangle \\
&= \sum_{k\neq i}\sum_{l\neq j}\int_{t_0}^{t}\mathrm{d}t_1\int_{t_0}^{t_1}\mathrm{d}t_2\,\lambda^{\mathrm{B}}_{\perp,jl}(t_1)\lambda^{\mathrm{A}}_{\perp,ik}(t_2) \\
&\quad\times \mathrm{Tr}_\phi\Big(\hat{D}_{\beta^{\mathrm{A}-}_{ii'}(t)+\beta^{\mathrm{B}-}_{jj'}(t)-\beta^{\mathrm{B}-}_{jl}(t_1)-\beta^{\mathrm{A}-}_{ik}(t_2)} \\
&\quad\times \hat{\phi}^{\alpha^{\mathrm{B}}}_{\mathrm{T},kl}(t_1)\hat{\phi}^{\alpha^{\mathrm{A}}}_{\mathrm{T},kl}(t_2)\,\langle k_{\mathrm{A}} l_{\mathrm{B}}|\hat{\rho}_0|i'_{\mathrm{A}} j'_{\mathrm{B}}\rangle\Big)e^{\zeta^{(\mathrm{BA},0)}_{ijlki'j'}(t,t_1,t_2)},
\end{aligned}
\tag{B.111}
$$

$$
\begin{aligned}
\zeta^{(\mathrm{AA},0)}_{ijski'j'}(t,t_1,t_2) &= -\vartheta_{iji'j'}(t) + C^{\mathrm{AA}}_{ii'is}(t,t_1) + C^{\mathrm{BA}}_{jj'is}(t,t_1) \\
&\quad + C^{\mathrm{AA}}_{ii'sk}(t,t_2) + C^{\mathrm{BA}}_{jj'sk}(t,t_2) \\
&\quad - C^{\mathrm{AA}}_{issk}(t_1,t_2) + \vartheta_{ijsj}(t_1) + \vartheta_{sjkj}(t_2), \\
\zeta^{(\mathrm{BB},0)}_{ijsli'j'}(t,t_1,t_2) &= -\vartheta_{iji'j'}(t) + C^{\mathrm{AB}}_{ii'js}(t,t_1) + C^{\mathrm{BB}}_{jj'js}(t,t_1) \\
&\quad + C^{\mathrm{AB}}_{ii'sl}(t,t_2) + C^{\mathrm{BB}}_{jj'sl}(t,t_2) \\
&\quad - C^{\mathrm{BB}}_{jssl}(t_1,t_2) + \vartheta_{ijis}(t_1) + \vartheta_{isil}(t_2), \\
\zeta^{(\mathrm{AB},0)}_{ijkli'j'}(t,t_1,t_2) &= -\vartheta_{iji'j'}(t) + C^{\mathrm{AA}}_{ii'ik}(t,t_1) + C^{\mathrm{BA}}_{jj'ik}(t,t_1) \\
&\quad + C^{\mathrm{AB}}_{ii'jl}(t,t_2) + C^{\mathrm{BB}}_{jj'jl}(t,t_2) \\
&\quad - C^{\mathrm{AB}}_{ikjl}(t_1,t_2) + \vartheta_{ijkj}(t_1) + \vartheta_{kjkl}(t_2), \\
\zeta^{(\mathrm{BA},0)}_{ijlki'j'}(t,t_1,t_2) &= -\vartheta_{iji'j'}(t) + C^{\mathrm{AB}}_{ii'jl}(t,t_1) + C^{\mathrm{BB}}_{jj'jl}(t,t_1) \\
&\quad + C^{\mathrm{AA}}_{ii'ik}(t,t_2) + C^{\mathrm{BA}}_{jj'ik}(t,t_2) \\
&\quad - C^{\mathrm{BA}}_{jlik}(t_1,t_2) + \vartheta_{ijil}(t_1) + \vartheta_{ilkl}(t_2).
\end{aligned}
\tag{B.112}
$$

B.4.2 Evolution of the state components for detectors initialized in pure product states

Now we particularize the expressions in the previous summary (Appendix B.4.1) for the case that the initial state is

$$\hat{\rho}_0 = |0_{\mathrm{A}}0_{\mathrm{B}}\rangle\langle 0_{\mathrm{A}}0_{\mathrm{B}}| \otimes \hat{\rho}_{\phi,0}. \tag{B.113}$$

The following expressions use the definitions stated in Appendix B.4.1 and the definitions of ξ_i^{ν}, $v_i^{\nu\nu}$, M_{ij} and $L_{ij}^{\mu\nu}$ from subsection 3.2.1,

$$\begin{aligned}
\xi_i^{\mathrm{A}} &= -\mathrm{i}\int_{t_0}^{t} \mathrm{d}t_1\, e^{\zeta^{(\mathrm{A},0)}_{i0000}(t,t_1)} \lambda^{\mathrm{A}}_{\perp,i0}(t_1) \\
&\quad \times \left\langle \hat{D}_{\beta^{\mathrm{A}-}_{i0}(t)-\beta^{\mathrm{A}-}_{i0}(t_1)} \hat{\phi}^{\alpha^{\mathrm{A}}}_{\mathrm{T},00}(t_1) \right\rangle_{\hat{\rho}_{\phi,0}}, \\
\xi_j^{\mathrm{B}} &= -\mathrm{i}\int_{t_0}^{t} \mathrm{d}t_1\, e^{\zeta^{(\mathrm{B},0)}_{0j000}(t,t_1)} \lambda^{\mathrm{B}}_{\perp,j0}(t_1) \\
&\quad \times \left\langle \hat{D}_{\beta^{\mathrm{B}-}_{j0}(t)-\beta^{\mathrm{B}-}_{j0}(t_1)} \hat{\phi}^{\alpha^{\mathrm{B}}}_{\mathrm{T},00}(t_1) \right\rangle_{\hat{\rho}_{\phi,0}},
\end{aligned} \tag{B.114}$$

$$\begin{aligned}
v_i^{\mathrm{AA}} &= \sum_{s\neq i,0} \int_{t_0}^{t} \mathrm{d}t_1 \int_{t_0}^{t_1} \mathrm{d}t_2\, e^{\zeta^{(\mathrm{AA},0)}_{i0s000}(t,t_1,t_2)} \lambda^{\mathrm{A}}_{\perp,is}(t_1)\lambda^{\mathrm{A}}_{\perp,s0}(t_2) \\
&\quad \times \left\langle -\hat{D}_{\beta^{\mathrm{A}-}_{i0}(t)-\beta^{\mathrm{A}-}_{is}(t_1)-\beta^{\mathrm{A}-}_{s0}(t_2)} \hat{\phi}^{\alpha^{\mathrm{A}}}_{\mathrm{T},00}(t_1)\hat{\phi}^{\alpha^{\mathrm{A}}}_{\mathrm{T},00}(t_2) \right\rangle_{\hat{\rho}_{\phi,0}}, \\
v_j^{\mathrm{BB}} &= \sum_{s\neq j,0} \int_{t_0}^{t} \mathrm{d}t_1 \int_{t_0}^{t_1} \mathrm{d}t_2\, e^{\zeta^{(\mathrm{BB},0)}_{0js000}(t,t_1,t_2)} \lambda^{\mathrm{B}}_{\perp,js}(t_1)\lambda^{\mathrm{B}}_{\perp,s0}(t_2) \\
&\quad \times \left\langle -\hat{D}_{\beta^{\mathrm{B}-}_{j0}(t)-\beta^{\mathrm{B}-}_{js}(t_1)-\beta^{\mathrm{B}-}_{s0}(t_2)} \hat{\phi}^{\alpha^{\mathrm{B}}}_{\mathrm{T},00}(t_1)\hat{\phi}^{\alpha^{\mathrm{B}}}_{\mathrm{T},00}(t_2) \right\rangle_{\hat{\rho}_{\phi,0}},
\end{aligned} \tag{B.115}$$

$$\begin{aligned}
&M_{ij} \\
&= -\int_{t_0}^{t} \mathrm{d}t_1 \int_{t_0}^{t_1} \mathrm{d}t_2\, e^{\zeta^{(\mathrm{AB},0)}_{ij0000}(t,t_1,t_2)} \lambda^{\mathrm{A}}_{\perp,i0}(t_1)\lambda^{\mathrm{B}}_{\perp,j0}(t_2) \\
&\times \left\langle \hat{D}_{\beta^{\mathrm{A}-}_{i0}(t)+\beta^{\mathrm{B}-}_{j0}(t)-\beta^{\mathrm{A}-}_{i0}(t_1)-\beta^{\mathrm{B}-}_{j0}(t_2)} \hat{\phi}^{\alpha^{\mathrm{A}}}_{\mathrm{T},00}(t_1)\hat{\phi}^{\alpha^{\mathrm{B}}}_{\mathrm{T},00}(t_2) \right\rangle_{\hat{\rho}_{\phi,0}} \\
&- \int_{t_0}^{t} \mathrm{d}t_1 \int_{t_0}^{t_1} \mathrm{d}t_2\, e^{\zeta^{(\mathrm{BA},0)}_{ij0000}(t,t_1,t_2)} \lambda^{\mathrm{B}}_{\perp,j0}(t_1)\lambda^{\mathrm{A}}_{\perp,i0}(t_2) \\
&\times \left\langle \hat{D}_{\beta^{\mathrm{A}-}_{i0}(t)+\beta^{\mathrm{B}-}_{j0}(t)-\beta^{\mathrm{B}-}_{j0}(t_1)-\beta^{\mathrm{A}-}_{i0}(t_2)} \hat{\phi}^{\alpha^{\mathrm{B}}}_{\mathrm{T},00}(t_1)\hat{\phi}^{\alpha^{\mathrm{A}}}_{\mathrm{T},00}(t_2) \right\rangle_{\hat{\rho}_{\phi,0}},
\end{aligned} \tag{B.116}$$

$$
\begin{aligned}
L^{\mathrm{AA}}_{ii'} &= \int_{t_0}^{t}\mathrm{d}t_1\int_{t_0}^{t}\mathrm{d}t_2\, e^{\zeta^{(\mathrm{A},\mathrm{A})}_{i00i'00}(t,t_1,t_2)}\lambda^{\mathrm{A}}_{\perp,i0}(t_1)\lambda^{\mathrm{A}}_{\perp,0i'}(t_2)\\
&\quad\times\Big\langle\hat{\phi}^{\alpha^{\mathrm{A}}}_{\mathrm{T},00}(t_2)\hat{D}_{\beta^{\mathrm{A}-}_{ii'}(t)-\beta^{\mathrm{A}-}_{i0}(t_1)+\beta^{\mathrm{A}-}_{i'0}(t_2)}\hat{\phi}^{\alpha^{\mathrm{A}}}_{\mathrm{T},00}(t_1)\Big\rangle_{\hat{\rho}_{\phi,0}},\\
L^{\mathrm{BB}}_{jj'} &= \int_{t_0}^{t}\mathrm{d}t_1\int_{t_0}^{t}\mathrm{d}t_2\, e^{\zeta^{(\mathrm{B},\mathrm{B})}_{0j00j'0}(t,t_1,t_2)}\lambda^{\mathrm{B}}_{\perp,j0}(t_1)\lambda^{\mathrm{B}}_{\perp,0j'}(t_2)\\
&\quad\times\Big\langle\hat{\phi}^{\alpha^{\mathrm{B}}}_{\mathrm{T},00}(t_2)\hat{D}_{\beta^{\mathrm{B}-}_{jj'}(t)-\beta^{\mathrm{B}-}_{j0}(t_1)+\beta^{\mathrm{B}-}_{j'0}(t_2)}\hat{\phi}^{\alpha^{\mathrm{B}}}_{\mathrm{T},00}(t_1)\Big\rangle_{\hat{\rho}_{\phi,0}},\\
L^{\mathrm{AB}}_{ij} &= \int_{t_0}^{t}\mathrm{d}t_1\int_{t_0}^{t}\mathrm{d}t_2\, e^{\zeta^{(\mathrm{A},\mathrm{B})}_{i00j0}(t,t_1,t_2)}\lambda^{\mathrm{A}}_{\perp,i0}(t_1)\lambda^{\mathrm{B}}_{\perp,0j}(t_2)\\
&\quad\times\Big\langle\hat{\phi}^{\alpha^{\mathrm{B}}}_{\mathrm{T},00}(t_2)\hat{D}_{\beta^{\mathrm{A}-}_{i0}(t)-\beta^{\mathrm{B}-}_{j0}(t)-\beta^{\mathrm{A}-}_{i0}(t_1)+\beta^{\mathrm{B}-}_{j0}(t_2)}\\
&\qquad\times\hat{\phi}^{\alpha^{\mathrm{A}}}_{\mathrm{T},00}(t_1)\Big\rangle_{\hat{\rho}_{\phi,0}}.
\end{aligned}
\tag{B.117}
$$

B.5 Eigenvalues of perturbed rank one Hermitian operators

This appendix is dedicated to finding perturbative expressions for the eigenvalues for operators of the following kind,

$$
\begin{aligned}
\hat{R} &= |\eta_0\rangle\langle\eta_0| + \lambda\big(\,|\eta_1\rangle\langle\eta_0| + |\eta_0\rangle\langle\eta_1|\,\big)\\
&\quad+\lambda^2\big(\,|\eta_2\rangle\langle\eta_0| + |\eta_0\rangle\langle\eta_2| + \hat{R}^{\perp}\big) + \mathcal{O}(\lambda^3),
\end{aligned}
\tag{B.118}
$$

where $\langle\eta_0|\eta_1\rangle = 0$, $\hat{R}^{\perp}|\eta_0\rangle = 0$, $\hat{R}^{\perp\dagger} = \hat{R}^{\perp}$, $\langle\eta_0|\eta_0\rangle = 1$, and $|\eta_1\rangle$, $|\eta_2\rangle$ are not normalized in general.

We are interested in such operators because $\hat{\rho}_{\mathrm{AB}}$ and $\hat{\rho}^{\top_{\mathrm{A}}}_{\mathrm{AB}}$ are of this form, for the scenario explored in Section 3.2. That is, the scenario where the detectors are initialized in a pure, longitudinal product state. The expression of $\hat{\rho}^{\top_{\mathrm{A}}}_{\mathrm{AB}}$ for this case, shown in Eq. (3.66), is

$$
\begin{aligned}
\hat{\rho}^{\top_{\mathrm{A}}}_{\mathrm{AB}} &= |0_{\mathrm{A}}0_{\mathrm{B}}\rangle\langle 0_{\mathrm{A}}0_{\mathrm{B}}| + |\psi_1\rangle\langle 0_{\mathrm{A}}0_{\mathrm{B}}| + |0_{\mathrm{A}}0_{\mathrm{B}}\rangle\langle\psi_1|\\
&\quad+|\psi_2\rangle\langle 0_{\mathrm{A}}0_{\mathrm{B}}| + |0_{\mathrm{A}}0_{\mathrm{B}}\rangle\langle\psi_2| + \hat{\sigma}_2 + \mathcal{O}\big(\lambda^3_{\perp}\big).
\end{aligned}
\tag{B.119}
$$

To verify that $\hat{\rho}^{\top_{\mathrm{A}}}_{\mathrm{AB}}$ is of the same form as $\hat{R}$, notice that $|\psi_1\rangle$ is of order $\lambda_{\perp}$, while $|\psi_2\rangle$ and $\hat{\sigma}_2$ are of order $\lambda^2_{\perp}$, and $\langle 0_{\mathrm{A}}0_{\mathrm{B}}|\psi_1\rangle = 0$, $\hat{\sigma}_2|0_{\mathrm{A}}0_{\mathrm{B}}\rangle = 0$, $\hat{\sigma}^{\dagger}_2 = \hat{\sigma}_2$, $\langle 0_{\mathrm{A}}0_{\mathrm{B}}|0_{\mathrm{A}}0_{\mathrm{B}}\rangle = 1$.

We now proceed to investigating the eigenvalues of Hermitian operators of the form of $\hat{R}$, perturbatively in the parameter λ. Consider any $|\kappa\rangle$ eigenvector of $\hat{R}$ with eigenvalue r, so that

$$\hat{R}\,|\kappa\rangle = r\,|\kappa\rangle\,. \tag{B.120}$$

Let us expand the eigenvector and eigenvalue in powers of λ,

$$\begin{aligned} r &= r_0 + \lambda r_1 + \lambda^2 r_2 + \mathcal{O}(\lambda^3) \\ |\kappa\rangle &= |\kappa_0\rangle + \lambda\,|\kappa_1\rangle + \lambda^2\,|\kappa_2\rangle + \mathcal{O}(\lambda^3). \end{aligned} \tag{B.121}$$

The eigenvalue equation must be true at every perturbative order. Therefore, it is convenient to expand both sides of the eigenvalue equation,

$$\begin{aligned} \hat{R}\,|\kappa\rangle &= \langle\eta_0|\kappa_0\rangle\,|\eta_0\rangle \\ &\quad + \lambda\big(\,\langle\eta_0|\kappa_1\rangle\,|\eta_0\rangle + \langle\eta_0|\kappa_0\rangle\,|\eta_1\rangle + \langle\eta_1|\kappa_0\rangle\,|\eta_0\rangle\,\big) \\ &\quad + \lambda^2\big(\,\langle\eta_0|\kappa_2\rangle\,|\eta_0\rangle + \langle\eta_0|\kappa_1\rangle\,|\eta_1\rangle + \langle\eta_1|\kappa_1\rangle\,|\eta_0\rangle \\ &\quad + \langle\eta_0|\kappa_0\rangle\,|\eta_2\rangle + \langle\eta_2|\kappa_0\rangle\,|\eta_0\rangle + \hat{R}^{\perp}\,|\kappa_0\rangle\,\big) + \mathcal{O}(\lambda^3), \\ r\,|\kappa\rangle &= r_0\,|\kappa_0\rangle \\ &\quad + \lambda\big(r_0\,|\kappa_1\rangle + r_1\,|\kappa_0\rangle\,\big) \\ &\quad + \lambda^2\big(r_0\,|\kappa_2\rangle + r_1\,|\kappa_1\rangle + r_2\,|\kappa_0\rangle\,\big) + \mathcal{O}(\lambda^3). \end{aligned} \tag{B.122}$$

Let us assume that $r_0 \neq 0$, and choose $||\,|\kappa_0\rangle\,|| = 1$, then,

$$\langle\eta_0|\kappa_0\rangle\,|\eta_0\rangle = r_0\,|\kappa_0\rangle \implies |\kappa_0\rangle = |\eta_0\rangle\,,\ r_0 = 1. \tag{B.123}$$

Then, substituting and equating the order λ,

$$\langle\eta_0|\kappa_1\rangle\,|\eta_0\rangle + |\eta_1\rangle = |\kappa_1\rangle + r_1\,|\eta_0\rangle \tag{B.124}$$

where we used $\langle\eta_1|\eta_0\rangle = 0$. Next, taking the inner product with $|\eta_0\rangle$,

$$\begin{aligned} &\langle\eta_0|\kappa_1\rangle = \langle\eta_0|\kappa_1\rangle + r_1 \\ &\implies r_1 = 0,\ |\kappa_1\rangle = \langle\eta_0|\kappa_1\rangle\,|\eta_0\rangle + |\eta_1\rangle\,. \end{aligned} \tag{B.125}$$

We can only choose one parameter, $\langle\eta_0|\kappa_1\rangle$, which is related to the freedom in the normalization of $|\kappa\rangle$[1]. For simplicity, we pick $\langle\eta_0|\kappa_1\rangle = 0$, and thus $|\kappa_1\rangle = |\eta_1\rangle$.

[1]The choice $\langle\eta_0|\kappa_1\rangle = 0$ turns out to be equivalent to imposing $\langle\kappa|\kappa\rangle = \langle\eta_0|\eta_0\rangle + \mathcal{O}(\lambda^2)$.

Finally, using the results above and equating the order λ^2,

$$\begin{aligned}&\langle\eta_0|\kappa_2\rangle\,|\eta_0\rangle + \langle\eta_1|\eta_1\rangle\,|\eta_0\rangle + |\eta_2\rangle + \langle\eta_2|\eta_0\rangle\,|\eta_0\rangle \\ &= |\kappa_2\rangle + r_2\,|\eta_0\rangle\,.\end{aligned} \tag{B.126}$$

Taking the inner product with $|\eta_0\rangle$, we find that

$$r_2 = \langle\eta_1|\eta_1\rangle + 2\,\mathrm{Re}\,\langle\eta_0|\eta_2\rangle\,. \tag{B.127}$$

Therefore,

$$|\kappa_2\rangle = \langle\eta_0|\kappa_2\rangle\,|\eta_0\rangle + |\eta_2\rangle - \langle\eta_0|\eta_2\rangle\,|\eta_0\rangle\,, \tag{B.128}$$

and picking $\langle\eta_0|\kappa_2\rangle = 0$,[2]

$$|\kappa_2\rangle = |\eta_2\rangle - \langle\eta_0|\eta_2\rangle\,|\eta_0\rangle\,. \tag{B.129}$$

Therefore, the following is one eigenvalue and eigenvector pair of $\hat{R}$,

$$\begin{aligned}r &= 1 + \lambda^2\big(\,\langle\eta_1|\eta_1\rangle + 2\,\mathrm{Re}\,\langle\eta_0|\eta_2\rangle\,\big) + \mathcal{O}(\lambda^3), \\ |\kappa\rangle &= |\eta_0\rangle + \lambda\,|\eta_1\rangle + \lambda^2(|\eta_2\rangle - \langle\eta_0|\eta_2\rangle\,|\eta_0\rangle) + \mathcal{O}(\lambda^3).\end{aligned} \tag{B.130}$$

This eigenvalue must be positive when we are in the perturbative regime, where $\lambda \ll 1$. Therefore, this eigenvalue will not affect negativity in perturbative calculations.

Therefore, let us search for the rest of eigenvalues of $\hat{R}$ to find the negative ones. Previously, we assumed $r_0 \neq 0$, therefore we now explore the other case, $r_0 = 0$,

$$\langle\eta_0|\kappa_0\rangle\,|\eta_0\rangle = r_0\,|\kappa_0\rangle \implies \langle\eta_0|\kappa_0\rangle = 0. \tag{B.131}$$

This constraint leaves $|\kappa_0^{\perp}\rangle = (\hat{\mathbb{1}} - |\eta_0\rangle\langle\eta_0|)\,|\kappa_0\rangle$ completely free. Next, substituting and equating the order λ,

$$\langle\eta_0|\kappa_1\rangle\,|\eta_0\rangle + \langle\eta_1|\kappa_0\rangle\,|\eta_0\rangle = r_1\,|\kappa_0\rangle\,. \tag{B.132}$$

Taking the inner product with $|\eta_0\rangle$,

$$\langle\eta_0|\kappa_1\rangle = -\,\langle\eta_1|\kappa_0\rangle \implies r_1 = 0. \tag{B.133}$$

Here, we also have complete freedom in $(\hat{\mathbb{1}} - |\eta_0\rangle\langle\eta_0|)\,|\kappa_1\rangle$.

[2]The choices $\langle\eta_0|\kappa_1\rangle = 0$ and $\langle\eta_0|\kappa_2\rangle = 0$ turn out to be equivalent to imposing $\langle\kappa|\kappa\rangle = \langle\eta_0|\eta_0\rangle + \mathcal{O}(\lambda^3)$.

Finally, for the order λ^2,

$$r_2 |\kappa_0\rangle = \langle\eta_0|\kappa_2\rangle |\eta_0\rangle - \langle\eta_1|\kappa_0\rangle |\eta_1\rangle + \langle\eta_1|\kappa_1\rangle |\eta_0\rangle + \langle\eta_2|\kappa_0\rangle |\eta_0\rangle + \hat{R}^{\perp} |\kappa_0\rangle , \tag{B.134}$$

and taking the inner product with $|\eta_0\rangle$,

$$\langle\eta_0|\kappa_2\rangle = - \langle\eta_1|\kappa_1\rangle - \langle\eta_2|\kappa_0\rangle , \tag{B.135}$$

which also allows complete freedom in $(\hat{\mathbb{1}} - |\eta_0\rangle\langle\eta_0|) |\kappa_2\rangle$. However, now we have the additional condition

$$r_2 |\kappa_0\rangle = - \langle\eta_1|\kappa_0\rangle |\eta_1\rangle + \hat{R}^{\perp} |\kappa_0\rangle = (\hat{R}^{\perp} - |\eta_1\rangle\langle\eta_1|) |\kappa_0\rangle , \tag{B.136}$$

which can be seen as an eigenvalue equation for the matrix $\hat{R}^{\perp} - |\eta_1\rangle\langle\eta_1|$, in the subspace of vectors orthogonal to $|\eta_0\rangle$, since $\langle\eta_0|\kappa_0\rangle = 0$.

Therefore, all the remaining eigenvalue and eigenvector pairs of $\hat{R}$ are of the form

$$r = \lambda^2 r_2 + \mathcal{O}(\lambda^3), \tag{B.137}$$

$$|\kappa\rangle = |\kappa_0^{\perp}\rangle + \lambda(|\kappa_1^{\perp}\rangle - \langle\eta_1|\kappa_0^{\perp}\rangle |\eta_0\rangle) + \lambda^2 \big(|\kappa_2^{\perp}\rangle - (\langle\eta_1|\kappa_1^{\perp}\rangle + \langle\eta_2|\kappa_0^{\perp}\rangle) |\eta_0\rangle \big) + \mathcal{O}(\lambda^3), \tag{B.138}$$

with the following restrictions: $|\kappa_i^{\perp}\rangle$ are vectors orthogonal to $|\eta_0\rangle$, i.e. $\langle\eta_0|\kappa_i^{\perp}\rangle = 0$. Moreover, $|\kappa_0^{\perp}\rangle$ is an eigenvector of $\hat{R}^{\perp} - |\eta_1\rangle\langle\eta_1|$ with eigenvalue r_2.

In conclusion, this calculation shows that the negative eigenvalues for $\hat{R}$ are of order λ^2. Specifically, the negative eigenvalues of $\hat{R}$ at leading order are equal to λ^2 times the negative eigenvalues of $\hat{R}^{\perp} - |\eta_1\rangle\langle\eta_1|$.

B.6 Computing expectation values for displacement and field operators

The expression we derived for $\hat{\rho}_{\text{AB}}$, perturbative in $\lambda_{\perp}$ and non-perturbative in $\lambda_{\parallel}$, provided in Appendix B.4.2, requires computing expectation values of combinations of field operators and displacement operators. Specifically, the expectation values we need to find are of the form

$$\big\langle \hat{D}_{\alpha} \big\rangle_{\hat{\rho}_{\phi}}, \ \big\langle \hat{D}_{\alpha} \hat{\phi}^{\beta} \big\rangle_{\hat{\rho}_{\phi}}, \ \big\langle \hat{D}_{\alpha} \hat{\phi}^{\beta} \hat{\phi}^{\gamma} \big\rangle_{\hat{\rho}_{\phi}}, \ \big\langle \hat{\phi}^{\alpha} \hat{D}_{\beta} \hat{\phi}^{\gamma} \big\rangle_{\hat{\rho}_{\phi}}. \tag{B.139}$$

In what follows, we will find expressions for these for zero-mean Gaussian states and particularize them for the vacuum state.

B.6.1 Zero-mean Gaussian states

Consider the field to be in a Gaussian state $\hat{\rho}_\phi$ with zero one-point function, which is also called a quasi-free state. Then, Wick's theorem lets us evaluate the expectation values in Eq. (B.139) and obtain

$$\begin{aligned}
\left\langle \hat{D}_\alpha \right\rangle_{\hat{\rho}_\phi} &= e^{-\frac{1}{2}W^{\alpha\alpha}}, \\
\left\langle \hat{D}_\alpha \hat{\phi}^\beta \right\rangle_{\hat{\rho}_\phi} &= -\mathrm{i}W^{\alpha\beta} e^{-\frac{1}{2}W^{\alpha\alpha}}, \\
\left\langle \hat{D}_\alpha \hat{\phi}^\beta \hat{\phi}^\gamma \right\rangle_{\hat{\rho}_\phi} &= (W^{\beta\gamma} - W^{\alpha\beta}W^{\alpha\gamma}) e^{-\frac{1}{2}W^{\alpha\alpha}}, \\
\left\langle \hat{\phi}^\alpha \hat{D}_\beta \hat{\phi}^\gamma \right\rangle_{\hat{\rho}_\phi} &= (W^{\alpha\gamma} - W^{\alpha\beta}W^{\beta\gamma}) e^{-\frac{1}{2}W^{\beta\beta}},
\end{aligned} \tag{B.140}$$

where we used the definitions

$$\hat{D}_\alpha = e^{-\mathrm{i}\hat{\phi}^\alpha}, \quad W^{\alpha\beta} = \left\langle \hat{\phi}^\alpha \hat{\phi}^\beta \right\rangle_{\hat{\rho}_\phi}. \tag{B.141}$$

We now derive the equalities in (B.140), starting from the following [115],

$$\left\langle e^{\hat{\phi}^\kappa} \right\rangle_{\hat{\rho}_\phi} = e^{\frac{1}{2}\left\langle (\hat{\phi}^\kappa)^2 \right\rangle}. \tag{B.142}$$

Here, and from now on in this appendix, expectation values are taken with respect to $\hat{\rho}_\phi$ implicitly, to keep the notation lighter.

Using the linearity of $\hat{\phi}^\kappa$ on its exponent, we obtain the first equation

$$\left\langle \hat{D}_\alpha \right\rangle = e^{-\frac{1}{2}W^{\alpha\alpha}}. \tag{B.143}$$

For the second equality, we can use the following trick

$$\left\langle \hat{D}_\alpha \hat{\phi}^\beta \right\rangle = \partial_u \left\langle e^{-\mathrm{i}\hat{\phi}^\alpha} e^{u\hat{\phi}^\beta} \right\rangle \Big|_{u=0}. \tag{B.144}$$

To evaluate the right hand side we proceed as follows,

$$\begin{aligned}
\left\langle e^{-\mathrm{i}\hat{\phi}^\alpha} e^{u\hat{\phi}^\beta} \right\rangle &= e^{-\mathrm{i}\frac{u}{2}\left[\hat{\phi}^\alpha, \hat{\phi}^\beta\right]} \left\langle e^{-\mathrm{i}\hat{\phi}^\alpha + u\hat{\phi}^\beta} \right\rangle \\
&= e^{-\mathrm{i}\frac{u}{2}\left\langle \hat{\phi}^\alpha \hat{\phi}^\beta - \hat{\phi}^\beta \hat{\phi}^\alpha \right\rangle} e^{\frac{1}{2}\left\langle (-\mathrm{i}\hat{\phi}^\alpha + u\hat{\phi}^\beta)^2 \right\rangle} \\
&= e^{-\frac{1}{2}W^{\alpha\alpha} - \mathrm{i}uW^{\alpha\beta} + \frac{u^2}{2}W^{\beta\beta}},
\end{aligned} \tag{B.145}$$

by using the Baker-Campbell-Hausdorff (BCH) formula and Eq. (B.142). Then,

$$\begin{aligned}\left\langle \hat{D}_\alpha \hat{\phi}^\beta \right\rangle &= \partial_u e^{-\frac{1}{2}W^{\alpha\alpha} - \mathrm{i}uW^{\alpha\beta} + \frac{u^2}{2}W^{\beta\beta}}\Big|_{u=0} \\ &= -\mathrm{i}W^{\alpha\beta} e^{-\frac{1}{2}W^{\alpha\alpha}},\end{aligned} \tag{B.146}$$

proving the second equality in (B.140).

To show the third equality, we follow the same strategy,

$$\left\langle \hat{D}_\alpha \hat{\phi}^\beta \hat{\phi}^\gamma \right\rangle = \partial_u \partial_v \left\langle e^{-\mathrm{i}\hat{\phi}^\alpha} e^{u\hat{\phi}^\beta} e^{v\hat{\phi}^\gamma} \right\rangle\Big|_{u=0,\, v=0}, \tag{B.147}$$

and using the BCH formula and Eq. (B.142),

$$\begin{aligned}&\left\langle e^{-\mathrm{i}\hat{\phi}^\alpha} e^{u\hat{\phi}^\beta} e^{v\hat{\phi}^\gamma} \right\rangle \\ &= e^{\frac{1}{2}\left[\hat{\phi}^\alpha, \hat{\phi}^\beta\right] + \frac{1}{2}\left[\hat{\phi}^\alpha + \hat{\phi}^\beta, \hat{\phi}^\gamma\right]} \left\langle e^{-\mathrm{i}\hat{\phi}^\alpha + u\hat{\phi}^\beta + v\hat{\phi}^\gamma} \right\rangle \\ &= e^{\frac{1}{2}(-W^{\alpha\alpha} + u^2 W^{\beta\beta} + v^2 W^{\gamma\gamma}) - \mathrm{i}uW^{\alpha\beta} - \mathrm{i}vW^{\alpha\gamma} + uvW^{\beta\gamma}}.\end{aligned} \tag{B.148}$$

Substituting Eq. (B.148) into Eq. (B.147), and computing the appropriate derivatives, we obtain

$$\left\langle \hat{D}_\alpha \hat{\phi}^\beta \hat{\phi}^\gamma \right\rangle = (W^{\beta\gamma} - W^{\alpha\beta}W^{\alpha\gamma}) e^{-\frac{1}{2}W^{\alpha\alpha}}. \tag{B.149}$$

The final equality,

$$\left\langle \hat{\phi}^\alpha \hat{D}_\beta \hat{\phi}^\gamma \right\rangle = (W^{\alpha\gamma} - W^{\alpha\beta}W^{\beta\gamma}) e^{-\frac{1}{2}W^{\beta\beta}}, \tag{B.150}$$

can be obtained through an analogous calculation. Alternatively, $\left\langle \hat{\phi}^\alpha \hat{D}_\beta \hat{\phi}^\gamma \right\rangle$ can be obtained using that

$$\begin{aligned}\hat{\phi}^\alpha \hat{D}_\beta &= \hat{D}_\beta \hat{\phi}^\alpha - \mathrm{i}\hat{D}_\beta [\hat{\phi}^\alpha, \hat{\phi}^\beta] \\ &= \hat{D}_\beta \hat{\phi}^\alpha - \mathrm{i}\hat{D}_\beta (W^{\alpha\beta} - W^{\beta\alpha}),\end{aligned} \tag{B.151}$$

in combination with Eqs. (B.146) and (B.149).

B.6.2 Vacuum state

Now, consider the field to be in the vacuum state,

$$\hat{\rho}_{\phi,0} = |0_\phi\rangle\langle 0_\phi| \,. \tag{B.152}$$

The vacuum is a Gaussian state. Moreover, its one-point function, the expectation of $\hat{\phi}$, is zero in the vacuum. Therefore, the results derived in the previous part of this appendix, shown in Eq. (B.140), apply.

Furthermore, we can now compute $W^{\alpha\beta}$,

$$\begin{aligned} W^{\alpha\beta} &= \langle 0_\phi | \hat{\phi}^\alpha \hat{\phi}^\beta | 0_\phi \rangle \\ &= \int_{\mathbb{R}^n} \mathrm{d}^n \boldsymbol{k} \int_{\mathbb{R}^n} \mathrm{d}^n \boldsymbol{k}' \, \alpha^*(\boldsymbol{k}) \beta(\boldsymbol{k}') \, \langle 0_\phi | \hat{a}_{\boldsymbol{k}} \hat{a}^\dagger_{\boldsymbol{k}} | 0_\phi \rangle \\ &= \int_{\mathbb{R}^n} \mathrm{d}^n \boldsymbol{k} \, \alpha^*(\boldsymbol{k}) \beta(\boldsymbol{k}), \end{aligned} \tag{B.153}$$

where we used that the vacuum is annihilated by the annihilation operator $\hat{a}_{\boldsymbol{k}} \, |0_\phi\rangle = 0$, $[\hat{a}_{\boldsymbol{k}}, \hat{a}^\dagger_{\boldsymbol{k}'}] = \delta(\boldsymbol{k} - \boldsymbol{k}') \hat{\mathbb{1}}$, and Eq. (3.2), which we write as

$$\hat{\phi}^\alpha = \mathrm{i} \int_{\mathbb{R}^n} \mathrm{d}^n \boldsymbol{k} \, \alpha(\boldsymbol{k}) \hat{a}^\dagger_{\boldsymbol{k}} - \alpha^*(\boldsymbol{k}) \hat{a}_{\boldsymbol{k}}. \tag{B.154}$$

Appendix C

Appendices for Chapter 4

C.1 Relating the variable gap detector and the spin-boson model

The spin-boson model [68], commonly used to model superconducting circuits, has the Hamiltonian

$$\begin{aligned}
\hat{H}_{\text{SB}} &= \hat{H}_{\text{S}} + \hat{H}_{\text{B}} + \hat{H}_{\text{INT-SB}}, \\
\hat{H}_{\text{S}} &= -\frac{\hbar\Omega}{2}\hat{\sigma}_z, \\
\hat{H}_{\text{B}} &= \sum_k \hbar\omega_k \hat{a}_k^\dagger \hat{a}_k, \\
\hat{H}_{\text{INT-SB}} &= \sum_k (g_k^x \hat{\sigma}_x + g_k^z \hat{\sigma}_z)\hat{a}_k^\dagger + \text{H.c.},
\end{aligned} \tag{C.1}$$

where the bosonic bath with $\hat{H}_{\text{B}}$ corresponds to a transmission line of finite length L, with $k \in \frac{2\pi}{L}\mathbb{Z}$.

Now, consider the variable gap detector model of Eq. (4.31). Then, in the Schrödinger picture, picking the detector position $x_{\text{QB}} = 0$, assuming the interaction is fully switched

on, $\chi(t) = 1$, and ignoring additive constants in $\hat{H}_{\text{TL}}$,

$$\begin{aligned}
\hat{H}_{\text{VGAP}} &= \hat{H}_{\text{QB}} + \hat{H}_{\text{TL}} + \hat{H}_{\text{INT}}, \\
\hat{H}_{\text{QB}} &= -\frac{\hbar(\Omega^0 + \Delta\Omega)}{2}\hat{\sigma}_z, \\
\hat{H}_{\text{TL}} &= \int \mathrm{d}k\, \hbar\omega_k \hat{a}_k^\dagger \hat{a}_k, \\
\hat{H}_{\text{INT}} &= \varphi_0 \gamma \hat{\sigma}_x \int \mathrm{d}k\ \mathrm{C}(\omega_k)\sqrt{\frac{\hbar\omega_k}{4\pi\ell_0}}\,\mathrm{sgn}(k)\mathrm{i}\hat{a}_k^\dagger + \mathrm{H.c.}
\end{aligned} \tag{C.2}$$

Therefore, comparing with the spin-boson model,

$$g_k^x = \varphi_0\gamma\sqrt{\frac{\hbar\omega_k}{4\pi\ell_0}}\,\mathrm{C}(\omega_k)\,\mathrm{sgn}(k),\ \ g_k^z = 0, \tag{C.3}$$

where the longitudinal coupling is zero because we only kept the transversal coupling in the variable gap detector model. The spectral density of the bosonic bath (the infinite transmission line in our case) is

$$\begin{aligned}
J(\omega) &= \frac{2\pi}{\hbar^2}\int \mathrm{d}k\, |g_k|^2 \delta(\omega - \omega_k) \\
&= 2\int_0^\infty \mathrm{d}\omega'\, \frac{\varphi_0^2\gamma^2}{2\hbar\ell_0 v}\omega'\,\mathrm{C}^2(\omega')\delta(\omega - \omega') \\
&= \frac{1}{8\pi}\frac{R_{\text{K}}}{Z_0}\gamma^2\omega e^{-\frac{\omega}{\Omega_{\text{cut}}}},
\end{aligned} \tag{C.4}$$

where we used the exponential cutoff from Eq. (4.9).

In the limit $\omega \ll \Omega_{\text{cut}}$,

$$J(\omega) = \pi\alpha\omega, \tag{C.5}$$

which is the spectral density of an Ohmic bath, with the dimensionless coupling constant α being

$$\alpha = \frac{R_{\text{K}}}{8\pi^2 Z_0}\gamma^2 \approx 6.54\cdot\gamma^2. \tag{C.6}$$

Since the numerical simulations predict $\gamma \in [-0.02, 0.22]$ (see subsection 4.2.1), then $\alpha \in [0, 0.32]$.

As the frequencies approach Ω_{cut}, the exponential cutoff becomes noticeable, modifying the spectral density,

$$J(\omega) = \pi\alpha\omega e^{-\frac{\omega}{\Omega_{\text{cut}}}}. \tag{C.7}$$

C.2 Computing the outcome of the harvesting protocol

Here we follow the perturbative procedure outlined in 4.3 to obtain the final state of the probes after they interact with the field. The result is computed to the leading perturbative order, $\mathcal{O}(\lambda^2)$, assuming that $\lambda_{\mathrm{A}} = \lambda_{\mathrm{B}} = \lambda$.

To simplify the calculations, we define the following operators,

$$\begin{aligned}\hat{\chi}_\nu(t) &= \chi_\nu(t)\hat{\mu}_\nu(t),\\ \hat{\phi}'_\nu(t) &= \partial_x\hat{\phi}_{\mathrm{C}}(t, x_\nu)\end{aligned} \tag{C.8}$$

This notation simplifies the interaction Hamiltonian of Eq. (4.37) to

$$\hat{H}_I = \sum_\nu \lambda\hat{\chi}_\nu\hat{\phi}'_\nu\,. \tag{C.9}$$

Substituting into Eq. (4.41),

$$\begin{aligned}\hat{U}^{(1)} &= -\,\mathrm{i}\lambda\int \mathrm{d}t\,\sum_\nu \hat{\chi}_\nu(t)\hat{\phi}'_\nu(t)\,,\\ \hat{U}^{(2)} &= -\,\lambda^2\int_{t>t'}\mathrm{d}t\,\mathrm{d}t'\,\sum_{\mu,\nu}\hat{\chi}_\mu(t)\hat{\chi}_\nu(t')\hat{\phi}'_\mu(t)\hat{\phi}'_\nu(t').\end{aligned} \tag{C.10}$$

Now, we can compute the leading order terms of the detectors' final state according to Eq. (4.46),

$$\hat{\rho}_{\mathrm{AB}} = \hat{\rho}_{\mathrm{AB},0} + \hat{\rho}^{(2,0)}_{\mathrm{AB}} + \hat{\rho}^{(1,1)}_{\mathrm{AB}} + \hat{\rho}^{(0,2)}_{\mathrm{AB}} + \mathcal{O}(\lambda^4)\,. \tag{C.11}$$

First,

$$\begin{aligned}\hat{\rho}^{(1,1)}_{\mathrm{AB}} &= \mathrm{Tr}_\phi\big(\hat{U}^{(1)}\hat{\rho}_{\mathrm{AB},0}\otimes\hat{\rho}_{\phi,0}\hat{U}^{(1)\dagger}\big)\\ &= \lambda^2\int \mathrm{d}t\,\mathrm{d}t'\,\sum_{\mu,\nu}\mathcal{W}_{xx'}(t', x_\nu, t, x_\mu)\hat{\chi}_\mu(t)\hat{\rho}_{\mathrm{AB},0}\hat{\chi}_\nu(t'),\end{aligned} \tag{C.12}$$

where

$$\mathcal{W}_{xx'}(t, x_\mu, t', x_\nu) = \mathrm{Tr}\big(\hat{\phi}'_\mu(t)\hat{\phi}'_\nu(t')\hat{\rho}_{\phi,0}\big), \tag{C.13}$$

which can be seen to match the definition of $\mathcal{W}_{xx'}$ given in Eq. (4.50), by using that $\hat{\phi}'_\nu(t) = \partial_x\hat{\phi}_{\mathrm{C}}(t, x_\nu)$.

Second,

$$\begin{aligned}\hat{\rho}_{\mathrm{AB}}^{(2,0)} &= \mathrm{Tr}_{\phi}\big(\hat{U}^{(2)}\hat{\rho}_{\mathrm{AB},0}\otimes\hat{\rho}_{\phi,0}\big)\\ &= -\lambda^2\int \mathrm{d}t\,\mathrm{d}t'\;\Theta(t-t')\sum_{\mu,\nu}\mathcal{W}_{xx'}(t,x_\mu,t',x_\nu)\hat{\chi}_\mu(t)\hat{\chi}_\nu(t')\hat{\rho}_{\mathrm{AB},0}\,,\end{aligned} \tag{C.14}$$

and finally, $\hat{\rho}_{\mathrm{AB}}^{(0,2)} = \hat{\rho}_{\mathrm{AB}}^{(2,0)\dagger}$. Notice that the equation for $\hat{\rho}_{\mathrm{AB}}^{(2,0)}$ can be rewritten as

$$\begin{aligned}\hat{\rho}_{\mathrm{AB}}^{(2,0)} = -\lambda^2\int \mathrm{d}t\,\mathrm{d}t'\,\Big(&G_{xx'}(t,x_{\mathrm{A}},t',x_{\mathrm{B}})\hat{\chi}_{\mathrm{A}}(t)\hat{\chi}_{\mathrm{B}}(t')\\ &+\sum_{\nu}\Theta(t-t')\mathcal{W}_{xx'}(t,x_\nu,t',x_\nu)\hat{\chi}_\nu(t)\hat{\chi}_\nu(t')\Big)\hat{\rho}_{\mathrm{AB},0},\end{aligned} \tag{C.15}$$

where we used the definition of $G_{xx'}$ given in Eq. (4.50), which states that

$$G_{xx'}(t,x_\mu,t',x_\nu) = \Theta(t-t')\mathcal{W}_{xx'}(t,x_\mu,t',x_\nu) + \Theta(t'-t)\mathcal{W}_{xx'}(t',x_\nu,t,x_\mu). \tag{C.16}$$

This completes the calculation of $\hat{\rho}_{\mathrm{AB}}$ for an arbitrary $\hat{\rho}_{\mathrm{AB},0}$. Next, we particularize to the the probes starting from the ground state,

$$\hat{\rho}_{\mathrm{AB},0} = |0_{\mathrm{A}}0_{\mathrm{B}}\rangle\langle 0_{\mathrm{A}}0_{\mathrm{B}}|\,. \tag{C.17}$$

Under this assumption, we compute the components of $\hat{\rho}_{\mathrm{AB}}$ in the basis $|0_{\mathrm{A}}0_{\mathrm{B}}\rangle$, $|1_{\mathrm{A}}0_{\mathrm{B}}\rangle$, $|0_{\mathrm{A}}1_{\mathrm{B}}\rangle$, $|1_{\mathrm{A}}1_{\mathrm{B}}\rangle$. To ease the calculation, we denote

$$\hat{A}_{\mu\nu}(t,t') = \hat{\chi}_\mu(t)\hat{\rho}_{\mathrm{AB},0}\hat{\chi}_\nu(t'), \tag{C.18}$$

Then,

$$\begin{aligned}
\langle k_{\mathrm{A}}l_{\mathrm{B}}|\hat{A}_{\mathrm{AA}}(t,t')|k'_{\mathrm{A}}l'_{\mathrm{B}}\rangle &= \delta_{0l}\delta_{0l'}\,\langle k_{\mathrm{A}}|\hat{\chi}_{\mathrm{A}}(t)|0_{\mathrm{A}}\rangle\,\langle 0_{\mathrm{A}}|\hat{\chi}_{\mathrm{A}}(t')|k'_{\mathrm{A}}\rangle\,,\\
\langle k_{\mathrm{A}}l_{\mathrm{B}}|\hat{A}_{\mathrm{BB}}(t,t')|k'_{\mathrm{A}}l'_{\mathrm{B}}\rangle &= \delta_{0k}\delta_{0k'}\,\langle l_{\mathrm{B}}|\hat{\chi}_{\mathrm{B}}(t)|0_{\mathrm{B}}\rangle\,\langle 0_{\mathrm{B}}|\hat{\chi}_{\mathrm{B}}(t')|l'_{\mathrm{B}}\rangle\,,\\
\langle k_{\mathrm{A}}l_{\mathrm{B}}|\hat{A}_{\mathrm{AB}}(t,t')|k'_{\mathrm{A}}l'_{\mathrm{B}}\rangle &= \delta_{0k'}\delta_{0l}\,\langle k_{\mathrm{A}}|\hat{\chi}_{\mathrm{A}}(t)|0_{\mathrm{A}}\rangle\,\langle 0_{\mathrm{B}}|\hat{\chi}_{\mathrm{B}}(t')|l'_{\mathrm{B}}\rangle\,,\\
\langle k_{\mathrm{A}}l_{\mathrm{B}}|\hat{A}_{\mathrm{BA}}(t,t')|k'_{\mathrm{A}}l'_{\mathrm{B}}\rangle &= \delta_{0k}\delta_{0l'}\,\langle l_{\mathrm{B}}|\hat{\chi}_{\mathrm{B}}(t)|0_{\mathrm{B}}\rangle\,\langle 0_{\mathrm{A}}|\hat{\chi}_{\mathrm{A}}(t')|k'_{\mathrm{A}}\rangle\,,
\end{aligned}$$

where, combining Eqs. (4.38) and (C.8) with the definition of $\chi_{\varphi_\nu}(t)$ given in Eq. (4.49),

$$\langle i|\hat{\chi}_\nu(t)|0\rangle = \delta_{1i}\chi_{\varphi_\nu}(t), \tag{C.19}$$

and $\langle 0|\hat{\chi}_\nu(t)|i\rangle = \langle i|\hat{\chi}_\nu(t)|0\rangle^*$. Therefore, only one component of each $\hat{A}_{\mu\nu}$ survives. Precisely, these components correspond to

$$\mathcal{L}_{\mu\nu} = \lambda^2 \int \mathrm{d}t\, \mathrm{d}t'\, \mathcal{W}_{xx'}(t', x_\nu, t, x_\mu)\chi_{\varphi_\mu}(t)\chi^*_{\varphi_\nu}(t'). \tag{C.20}$$

Then,

$$\begin{aligned}\hat{\rho}^{(1,1)}_{\mathrm{AB}} = \mathcal{L}_{\mathrm{AA}} \left|1_\mathrm{A}0_\mathrm{B}\right\rangle\!\left\langle 1_\mathrm{A}0_\mathrm{B}\right| + \mathcal{L}_{\mathrm{BB}} \left|0_\mathrm{A}1_\mathrm{B}\right\rangle\!\left\langle 0_\mathrm{A}1_\mathrm{B}\right| \\ + \mathcal{L}_{\mathrm{AB}} \left|1_\mathrm{A}0_\mathrm{B}\right\rangle\!\left\langle 0_\mathrm{A}1_\mathrm{B}\right| + \mathcal{L}_{\mathrm{BA}} \left|0_\mathrm{A}1_\mathrm{B}\right\rangle\!\left\langle 1_\mathrm{A}0_\mathrm{B}\right|.\end{aligned} \tag{C.21}$$

Moving onto $\hat{\rho}^{(2,0)}_{\mathrm{AB}}$, define for convenience

$$\hat{B}_{\mu\nu}(t, t') = \hat{\chi}_\mu(t)\hat{\chi}_\nu(t')\hat{\rho}_{\mathrm{AB},0}. \tag{C.22}$$

Then,

$$\begin{aligned}\langle k_\mathrm{A} l_\mathrm{B}|\hat{B}_{\mathrm{AA}}(t,t')|k'_\mathrm{A} l'_\mathrm{B}\rangle &= \delta_{0l}\delta_{0l'}\delta_{0k'}\, \langle k_\mathrm{A}|\hat{\chi}_\mathrm{A}(t)\hat{\chi}_\mathrm{A}(t')|0_\mathrm{A}\rangle\,, \\ \langle k_\mathrm{A} l_\mathrm{B}|\hat{B}_{\mathrm{BB}}(t,t')|k'_\mathrm{A} l'_\mathrm{B}\rangle &= \delta_{0k}\delta_{0k'}\delta_{0l'}\, \langle l_\mathrm{B}|\hat{\chi}_\mathrm{B}(t)\hat{\chi}_\mathrm{B}(t')|0_\mathrm{B}\rangle\,, \\ \langle k_\mathrm{A} l_\mathrm{B}|\hat{B}_{\mathrm{AB}}(t,t')|k'_\mathrm{A} l'_\mathrm{B}\rangle &= \delta_{0k'}\delta_{0l'}\, \langle k_\mathrm{A}|\hat{\chi}_\mathrm{A}(t)|0_\mathrm{A}\rangle\, \langle l_\mathrm{B}|\hat{\chi}_\mathrm{B}(t')|0_\mathrm{B}\rangle\,.\end{aligned} \tag{C.23}$$

Then, using Eqs. (4.38), (4.49) and (C.8),

$$\langle i|\hat{\chi}_\nu(t)\hat{\chi}_\nu(t')|0\rangle = \delta_{0i}\chi^*_{\varphi_\nu}(t)\chi_{\varphi_\nu}(t'). \tag{C.24}$$

Together with the former Eq. (C.19), we see that only one component of each $\hat{B}_{\mu\nu}$ survives, resulting in

$$\hat{\rho}^{(2,0)}_{\mathrm{AB}} = \mathcal{M}\left|1_\mathrm{A}1_\mathrm{B}\right\rangle\!\left\langle 0_\mathrm{A}0_\mathrm{B}\right| + \sum_\nu \mathcal{K}_\nu \left|0_\mathrm{A}0_\mathrm{B}\right\rangle\!\left\langle 0_\mathrm{A}0_\mathrm{B}\right|, \tag{C.25}$$

where

$$\begin{aligned}\mathcal{M} &= -\lambda^2 \int \mathrm{d}t\, \mathrm{d}t'\, G_{xx'}(t, x_\mathrm{A}, t', x_\mathrm{B})\chi_{\varphi_\mathrm{A}}(t)\chi_{\varphi_\mathrm{B}}(t'), \\ \mathcal{K}_\nu &= -\lambda^2 \int \mathrm{d}t\, \mathrm{d}t'\, \Theta(t-t')\mathcal{W}_{xx'}(t, x_\nu, t', x_\nu)\chi^*_{\varphi_\nu}(t)\chi_{\varphi_\nu}(t').\end{aligned} \tag{C.26}$$

Notice that comparing this expression for $\mathcal{K}_\nu$ to the one for $\mathcal{L}_{\nu\nu}$ in Eq. (C.20) shows that

$$\mathcal{K}_\nu + \mathcal{K}^*_\nu = -\mathcal{L}_{\nu\nu}, \tag{C.27}$$

by using that

$$\mathcal{W}^*_{xx'}(t,x_\nu,t',x_\nu)=\mathcal{W}_{xx'}(t',x_\nu,t,x_\nu). \tag{C.28}$$

Then, when adding to $\hat{\rho}^{(2,0)}_{\mathrm{AB}}$ its Hermitian conjugate $\hat{\rho}^{(0,2)}_{\mathrm{AB}}$,

$$\begin{aligned}\hat{\rho}^{(2,0)}_{\mathrm{AB}}+\hat{\rho}^{(0,2)}_{\mathrm{AB}} =&\mathcal{M}\,|1_{\mathrm{A}}1_{\mathrm{B}}\rangle\langle 0_{\mathrm{A}}0_{\mathrm{B}}|+\mathcal{M}^*\,|0_{\mathrm{A}}0_{\mathrm{B}}\rangle\langle 1_{\mathrm{A}}1_{\mathrm{B}}|\\ &-\sum_\nu \mathcal{L}_{\nu\nu}\,|0_{\mathrm{A}}0_{\mathrm{B}}\rangle\langle 0_{\mathrm{A}}0_{\mathrm{B}}|\,,\end{aligned} \tag{C.29}$$

Therefore, putting together all the results in this appendix and taking $\hat{\rho}_{\mathrm{AB},0}=|0_{\mathrm{A}}0_{\mathrm{B}}\rangle\langle 0_{\mathrm{A}}0_{\mathrm{B}}|$ causes $\hat{\rho}_{\mathrm{AB}}$ to become, in the basis $|0_{\mathrm{A}}0_{\mathrm{B}}\rangle$, $|1_{\mathrm{A}}0_{\mathrm{B}}\rangle$, $|0_{\mathrm{A}}1_{\mathrm{B}}\rangle$, $|1_{\mathrm{A}}1_{\mathrm{B}}\rangle$,

$$\hat{\rho}_{\mathrm{AB}}=\begin{pmatrix}1-\mathcal{L}_{\mathrm{AA}}-\mathcal{L}_{\mathrm{BB}} & 0 & 0 & \mathcal{M}^*\\ 0 & \mathcal{L}_{\mathrm{AA}} & \mathcal{L}_{\mathrm{AB}} & 0\\ 0 & \mathcal{L}_{\mathrm{BA}} & \mathcal{L}_{\mathrm{BB}} & 0\\ \mathcal{M} & 0 & 0 & 0\end{pmatrix}+\mathcal{O}(\lambda^4), \tag{C.30}$$

where from Eqs. (C.20) and (C.26),

$$\begin{aligned}\mathcal{L}_{\mu\nu}&=\lambda^2\int \mathrm{d}t\,\mathrm{d}t'\,\mathcal{W}_{xx'}(t',x_\nu,t,x_\mu)\chi_{\varphi_\mu}(t)\chi^*_{\varphi_\nu}(t'),\\ \mathcal{M}&=-\lambda^2\int \mathrm{d}t\,\mathrm{d}t'\,G_{xx'}(t,x_{\mathrm{A}},t',x_{\mathrm{B}})\chi_{\varphi_{\mathrm{A}}}(t)\chi_{\varphi_{\mathrm{B}}}(t'),\end{aligned} \tag{C.31}$$

finishing the derivation of $\hat{\rho}_{\mathrm{AB}}$.

C.3 Simplifying the integrals needed to compute negativity

C.3.1 Symmetric switching functions equal up to a time shift and equal detectors

We can further simplify the equations $\mathcal{L}_{\mu\nu}$ and $\mathcal{M}$ for the type of $\chi_\nu(t)$ explored in this article, which satisfy

$$\chi_\nu(t)=\chi(t-t_\nu), \tag{C.32}$$

with $\chi(t)=\chi(-t)$, and t_ν controlling the time at which the detector ν is switched on. Moreover, we assume that the energy gap of both detectors depends linearly on their switching functions, as in Eq. (4.29), as follows,

$$\Omega_\nu(t)=\Omega^0_\nu+\Delta\Omega_\nu\chi_\nu(t). \tag{C.33}$$

For simplicity, we pick $\Omega^0 = \Omega^0_\nu$, $\Delta\Omega = \Delta\Omega_\nu$.

Under the assumptions above, the expression for χ_{φ_ν} becomes

$$\chi_{\varphi_\nu}(t) = e^{-\mathrm{i}\varphi(-t_\nu)}\chi_\varphi(t - t_\nu), \tag{C.34}$$

where we defined

$$\begin{aligned}\chi_\varphi(t) &= e^{\mathrm{i}\varphi(t)}\chi(t),\\ \varphi(t) &= \Omega^0 t + \Delta\Omega \int_0^t \mathrm{d}t'\, \chi(t').\end{aligned} \tag{C.35}$$

Moreover, $\chi(t) = \chi(-t)$ implies

$$\varphi(-t) = -\varphi(t), \quad \chi_\varphi(-t) = \chi_\varphi(t)^*. \tag{C.36}$$

Integrating field modes last

Substituting Eq. (C.34) into Eq. (4.55),

$$\begin{aligned}\mathcal{L} &= \frac{\lambda^2}{2\pi}\int_0^\infty \mathrm{d}\omega\, \omega\, \mathrm{C}(\omega)^2 |\widetilde{\chi_\varphi}(\omega)|^2,\\ \mathcal{L}_{\mathrm{AB}} &= \frac{\lambda^2}{2\pi} e^{-\mathrm{i}(\varphi(-t_\mathrm{A}))-\varphi(-t_\mathrm{B}))} \int_0^\infty \mathrm{d}\omega\, \omega\, \mathrm{C}(\omega)^2 \cos(\omega t_d) e^{-\mathrm{i}\omega t_\Delta} |\widetilde{\chi_\varphi}(\omega)|^2,\end{aligned} \tag{C.37}$$

where we defined $\mathcal{L} = \mathcal{L}_{\mathrm{AA}} = \mathcal{L}_{\mathrm{BB}}$. Moreover,

$$\begin{aligned}\mathcal{M} &= -\frac{\lambda^2}{2\pi} e^{-\mathrm{i}(\varphi(-t_\mathrm{A}))+\varphi(-t_\mathrm{B}))}\mathrm{M},\\ \mathrm{M} &= \int_0^\infty \mathrm{d}\omega\, \omega\, \mathrm{C}(\omega)^2 \cos(\omega t_d) \int \mathrm{d}t\, \mathrm{d}t'\, e^{-\mathrm{i}\omega|t-t'-t_\Delta|}\chi_\varphi(t)\chi_\varphi(t').\end{aligned} \tag{C.38}$$

Here, we also defined the delay between the times of switching $t_\Delta = t_\mathrm{B} - t_\mathrm{A}$ and used that

$$\widetilde{\chi_{\varphi_\nu}}(\omega) = e^{\mathrm{i}(\omega t_\nu - \varphi(-t_\nu))}\widetilde{\chi_\varphi}(\omega). \tag{C.39}$$

Moreover due to $\chi(t) = \chi(-t)$,

$$\begin{aligned}\mathrm{Re}(\mathrm{M}) &= \int_0^\infty \mathrm{d}\omega\, \omega\, \mathrm{C}(\omega)^2 \cos(\omega t_d)\cos(\omega t_\Delta)\widetilde{\chi_\varphi}(\omega)\widetilde{\chi_\varphi}(-\omega),\\ \mathrm{Im}(\mathrm{M}) &= -\int_0^\infty \mathrm{d}\omega\, \mathrm{d}t\, \mathrm{d}t'\, \omega\, \mathrm{C}(\omega)^2 \cos(\omega t_d)\sin(\omega|t-t'-t_\Delta|)\chi_\varphi(t)\chi_\varphi(t').\end{aligned} \tag{C.40}$$

These expressions for Re(M) and Im(M) follow from using that

$$\mathrm{M}^* = \int_0^\infty \mathrm{d}\omega\, \omega\, \mathrm{C}(\omega)^2 \cos(\omega t_d) \int \mathrm{d}t\, \mathrm{d}t'\, e^{\mathrm{i}\omega|t-t'-t_\Delta|} \chi_\varphi(t)\chi_\varphi(t'), \tag{C.41}$$

which in turn was obtained by performing the change of variables $t \to -t'$, $t' \to -t$ in Eq. (C.38) and then applying Eq. (C.36).

When comparing Eq. (C.38) to Eq. (C.41), we see that complex conjugating M is equivalent to complex conjugating $\mathcal{W}_{\text{vac}}$, since we only need to conjugate the complex phase $e^{-\mathrm{i}\omega|t-t'-t_\Delta|}$, which comes from $\mathcal{W}_{\text{vac}}$, and not χ_φ. Consequently, for the switching functions considered in this appendix (of the kind defined in Eq. (C.32), with $\chi(t) = \chi(-t)$), we have a shortcut to compute $\mathcal{M}^\pm$,

$$\begin{aligned}
\mathcal{M}^+ &= -\frac{\lambda^2}{2\pi} e^{-\mathrm{i}(\varphi(-t_\mathrm{A}))+\varphi(-t_\mathrm{B}))}\, \mathrm{Re}(\mathrm{M}), \\
\mathcal{M}^- &= -\frac{\lambda^2}{2\pi} e^{-\mathrm{i}(\varphi(-t_\mathrm{A}))+\varphi(-t_\mathrm{B}))}\, \mathrm{Im}(\mathrm{M}),
\end{aligned} \tag{C.42}$$

with M as defined in Eq. (C.38) and $\varphi(t)$ from Eq. (C.35). Additional expressions for $\mathcal{L}$, $\mathcal{L}_{\mathrm{AB}}$ and M are provided next.

Integrating field modes first

Substituting Eq. (C.34) into Eq. (4.59),

$$\begin{aligned}
\mathcal{L} &= \frac{\lambda^2}{2\pi} \int \mathrm{d}t\, \mathrm{d}t'\, \mathcal{J}(t'-t)\chi_\varphi(t)\chi_\varphi^*(t'), \\
\mathcal{L}_{\mathrm{AB}} &= \frac{\lambda^2}{2\pi} e^{-\mathrm{i}(\varphi(-t_\mathrm{A}))-\varphi(-t_\mathrm{B}))} \int \mathrm{d}t\, \mathrm{d}t'\, \mathcal{I}(t'-t+t_\Delta)\chi_\varphi(t)\chi_\varphi^*(t'), \\
\mathcal{M} &= -\frac{\lambda^2}{2\pi} e^{-\mathrm{i}(\varphi(-t_\mathrm{A}))+\varphi(-t_\mathrm{B}))} \mathrm{M}, \\
\mathrm{M} &= \int \mathrm{d}t\, \mathrm{d}t'\, \mathcal{I}(|t-t'-t_\Delta|)\chi_\varphi(t)\chi_\varphi(t'),
\end{aligned} \tag{C.43}$$

where $\mathcal{L} = \mathcal{L}_{\mathrm{AA}} = \mathcal{L}_{\mathrm{BB}}$, and $\mathcal{J}(t)$ and $\mathcal{I}(t)$ are defined as in Eq. (4.57) and Eq. (4.59) respectively.

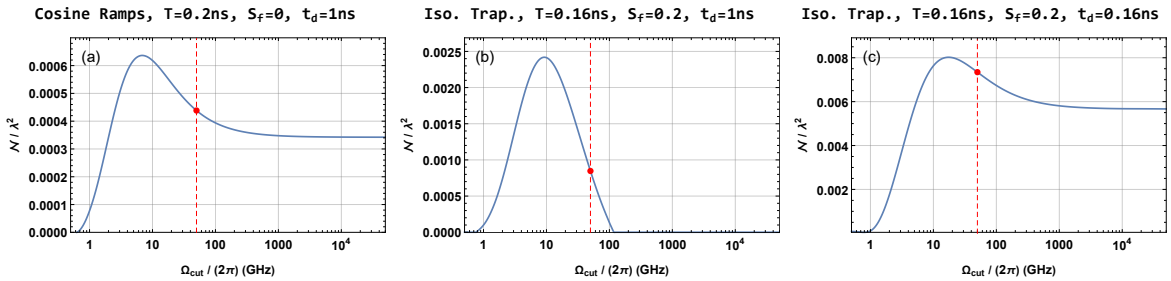


Figure C.1: $\mathcal{N}/\lambda^2$ plotted against the cutoff frequency $\Omega_{\text{cut}}/(2\pi)$, for $\Omega^0/(2\pi) = 7.3\,\text{GHz}$, $\Delta\Omega = 0$, $|t_\Delta| = t_d - T$ (spacelike detector interactions). The cutoff frequency $\Omega_{\text{cut}}/(2\pi) = 50\text{GHz}$, used throughout this work, is highlighted with a vertical dashed line. The subfigures are for: (a) Cosine ramps switching, $T = 0.2\,\text{ns}$, $S_f = 0$, $t_d = 1\,\text{ns}$. (b) Isosceles trapezoid switching, $T = 0.16\,\text{ns}$, $S_f = 0.2$, $t_d = 1\,\text{ns}$. (c) Isosceles trapezoid switching, $T = 0.16\,\text{ns}$, $S_f = 0.2$, $t_d = 0.16\,\text{ns}$. We emphasize that for all the scenarios analyzed the detectors are in strict spacelike separation.

Moreover, due to $\chi(t) = \chi(-t)$,

$$\begin{aligned}\text{Re(M)} &= \int \text{d}t\,\text{d}t'\ \text{Re}\big(\mathcal{I}(t-t'-t_\Delta)\big)\chi_\varphi(t)\chi_\varphi(t'),\\ \text{Im(M)} &= \int \text{d}t\,\text{d}t'\ \text{Im}\big(\mathcal{I}(|t-t'-t_\Delta|)\big)\chi_\varphi(t)\chi_\varphi(t').\end{aligned} \tag{C.44}$$

These expressions for Re(M) and Im(M) follow from using that $\mathcal{I}(-t) = \mathcal{I}^*(t)$ together with

$$\text{M}^* = \int \text{d}t\,\text{d}t'\,\mathcal{I}^*(|t-t'-t_\Delta|)\chi_\varphi(t)\chi_\varphi(t'). \tag{C.45}$$

In turn, this expression was obtained by performing the change of variables $t \to -t'$, $t' \to -t$ in Eq. (C.43) and then applying Eq. (C.36).

C.3.2 Changing variables to partially decouple time integrals

The follwing change of variables facilitates numerical integration by uncoupling one of the time integrals from $\mathcal{J}$ and $\mathcal{I}$ in the expressions for $\mathcal{L}_{\mu\nu}$ and $\mathcal{M}$,

$$t_\pm = t \pm t', \tag{C.46}$$

with absolute value of the Jacobian

$$\left|\frac{\partial(t_+,t_-)}{\partial(t,t')}\right| = 2. \tag{C.47}$$

Then, performing the change of variables in Eq. (C.43),

$$\begin{aligned}
\mathcal{L} &= \frac{\lambda^2}{4\pi}\int \mathrm{d}t_-\, \mathcal{J}^*(t_-)I_L(t_-),\\
\mathcal{L}_{\mathrm{AB}} &= \frac{\lambda^2}{4\pi}e^{-\mathrm{i}(\varphi(-t_{\mathrm{A}}))-\varphi(-t_{\mathrm{B}}))}\int \mathrm{d}t_-\, \mathcal{I}^*(t_- - t_\Delta)I_L(t_-),\\
\mathcal{M} &= -\frac{\lambda^2}{2\pi}e^{-\mathrm{i}(\varphi(-t_{\mathrm{A}}))+\varphi(-t_{\mathrm{B}}))}\mathrm{M},\\
\mathrm{M} &= -\frac{\lambda^2}{4\pi}\int \mathrm{d}t_-\, \mathcal{I}(|t_- - t_\Delta|)I_M(t_-),
\end{aligned} \tag{C.48}$$

where we used $\mathcal{J}(-t)=\mathcal{J}^*(t)$, $\mathcal{I}(-t)=\mathcal{I}^*(t)$, and defined

$$\begin{aligned}
I_L(t_-) &= \int \mathrm{d}t_+\, \chi_\varphi\left(\frac{t_+ + t_-}{2}\right)\chi^*_\varphi\left(\frac{t_+ - t_-}{2}\right),\\
I_M(t_-) &= \int \mathrm{d}t_+\, \chi_\varphi\left(\frac{t_+ + t_-}{2}\right)\chi_\varphi\left(\frac{t_+ - t_-}{2}\right).
\end{aligned} \tag{C.49}$$

For finite time switching functions supported on $[-\frac{T}{2},\frac{T}{2}]$, the integration limits for $t_\pm$ are

$$-T \le t_- \le T, \quad -T+|t_-| \le t_+ \le T-|t_-|. \tag{C.50}$$

Moreover, when $\chi(t)=\chi(-t)$ and thus $\chi_\varphi(-t)=\chi^*_\varphi(t)$,

$$\begin{aligned}
I_L(t_-) &= 2\int_0^\infty \mathrm{d}t_+\, \chi_\varphi\left(\frac{t_+ + t_-}{2}\right)\chi^*_\varphi\left(\frac{t_+ - t_-}{2}\right),\\
I_M(t_-) &= 2\int_0^\infty \mathrm{d}t_+\, \mathrm{Re}\left(\chi_\varphi\left(\frac{t_+ + t_-}{2}\right)\chi_\varphi\left(\frac{t_+ - t_-}{2}\right)\right).
\end{aligned} \tag{C.51}$$

C.4 Spacelike harvesting in the large cutoff limit

The model explored in this article includes an exponential cutoff, which can be reinterpreted as the detector being smeared in space according to Eq. (4.13). This relationship is shown

in subsection 4.1.1 and further discussion can be found in [67]. This effective smearing can raise the question of whether the harvesting found in section 4.5 for spacelike separated point-like detectors is truly present or is merely a byproduct of their effective size induced by the cutoff.

In this appendix, we show that spacelike entanglement harvesting can be achieved in the explored scenarios. Specifically, we provide examples of $\mathcal{N}$ tending to positive values as Ω_{cut} grows large. This corresponds to the limit where the effective detector size becomes negligible. Three spacelike harvesting examples are presented in Figure C.1. For the cosine ramps switching example in Figure C.1(a), harvesting remains possible as $\Omega_{\text{cut}} \to \infty$. There is only a 20% reduction of $\mathcal{N}$ in the limit $\Omega_{\text{cut}} \to \infty$ with respect to $\Omega_{\text{cut}}/(2\pi) = 50\text{GHz}$. For the isosceles trapezoid switching, the cutoff seems to play a larger role when $t_d = 1\,\text{ns}$, as shown in Figure C.1(b), where spacelike harvesting becomes impossible as $\Omega_{\text{cut}} \to \infty$. However, spacelike harvesting for isosceles trapezoid swithching and $\Omega_{\text{cut}} \to \infty$ is still possible by reducing the distance between the detectors to $t_d = 0.16\,\text{ns}$, as shown in Figure C.1(c).